Reformage et synthèse des diméthoxyméthane et diméthyléther pour la production d'hydrogène

Qing Sun

N° d'ordre : 110 - 2007 Année 2007

THESE

présentée devant

l'UNIVERSITE CLAUDE BERNARD – LYON 1

ECOLE DOCTORALE DE CHIMIE – Spécialité CHIMIE

pour l'obtention du

DIPLOME DE DOCTORAT EN CO-TUTELLE
(arrêté du 25 avril 2002)
avec L'UNIVERSITE DE NANJING

Présentée et soutenue publiquement le 12 Juillet 2007

par

Qing SUN

TITRE:

Reformage et synthèse des diméthoxyméthane et diméthyléther pour la production d'hydrogène

Directeur de thèse: M^{me} Aline AUROUX
Co-Directeur de thèse: M. Jianyi SHEN

JURY:	M. J.J. COUNIOUX	Président
	M. X. GE	Examinateur
	Mme V. RAKIC	Rapporteur
	Mme A. AUROUX	Directeur de Thèse
	M. J. SHEN	Co-Directeur de Thèse
	M. J.C. VEDRINE	Rapporteur
	M. P. GELIN	Membre invité
	Mme S. BENNICI	Membre invité

UNIVERSITE CLAUDE BERNARD - LYON I

Président de l'Université	**M. le Professeur L. COLLET**
Vice-Président du Conseil Scientifique	M. le Professeur J.F. MORNEX
Vice-Président du Conseil d'Administration	M. le Professeur J. LIETO
Vice-Président du Conseil des Etudes et de la Vie Universitaire	M. le Professeur D. SIMON
Secrétaire Général	M. G. GAY

SECTEUR SANTE

Composantes

UFR de Médecine Lyon R.T.H. Laënnec	Directeur : M. le Professeur D. VITAL-DURAND
UFR de Médecine Lyon Grange-Blanche	Directeur : M. le Professeur X. MARTIN
UFR de Médecine Lyon-Nord	Directeur : M. le Professeur F. MAUGUIERE
UFR de Médecine Lyon-Sud	Directeur : M. le Professeur F.N. GILLY
UFR d'Odontologie	Directeur : M. O. ROBIN
Institut des Sciences Pharmaceutiques et Biologiques	Directeur : M. le Professeur F. LOCHER
Institut Techniques de Réadaptation	Directeur : M. le Professeur MATILLON
Département de Formation et Centre de Recherche en Biologie Humaine	Directeur : M. le Professeur P. FARGE

SECTEUR SCIENCES

Composantes

UFR de Physique	Directeur : M. le Professeur A. HOAREAU
UFR de Biologie	Directeur : M. le Professeur H. PINON
UFR de Mécanique	Directeur : M. le Professeur H. BEN HADID
UFR de Génie Electrique et des Procédés	Directeur : M. le Professeur A. BRIGUET
UFR Sciences de la Terre	Directeur : M. le Professeur P. HANTZPERGUE
UFR de Mathématiques	Directeur : M. le Professeur M. CHAMARIE
UFR d'Informatique	Directeur : M. le Professeur M. EGEA
UFR de Chimie Biochimie	Directeur : Mme. le Professeur H. PARROT
UFR STAPS	Directeur : M. COLLIGNON
Observatoire de Lyon	Directeur : M. le Professeur R. BACON
Institut des Sciences et des Techniques de l'Ingénieur de Lyon	Directeur : M. le Professeur J. LIETO
IUT A	Directeur : M. le Professeur M. C. COULET
IUT B	Directeur : M. le Professeur R. LAMARTINE
Institut de Science Financière et d'Assurances	Directeur : M. le Professeur J.C. AUGROS

Acknowledgements

I am grateful to all the people who made possible the success of this scientific project and who gave me three wonderful and unforgettable years. This work has been accomplished from September 2004 to July 2007 in the French and Chinese collaborating laboratories of IRCELYON (Villeurbanne, France) and Chemistry Department, Nanjing University (Nanjing, China), respectively.

My deepest gratitude goes first and foremost to my supervisors. Without their constant and illuminating instruction, this thesis could not have reached its present form.

Mr. Jianyi Shen, Professor, Chairman of Chemistry Department in Nanjing University, who led me into the world of catalysis chemistry, gave me the first view of the research and introduced me to the concept and method about how to make a research. “Extensive reading, intensive thinking, smart design, skilled experimental techniques, and scientific insight” - what he taught me are always echoed in my mind. His guide, his broad-mindedness and his human and professional qualities have been of fundamental help for my whole thesis, even for my whole life.

Madame Aline Auroux, directeur de recherche, in IRCELYON, head of the “clean and renewable energies” group, welcomes me warmly into her group and supported me so much in all my stay in France. I was blessed in the three years, with her guidance, encouragement, unreserved help, hospitality, motivation, enthusiasm, immense knowledge, invaluable technical and editorial advice, which really supported me through my whole PhD studies. Not only in science but also in life experience, her cordial help started from the first day of this thesis and never stopped until the end of the thesis.

I also gratefully acknowledge the precious work of Mr. Yuchuan Fu, who generously shared his very valuable knowledge and technique expertise with me. Without his pioneering works, the achievement of this work would be unimaginable.

I gratefully thank Prof. J.J. Counioux from Université Lyon 1, Prof. J.C. Védrine from Université Paris VI, Prof. V. Rakic from University of Belgrade and Prof. X. Ge

from Nanjing University for accepting to refer and judge this manuscript as members of my PhD jury, and Dr. P. Gelin and Dr. S. Bennici from IRCELYON as invited members.

I must also express my deepest gratitude and thanks to those who gave me a lot of instructions and technical supports during my experiments.

Mr. Bernard Bonnetot, directeur de recherche in LMI, UCB LYON 1, gave a lot of help for the TG and XRD analysis of my samples.

Mr. Claude Guimon, directeur de recherche in CNRS, Directeur du laboratoire IPREM – ECP in Université de Pau et des Pays de l'Adour, provided the NH_3 adsorption XPS analysis helping me a lot for the acidic properties characterization of my samples.

Madame Vesna Rakic, teached me the operating of the TG-DSC-MS apparatus and gave me much guidance about this technique.

Mr. Swamy Prakash, gave me so much help and valuable discussions for using the FT-IR apparatus.

Mr. Alain Tuel, provided me with many experimental facilities during the experiments of my samples preparation.

Thanks also go to Prof. Jingwen Song, Prof. Xin Ge and Prof. Huiliang Zhang, who provided me with constant inspirations, advices and encouragements, as well as their valuable experiences and discussions.

I had a real pleasure to work with my colleagues who were in the GIPE or Energy Group at IRCELYON in France during my stay: Simona Bennici, Georgeta Postole and Brandusa Drăgoi; and those who are in the Chemistry Department of Nanjing University in China: Yu'an Huang, Shenghua, Hu, Songlin Zuo, Zheng Xu, Mingwei Xue, Jingwei Liu, Haixia Yang, Guojun Shi, Jiazhen Ge, Hui Chen, Chenghui Han, Binghua Liu, Haiyan Zhu, Yupei Zhao, Suming Wang, Lanxiang Liu, Xiaolin Xing, Hongying Zhao, Xiaoyan Zhang, Dongmei Fang, Jianan Yu, Yang Yang, Yanhua Lei.

Acknowledgements

Let me say “Thank you” to all of you for your continually unselfish help and all the happy time working together.

I also owe my earnest gratitude to all my friends both in France and in China who gave me their help and encouragement.

Thank to CBMM Company in Brazil providing the niobium samples studied in this work.

I also wish to express my appreciation to all the facilities at IRCELYON in France and in Chemistry Department of Nanjing University in China, for the convenient scientific and technical services for the analysis of my samples.

I would like to thank both IRCELYON and Chemistry Department in Nanjing University for providing resources and facilities for my research assistantship.

I gratefully acknowledge the French Government and le Centre National des Œuvres Universitaires et Scolaires (CNOUS). Without their financial support provided for my PhD studies, I could not achieve this work.

I own especially thanks to my girl friend Zhilin Cheng for her patience, love and encouragement during these years of my studies. Finally, I would like to thank my parents for their support and love while have been separated for these years.

Contents

List of Publications

The results of this thesis have been published or submitted into several international journals which are listed in the following:

I. **Qing Sun**, Aline Auroux and Jianyi Shen, Surface acidity of porous niobium phosphate (NbP) and steam reforming of dimethoxymethane over Cu/ZnO/Al_2O_3-NbP complex catalysts, *J. Catal.*, 216 (2006) 1-9.

II. **Qing Sun**, Jianyi Shen and Aline Auroux, Hydrogen production from steam reforming of dimethoxymethane over CuZnO/Al_2O_3-niobium phosphate hybrid catalysts, 16th World Hydrogen Energy Conference, 2006, 8 pages

III. **Qing Sun**, Lanxiang Liu, Xiaoling Xing, Aline Auroux and Jianyi Shen, Catalytic effects of niobium, *Petrochemical Technology*, 36 (2007) 319-328.

IV. **Qing Sun,** Dongmei Fang, Suming Wang, Jianyi Shen, Aline Auroux, **S**tructural, acidic and redox properties of V_2O_5/NbP catalysts, *Appl. Catal. A: General*, in press.

V. **Qing Sun**, Yuchuan Fu, Haixia Yang, Aline Auroux and Jianyi Shen, Dehydration of methanol to dimethyl ether over Nb_2O_5 and NbP catalysts: Microcalorimetric and FT-IR studies, *J. Mol. Catal. A: Chemical*, accepted.

VI. **Qing Sun**, Yuchuan Fu, Jingwei Liu, Jianyi Shen and Aline Auroux, Structural, acidic and redox properties of V_2O_5-TiO_2-SO_4^{2-} catalysts, submitted to *Appl. Catal. A: General*

VII. Hao Shen, Yuchuan Fu, **Qing Sun**, Songlin Zuo, Aline Auroux and Jianyi Shen, High surface area carbons as acidic components with Cu-ZnO/Al_2O_3 for the reforming of dimethoxymethane, submitted to *Catal. Comm.*

List of Communications

I. 16th World Hydrogen Energy Conference, June 13 – 16, 2005, Lyon, France, "Hydrogen production from steam reforming of dimethoxymethane over $CuZnO/Al_2O_3$-niobium phosphate hybrid catalysts", **Qing Sun**, Jianyi Shen, Aline Auroux.

II. 13th National Conference of Catalysis, September 17 – 21, 2006, Lanzhou, China, "Surface acidity and acid catalytic activity of NbP", **Qing Sun**, Yuchuan Fu, Jianyi Shen, Aline Auroux.

III. Gecat 2007, May 29 – June 1, 2007, La Grande Motte, "Structural, acidic and redox properties of V_2O_5/NbP catalysts" **Qing Sun**, Yuchuan Fu, Jianyi Shen, Aline Auroux.

IV. EUROPACAT VIII, Turku, Finland, August 26 – 31, 2007, "The acidic-redox properties of V_2O_5/NbP catalysts in methanol oxidation reaction" **Qing Sun**, Yuchuan Fu, Jianyi Shen, Aline Auroux.

1. Background and Introduction

This work is related to the subject "Clean Energy".

In the last two decades of the 20th century, there has been growing concern about pollution in major cities, and in particular about the large contribution made by road transportation sources to this problem. Additionally, there has been parallel concerns about the emissions of carbon dioxide, from both transportation and stationary power sources, and their influence on climate change ("global warming") via the "greenhouse effect". While the true extent and consequences of global warming are still fiercely debated, it is generally agreed that action needs to be taken to curb emissions of carbon dioxide. Taken together, these environmental problems argue the case for the development and introduction of fuel-cell vehicles (FCVs), since they produce zero or almost zero tailpipe emissions of regulated pollutants such as NOx, CO, SOx and hydrocarbons, offer high efficiency, and emit significantly lower amounts of CO_2 than the conventional internal combustion engines (ICEs) [1, 2].

One of the key techniques to do so is the development of mobile hydrogen sources for fuel cells [3, 4]. Generally speaking, a large-scale production of H_2 in industry is available which can be realized by hydrocarbon reforming or coal gasification combined with water gas shift reaction [5, 6]. What is much more costly is the process of storage and transportation of H_2 [5, 6]. One solution is transferring H_2 into materials like methanol which are of high hydrogen content and easy to store and transport [3-8]. When needed, the H_2 can be released again by decomposition of such materials.

H_2 can be produced by steam reforming of gasoline [9], natural gas, methanol [10-12], dimethyl ether [13-15], and also by decomposition of ammonia [16-18]. However, the reforming temperatures of natural gas and gasoline are high [19] (above 873 K for natural gas and above 1073 K for gasoline) requiring high energy input and the stability of catalysts and refractory reactors are also problems. Methanol is synthesized from syngas [20] and its reforming is relatively easy to perform around 523-573 K. The disadvantage of using methanol as H_2 source is that it is highly toxic.

1. Background and Introduction

The reforming of dimethylether (DME) has been performed to produce H_2. However, the thermodynamic calculation suggests that the reforming of DME might be limited by its low rate of hydrolysis.

DMM (dimethoxymethane) is a preferring material for steam reforming process to produce H_2. It has the advantages of high content of hydrogen, extremely low toxicity, environmentally benign. Furthermore, it is a liquid and easy for storage and transportation at ambient conditions.

Thus, in this work, DMM is studied to be reformed to produce H_2. Steam reforming of DMM consists of the hydrolysis of DMM to methanol and formaldehyde, which are further reformed to produce H_2 and CO_2.

$$CH_3OCH_2OCH_3 + H_2O = 2CH_3OH + CH_2O \quad (1)$$

$$CH_3OH + H_2O = 3H_2 + CO_2 \quad (2)$$

$$CH_2O + H_2O = 2H_2 + CO_2 \quad (3)$$

The overall reaction can then be expressed as,

$$CH_3OCH_2OCH_3 + 4H_2O = 8H_2 + 3CO_2 \quad (4)$$

Thus, the catalysts for the reforming of DMM must consist of a solid acid for the hydrolysis of DMM and a component for the reforming of methanol and formaldehyde. The latter is usually $CuZnO/Al_2O_3$ (CuZnAl) that has been extensively studied [10, 11, 21-25]. The acidic component must be carefully chosen. It should catalyze the hydrolysis of DMM effectively, but does not affect the performance of $CuZnO/Al_2O_3$ for the reforming reactions.

Niobium pentoxides (Nb_2O_5) and niobium phosphates (NbP) possess strong surface acidity and are used as solid acid catalysts [26-29]. The acidity and reactivity of these systems have been studied by different techniques during the past years [30-38]. The preparation, characterization and application of niobium-containing materials were reviewed by Nowak and Ziolek [26, 27]. Tanabe summarized the catalytic applications of niobium compounds [28, 29].

1. Background and Introduction

Niobium pentoxide (Nb_2O_5) is a white, air-stable and water insoluble solid. It generally possesses an octahedrally coordinated NbO_6 distorted to different extents depending on whether its polyhedra are corner-shared or edge-shared [39, 40]. Hydrated niobium oxide ($Nb_2O_5 \cdot nH_2O$) exhibits strong acidity according to the Hammett titration ($H_0 \leq -5.6$). Its acid strength is equivalent to about 70% sulfuric acid [41]. It possesses both Lewis and Brønsted acid sites [40]. The surface acid sites remained after outgassing at 673 K for 10 h, as determined by using ammonia adsorption microcalorimetry [30]. It usually exhibits high activity for the acid catalyzed reactions in which water molecules participate [41, 42].

Niobium phosphate (NbP or $NbOPO_4$) has a similar structure to Nb_2O_5 [26], but with higher acid strength ($H_0 \leq -8.2$). It has a distorted octahedra (NbO_6) connected by PO_4 tetrahedra via sharing corners [27]. Both terminal POH and NbOH groups are present in bulk and coated niobium phosphate catalysts [26]. The POH are stronger Brønsted acids than NbOH in niobium phosphates [43]. The Lewis acid sites in niobium phosphates are those coordinatively unsaturated Nb^{5+} cations [43].

Thus, both Nb_2O_5 and NbP could be used as an acid component to mix with $CuZnO/Al_2O_3$ forming a complex catalyst for steaming reforming of DMM to produce H_2. Nb_2O_5, NbP and the complex catalyst are studied in this work.

Since DMM is used as a H_2 containing compound for H_2 production, thus, the synthesis of DMM is also studied in this work.

Generally DMM is produced via a condensation of formaldehyde with methanol over acid catalysts [44]. It was reported that DMM could also be synthesized by the direct oxidation of methanol on crystalline $SbRe_2O_6$ [45], $Re/\gamma\text{-}Fe_2O_3$ [45], heteropolyacids [47], and RuO_x/SiO_2 [48]. The direct synthesis of DMM would be more efficient if the process is industrialized. The selective oxidation of methanol to DMM may involve two steps: (1) oxidation of methanol to formaldehyde on redox sites and (2) condensation of formaldehyde produced with additional methanol to DMM on acidic sites. Thus, bi-functional catalysts with redox and acidic characters are required for the reaction.

1. Background and Introduction

Tatibouët summarized [49], in methanol oxidation, methanol is first dissociatively adsorbed to form methoxy groups. Further transformation of methoxy group will depend on the acid strength of the adsorption site, and on the nature of the active centers in close proximity. The redox sites close to the methoxy group will lead to the break of a C-H bond, while weak acid sites will favor the desorption of the reaction products. Thus, the formation of formaldehyde requires both redox and weak acid sites to limit the H abstraction and to prevent a too strong adsorption of formaldehyde, respectively. Strong acid sites prolong the residence time of formaldehyde species to form dioxymethylene species, able to react with methanol to form DMM. If the redox sites are stronger than those needed for DMM formation, dioxymethylene species will be oxidized into formate species which quickly react with methanol to form methyl formate or are further oxidized to COx. If only strong acid sites are present, only dimethyl ether is formed. The acid-redox strength diagram is summarized in Fig. 1.1. Supported V_2O_5 catalysts were usually used in the reaction of methanol oxidation [49, 50]. Therefore, we prepared catalysts of V_2O_5 supported on different supports (NbP and TiO_2), which were used to synthesis of DMM via selective oxidation of methanol.

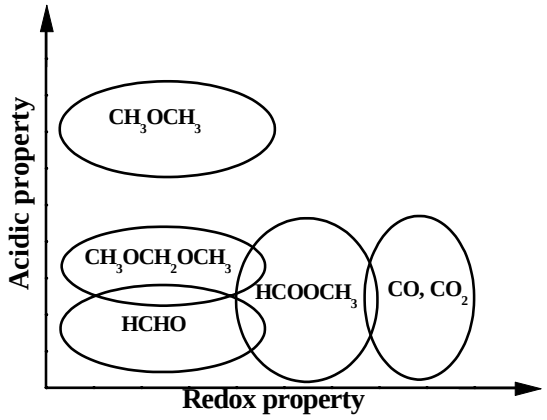

Fig. 1.1 Acidic properties vs. redox properties in methanol oxidation

Dimethyl ether (DME) has been widely used as an aerosol propellant to replace chlorofluoro carbons [51]. Additionally, it is an important chemical intermediate for producing many valuable chemicals such as lower olefins, methyl acetate, dimethyl sulfate, etc. [52, 53]. In recent years, it has attracted global attention as a potential clean fuel substitute for LPG (liquefied petroleum gas) and diesel oil for its cleanness, non-toxic and environmentally benign behaviour [54, 55].

1. Background and Introduction

DME is generally synthesized by dehydration of methanol over solid acidic catalysts [56-59]. It can also be synthesized directly from syngas via a so-called STD (syngas to DME) process by employing a hybrid catalyst comprising a methanol synthesis component and a solid acid [60, 61], which is more attractive in consideration of the equilibrium limitation. Typically, the $Cu/ZnO/Al_2O_3$ catalyst is used as a methanol synthesis component in the hybrid catalyst [61, 62], and the solid acids used for the dehydration of methanol are H-ZSM-5, H-Y zeolite, γ-Al_2O_3, modified γ-Al_2O_3, silica-alumina and so on [57, 59, 61, 63, 64].

Nb_2O_5 are reported to be active catalyst in the alcohol dehydration reactions [28, 29]. However, the reactions of methanol dehydration on Nb_2O_5 and NbP samples have never been studied intensively especially for the adsorption properties of methanol, H_2O and DME. Therefore, in this work, Nb_2O_5 and NbP samples are studied by adsorption microcalorimetry, FT-IR and TPD using different gas (NH_3, methanol, water and DME) as probe molecules. The catalytic activities of Nb_2O_5 and NbP were evaluated in the reaction of methanol dehydration to DME.

To summarize, the object of this work is to study:

(1) Steam reforming of DMM to produce H_2:

Dimethoxymethane (DMM) is nontoxic and of high hydrogen content, and may be used as a H_2 storage material for small H_2 sources. Steam reforming of DMM needs a bi-functional catalyst composed of an acidic component and a traditional copper catalyst, on which DMM is hydrolyzed on the acidic sites to methanol and formaldehyde which are then further reformed to H_2 and CO_2 on metallic copper sites. Samples of NbP with high surface areas were synthesized, characterized and tested for the hydrolysis of DMM and used as acidic components for the reforming of DMM to produce H_2. The structure and surface areas of these samples were characterized and the activity for the hydrolysis of DMM was correlated to the surface acidities.

The activity for H_2 production on $CuZnO/Al_2O_3$-NbP bi-functional catalysts from steam reforming of DMM was evaluated.

(2) Selective oxidation of methanol to DMM:

Two catalysts series of V_2O_5/NbP and V_2O_5-TiO_2-SO_4^{2-} were prepared by the wetness impregnation and co-precipitation methods respectively. The structural properties were characterized by O_2 chemisorption, X-ray diffraction (XRD), Raman spectroscopy (LRS) and X-ray photoelectron spectroscopy (XPS). The surface acidity was determined by the techniques of microcalorimetry and infrared spectroscopy (FTIR) using NH_3 as a probe molecule. Isopropanol (IPA) and methanol oxidation reactions with the presence of O_2 were employed to provide the information about the surface acidity and redox property simultaneously.

(3) Dehydration of methanol to produce DME:

Nb_2O_5 and NbP catalysts were developed for the dehydration of methanol to form DME. The interactions of ammonia, methanol, water and dimethyl ether with Nb_2O_5 and NbP were investigated by means of adsorption microcalorimetry, adsorption infrared spectroscopy (FT-IR) and temperature-programmed desorption (TPD) techniques. NH_3 adsorption microcalorimetry was used to titrate the strength and number of surface acid sites while the nature of acid sites was probed by NH_3 adsorption FT-IR. Methanol, water and DME were used as probe molecules to determine the strength, strength distribution and nature of adsorption sites by means of adsorption microcalorimetry, adsorption FT-IR and TPD techniques. The activities for the reaction of methanol dehydration were evaluated on Nb_2O_5 and NbP, which were compared with the conventional solid acid catalysts such as H-ZSM-5, etc.

2. Experimental descriptions

The following chapter describes the catalysts preparation and experimental techniques used in this work.

2.1 Catalyst preparation

2.1.1 Niobium oxide (Nb_2O_5) and niobium phosphate (NbP) catalysts

Nb_2O_5 was prepared by calcining a commercial niobic acid ($Nb_2O_5 \cdot nH_2O$, CBMM, Brazil) at 623 K for 4 h in flowing air. NbP1 was a commercial niobium phosphate provided by CBMM in Brazil. NbP2 was a niobium phosphate prepared with the impregnation method. In short, 6.35 g of niobic acid was added into 120 ml aqueous solution of H_3PO_4 (1 M) and stirred for 48 h at room temperature. The slurry was filtered, dried at 373 K overnight and then calcined at 673 K for 4 h. A high surface area niobium phosphate (NbP3) was prepared by following a procedure previously described [65]. 2.73 g of $NbCl_5$ (Alfa Aesar, 99%) were partially hydrolyzed in 50 ml H_2O followed by the addition of 2.30 g H_3PO_4 (Aldrich, 85% aqueous solution) to initiate a vigorous hydrolysis reaction. An additional 50 ml H_2O was then added and the reaction mixture was stirred for 30 min. The pH of the reaction mixture was adjusted to 2.6 by ammonia solution. After stirring, the slurry was filtered and washed with deionized water to obtain a chlorine-free gel. The gel was mixed with 10 ml H_2O and 1.45 g hexadecylamine (Aldrich, 90%) and stirred for 30 min. Then, 0.92 g H_3PO_4 (85 wt%) was added and the pH of the mixture was adjusted to 3.9. After complete mixing, the slurry was heated in a Teflon lined stainless steel autoclave at 338 K under autogeneous pressure for 2 days. The final product was filtered, washed with deionized water, dried at 373 K overnight and calcined at 723 K in air for 40 h.

2.1.2 $CuZnO/Al_2O_3$ catalysts

The $CuZnO/Al_2O_3$ is a commercial catalyst (CF105, a product of the Research Institute of Nanjing Chemical Industry Group, China) with the molar ratio of 63% Cu, 21% Zn and 16% Al.

2.1.3 V_2O_5/NbP (V/NbP) and V_2O_5 catalysts

The V_2O_5/NbP catalysts with various loadings (5-25 wt% of V_2O_5) were prepared by using the incipient wetness impregnation method. Specifically, for each preparation, a known amount of NbP (prepared by using a template) was added into the aqueous solution containing the desired amount of vanadium oxalate and stirred. After being kept at room temperature overnight, it was dried at 383 K overnight and then calcined in air at 673 K for 5 h. Bulk V_2O_5 was obtained from the calcination of ammonium metavanadate in air at 673 K for 5h.

2.1.4 V_2O_5-TiO_2 (VT) and V_2O_5-TiO_2-SO_4^{2-} (VTS) catalysts

The V_2O_5-TiO_2 (termed as VT) catalysts were prepared by a co-precipitation method described as the following. Specifically, stoichiometric $TiCl_4$ (99.9%) was dissolved in C_2H_5OH (1g $TiCl_4$ in 20 ml C_2H_5OH) in ice bath, which formed a titanium containing solution (S1), while a niobium containing solution (S2) was obtained by dissolving $VOCl_3$ (99.9%, Aldrich) into H_2O (1g $VOCl_3$ in 20 ml H_2O). Then S1 was slowly dropped into S2 in a continual stirring condition to form a mixed solution (S3). Then an excess amount of diluted $NH_3.H_2O$ (4 wt % NH_3) was dropped into S3 under a violent stirring in ice bath and a brown precipitate formed immediately. This precipitate was aging for 3 h at room temperature. Subsequently the precipitate was filtered, washed with deionized water until no chloride ions were detected, dried at 373 K overnight, and calcined at 673 K in air for 6 h. Pure TiO_2 and V_2O_5 were prepared with the same method. The V_2O_5-TiO_2-SO_4^{2-} (VTS) samples were prepared by incipient wetness impregnating 1 g of above mentioned VT catalyst with an aqueous solution containing 50 mg $Ti(SO_4)_2$. After being kept at room temperature overnight, they were dried at 373 K overnight and then calcined in air at 673 K for 4 h.

2.2 Catalyst characterization

Different techniques were used to characterize the physico-chemical properties of the catalysts which are listed as the following.

The surface area and pore size were measured by nitrogen adsorption at 77 K after heat pretreatment under vacuum at 623 K for 4 h in an automatic system built up in IRCELYON (see Fig. 2.2.1.)

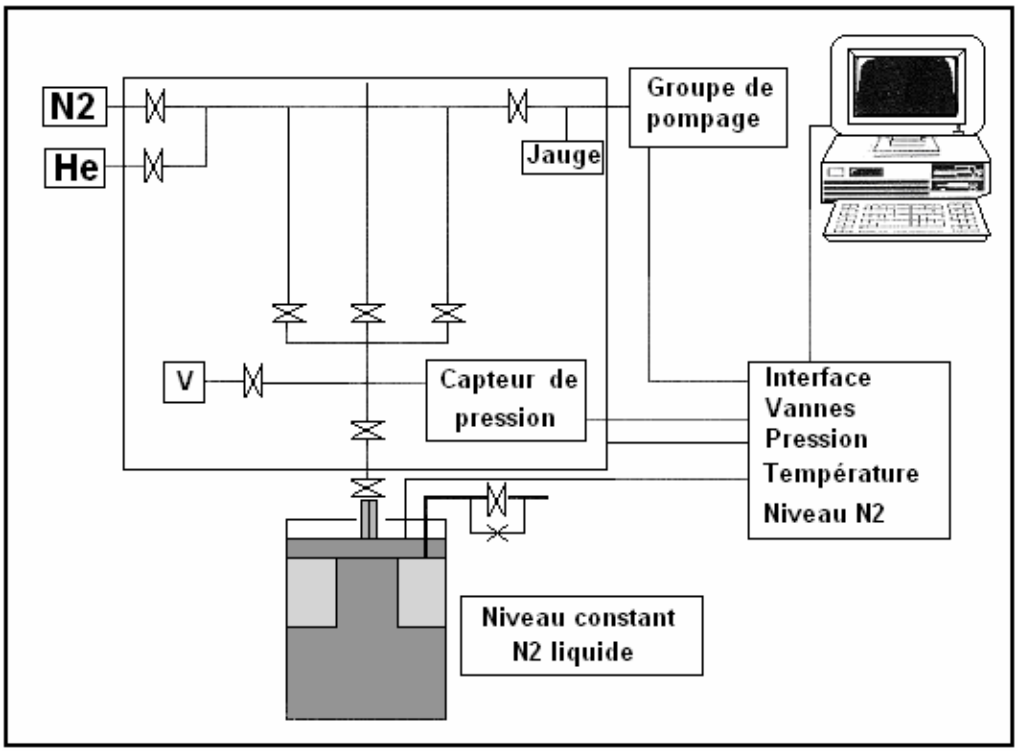

Fig. 2.2.1 Scheme of the system for S_{BET} and pore size measurements (IRCELYON).

The X-ray diffraction (XRD) measurements were carried out on a Bruker D5005 diffractometer scanning from 3^o to 80^o (2θ) at a rate of 0.02 degree·s^{-1} and from 1^o to 10^o (2θ) at a rate of 0.002 degree·s^{-1} using a Cu Kα radiation (λ = 0.15418 nm) source. The applied voltage and current were 50 kV and 35 mA, respectively.

Elemental analysis was performed using the ICP atomic emission spectroscopy (Spectroflame-ICP D, Spectro).

The UV-Vis spectra were recorded with a Perkin-Elmer Lambda 19 spectrophotometer.

2. Experimental descriptions

Raman spectra were obtained using a Dilor XY spectrometer coupled to an Olympus BH-2 microscope. The excitation was provided by the 514.5 nm line of an Ar+ ion laser (Spectra Physics) employing a laser power of 2.5 mW. The range and resolution applied were 100-1100 cm^{-1} and 0.5 cm^{-1}, respectively.

The transmission electron microscopy (TEM) was carried out using a JEM 2010 operating at 200 kV in bright and dark field modes.

The X-ray photoelectron spectra (XPS) were measured on a SSI 301 instrument (Bruker) equipped with a hemispherical electron analyzer and an Al anode (Al Kα =1486.6 eV) powered at 100 W. The residual pressure in the spectrometer chamber was 5×10^{-8} Pa during data acquisition. (Fig. 2.2.2)

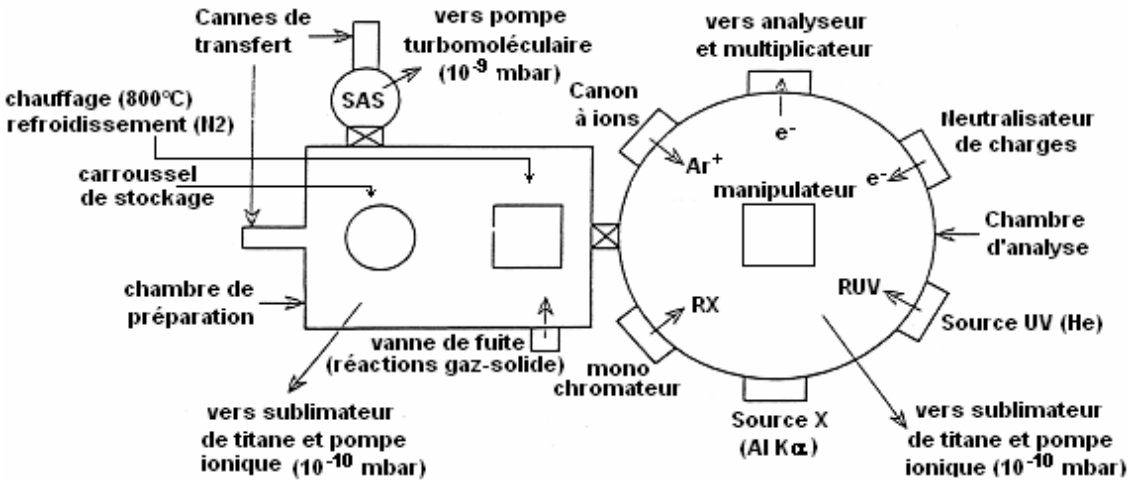

Figure 2.2.2 Scheme of spectrometer SSI

The microcalorimetric studies of methanol, water and DME adsorption were performed at 303 K while ammonia adsorption at 423 K in a heat flow calorimeter (C80 from Setaram) linked to a conventional volumetric apparatus equipped with a Barocel capacitance manometer for pressure measurements. All gases used for measurements (purity > 99.9%) were purified by successive freeze–pump–thaw cycles. About 100 mg of sample was pretreated in a quartz cell under evacuation overnight at 623 K. The differential heats of adsorption were measured as a function of coverage by repeatedly introducing small doses of ammonia gas onto the catalyst until an equilibrium pressure of about 66 Pa was reached [66]. The sample was then

outgassed for 30 min at the same temperature and a second adsorption was performed at the same temperature as adsorption until an equilibrium pressure of about 27 Pa was attained in order to calculate the irreversibly chemisorbed amount of absorbed gases at this pressure. (Fig. 2.2.3)

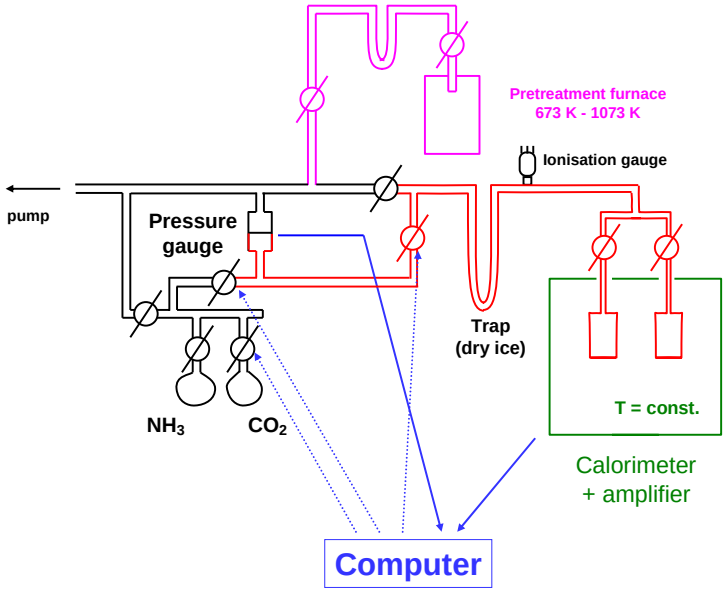

Fig. 2.2.3 Scheme of adsorption microcalorimetry system (IRCELYON).

Temperature-programmed ammonia (water, methanol) desorption was performed on a Setaram TG-DSC 111 equipment coupled with a mass spectrometer (Thermostar from Pfeifer) as a detector. Capillary-coupling system was used. The TPD experiments were carried out in a flow, with helium as the carrier gas (10 ml·min^{-1}). For each experiment, about 30 mg of a sample with ammonia adsorbed in previously done microcalorimetry experiment was used. Initially, the samples were purged with helium at 373 K for 30 min to remove most of adsorbed water and heated at 5 K·min^{-1} in helium up to 873 K. During this temperature increase, the mass spectrometer was set at m/e = 15 in order to avoid the interference of water fragmentation masses. For water and methanol desorption, the gas phase composition was analyzed by setting the mass spectrometer m/e = 15 and 16 for methane, m/e = 31 for methanol, m/e = 18 for H_2O and m/e = 45 for DME. (see Fig. 2.2.4)

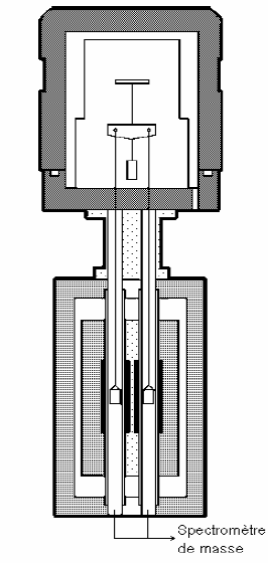

Fig. 2.2.4 Scheme of TG-DSC 111 system

The gas phase adsorption FT-IR spectra were recorded with a Bruker Vector 22 FTIR spectrophotometer (DTGS detector). The range, resolution and acquisition applied were 4000–400, 2 cm^{-1} and 50 scans, respectively. The self-supporting wafer (10–30 mg, 18mm diameter) was first activated in an in-situ IR cell at 673 K in flowing O_2 for 12 h, evacuated at the same temperature for 2 h, and then exposed to different gases (NH_3, methanol and dimethyl ether) (purity>99.9%) at room temperature for 5 minutes. The desorption was carried out by evacuation for 30 min each at 300, 373, 473, 523, 573 and 673 K. A spectrum was recorded at room temperature after desorption at each temperature. (see scheme Fig. 2.2.5)

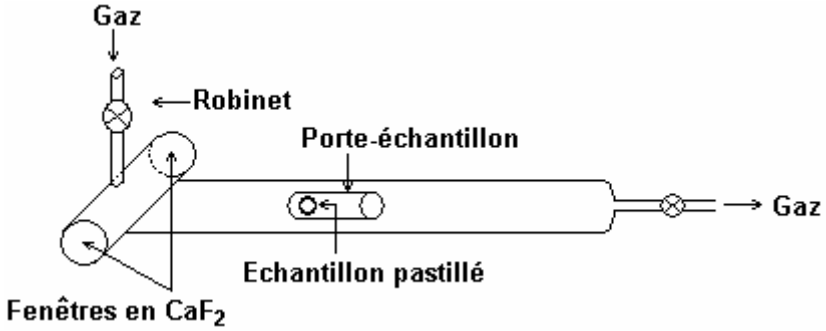

Fig. 2.2.5 Scheme of the in-situ cell for adsorption FT-IR (IRCELYON).

2. Experimental descriptions

H_2-TPR measurements were carried out with a continuous mode using a U-type quartz microreactor (3.5 mm in diameter). A sample of about 50 mg was contacted with a H_2:N_2 mixture (5.13% volume of H_2 in N_2) at a total flow rate of 40 ml·min^{-1}. The sample was heated at a rate of 10 K·min^{-1} from room temperature to 1250 K. The hydrogen consumption was monitored using a thermal conductive detector (TCD). The reducing gas was first passed through the reference arm of the TCD before entering the reactor. The reactor exit was directed through a trap filled with $Mg(ClO_4)_2$ (to remove water product) and then to the second arm of the TCD.

2.3 Catalytic reaction

Isopropanol probe reaction was used to characterize the surface acidity. The probe reaction was carried out in a fixed-bed glass tube reactor. About 100 mg sample was loaded for the reaction. Isopropanol was introduced to the catalysts by bubbling N_2 (99.999%) or air through a glass saturator filled with isopropanol maintained at 295 K. Isopropanol and reaction products were analyzed by an online gas chromatograph, using a PEG 20M packed column connected to a Flame Ionization Detector (FID). Each catalyst was pretreated by heating in N_2 or air at 673 K for 1 h and then cooled in the same flow to the reaction temperature.

The hydrolysis of dimethoxymethane (DMM) was performed in a fixed-bed micro-reactor made of glass with an inner diameter of 6 mm. The DMM and H_2O were introduced to the reaction zone by bubbling N_2 (99.999%) through a glass saturator filled with DMM (Aldrich, 99%) maintained at 273 K and a glass saturator filled with H_2O maintained at 333 K. In each test, 50 mg catalyst was loaded, and the gas hourly space velocity (GHSV) used was 90000 ml·g^{-1}·h^{-1}. The feed composition was maintained at N_2:H_2O:DMM = 24:5:1 (v/v). The tail gas out of the reactor was analyzed by an on-line GC equipped with a FID detector. The column used was Porapak N for the separation of methanol, DMM and other organic compounds. The gas lines were kept at 373 K to prevent condensation of the reactant and products. The reaction was carried out at atmospheric pressure.

2. Experimental descriptions

The steam reforming of methanol (or DMM) was carried out in a same way as the hydrolysis of DMM. An acidic component was mixed with $CuZnO/Al_2O_3$ in a weight ratio of 1/7. About 500 mg catalyst was loaded and the GHSV used was 10000 $ml \cdot g^{-1} \cdot h^{-1}$ for methanol and 4550 $ml \cdot g^{-1} \cdot h^{-1}$ for DMM. The feed composition was maintained at N_2:H_2O:methanol = 8.8:1.25:1 or N_2:H_2O:DMM = 24:5:1 (v/v). The products were analyzed by an on-line GC equipped with FID and TCD detectors. The FID was connected to a Porapak N column for the separation of methanol, DMM and other organic compounds, while the TCD was connected to a TDX-01 column for the analysis of methane, CO_X and N_2. The amount of H_2 produced was usually calculated according to the conversion of DMM and the composition of other products, and was checked by using another GC.

The oxidation of methanol (or dehydration of methanol) was carried out in a fixed-bed micro-reactor made of glass with an inner diameter of 6 mm. The methanol was introduced to the reaction zone by bubbling O_2/N_2 (1/5) (pure N_2 for methanol dehydration) through a glass saturator filled with methanol (99.9%) maintained at 278 K. In each test, 0.2 g catalyst was loaded, and the gas hourly space velocity (GHSV) was 11400 $ml.g^{-1}.h^{-1}$. The feed composition was maintained as methanol:O_2:N_2=1:3:15 (v/v). The tail gas out of the reactor was analyzed by an on-line GC equipped with a FID detector and a TCD detector. The column used was PORAPAK N for the separation of methanol, DMM and other organic compounds. The gas lines were kept at 373 K to prevent condensation of the reactant and products. The reaction was carried out at atmospheric pressure.

3. List of Catalysts

Table 1 Brief description of the catalysts used in this work

Catalyst	Description	Calcination Temp.[a] (K)	Publication
Nb_2O_5	Niobic acid (CBMM) calcined	623	I, II, V
NbP1	Commercial niobium phosphate (CBMM)	673	I, II
NbP2	Niobium phosphate prepared by impregnation method	673	I, II
NbP3	Niobium phosphate prepared by using a template	723	I, II
NbP (280 m^2/g)	Niobium phosphate prepared by using a template	723	IV
NbP (511 m^2/g)	Niobium phosphate prepared by using a template	723	V
5V/NbP	5 wt% V_2O_5 supported on NbP prepared by impregnation method	673	III
15V/NbP	15 wt% V_2O_5 supported on NbP prepared by impregnation method	673	IV
25V/NbP	25 wt% V_2O_5 supported on NbP prepared by impregnation method	673	IV
V_2O_5	Bulk V_2O_5 prepared by calcination of NH_4VO_3	673	IV
15VT	Ti^{4+} and V^{3+} co-precipitated by NH_4OH (15 wt% V_2O_5 - 85 wt% TiO_2)	673	VI
25VT	Ti^{4+} and V^{3+} co-precipitated by NH_4OH (25 wt% V_2O_5 - 75 wt% TiO_2)	673	VI
50VT	Ti^{4+} and V^{3+} co-precipitated by NH_4OH (50 wt% V_2O_5 - 50 wt% TiO_2)	673	VI
75VT	Ti^{4+} and V^{3+} co-precipitated by NH_4OH (75 wt% V_2O_5 - 25 wt% TiO_2)	673	VI
15VTS	15VT impregnated with 4 wt% of SO_4^{2-}	673	VI
25VTS	25VT impregnated with 4 wt% of SO_4^{2-}	673	VI
50VTS	50VT impregnated with 4 wt% of SO_4^{2-}	673	VI
TiO_2	Ti^{4+} precipitated by NH_4OH	673	VI
V_2O_5	V^{5+} precipitated by NH_4OH	673	VI

[a] All catalysts were calcined in air

References

[1] B.D. McNicol, D.A.J. Rand, K.R. Williams, J. Power Sources 100 (2001) 47.

[2] P.K. Cheekatamarla, C.M. Finnerty, J. Power Sources 160 (2006) 490.

[3] J.C. Amphlett, K.A.M. Creber, J.M. Davis, R.F. Mann, B.A. Peppley, D.M. Stokes, Int. J. Hydrogen Energy 19 (1994) 131.

[4] L. Carrette, K.A. Friedrich, U. Stimming, Chemphyschem 1 (2000) 162.

[5] D.L. Trimm, Z.I. Onsan, Catal. Rev. Sci. Eng. 43 (2001) 31.

[6] C.S. Song, Catal. Today 77 (2002) 17.

[7] G.J.K. Acres, J. Power Sources 100 (2001) 60.

[8] A. Heinzel, V.M. Barragan, J. Power Sources 84 (1999) 70.

[9] A.D. Qi, S.D. Wang, G.Z. Fu, C.J. Ni, D.Y. Wu, Appl. Catal. A 281 (2005) 233.

[10] J.C. Amphlett, M.J. Evans, R.A. Jones, R.F. Mann, R.D. Weir, Can. J. Chem. Eng. 59 (1981) 720.

[11] B. Emonts, J.B. Hansen, S.L. Jorgensen, B. Hohlein, R. Peters, J. Power Sources 71 (1998) 288.

[12] J.-P. Shen, C.S. Song, Catal. Today 77 (2002) 89.

[13] K. Takeishi, H. Suzuki, Appl. Catal. A 260 (2004) 111.

[14] V.V. Galvita, G.L. Semin, V.D. Belyaev, T.M. Yurieva, V.A. Sobyanin, Appl. Catal. A 216 (2001) 85.

[15] V.A. Sobyanin, S. Cavallaro, S. Freni, Energy Fuels 14 (2000) 1139.

[16] S.F. Yin, B.Q. Xu, X.P. Zhou, C.T. Au, Appl. Catal. A 277 (2004) 1.

[17] T.V. Choudhary, C. Sivadinarayana, D.W. Goodman, Catal. Lett. 72 (2001) 197.

[18] F. Vitse, M. Cooper, G.G. Botte, J. Power Sources 142 (2005) 18.

[19] C.S. Song, K.M. Reddy, Appl. Catal. A 176 (1999) 1.

[20] K. Klier, Adv. Catal. 31 (1982) 243.

[21] T. Takeguchi, Y. Kani, M. Inoue, K. Eguchi, Catal. Lett. 83 (2002) 49.

[22] J.P. Breen, J.R.H. Ross, Catal. Today 51 (1999) 521.

[23] C.J. Jiang, D.L. Trimm, M.S. Wainwright, N.W. Cant, Appl. Catal. A 97 (1993) 145.

References

[24] B.A. Peppley, J.C. Amphlett, L.M. Kearns, R.F. Mann, Appl. Catal. A 179 (1999) 21.

[25] B.A. Peppley, J.C. Amphlett, L.M. Kearns, R.F. Mann, Appl. Catal. A 179 (1999) 31.

[26] I. Nowak, M. Ziolek, Chem. Rev. 99 (1999) 3603.

[27] M. Ziolek, Catal. Today 78 (2003) 47.

[28] K. Tanabe, Catal. Today 78 (2003) 65.

[29] K. Tanabe, S. Okazaki, Appl. Catal. A 133 (1995) 191.

[30] P. Carniti, A. Gervasini, S. Biella, A. Auroux, Chem. Mater. 17 (2005) 6128.

[31] K. Asakura, Y. Iwasawa, Chem. Lett. (1986) 859.

[32] J.M. Jehng, A.M. Turek, I.E. Wachs, Appl. Catal. A 83 (1992) 179.

[33] A. Florentino, P. Cartraud, P. Magnoux, M. Guisnet, Appl. Catal. A 89 (1992) 143.

[34] T. Ushikubo, T. Iizuka, H. Hattori, K. Tanabe, Catal. Today 16 (1993) 291.

[35] T. Tanaka, H. Nojima, H. Yoshida, H. Nakagawa, T. Funabiki, S. Yoshida, Catal. Today 16 (1993) 297.

[36] J.C. Védrine, G. Coudurier, A. Ouqour, P.G.P. deOliveira, J.C. Volta, Catal. Today 28 (1996) 3.

[37] P. Batamack, R. Vincent, J. Fraissard, Catal. Lett. 36 (1996) 81.

[38] C.L.T. da Silva, V.L.L. Camorim, J.L. Zotin, M. Pereira, A.D. Faro, Catal. Today 57 (2000) 209.

[39] J.-M. Jehng, I.E. Wachs, Chem. Mater. 3 (1991) 100.

[40] J.-M. Jehng, I.E. Wachs, Catal. Today 8 (1990) 37.

[41] K. Tanabe, Mater. Chem. Phys. 17 (1987) 217.

[42] K. Tanabe, Catal. Today 8 (1990) 1.

[43] T. Armaroli, G. Busca, C. Carlini, M. Giuttari, A.M.R. Galletti, G. Sbrana, J. Mole. Catal. A 151 (2000) 233.

[44] S. Satoh, Y. Tanigawa, US Patent 6379507 (2002).

[45] Y.Z. Yuan, H.C. Liu, H. Imoto, T. Shido, Y. Iwasawa, J. Catal. 195 (2000) 51.

[46] Y.Z. Yuan, T. Shido, Y. Iwasawa, Chem. Comm. 15 (2000) 1421.

References

[47] H.C. Liu, N. Bayat, E. Iglesia, Angew. Chem. Int. Ed. 42 (2003) 5072.

[48] H.C. Liu, E. Iglesia, J. Phys. Chem. B 107 (2003) 10840.

[49] J.M. Tatibouet, Appl. Catal. A 148 (1997) 213.

[50] P. Forzatti, E. Tronconi, A.S. Elmi, G. Busca, Appl. Catal. A 157 (1997) 387.

[51] T. Shikada, K. Fujimoto, M. Miyauchi, H. Tominaga, Appl. Catal. 7 (1983) 361.

[52] W.W. Kaeding, S.A. Butter, J. Catal. 61 (1980) 155.

[53] G.Y. Cai, Z.M. Liu, R.M. Shi, C.Q. He, L.X. Yang, C.L. Sun, Y.J. Chang, Appl. Catal. A 125 (1995) 29.

[54] T.H. Fleisch, A. Basu, M.J. Gradassi, J.G. Masin, Natural Gas Conversion Iv, 1997, pp. 117.

[55] J. Sehested, T. Mogelberg, T.J. Wallington, E.W. Kaiser, O.J. Nielsen, J. Phys. Chem. 100 (1996) 17218.

[56] J.C. Woodhouse, US Patent 2014408 (1935).

[57] J.H. Kim, M.J. Park, S.J. Kim, O.S. Joo, K.D. Jung, Appl. Catal. A 264 (2004) 37.

[58] M.T. Xu, J.H. Lunsford, D.W. Goodman, A. Bhattacharyya, Appl. Catal. A 149 (1997) 289.

[59] Y.C. Fu, T. Hong, J.P. Chen, A. Auroux, J.Y. Shen, Thermochim. Acta 434 (2005) 22.

[60] W.K. Bell, C.D. Chang, US Patent 4 423 155 (1983).

[61] T. Takeguchi, K. Yanagisawa, T. Inui, M. Inoue, Appl. Catal. A 192 (2000) 201.

[62] J. Topp-Jorgensen, US Patent 4536485 (1985).

[63] G. Pagani, US Patent 4098809 (1978).

[64] G.C. Chinchen, J.R. Jennings, US Patent 4863894 (1989).

[65] N.K. Mal, M. Fujiwara, Chem. Commun. (2002) 2702.

[66] A. Auroux, Top. Catal. 4 (1997) 71.

Published Results

Publication I

Available online at www.sciencedirect.com
ScienceDirect
Journal of Catalysis 244 (2006) 1–9
JOURNAL OF CATALYSIS
www.elsevier.com/locate/jcat

Surface acidity of niobium phosphate and steam reforming of dimethoxymethane over $CuZnO/Al_2O_3$–NbP complex catalysts

Qing Sun [a,b], Aline Auroux [b], Jianyi Shen [a,b,*]

[a] *Lab of Mesoscopic Chemistry, School of Chemistry and Chemical Engineering, Nanjing University, Nanjing 210093, China*
[b] *Institut de Recherches sur la Catalyse, CNRS, 2 Av. Einstein, 69626 Villeurbanne Cedex, France*

Received 14 May 2006; revised 15 July 2006; accepted 18 July 2006
Available online 25 September 2006

Abstract

Dimethoxymethane (DMM) is nontoxic and of high hydrogen content and may be used as a H_2 storage material for small H_2 sources. Steam reforming of DMM requires a bifunctional catalyst composed of an acidic component and a traditional copper catalyst, on which DMM is hydrolyzed on the acidic sites to methanol and formaldehyde, which are then further reformed to H_2 and CO_2 on metallic copper sites. In this work, samples of niobium phosphate with high surface areas were synthesized, characterized, and tested for the hydrolysis of DMM and used as acidic components for the reforming of DMM to produce H_2. The structure and surface areas of these samples were characterized, and the activity for the hydrolysis of DMM was correlated with the surface acidities. It was found that all of the niobium phosphate samples exhibited high activity for the hydrolysis of DMM. The one with a high surface area (394 m^2/g) was highly acidic with mainly Brønsted acid sites and thus was the most active for the hydrolysis of DMM among the niobium samples studied in this work. Mixing the niobium phosphate with $CuZnO/Al_2O_3$ did not affect the activity of $CuZnO/Al_2O_3$ for the reforming of methanol. The activity and selectivity to H_2 were low for the steam reforming of DMM over traditional $CuZnO/Al_2O_3$ alone. Mechanically mixing niobium phosphate with $CuZnO/Al_2O_3$ greatly enhanced the conversion of DMM (e.g., 100% at 493 K) with high selectivity to H_2. This indicates that niobium phosphate is an effective acidic component for the hydrolysis of DMM and can be used with $CuZnO/Al_2O_3$ for reforming DMM to produce H_2.

Keywords: Niobium phosphate; Hydrolysis of dimethoxymethane; Steam reforming; Hydrogen production; Adsorption microcalorimetry; Surface acidity

1. Introduction

Fuel cell systems have attracted much attention as potential electricity generation devices for household and automotive applications [1–3]. These systems have the advantages of cleanness, high energy density, compactness, and highly efficient energy transformation. Hydrogen is the most promising fuel for such applications. H_2 can be produced by steam reforming of gasoline [4], natural gas, methanol [5–8], dimethyl ether [9–11], and other products, as well as decomposition of ammonia [12–14]. However, the reforming temperatures of natural gas and gasoline are high [15] (above 873 K for natural gas and above 1073 K for gasoline), requiring significant energy input, and the stability of catalysts and refractory reactors is also problematic. Methanol is synthesized from syngas [16], and its reforming is relatively easy at around 523–573 K. The disadvantage of using methanol as an H_2 source is that it is highly toxic. Thus, reforming of dimethyl ether (DME) has been performed to produce H_2 [9–11]. However, reforming of DME might be limited by the low rate of hydrolysis.

In this work, we studied the reforming of dimethoxymethane (DMM) for the production of hydrogen. DMM is nontoxic and environmentally benign. It can be easily stored and handled, because it is a liquid under atmospheric pressure. In addition, steam reforming of DMM can be done at low temperature (below 533 K) [17]. DMM may be synthesized from direct oxidation of methanol. Liu et al. studied the oxidation of methanol to DMM using heteropoly acids [18]. Yuan et al. found that Re/γ-Fe_2O_3 was active for the oxidation of methanol to DMM [19,20]. V_2O_5/TiO_2 catalysts also have been found to be active for this reaction [17].

* Corresponding author. Fax: +86 25 83317761.
E-mail address: jyshen@nju.edu.cn (J. Shen).

0021-9517/$ – see front matter
doi:10.1016/j.jcat.2006.07.027

Steam reforming of DMM involves the hydrolysis of DMM to methanol and formaldehyde, which are further reformed to produce H_2 and CO_2,

$$CH_3OCH_2OCH_3 + H_2O = 2CH_3OH + CH_2O, \quad (1)$$

$$CH_3OH + H_2O = 3H_2 + CO_2, \quad (2)$$

$$CH_2O + H_2O = 2H_2 + CO_2. \quad (3)$$

The overall reaction can then be expressed as

$$CH_3OCH_2OCH_3 + 4H_2O = 8H_2 + 3CO_2. \quad (4)$$

Thus, the catalysts for the reforming of DMM must consist of a solid acid for the hydrolysis of DMM and a component for the reforming of methanol and formaldehyde. The latter is usually $CuZnO/Al_2O_3$ (CuZnAl), which has been studied extensively [5–8]. The acidic component must be chosen carefully; it should effectively catalyze the hydrolysis of DMM, but not affect the performance of $CuZnO/Al_2O_3$ for the reforming reactions.

Niobium oxides and niobium phosphates have strong surface acidity and are used as solid acid catalysts [21–24]. The acidity and reactivity of these systems have been studied by different techniques [25–33]. The preparation, characterization, and application of niobium-containing materials were reviewed by Nowak and Ziolek [21,22]. Tanabe summarized the catalytic applications of niobium compounds [23,24].

Niobium pentoxide (Nb_2O_5) is a white, air-stable, and water-insoluble solid that generally has an octahedrally coordinated NbO_6 distorted to different extent, depending on whether its polyhedra are corner-shared or edge-shared [34,35]. Hydrated niobium oxide ($Nb_2O_5{\cdot}nH_2O$) exhibits strong acidity according to the Hammett titration ($H_0 \leqslant -5.6$). Its acid strength is equivalent to about 70% sulfuric acid [36]. It has both Lewis and Brønsted acid sites [34]. The surface acid sites remain after outgassing at 673 K for 10 h, as determined by ammonia adsorption microcalorimetry [25]. It usually exhibits high activity for the acid-catalyzed reactions in which water molecules participate [36,37].

Niobium phosphate has a similar structure to Nb_2O_5 [21] but with higher acid strength ($H_0 \leqslant -8.2$). It has a distorted octahedra (NbO_6) connected by PO_4 tetrahedra via shared corners [22]. Both terminal POH and NbOH groups are present in bulk and impregnated niobium phosphate catalysts [22]. The POH are stronger Brønsted acids than NbOH in niobium phosphates [38]. The Lewis acid sites in niobium phosphates are coordinatively unsaturated Nb^{5+} cations [38].

Porous niobium oxides and niobium-containing materials can be synthesized by various methods [39–44]. Recently, porous niobium phosphates with high surface areas were prepared and used as solid acid catalysts by Mal and Fujiwara [45].

In this work, we prepared and characterized porous niobium phosphates and compared them with a niobium oxide and a commercial niobium phosphate (supplied by CBMM). The surface acidities of these samples were studied by adsorption microcalorimetry of ammonia, infrared spectroscopy (IR), and isopropanol probe reaction and were correlated with the activities for the hydrolysis of DMM. In addition, these samples were mixed with the traditional $CuZnO/Al_2O_3$ to form complex catalysts for the reforming of DMM to produce H_2.

2. Experimental

2.1. Catalyst preparation

Nb_2O_5 was prepared by calcining a commercial niobic acid ($Nb_2O_5{\cdot}nH_2O$, CBMM, Brazil) at 623 K for 4 h in flowing air. NbP1 is a commercial niobium phosphate provided by the CBMM in Brazil. NbP2 is a niobium phosphate prepared by the impregnation method [38]. In short, 6.35 g of niobic acid was added to 120 ml of aqueous solution of H_3PO_4 (1 M) and stirred for 48 h at room temperature. The slurry was filtered, dried at 373 K overnight, and then calcined at 673 K for 4 h. A high-surface area niobium phosphate (NbP3) was prepared as described previously [45]. Specifically, 2.73 g of $NbCl_5$ (Alfa Aesar, 99%) was partially hydrolyzed in 50 ml of H_2O, followed by the addition of 2.30 g of H_3PO_4 (Aldrich, 85% aqueous solution) to initiate a vigorous hydrolytic reaction. An additional 50 ml of H_2O was then added, and the reaction mixture was stirred for 30 min. The pH of the reaction mixture was adjusted to 2.60 by ammonia solution. After stirring, the slurry was filtered and washed with deionized water to obtain a chlorine-free gel. The gel was mixed with 10 ml of H_2O and 1.45 g of hexadecylamine (Aldrich, 90%) and stirred for 30 min. Then 0.92 g H_3PO_4 (85%) was added, and the pH of the mixture was adjusted to 3.88. After mixing was complete, the slurry was heated in a Teflon-lined stainless steel autoclave at 338 K under autogenous pressure for 2 days. The final product was filtered, washed with deionized water, dried at 373 K overnight, and calcined at 723 K in air for 40 h. $CuZnO/Al_2O_3$ is a commercial catalyst (CF105, a product of the Research Institute of Nanjing Chemical Industry Group, China) with a molar ratio of 63% Cu, 21% Zn, and 16% Al.

2.2. Catalyst characterization

The X-ray diffraction (XRD) measurements were done using a Bruker D5005 diffractometer scanning from 3° to 80° (2θ) at a rate of 0.02 degree s^{-1} and from 1° to 10° (2θ) at a rate of 0.002 degree s^{-1} using a Cu$K\alpha$ radiation ($\lambda = 0.15418$ nm) source. The applied voltage and current were 50 kV and 35 mA, respectively. Elemental analysis was performed by ICP atomic emission spectroscopy (Spectroflame-ICP D, Spectro). The surface area and pore size were measured by nitrogen adsorption at 77 K after heat pretreatment under vacuum at 623 K for 4 h. Transmission electron microscopy (TEM) was done using a JEM 2010 operating at 200 kV in bright- and dark-field modes. The X-ray photoelectron spectra (XPS) were measured on a SSI 301 instrument equipped with a hemispherical electron analyzer and an Al anode (Al$K\alpha = 1486.6$ eV) powered at 100 W. The residual pressure in the spectrometer chamber during data acquisition was 5×10^{-8} Pa.

The microcalorimetric studies of ammonia adsorption were performed at 423 K in a heat flow calorimeter (Setaram C80) linked to a conventional volumetric apparatus equipped with

a Barocel capacitance manometer for pressure measurements. Ammonia used for measurements (purity >99.9%) was purified by successive freeze–pump–thaw cycles. About 100 mg of sample was pretreated in a quartz cell under evacuation overnight at 623 K. The differential heat of adsorption was measured as a function of coverage by repeatedly introducing small doses of ammonia gas onto the catalyst until an equilibrium pressure of about 66 Pa was reached [46]. The sample was then outgassed for 30 min at the same temperature, and a second adsorption was performed at 423 K until an equilibrium pressure of about 27 Pa was attained, to calculate the irreversibly chemisorbed amount of ammonia at this pressure, which gives an estimation of number of strong acid sites.

Temperature-programmed ammonia desorption was performed on a Setaram TG-DSC 111 device coupled with a mass spectrometer (Thermostar, Pfeifer) as a detector. A capillary-coupling system was used. The TPD experiments were carried out in a flow with helium as the carrier gas (10 ml min^{-1}). For each experiment, about 30 mg of a sample with ammonia absorbed in previous microcalorimetric experiments was used. Initially, the samples were purged with He at 373 K for 30 min to remove most of absorbed water and heated at 5 K min^{-1} in He up to 873 K. During this temperature increase, the mass spectrometer was set at $m/e = 15$, to avoid the interference of water fragmentation masses.

The NH_3 adsorption IR spectra were recorded with a Bruker Vector 22 FTIR spectrophotometer (DTGS detector) with a range of 4000–400, a resolution of 2 cm^{-1}, and 50 acquisition scans. The self-supporting wafer (10–30 mg, 18 mm diameter) was activated in situ in the IR cell at 673 K in flowing O_2 for 12 h, evacuated at the same temperature for 2 h, and then exposed to NH_3 (purity >99.9%) at room temperature for 5 min. Desorption was carried out by evacuation for 30 min at room temperature, 323, 373, 473, 523, 573, and 673 K. A spectrum was recorded at room temperature after desorption at each temperature.

2.3. Catalytic reaction

An isopropanol probe reaction carried out in a fixed-bed glass tube reactor was used to characterize the surface acidity. About 100 mg of sample was loaded for the reaction. Isopropanol was introduced to the catalysts by bubbling N_2 (99.999%) or air through a glass saturator filled with isopropanol maintained at 295 K. Isopropanol and reaction products were analyzed by an on-line gas chromatograph, using a PEG 20M packed column connected to a flame ionization detector (FID). Each catalyst was pretreated by heating in N_2 or air at 673 K for 1 h and then cooled in the same flow to the reaction temperature.

The hydrolysis of DMM was performed in a glass fixed-bed microreactor with an inner diameter of 6 mm. The DMM and H_2O were introduced to the reaction zone by bubbling N_2 (99.999%) through a glass saturator filled with DMM (Aldrich, 99%) maintained at 273 K and a glass saturator filled with H_2O maintained at 333 K. In each test, 50 mg of catalyst was loaded, and a gas hourly space velocity (GHSV) of 90,000 ml g^{-1} h^{-1} was used. The feed composition was maintained at N_2:H_2O:DMM = 24:5:1 (v/v). The tail gas out of the reactor was analyzed by an on-line gas chromatograph equipped with an FID and a Porapak N column for the separation of methanol, DMM, and other organic compounds. The gas lines were kept at 373 K to prevent condensation of the reactant and products. The reaction was carried out at atmospheric pressure.

The steam reforming of methanol (or DMM) was carried out in a same way as the hydrolysis of DMM. An acidic component was mixed with $CuZnO/Al_2O_3$ in a weight ratio of 1/7. About 500 mg of catalyst was loaded, and the GHSV was 10,000 ml g^{-1} h^{-1} for methanol and 4550 ml g^{-1} h^{-1} for DMM. The feed composition was maintained at N_2:H_2O:methanol = 8.8:1.25:1 or N_2:H_2O:DMM = 24:5:1 (v/v). The products were analyzed by an on-line gas chromatograph equipped with an FID and a thermal conductivity detector (TCD). The FID was connected to a Porapak N column for the separation of methanol, DMM, and other organic compounds, whereas the TCD was connected to a TDX-01 column for the analysis of methane, CO_x, and N_2. The amount of H_2 produced was usually calculated according to the conversion of DMM and the composition of other products and was checked using another gas chromatograph.

3. Results and discussion

3.1. Structural characterizations

The XRD results shown in Fig. 1 indicated that the Nb_2O_5 and niobium phosphate samples studied in this work were amorphous. They exhibited mainly two broad 2θ peaks at around 25° and 52°. The peaks were shifted to lower angles for the sample NbP3, implying some difference in bonding in this high-surface area sample.

Results of bulk and surface elemental analysis, as well as the surface area and porosity data for the samples, are given in Table 1. The NbP3 prepared using a template had a significantly greater surface area (394 m^2 g^{-1}) than the other samples. In addition, chemical analysis showed that this sample had a much higher P content (12.4 wt%), which is close to the Nb/P atomic ratio of 1/1, than the other niobium phosphate samples. XPS results indicated that P might be slightly enriched on the surface of these niobium phosphate samples.

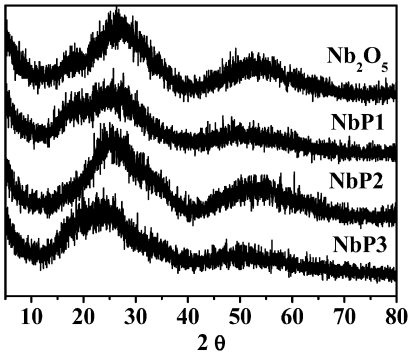

Fig. 1. X-ray diffraction (XRD) patterns of Nb_2O_5 and niobium phosphate catalysts.

Table 1
Chemical analysis, X-ray photoelectron spectroscopic data, BET surface area, and average pore radius of the samples

Sample	C.A. (wt%)		XPS (AT%)		BET ($m^2\ g^{-1}$)	Average pore radius (nm)
	Nb	P	Nb	P		
Nb_2O_5	69.2	–	–	–	110	Not determined
NbP1	46.6	5.0	13.4	8.9	142	3.0
NbP2	46.7	4.0	18.7	5.6	81	Not determined
NbP3	42.6	12.4	12.1	12.7	394	<1.5

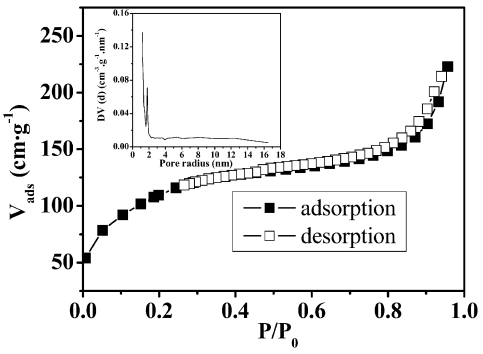

Fig. 2. N_2 adsorption–desorption isotherms of NbP3. (Inset: Pore radius distribution curve from the desorption branch of the isotherm.)

The N_2 adsorption–desorption isotherms and pore size distribution for NbP3 are depicted in Fig. 2. The adsorption–desorption isotherms are similar to type II and show no significant hysteresis loop, explaining the "supermicroporous" nature of the sample as suggested by Blanchard et al. [47]. The results agree well with those reported by Mal and Fujiwara [45]. The pore radius thus measured for NbP3 was <1.5 nm, which is lower than that of NbP1 (3 nm), a niobium phosphate provided by CBMM. The small-angle XRD showed the two diffraction peaks at $2\theta = 1.9$ and 4.2 for the NbP3 before calcination, corresponding to (100) and (110) reflections [45] and indicating the ordered structure of NbP3.

The TEM images of Nb_2O_5 and NbP3 are shown in Fig. 3. Both samples exhibit pore structures with diameters of 1–5 nm.

Temperature-programmed reduction experiments revealed no significant hydrogen consumption peaks for the Nb_2O_5 and niobium phosphates up to 1100 K, indicating that reduction of these samples was difficult [22].

The skeletal IR spectra are reported in Fig. 4. All of the samples exhibited a band around 1628 cm^{-1}, due to the scissoring mode of adsorbed molecular water. A sharp band at around 1385 cm^{-1} for NbP1, probably due to the O–C–O symmetric vibration of impurities of potassium carbonate in NbP1 (a commercial product), can be seen. This peak was also observed for the other three samples, although its intensity was weak. Chemical analysis showed that the niobic acid from CBMM contained a small amount of K (0.1%). Thus, the samples prepared using the niobic acid may contain K_2CO_3 formed during the preparation stage. In addition, all of the samples exhibited a broad band at around 600 cm^{-1}, probably due to the Nb–O–Nb stretching mode related to the slightly disordered octahedral NbO_6. A broad band around 1000 cm^{-1} was observed for Nb_2O_5 and NbP2, which could be assigned to the stretching

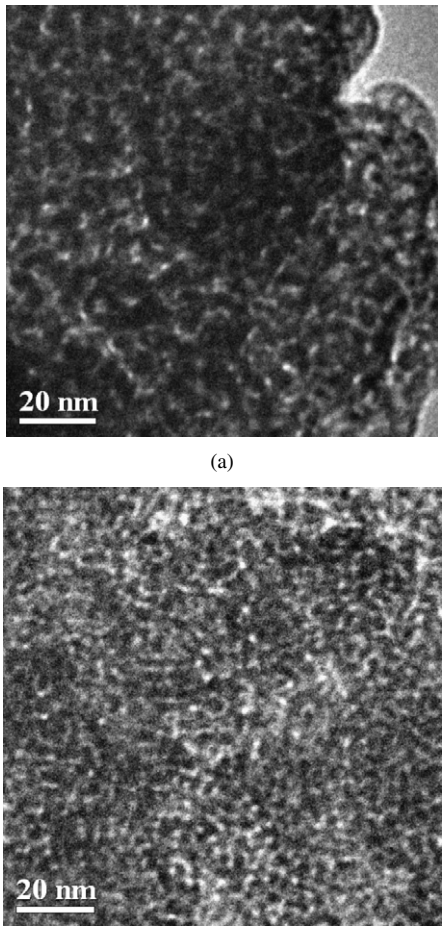

(a)

(b)

Fig. 3. Transmission electron microscopy (TEM) images of (a) Nb_2O_5 and (b) NbP3.

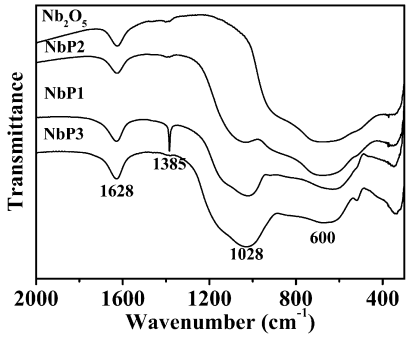

Fig. 4. FTIR skeletal spectra (KBr pressed disks with 2 mg sample in 198 mg KBr) of Nb_2O_5 and NbP catalysts.

mode of the short Nb=O bond in a highly disordered octahedral NbO_6. The different extent of NbO_6 disordering may suggest the stability of NbO_6 on the addition of P [21,22]. Furthermore, the addition of P to Nb_2O_5 also resulted in an additional broad band located at around 1028 cm^{-1}, possibly due to the O=P=O asymmetric stretching mode of phosphate or polyphosphate species. The intensity of this band increased with increasing P content in NbP. These results agree well with those reported by Armaroli et al. [38].

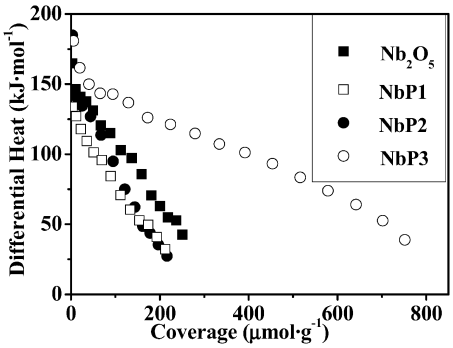

Fig. 5. Differential heat versus coverage (in μmol g^{-1}) for ammonia adsorption at 423 K over Nb_2O_5 and niobium phosphate catalysts.

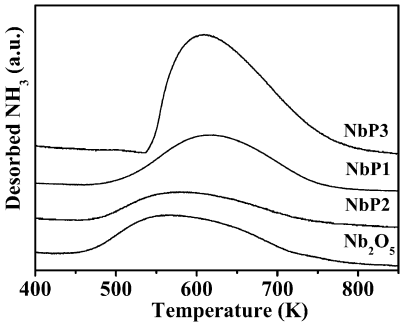

Fig. 6. Temperature-programmed desorption (TPD) profiles of adsorbed NH_3 on Nb_2O_5 and niobium phosphate catalysts.

3.2. Surface acidity

Surface acidity, in terms of number of acid sites and site strengths, was titrated by adsorption microcalorimetry of ammonia; the results are presented in Fig. 5. The initial heat for ammonia adsorption on Nb_2O_5 was found to be about 165 kJ mol^{-1}, which is higher than that of acidic solids such as γ-Al_2O_3. In fact, Nb_2O_5 is considered a strong acid according to Hammett titration [36]. The two niobium phosphate samples, NbP1 and NbP2, behaved similarly to Nb_2O_5 in terms of the heat versus coverage curves for ammonia adsorption, indicating that the addition of P to Nb_2O_5 did not seem to enhance surface acidity. However, the saturation coverage of ammonia on NbP3 was found to be about 750 μmol g^{-1}, much higher than that for the other samples in this work. This is apparently due to the much higher surface area of NbP3 as compared with the other samples. In fact, when the surface coverage was expressed in terms of the amount of ammonia adsorbed on a unit surface area, the coverage on NbP3 was lower than that on other samples.

Fig. 6 shows the NH_3-TPD results for the Nb_2O_5 and niobium phosphate samples. All of the samples exhibited a desorption peak so broad as to reveal the heterogeneous strength distribution of the acid sites in these samples. It is usually not accurate to rank the acid strengths by simply comparing the desorption maxima because of the complex diffusion effect, especially for the porous materials. However, the temperatures of the peak maxima were higher for the niobium phosphate samples than for Nb_2O_5, implying the stronger acidity of niobium phosphate compared with Nb_2O_5. In addition, the areas of desorption peaks reflected the relative populations of acid sites. It is clearly shown that the NbP3 had many more acid sites than the other samples, agreeing well with the microcalorimetric adsorption results.

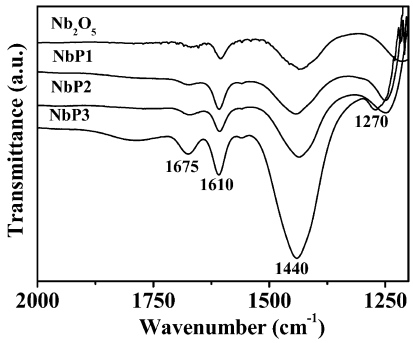

Fig. 7. FTIR spectra for NH_3 adsorption and desorption at room temperature on Nb_2O_5 and niobium phosphate catalysts.

Table 2
Results of isopropanol probe reaction in N_2 at 413 K

Sample	Conversion (%)	Selectivity (%)		
		PPE	DIPE	ACE
Nb_2O_5	0.3	81.0	19.0	0
NbP1	1.0	74.5	25.5	0
NbP2	2.0	74.8	25.2	0
NbP3	15.2	78.3	21.7	0

Note. PPE, DIPE, and ACE denote propylene, diisopropyl ether, and acetone, respectively.

Fig. 7 shows the FTIR spectra of the samples for ammonia adsorption. Both Brønsted and Lewis acid sites were present on the samples. The bands at around 1675 and 1440 cm^{-1} were due to the deformation vibration of NH_4^+ formed by the interaction of NH_3 with Brønsted acid sites, whereas the bands at 1610 and 1270 cm^{-1} originated from the asymmetric and symmetric deformation vibrations, respectively, for NH_3 coordinated to Nb^{5+}. IR spectra from adsorbed pyridine [48] and acetonitrile [38] also revealed the presence of both Brønsted and Lewis acidity on niobium phosphates. It should be mentioned that the NbP3 sample seemed to exhibit more Brønsted acid sites than the other samples according to the relative intensities of the peak at around 1440 cm^{-1}. On evacuation at 473 K, all of the IR peaks for adsorbed ammonia disappeared for the Nb_2O_5, NbP1, and NbP2 samples, whereas these peaks remained for the NbP3 sample (data not shown). These results indicate that the NbP3 sample exhibited the strongest surface acidity of all the samples studied in this work.

3.3. Isopropanol probe reaction

The results of isopropanol (IPA) probe reaction over the samples in flowing N_2 are presented in Table 2 and Fig. 8. It is well known that IPA undergoes dehydration reactions to produce propylene (PPE) and diisopropyl ether (DIPE) on acid sites, and undergoes a dehydrogenation reaction to acetone (ACE) on base sites in inert atmosphere [49,50]. Thus, the con-

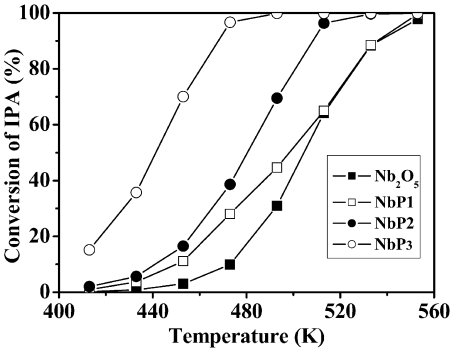

Fig. 8. Conversion of isopropanol (IPA) in N_2 at different temperatures over Nb_2O_5 and niobium phosphate catalysts.

version of IPA and selectivity to PPE, DIPE, and ACE in N_2 can be used to probe the strengths of surface acidity and basicity. In addition, IPA can also be oxidatively dehydrogenated to ACE in an oxidation atmosphere, which can be used to probe the surface redox properties.

Results in Table 2 show that the Nb_2O_5 and niobium phosphates exhibited only surface acidity, because only the products PPE and DIPE were formed. The conversion of IPA was significantly higher on the niobium phosphate samples than on Nb_2O_5, indicating that niobium phosphates are more acidic than Nb_2O_5. In addition, NbP3 exhibited much higher IPA conversion than the other niobium phosphates. Fig. 8 compares the conversion of IPA at different temperatures over the Nb_2O_5 and niobium phosphates. The results clearly show that NbP3 was much more active than the other samples over the whole range of reaction temperatures. Below 500 K, NbP1 and NbP2 were also more active than Nb_2O_5. Further data showed that IPA probe reaction over Nb_2O_5 and niobium phosphates in both N_2 and air did not produce any ACE, indicating that these samples were neither basic nor oxidative under the reaction conditions. The conversions of IPA and selectivity were similar for the reaction performed in N_2 and air. These results are not completely consistent with those of microcalorimetric adsorption of ammonia presented above; the inconsistency may be due to the different treatments in the experiments for microcalorimetric adsorption and the probe reaction. The evacuation treatment for the microcalorimetric adsorption may have removed more hydroxyl groups on the surface of the samples, decreasing the surface acidity. On the other hand, the IPA dehydration reaction produced water and hydrolyzed the surface of the samples, possibly enhancing the surface acidity of the samples.

3.4. Hydrolysis of DMM

DMM is hydrolyzed to methanol (MeOH) and formaldehyde (FA) according to Eq. (1). Table 3 gives the results for the hydrolysis of DMM over the Nb_2O_5 and niobium phosphate catalysts. MeOH and FA were the main products, with selectivity >96%. Other products were DME and methyl formate (MF), with total selectivity <4%. The conversion of DMM increased with increasing temperature for all of the samples. At lower temperatures, the conversion of DMM was higher over the catalysts with higher surface acidity as probed by the IPA reaction. At temperatures above 493 K, the conversion of DMM approached 100% over all of the samples. Our previous studies revealed that at 493 K, DMM was converted mainly to MeOH and FA, with low conversion (<10%) on γ-Al_2O_3, whereas >75% of DMM was converted to DME over H-ZSM-5 even though the conversion was high (99%) [17]. Thus, the Nb_2O_5 and niobium phosphate catalysts seemed to be active and suitable for the hydrolysis of DMM and may be used as acidic components with the traditional CuZnAl catalyst for the reforming of DMM to produce H_2. DMM itself did not hydrolyze without a catalyst at temperatures as high as 533 K.

Table 3
Conversion and selectivity for the hydrolysis of DMM over the Nb_2O_5 and NbP catalysts

Sample	Temperature (K)	Conversion (%)	Selectivity (%)		
			DME	MF	MeOH and FA
Nb_2O_5	413	49	0.8	3	97
	433	63	0.6	4	96
	453	77	0.4	3	97
	473	86	0.3	3	97
	493	94	0.5	3	97
	513	98	0.4	2	98
	533	100	0.4	2	98
NbP1	413	70	0.7	1	98
	433	82	0.7	3	96
	453	87	0.5	2	97
	473	93	0.6	2	97
	493	97	0.6	3	97
	513	99	0.5	3	97
	533	100	0.5	1	98
NbP2	413	72	1	0.0	99
	433	80	0.9	0.2	99
	453	87	1	0.2	99
	473	92	0.5	0.2	99
	493	98	1	0.2	99
	513	99	0.8	0.2	99
	533	100	0.6	0.2	99
NbP3	413	78	1	0.0	99
	433	87	0.6	0.4	99
	453	93	0.8	1	98
	473	95	0.8	0.4	99
	493	99	1	0.4	99
	513	99	1	0.2	99
	533	100	0.9	0.1	99

Note. DME, MF, MeOH, and FA denote dimethyl ether, methyl formate, methanol, and formaldehyde, respectively. Reaction conditions: $N_2/H_2O/DMM = 24/5/1$ (v/v), GHSV = 90,000 ml g^{-1} h^{-1}.

3.5. Reforming of methanol

Traditional CuZnAl catalyst is usually used for the reforming of methanol to produce H_2 [5–8]. The catalyst has been characterized in detail and used for the reforming of methanol by Murcia-Mascaros et al. [51] and Turco et al. [52]. In the present work, we examined the effect of adding Nb_2O_5 and NbP3 on the reforming of methanol over CuZnAl. The results, given in Fig. 9, clearly show that the addition of Nb_2O_5 or NbP3 did not affect the conversion of methanol on CuZnAl at 453–

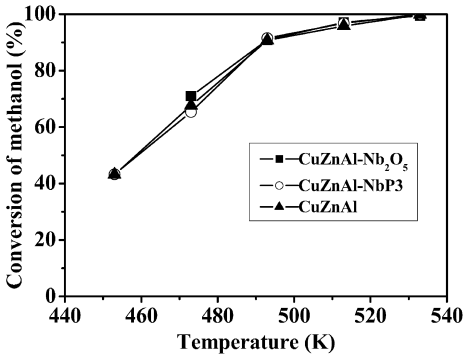

Fig. 9. Reforming of methanol over CuZnAl–Nb_2O_5 and CuZnAl–NbP catalysts.

533 K. In addition, no DME or other organic compounds were observed for the reforming of methanol on these catalysts. The only products detected were CO_x and H_2. Thus, both Nb_2O_5 and NbP seem to be suitable hydrolysis components for the reforming of DMM.

3.6. Reforming of DMM

We mixed an industrial CuZnAl catalyst with our Nb_2O_5 and NbP3 to form the complex catalysts for the reforming of DMM. The weight ratio of CuZnAl to acid component was 7/1, and a complex catalyst contained only 12.5% of the acidic component. This is because the hydrolysis of DMM on the acidic components was rapid, as discussed above. A GHSV of 4550 ml g^{-1} h^{-1} was used for the complex catalysts, corresponding to the GHSV of 36,400 ml g^{-1} h^{-1} on the acid component, which was lower than that for the hydrolysis of DMM (90,000 ml g^{-1} h^{-1}) used above. Thus, the rate of DMM reforming on the complex catalysts should be limited mainly by the methanol reforming on the CuZnAl component.

Table 4 shows that the CuZnAl catalyst exhibited low conversion for the reforming of DMM and produced a substantial amount of DME. Addition of either a niobium oxide or NbP3 component greatly enhanced the conversion of DMM and inhibited the formation of DME. For example, almost no DMM conversion was observed on the CuZnAl at 453 K, whereas the DMM conversion was 94% at this temperature with the addition of Nb_2O_5. The conversion of DMM reached 100% on the CuZnAl–NbP3 at 453 K. These results clearly demonstrate that the acidic component is essential for the reforming of DMM. Below 493 K, methanol was detected in the products for the reforming of DMM on CuZnAl–Nb_2O_5 or CuZnAl–NbP3, revealing that the rate of DMM hydrolysis was faster than that of methanol reforming. Thus, the reforming of methanol appears to be the rate-determining step for the reforming of DMM below 493 K. Above 493 K, the rate of reforming of methanol on CuZnAl was sufficiently fast so that no methanol was detected. The rate of hydrogen production was also significantly improved by the addition of an acidic niobium component. The highest rate of H_2 production obtained in this work for the reforming of DMM was 1185 ml g^{-1} h^{-1} at 493 K, which was lower than 2438 ml g^{-1} h^{-1} for the reforming of methanol at the same temperature. This does not mean that the rate of H_2 production from the reforming of DMM is always lower than that from the reforming of methanol. The rate of H_2 production depends on the activity of catalysts and the space velocity of feed gas. A thorough comparison between the reforming of DMM and that of methanol for the production of H_2 requires data for the complete conversion of DMM and methanol at the maximum space velocities. The rate of H_2 production from the reforming of DMM over the CuZnAl–H-CNF (where H-CNF denotes acidic carbon nanofiber) was found to be about 80% of that from the reforming of methanol on the CuZnAl [17].

3.7. CO concentration and the water–gas shift reaction

CO concentration is a critical issue for fuel cell applications, because one of the most promising types of fuel cells, the

Table 4
Conversion and selectivity for the steam reforming of DMM over the CuZnAl and hybrid catalysts (CuZnAl/acid component = 7/1 wt)

Sample	Temperature (K)	Conversion (%)	Selectivity (%)					R_{H_2} (ml g^{-1} h^{-1})
			CH_4	DME	MeOH	CO	CO_2	
CuZnAl–Nb_2O_5	453	94	0	0	61	0	39	620
	473	100	0	0	9	1	90	1116
	493	100	0	0	0	3	97	1174
	513	100	0	0	0	5	95	1156
	533	100	0	0	0	6	94	1141
CuZnAl–NbP3	453	100	0	0.1	45	0	55	803
	473	100	0	0.1	3	2	95	1163
	493	100	0	0.1	0	2	98	1185
	513	100	0	0.1	0	4	96	1159
	533	100	0	0.1	0	6	94	1146
CuZnAl	453	1.5	1	19	8	0	72	14
	473	4.7	1	16	7	0	76	47
	493	11	1	21	6	0	72	106
	513	31	0.4	13	1	0.9	84	330
	533	47	1	22	1	2	75	458

Note. DME, MeOH, and R_{H_2} denote dimethyl ether, methanol, and rate of hydrogen production, respectively. Reforming conditions: $N_2/H_2O/DMM = 24/5/1$ (v/v), GHSV = 4550 ml g^{-1} h^{-1}.

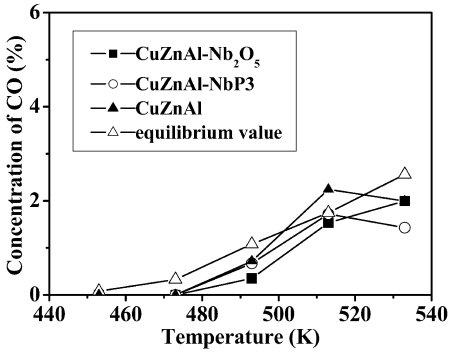

Fig. 10. Concentration of CO in products over CuZnAl–Nb_2O_5 and CuZnAl–NbP3 catalysts for the reforming of methanol.

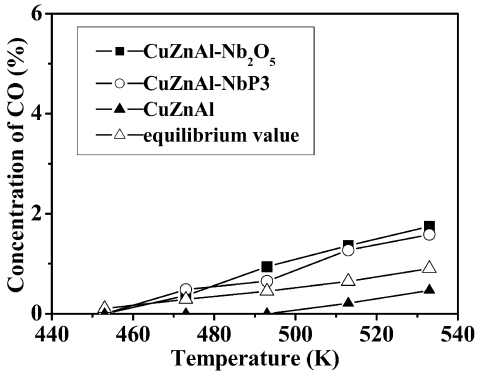

Fig. 11. Concentration of CO in products over CuZnAl–Nb_2O_5 and CuZnAl–NbP3 catalysts for the reforming of DMM.

proton-exchange-membrane fuel cell (PEMFC), is extremely susceptible to poisoning by CO in the anode feed gas. CO concentrations <10 ppm are desirable in a fuel for a PEMFC. Figs. 10 and 11 show that the selectivity to CO increased with increasing of temperature for the reforming of both methanol and DMM, possibly due to the reversed water gas shift reaction (RWGSR: $CO_2 + H_2 = CO + H_2O$) shift to the right with increasing temperature. In fact, the concentration of CO in the tail gas from the reforming of methanol or DMM is close to the equilibrium value, and the maximum CO concentration is <2%. It seemed that the addition of niobium component did not affect the equilibrium of the RWGSR over CuZnAl. The concentration of CO in the tail gas is known to depend on the concentration of H_2O in the feed gas for the reforming of methanol. When the concentration of H_2O is insufficient in the feed gas, methanol directly decomposes to CO and H_2 on CuZnAl, and the rate of such decomposition is much slower than that of the reforming of methanol [53]. On the other hand, excessive H_2O would entail excessive energy costs. This situation also holds for the reforming of DMM, because it involves the hydrolysis of DMM and the reforming of methanol. The ratios of H_2O/methanol and H_2O/DMM applied in this work were 2 and 5, respectively, slightly higher than the respective stoichiometric ratios (1 and 4), to minimize the CO concentrations without entailing an excessive energy cost.

4. Conclusion

Niobium phosphates were prepared by different methods in which porous NbOPO4 with high surface area (394 $m^2\,g^{-1}$) was obtained using hexadecylamine as a template. The Nb_2O_5 and niobium phosphate samples studied in this work had similar amorphous structures. The niobium phosphates were found to be more acidic than Nb_2O_5, especially that with a high surface area. Both Brønsted and Lewis acid sites were present on the surface of Nb_2O_5 and niobium phosphates, with niobium phosphates having more Brønsted sites than Nb_2O_5. The high-surface area niobium phosphate exhibited numerous surface acid sites (~750 μmol g^{-1}) and was active in catalyzing the dehydration of isopropanol and the hydrolysis of DMM. The complex catalysts resulting from combining Nb_2O_5 or niobium phosphate with an industrial $CuZnO/Al_2O_3$ were effective for the reforming of DMM to produce H_2 at above 493 K. DMM could be completely reformed into CO_x and H_2 over the complex catalysts at 493 K. Because DMM is more environmentally benign than methanol, our findings indicate that it is possible to reform DMM directly using a proper acidic component with the traditional $CuZnO/Al_2O_3$ catalyst.

Acknowledgments

The authors acknowledge financial support from CNRS-France, the French Ministry of Education, the French–Chinese joint program PRA E 03-01, and the Ministry of Science and Technology of China (Grants 2004DFB02900 and 2005 CB221400).

References

[1] P.G. Gray, M.I. Petch, Platinum Metals Rev. 44 (2000) 108.
[2] S. Golunski, Platinum Metals Rev. 42 (1998) 2.
[3] N. Edwards, S.R. Ellis, J.C. Frost, S.E. Golunski, A.N.J. van Keulen, N.G. Lindewald, J.G. Reinkingh, J. Power Sources 71 (1998) 123.
[4] A.D. Qi, S.D. Wang, G.Z. Fu, C.J. Ni, D.Y. Wu, Appl. Catal. A 281 (2005) 233.
[5] J.C. Amphlett, M.J. Evans, R.A. Jones, R.F. Mann, R.D. Weir, Can. J. Chem. Eng. 59 (1981) 720.
[6] B. Emonts, J.B. Hansen, S.L. Jorgensen, B. Hohlein, R. Peters, J. Power Sources 71 (1998) 288.
[7] T. Takeguchi, Y. Kani, M. Inoue, K. Eguchi, Catal. Lett. 83 (2002) 49.
[8] J.-P. Shen, C.S. Song, Catal. Today 77 (2002) 89.
[9] K. Takeishi, H. Suzuki, Appl. Catal. A 260 (2004) 111.
[10] V.V. Galvita, G.L. Semin, V.D. Belyaev, T.M. Yurieva, V.A. Sobyanin, Appl. Catal. A 216 (2001) 85.
[11] V.A. Sobyanin, S. Cavallaro, S. Freni, Energy Fuels 14 (2000) 1139.
[12] S.F. Yin, B.Q. Xu, X.P. Zhou, C.T. Au, Appl. Catal. A 277 (2004) 1.
[13] T.V. Choudhary, C. Sivadinarayana, D.W. Goodman, Catal. Lett. 72 (2001) 197.
[14] F. Vitse, M. Cooper, G.G. Botte, J. Power Sources 142 (2005) 18.
[15] C.S. Song, K.M. Reddy, Appl. Catal. A 176 (1999) 1.
[16] K. Klier, Adv. Catal. 31 (1982) 243.
[17] Y.C. Fu, Studies of Some Catalytic Reactions for the Synthesis and Conversion of Methanol-Derived Chemicals, Ph.D. thesis, Nanjing University, 2005.
[18] H.C. Liu, N. Bayat, E. Iglesia, Angew. Chem. Int. Ed. 42 (2003) 5072.
[19] Y.Z. Yuan, H.C. Liu, H. Imoto, T. Shido, Y. Iwasawa, J. Catal. 195 (2000) 51.
[20] Y.Z. Yuan, T. Shido, Y. Iwasawa, Chem. Commun. 15 (2000) 1421.

[21] I. Nowak, M. Ziolek, Chem. Rev. 99 (1999) 3603.
[22] M. Ziolek, Catal. Today 78 (2003) 47.
[23] K. Tanabe, S. Okazaki, Appl. Catal. A 133 (1995) 191.
[24] K. Tanabe, Catal. Today 78 (2003) 65.
[25] P. Carniti, A. Gervasini, S. Biella, A. Auroux, Chem. Mater. 17 (2005) 6128.
[26] K. Asakura, Y. Iwasawa, Chem. Lett. (1986) 859.
[27] J.M. Jehng, A.M. Turek, I.E. Wachs, Appl. Catal. A 83 (1992) 179.
[28] A. Florentino, P. Cartraud, P. Magnoux, M. Guisnet, Appl. Catal. A 89 (1992) 143.
[29] T. Ushikubo, T. Iizuka, H. Hattori, K. Tanabe, Catal. Today 16 (1993) 291.
[30] T. Tanaka, H. Nojima, H. Yoshida, H. Nakagawa, T. Funabiki, S. Yoshida, Catal. Today 16 (1993) 297.
[31] J.C. Vedrine, G. Coudurier, A. Ouqour, P.G.P. de Oliveira, J.C. Volta, Catal. Today 28 (1996) 3.
[32] P. Batamack, R. Vincent, J. Fraissard, Catal. Lett. 36 (1996) 81.
[33] C.L.T. da Silva, V.L.L. Camorim, J.L. Zotin, M. Pereira, A.D. Faro, Catal. Today 57 (2000) 209.
[34] J.-M. Jehng, I.E. Wachs, Catal. Today 8 (1990) 37.
[35] J.-M. Jehng, I.E. Wachs, Chem. Mater. 3 (1991) 100.
[36] K. Tanabe, Mater. Chem. Phys. 17 (1987) 217.
[37] K. Tanabe, Catal. Today 8 (1990) 1.
[38] T. Armaroli, G. Busca, C. Carlini, M. Giuttari, A.M.R. Galletti, G. Sbrana, J. Mol. Catal. A 151 (2000) 233.
[39] D.M. Antonelli, J.Y. Ying, Angew. Chem. Int. Ed. Engl. 35 (1996) 426.
[40] M. Ziolek, I. Nowak, J.C. Lavalley, Catal. Lett. 45 (1997) 259.
[41] R. Abe, K. Shinohara, A. Tanaka, M. Hara, J.N. Kondo, K. Domen, J. Mater. Res. 13 (1998) 861.
[42] D.M. Antonelli, Micropor. Mesopor. Mater. 33 (1999) 209.
[43] B. Lee, D.L. Lu, J.N. Kondo, K. Domen, J. Am. Chem. Soc. 124 (2002) 11256.
[44] S. Murray, M. Trudeau, D.M. Antonelli, Adv. Mater. 12 (2000) 1339.
[45] N.K. Mal, M. Fujiwara, Chem. Commun. (2002) 2702.
[46] A. Auroux, Top. Catal. 4 (1997) 71.
[47] J. Blanchard, F. Schuth, P. Trens, M. Hudson, Micropor. Mesopor. Mater. 39 (2000) 163.
[48] S. Okazaki, N. Wada, Catal. Today 16 (1993) 349.
[49] A. Gervasini, J. Fenyvesi, A. Auroux, Catal. Lett. 43 (1997) 219.
[50] X.D. Gu, C. Hui, J.Y. Shen, Chin. J. Catal. 24 (2003) 885.
[51] S. Murcia-Mascaros, R.M. Navarro, L. Gomez-Sainero, U. Costantino, M. Nocchetti, J.L.G. Fierro, J. Catal. 198 (2001) 338.
[52] M. Turco, G. Bagnasco, U. Costantino, F. Marmottini, T. Montanari, G. Ramis, G. Busca, J. Catal. 228 (2004) 43.
[53] B.A. Peppley, J.C. Amphlett, L.M. Kearns, R.F. Mann, Appl. Catal. A 179 (1999) 21.

Publication II

Hydrogen production from steam reforming of dimethoxymethane over $CuZnO/Al_2O_3$-niobium phosphate hybrid catalysts

Qing Sun[a, b], Jianyi Shen[a, b] and Aline Auroux[b]

[a] *Department of Chemistry, Nanjing University, Nanjing 210093, China*
[b] *Institut de Recherches sur la Catalyse, CNRS, 2 Av. Einstein, 69626 Villeurbanne Cedex, France, aline.auroux@catalyse.cnrs.fr*

ABSTRACT:

The high hydrogen content of dimethoxymethane (DMM) and nontoxicity make it suitable as a resource for hydrogen production used for applications like mobile systems. In this work, samples of niobium phosphate with high surface areas were synthesized, characterized and tested for the hydrolysis of DMM and were used as acidic components for the reforming of DMM to produce H_2. Ammonia adsorption microcalorimetry and isopropanol conversion results showed the high acidity of niobium phosphate with high surface area (394 m^2/g). When this sample was mixed mechanically with $CuZnO/Al_2O_3$, the conversion of DMM was greatly enhanced comparing with using $CuZnO/Al_2O_3$ alone. At 533 K, almost 100% theoretical yield to H_2 was achieved and the corresponding hydrogen production rate was found to be 1100 $ml.g^{-1}.h^{-1}$.

KEYWORDS: *hydrogen production; steam reforming of dimethoxymethane; niobium phosphate; surface acidity; adsorption microcalorimetry*

1. Introduction

In recent years increasing attention has been focused on the fuel cell systems, which are regarded as potential electricity generation devices for many applications.[1,2] Hydrogen is the most suitable fuel for fuel cells. H_2 can be produced by lots of ways.[3-7] In this work, we studied production of H_2 by the reforming of dimethoxymethane (DMM). DMM is not only nontoxic and environmentally benign, but also can be easily stored and handled since it is a liquid under atmospheric pressure. In addition, DMM can be reformed at low temperature (below 533 K)[8] and it might be synthesized from direct oxidation of methanol.[8-10]

In the reaction of DMM steam reforming, DMM is hydrolyzed to methanol and formaldehyde, which are further reformed to produce H_2 and CO_2.

$$CH_3OCH_2OCH_3 + H_2O = 2CH_3OH + CH_2O \quad (1)$$
$$CH_3OH + H_2O = 3H_2 + CO_2 \quad (2)$$
$$CH_2O + H_2O = 2H_2 + CO_2 \quad (3)$$

The overall reaction can then be expressed as,

$$CH_3OCH_2OCH_3 + 4H_2O = 8H_2 + 3CO_2 \quad (4)$$

Thus, the catalysts for the reforming of DMM can be consisted of a solid acid for the hydrolysis of DMM and a component for the reforming of methanol and formaldehyde (usually using $CuZnO/Al_2O_3$ catalysts)[4-5]. The acidic component should catalyze the hydrolysis of DMM effectively without affecting the performance of $CuZnO/Al_2O_3$ for the reforming reactions.

Niobium oxide and niobium phosphate have strong surface acidities and are used as solid acid catalysts.[11-16] Nowak and Ziolek have reviewed the preparation, characterization and application of niobium-containing materials.[11,12] The catalytic application of niobium compounds was summarized by Tanabe.[13,14]

In this work, we prepared and characterized two different niobium phosphates and compared them with commercial niobium oxide and niobium phosphate (supplied by CBMM). We studied the surface acidities of these samples by using adsorption microcalorimetry of ammonia and isopropanol conversion reaction (IPA probe reactions), which are correlated to the activities in the reactions of DMM hydrolysis and H_2 production from steam reforming of DMM.

2. Experimental Section

2.1 Catalyst preparation

Nb_2O_5 was prepared by heating a niobic acid ($Nb_2O_5 \cdot nH_2O$, CBMM, Brazil) at 623 K for 4 h. NbP is the abbreviation for niobium phosphate. NbP1 was also provided by CBMM. NbP2 was prepared by an impregnation method according to the literature.[15] NbP3 with high surface area, was prepared by following a procedure previously described.[16] $CuZn/Al_2O_3$ is a commercial catalyst (CF105, Research Institute of Nanjing Chemical Industry Group, China).

2.2 Catalyst characterization

XRD patterns were obtained in a Bruker D5005 diffractometer (50kV, 35 mA) using a Cu Kα source.

Elemental analysis was performed using the ICP atomic emission spectroscopy.

BET surface areas were determined by N_2 adsorption at 77 K after outgassing at 623 K for 4 h.

XPS spectra were measured on a SSI 301 instrument equipped with an Al Kα X-ray source.

The TPR apparatus used was a home-made unit. The H_2 consumption was monitored by a TCD. About 50 mg sample was hold in a U-type reactor. A 5.13 % H_2/N_2 gas was used with a flow rate of 40 ml/min.

The UV-Vis spectra were recorded with a Perkin-Elmer Lambda 19 spectrophotometer.

The IR spectra were recorded on an FT-IR Bruker IFS-48 Vector 22 spectrometer.

The NH_3 adsorption microcalorimetry was performed at 423 K in a heat flow calorimeter (C80, Setaram). About 100 mg of sample was pretreated in vacuum in a quartz cell overnight at 623 K. Small repeated doses of NH_3 were sent onto the samples until an equilibrium pressure of about 66 Pa was reached.

2.3 Catalytic reaction

The isopropanol probe reactions were carried out in a home-made fixed-bed micro-reactor connected to a gas chromatograph. For each test, about 100 mg sample was loaded. The carrier gas N_2 with a flow rate of 60 ml·min^{-1} was passed through a liquid saturator containing isopropanol at 295 K. The reaction products were analyzed on-line with a gas chromatograph using a PEG 20000 column and a FID.

The hydrolysis of dimethoxymethane (DMM) was performed in a fixed-bed micro-reactor connected to a gas chromatograph. The DMM and H_2O reactants were introduced to the reaction zone by bubbling N_2 through a glass saturator filled with DMM (Aldrich, 99%) maintained at 273 K and a glass saturator filled with H_2O maintained at 333 K. About 50 mg catalyst was loaded for each test. The feed composition was maintained at N_2:H_2O:DMM = 24:5:1 (v/v). The reaction products were analyzed by an on-line GC equipped with a FID detector. The packed column used was Porapak N for the separation of organic compounds.

The steam reforming of DMM was carried out in a same way as the hydrolysis of DMM. The products were analyzed by an on-line GC equipped with FID and TCD detectors. The FID was connected to a Porapak N column for the separation of organic compounds, while the TCD was connected to a TDX-01 column to analyze methane, COx and N_2. The amount of H_2 produced was usually calculated according to the conversion of DMM and the composition of other products (as given in Table 2), and was checked by using another GC.

3. Results and discussion:

3.1 Structural characterizations

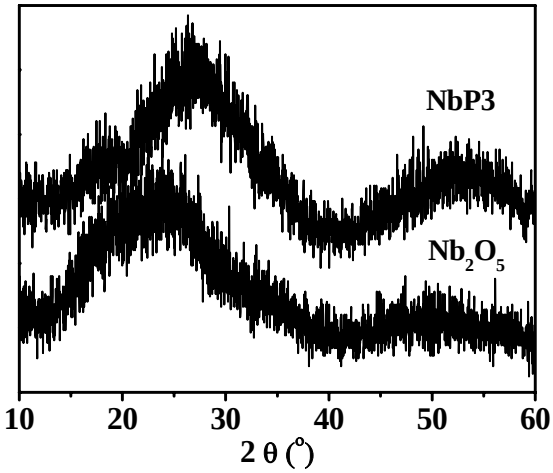

Figure 1. X-ray diffraction (XRD) patterns of Nb_2O_5 and NbP3 catalysts.

Figure 1 shows the XRD results indicating that Nb_2O_5 and NbP3 were amorphous. On NbP3, the peaks were shifted to lower angles, suggesting different bonding situations in NbP3 comparing to Nb_2O_5.

Table 1. Chemical analysis, XPS analysis and BET surface area of the samples

Sample	C.A. (wt%)		XPS (AT%)		BET (m^2/g)
	Nb	P	Nb	P	
Nb_2O_5	69.2	---	---	---	110
NbP1	46.6	5.0	13.4	8.9	142
NbP2	46.7	4.0	18.7	5.6	81
NbP3	42.6	12.4	12.1	12.7	394

Bulk and surface elemental analysis and the surface area for the samples are presented in Table 1. NbP3 prepared by using a template showed a surface area (394 $m^2 \cdot g^{-1}$) that is much higher than other samples. In addition, in the case of niobium phosphate samples, chemical analysis showed that NbP3 has the highest P content (12.4 wt%) close to the Nb/P atomic ratio of 1/1. XPS results showed that P might be enriched slightly on the surface of these niobium phosphate samples.

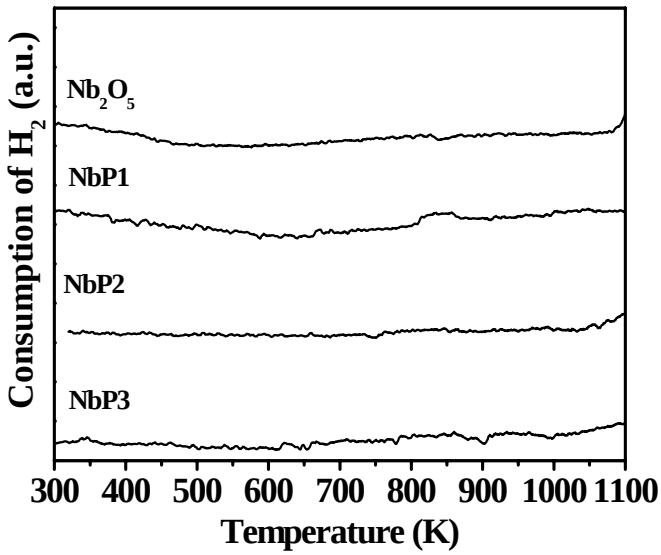

Figure 2. Temperature-programmed reduction (TPR) profiles of Nb_2O_5 and NbP catalysts.

TPR is frequently used to study the redox properties of metal oxide catalysts. In figure 2, until 1100 K, there is no significant hydrogen consumption shown, indicating that niobium oxide is very difficult to reduce.[22]

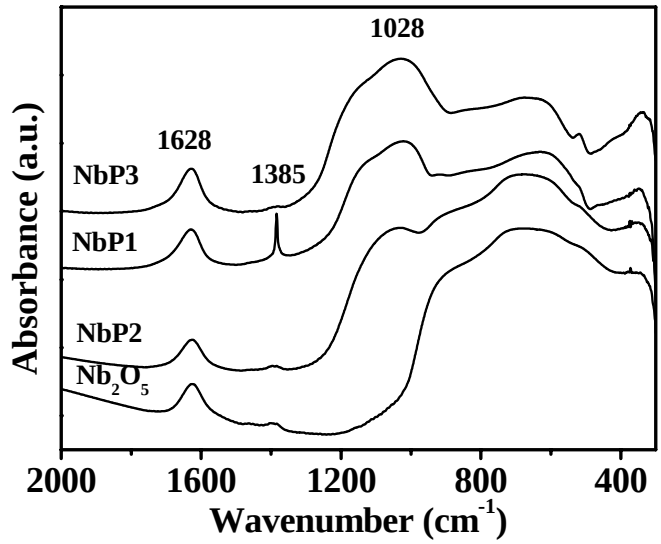

Figure 3. FT-IR skeletal spectra (KBr pressed disks, 2 mg sample in 198mg KBr) of Nb_2O_5 and NbP catalysts.

Figure 3 presents the skeletal IR spectra of samples. The bands at around 1628 cm^{-1}, due to the scissoring mode of adsorbed molecular water are shown on all the samples. The sharp band shown at 1385 cm^{-1} on NbP1 probably comes from the impurity of potassium-containing materials in NbP1 (commercial catalyst). The broad bands about 600 cm^{-1} for all the samples are mainly due to Nb-O-Nb stretching modes. For Nb_2O_5 and NbP2, a broad band also appears about below 1000 cm^{-1}, which could be assigned to the stretching mode of short Nb=O bonds. There is a broad band apparently located around 1028 cm^{-1}, on NbP samples, maybe due to the P=O=P asymmetric stretching modes. This band enhances with the increasing of P content in NbP. These results well agree with spectra got by Armaroli et al..[15]

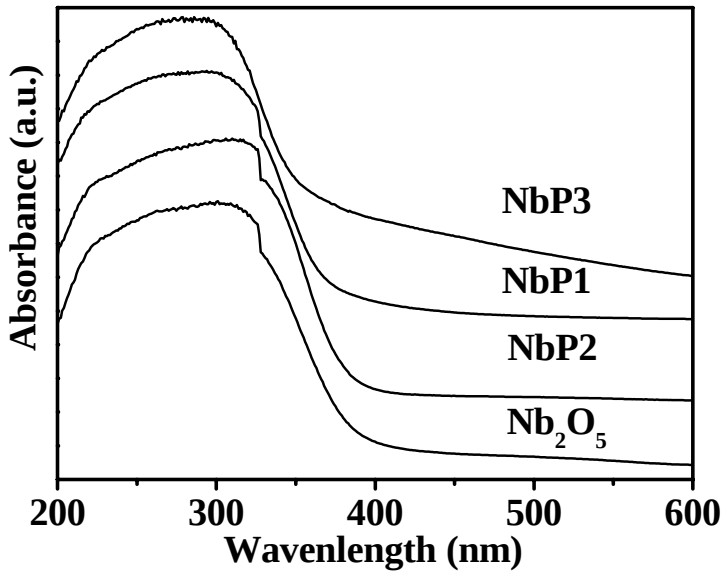

Figure 4.UV-Vis spectra of Nb_2O_5 and NbP catalysts.

Figure 4 shows the UV-Vis spectra of niobium based samples. In all cases, broad transitions were observed which can be due to the charge transfer transitions $O^{2-} \rightarrow Nb^{5+}$ associated to the energy gap between the O 2p valence band and the Nb 4d conduction band.[15] Comparing the beginning and maximum adsorption wavelengths of the samples, the transitions of NbP1 and NbP3 seem to be shifted to lower wavelength than Nb_2O_5 and NbP2 samples. As seen in the above skeletal IR, Nb_2O_5 and NbP2 are in distorted octahedral coordination. Thus these shifts indicate that NbP1 and NbP3 have different coordination states compared to Nb_2O_5 and NbP2.

3.2 Surface acidity

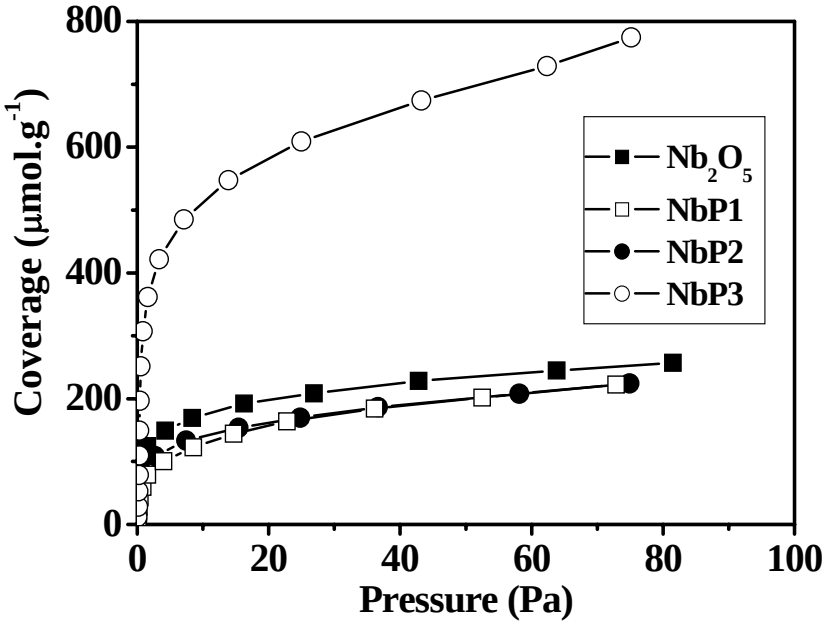

Figure 5. Isotherms for NH_3 adsorption at 423 K over Nb_2O_5 and NbP catalysts.

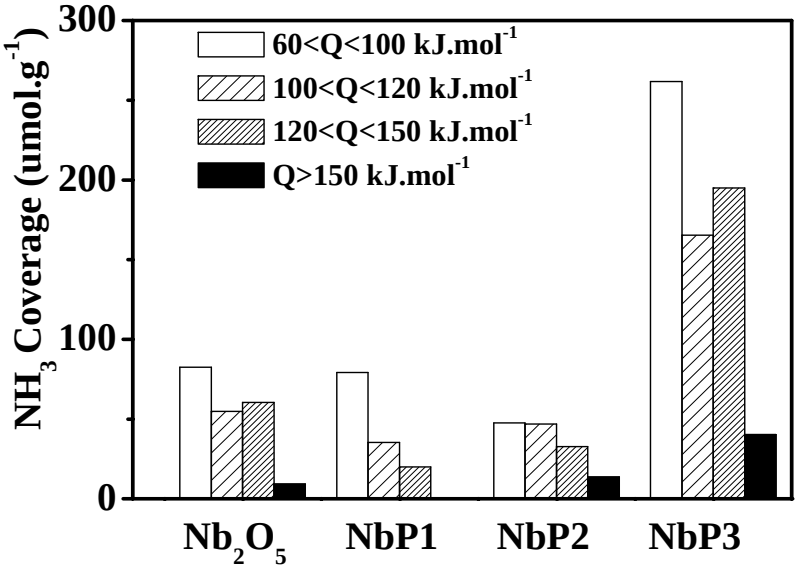

Figure 6. Acid sites distribution for NH_3 adsorption at 423 K over Nb_2O_5 and niobium phosphate catalysts.

NH_3 adsorption microcalorimetry was performed in order to determine the number, strength and strength distribution of surface acid sites of catalysts.[17] The adsorption isotherms are plotted in figure 6, and the strength distribution of surface acid sites are drawn in figure 7. NbP1 and NbP2 behaved quite similar to Nb_2O_5 in terms of isotherms curves and for ammonia adsorption. This indicates that the addition of P into Nb_2O_5 did not seem to enhance the surface acidity. However, on NbP3, a big difference can be observed. The saturation coverage of ammonia on NbP3 was found to be about 750 μmol·g^{-1} (at 66 Pa), much higher than those for other samples in this work. Beyond that, the amount of strong sites (Q > 100 kJ.mol^{-1}) and the amount of weak sites (100 > Q > 60 kJ.mol^{-1}) both increased. (see figure 7) Apparently, this should be attributed to the much higher surface area of NbP3 as compared to the other samples. When considering the NH_3 coverage per unit surface area, the coverage on NbP3 was slightly lower than that on Nb_2O_5 sample.

3.3 Isopropanol probe reaction

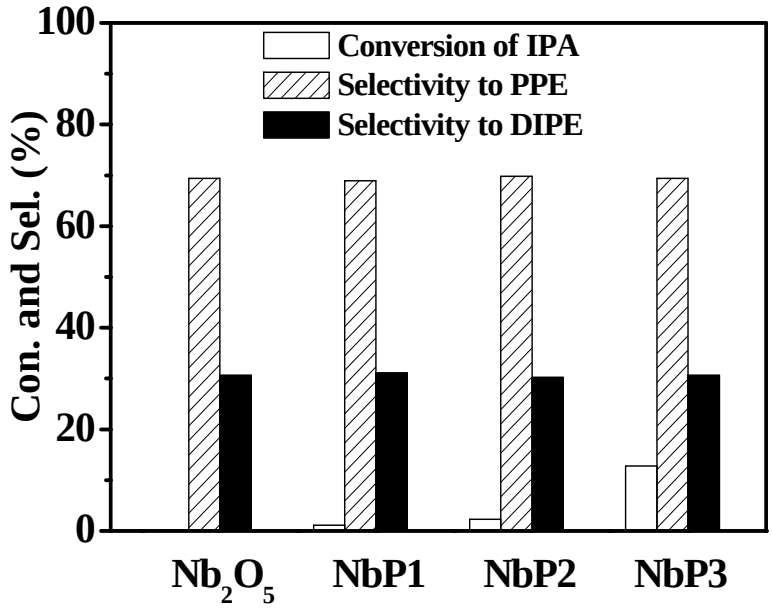

Figure 7. Conversion of IPA and selectivity of PPE and DIPE in N_2 at 413K.
Notes: IPA, PPE, DIPE and ACE denoted isopropanol, propylene, diisopropoxy ether and acetone, respectively.

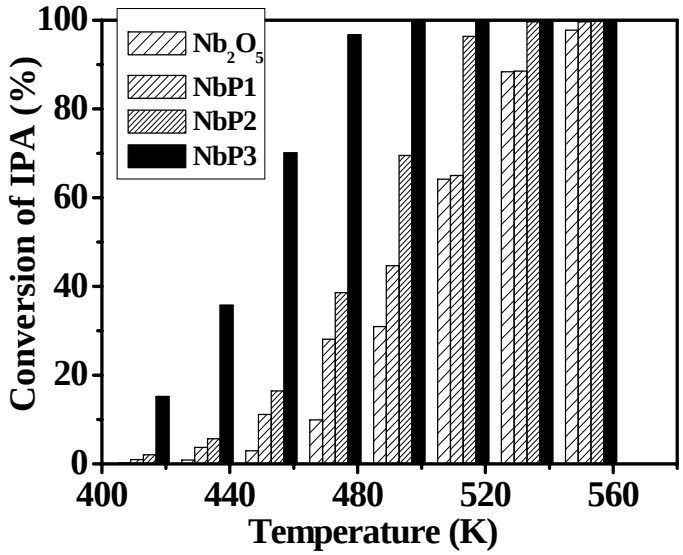

Figure 8. Conversion of isopropanol (IPA) in N_2 at different temperatures over Nb_2O_5 and NbP catalysts.

The results of isopropanol (IPA) probe reaction over the samples in N_2 gas flow are presented in Figure 7 and Figure 8. The IPA probe reaction has been extensively used to characterize the surface acid/base properties. It is well known that IPA undergoes hydration reactions to produce propylene (PPE) and diisopropoxy ether (DIPE) on acid sites while it via a dehydrogenation reaction to acetone (ACE) on base sites in inert atmosphere[18]. Thus, the conversion of IPA and selectivity to PPE, DIPE and ACE in N_2 gas flow can be used to probe the strength of surface acidity and basicity.

Results in Figure 7 showed that all the niobium catalysts in this work exhibited only surface acidity since only the products PPE and DIPE were formed, implying the non-basicity of these samples. Besides, on NbP samples, the conversion of IPA was quite higher than on Nb_2O_5, indicating that niobium phosphates were more acidic than Nb_2O_5. Among the niobium phosphates, NbP3 sample exhibited much higher IPA conversion than the other niobium phosphate catalysts. The conversion of IPA at different temperatures over the Nb_2O_5 and niobium phosphate catalysts is reported in Figure 8. The plots evidently showed that NbP3 was much more active than the other samples during the whole range of reaction temperatures. Below 500 K, NbP1 and NbP2 were also more active than Nb_2O_5.

3.4 Hydrolysis of DMM

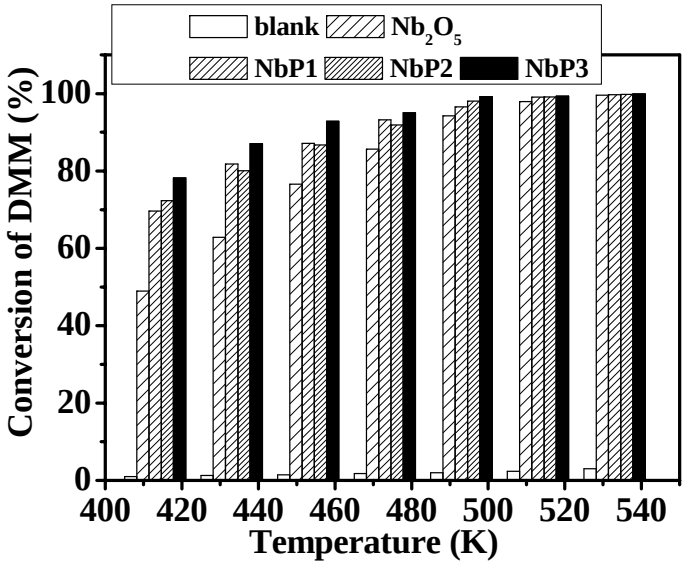

Figure 9. Conversion of dimethoxymethane (DMM) over Nb_2O_5 and NbP samples.
$N_2/H_2O/DMM$ = 24/5/1 (v/v), GHSV = 90000 $ml \cdot g^{-1} \cdot h^{-1}$, note "blank" represents without loading any catalyst in the reactor.

According to equation (1), DMM is hydrolyzed to form methanol (MeOH) and formaldehyde (FA). Figure 9 gives the conversion of DMM over niobium catalysts versus temperature. In blank experiments, DMM nearly did not hydrolyze showing its stability in the range of reaction temperature. On all the niobium samples used in the experiments, the conversion of DMM increased with temperature increasing. At lower temperatures, the conversion of DMM was higher over the more acidic catalysts as probed by IPA probe reaction. At temperatures higher than 493 K, on all the niobium samples, the conversion of DMM approached to 100%, and differences no longer appear. In the whole range of reaction temperature, the main products were methanol and formaldehyde, while the by-products were dimethyl ether (DME) and methyl formate (MF) with a total selectivity lower than 4%. So, the above niobium samples were active for the hydrolysis of DMM and may be used as acidic components combined with the traditional CuZnAl catalyst for the reforming of DMM to produce H_2.

3.5 Reforming of DMM

Table 2. Conversion and selectivity for the steam reforming of DMM over the hybrid catalysts

Sample	Temp. (K)	Conversion (%)	Selectivity/%		
			DME+MF	MeOH	H_2
CuZnAl	453	1.5	----	----	----
	493	11.0	----	----	76
	533	46.9	----	----	85
CuZnAl-Nb_2O_5	453	80.2	0.1	59.5	40.4
	493	94.3	0.1	18.0	81.9
	533	99.4	0.4	5.2	94.4
CuZnAl-NbP1	453	84.9	0.1	68.9	31.1
	493	89.5	4.3	62.0	33.7
	533	100.0	0.4	0.2	99.4
CuZnAl-NbP2	453	87.7	0.1	80.8	19.1
	493	94.5	3.1	60.1	36.8
	533	100.0	0.4	0.8	98.8
CuZnAl-NbP3	453	88.9	0.1	89.1	10.8
	493	90.5	1.8	53.8	44.4
	533	100.0	0.9	0.1	99.0

DME, MF, MeOH and FA denoted as dimethyl ether, methyl formate, methanol and formaldehyde, respectively.
Reforming conditions: $N_2/H_2O/DMM$ = 24/5/1 (v/v), GHSV = 4550 $ml \cdot g^{-1} \cdot h^{-1}$, CuZnAl/acid component = 1/7 (wt ratio)

CuZnAl catalyst is normally used for the reforming of methanol to produce H_2.[5-8] In this work, we made hybrid catalysts by mechanically mixing an industrial CuZnAl catalyst with our niobium components for the reforming of DMM. In the results, we included CO into the selectivity to H_2, since CO could be converted into H_2 via WGSR reaction. It was usually lower than 20% in our reforming reactions.

Table 2 gives a main feature for the reforming of DMM over the complex catalysts. CuZnAl catalyst alone exhibited low conversion for the reforming of DMM. Although the conversion of DMM increased with temperature, it was lower than 50% even at 533 K, the highest temperature employed in this work. Addition of any niobium sample we used in this work greatly raised the conversion of DMM. For example, at 453 K, almost no DMM was converted on CuZnAl, while the DMM conversion achieved higher than 80% with addition of one of the niobium samples. This result indicated the importance of adding an acidic component for the reforming of DMM over CuZnAl. Comparing with the selectivity to H_2 on all hybrid catalysts, the CuZnAl-Nb_2O_5 exhibited higher than the other catalysts when the temperature was lower than 493 K. At 533 K, all the catalysts exhibited selectivity to H_2 higher than 94% meanwhile the conversion of DMM was about 100%. Thus, all the complex catalysts composed of CuZnAl and niobium samples worked well for the reforming of DMM to produce H_2 at 533 K, with a H_2 production rate of about 1100 $ml.g^{-1}.h^{-1}$. Below 533 K, there was a substantial amount of methanol in the products. This indicates that the activity of CuZnAl component was not enough to convert methanol and H_2O to H_2 and COx completely. Considering the high ratio of CuZnAl to the acidic niobium component (7/1), it was difficult to increase the activity of methanol reforming by simply increasing the amount of CuZnAl. Additionally, it was shown that Nb_2O_5 and other niobium phosphates behaved differently. From the previous data, Nb_2O_5 was less acidic and thus less active for the hydrolysis of DMM than the niobium phosphates, it exhibited lower activity for the reforming of DMM at lower temperatures. However, it gave rise to higher selectivity to H_2 (with lower amount of methanol remained) at lower temperatures as compared to the niobium phosphates. Moreover, the niobium phosphate with different P content also showed different selectivity to H_2 from each other at low temperature. Thus, it seems that P in the niobium phosphates might have a negative effect on the performance of CuZnAl catalyst for the reforming of methanol.

4. Conclusions

We prepared niobium phosphates in different ways, in which we could obtain NbP with high surface area (394 $m^2 \cdot g^{-1}$) by using the template, hexadecylamine. The Nb_2O_5 and niobium phosphate samples studied in this work possessed similar amorphous structure. The niobium phosphates were found to be more acidic than Nb_2O_5, especially the one with high surface area. The high surface area niobium phosphate exhibited great amount of surface acid sites (~750 $\mu mol \cdot g^{-1}$) and was active in catalyzing the dehydration of isopropanol and the hydrolysis of dimethoxymethane (DMM). By combining Nb_2O_5 or niobium phosphate with an industrial $CuZnO/Al_2O_3$ catalyst, the complex catalysts were effective for the direct reforming of DMM to produce H_2 at 533 K. The conversion of DMM was higher than 94% with selectivity to H_2 (and CO) higher than 96% at 533 K, and a H_2 production rate of about 1100 $ml.g^{-1}.h^{-1}$. Since DMM is more environmentally benign than methanol, our present work indicated that it is possible to reform DMM directly if a proper acidic component is added in the traditional $CuZnO/Al_2O_3$ catalyst.

Acknowledgements

We acknowledge the financial supports from CNRS-France, Ministry of Science and Technology of China (2004DFB02900), French Ministry of Education and French-Chinese joint program PRA E 03-01.

References:

(1) Wasmus,S.; Kuver,A., Methanol oxidation and direct methanol fuel cells: a selective review, J. Electroanal. Chem., 461, 14, 1999.
(2) Song,C.S., Fuel processing for low-temperature and high-temperature fuel cells - Challenges, and opportunities for sustainable development in the 21st century, Catal. Today, 77, 17, 2002.
(3) Qi, A. D.; Wang, S. D.; Fu, G. Z.; Ni, C. J.; Wu, D. Y., La-Ce-Ni-O monolithic perovskite catalysts potential for gasoline autothermal reforming system, Appl. Catal., A 281, 233, 2005.
(4) Amphlett, J. C.; Evans, M. J.; Jones, R. A.; Mann, R. F.; Weir, R. D., Hydrogen production by the catalytic steam reforming of methanol. Part 1. The thermodynamics, Can. J. Chem. Eng. 59, 720, 1981.
(5) Emonts, B.; Hansen, J. B.; Jørgensen, S.; Höhlein, B.; Peters, R. J., Compact methanol reformer test for fuel-cell powered light-duty vehicles, Power sources 71, 288, 1998.
(6) Takeishi, K.; Suzuki, H., Steam reforming of dimethyl ether, Appl. Catal., A 260, 111, 2004.
(7) Yin, S. F.; Xu, B. Q.; Zhou, X. P.; Au, C. T., A mini-review on ammonia decomposition catalysts for on-site generation of hydrogen for fuel cell applications, Appl. Catal., A 277, 1, 2004.
(8) Fu, Y.C. doctoral thesis, Studies of Some Catalytic Reactions for the Synthesis and Conversion of Methanol-derived Chemicals, Nanjing University, 2005
(9) Liu, H. C.; Bayat, N.; Iglesia, E., Site titration with organic bases during catalysis: Selectivity modifier and structural probe in methanol oxidation on Keggin clusters, Angew. Chem. Int. Edit. 42, 5072, 2003.
(10) Yuan, Y. Z.; Shido, T.; Iwasawa, Y., The new catalytic property of supported rhenium oxides for selective oxidation of methanol to methylal, Chem. Comm. 15, 1421, 2000.
(11) Nowak, I.; Ziolek, M., Niobium compounds: Preparation, characterization, and application in heterogeneous catalysis, Chem. Rev. 99, 3603, 1999.
(12) Ziolek, M., Niobium-containing catalysts - the state of the art, Catal. Today 78, 47, 2003.
(13) Tanabe, K.; Okazaki, S., Various reactions catalyzed by niobium compounds and materials, Appl. Catal. A 133, 191, 1995.
(14) Tanabe, K., Catalytic application of niobium compounds, Catal. Today 78, 65., 2003
(15) Armaroli, T.; Busca, G.; Carlini, C.; Giuttari, M.; Galletti, A. M. R.; Sbrana. G., Acid sites characterization of niobium phosphate catalysts and their activity in fructose dehydration to 5-hydroxymethyl-2-furaldehyde, J. Mol. Catal., A 151, 233, 2000.
(16) Mal, N. K.; Fujiwara, M., Synthesis of hexagonal and cubic super-microporous niobium phosphates with anion exchange capacity and catalytic properties, Chem. Comm. 22, 2702, 2002.
(17) Auroux, A., Acidity characterization by microcalorimetry and relationship with reactivity, Top. Catal. 4, 71, 1997.
(18) Gervasini, A.; Fenyvesi, J.; Auroux, A., Study of the acidic character of modified metal oxide surfaces using the test of isopropanol decomposition, Catal. Lett. 43, 219, 1997.

Publication III

特约述评

铌的催化作用

孙 清[1,2],刘兰香[1],邢晓玲[1],Aline Auroux[2],沈俭一[1]
(1. 南京大学 化学化工学院介观化学重点实验室,江苏 南京 210093;
2. Institut de Recherches sur la Catalyse, CNRS, 2 Av. Einstein, 69626 Villeurbanne, Cedex, France)

[摘要] 综述了铌在酸催化和氧化催化反应中的作用。铌化合物为新型催化材料,在催化反应中,既可作为催化剂,也可作为催化剂载体或助剂。铌酸和磷酸铌在水解、水合等很多酸催化反应中具有良好的催化活性。在含铌负载的金属催化剂中,存在着载体与金属间的强相互作用,可用于选择性催化加氢反应。铌氧化物具备一定的氧化-还原能力,能增强用其掺杂或负载的氧化物催化剂的催化氧化活性。铌作为催化助剂,在低碳烃选择氧化反应中,可提高目标产物烯烃、醛、酸或腈的收率。铌催化剂还在光催化制氢等反应中显示出特殊的活性。

[关键词] 铌;催化作用;助催化作用;载体;固体酸催化;选择氧化;光催化
[文章编号] 1000-8144(2007)04-0000-00 [中图分类号] TQ 426.8 [文献标识码] A

Catalysis of Niobium

Sun Qing[1,2], *Liu Lanxiang*[1], *Xing Xiaoling*[1], *Auroux Aline*[2], *Shen Jianyi*[1]
(1. Lab of Mesoscopic Chemistry, School of Chemistry and Chemical Engineering, Nanjing University, Nanjing Jiansu 210093, China; 2. Institut de Recherches sur la Catalyse, CNRS, 2 Av. Einstein, 69626 Villeurbanne Cedex, France)

[**Abstract**] Catalysis of niobium in various reactions especially in acid catalyzed and selective oxidative reactions were reviewed. Niobium compounds can be used as active components, supports or promoters in catalytic reactions. Niobic acid and niobium phosphate exhibit strong surface acidity and therefore exhibit high catalytic activities in acid catalyzed reactions such as hydrolysis and hydration of organic compounds. Strong interactions of metal with support exist in niobium pentoxide supported metallic catalysts. This effect can be used to improve activities and selectivities of metallic catalysts for hydrogenations. Another important property of niobium oxides is its weak redox behavior which enhances redox ability of other metallic oxides supported on or doped with niobium oxides. As a promoter, niobium has been doped into complex oxides mainly consisted of V and Mo to raise catalytic activity and selectivity for selective oxidation of light paraffins to corresponding olefins, organic acids and nitriles. Moreover complex niobium oxides with layered structures have been found to be photo-catalytically active for decomposition of H_2O to produce H_2.

[**Keywords**] niobium; catalysis; co-catalysis; support; solid acid catalysis; selective oxidation; photocatalysis

铌化合物作为一类新型的催化材料,既可作为催化剂,也可作为催化剂载体或助剂,它们在酸催化和氧化催化反应中的应用已引起人们的注意[1~6]。国内外有关将铌用于催化反应的文献数量逐年递增,这也说明铌的催化作用越来越受到重视。

本文综述了近五年来国内外文献中有关铌催化作用的研究进展。

[收稿日期] 2006-11-15;[修改稿日期] 2006-11-23。
[作者简介] 孙清(1978—),男,江苏省南京市人,博士生。联系人:沈俭一,电话 025-83594305,电邮 jyshen@nju.edu.cn。
[基金项目] 科技部国际合作项目(2004DFB02900);国家自然科学基金项目(20373023)。

1 元素铌和铌材料

1.1 元素铌

铌与钒同属于元素周期表的第五族。铌主要来源于铌铁矿,巴西是目前世界上最大的铌产地[4]。目前,铌在工业上主要作为合金元素用于制造高强度、耐腐蚀钢铁,还应用于催化、原子能、电容材料、陶瓷工业、非线性光学材料等领域[4]。

1.2 氧化铌和磷酸铌

五氧化二铌(Nb_2O_5)是铌最常见的氧化物形态,为白色粉末,在空气中稳定,不溶于水。在分子结构上,由 NbO_6 八面体结构单元通过共边或共角构成[7]。水化的 Nb_2O_5 称为铌酸($Nb_2O_5 \cdot nH_2O$)[8]。铌酸表现出强酸性(酸强度 $H_0 = -5.6 \sim 8.2$,相当于质量分数为 70% 的 H_2SO_4 酸强)[9],氨吸附量热结果表明,铌酸为中强酸(初始吸附热为 165 kJ/mol)[10]。铌酸的酸性来源于表面的 Nb — OH(B 酸中心)和配位未饱和的 Nb^{5+}(L 酸中心)[11]。经高温(高于 773 K)焙烧,铌酸变为结晶态,表面积下降,同时大量表面羟基脱除,酸性消失[4]。为了提高铌酸的高温稳定性,可用磷酸处理铌酸,得到磷酸铌($NbOPO_4 \cdot nH_2O$)。磷酸铌的酸性更强($H_0 \leqslant -8.2$,相当于质量分数为 90% 的 H_2SO_4 强度)[2],与铌酸相比,磷酸铌的高温稳定性增强,因为加入的磷酸阻碍了铌酸在高温下的结晶,维持了铌酸较大的表面积[4]。磷酸铌中 B 酸中心为 Nb — OH和 P — OH,由于 P 的电负性比铌略大,因此 P OH 中心比 Nb — O — H 中心的酸性略强,L 酸中心仍为未饱和的 Nb^{5+}[12]。

铌酸或 Nb_2O_5 可通过铌的氯化物或醇盐水解制备[13,14]。自 Mobil 公司[15,16]首次报道了 MCM-41 分子筛的合成后,中孔材料的合成取得了很大进展[17~19]。Antonelli 等[20,21]首先用烷基胺作模板剂合成了 Nb — O 中孔材料。通过改变模板剂或制备条件,可获得不同孔道结构和孔径的 Nb — O孔材料[22~25]。Mal 等通过模板法合成了微孔[26,27]和中孔[28,29]的磷酸铌。

1.3 Nb-Si-O 孔材料

1997 年,Ziolek 等[30]首次合成了铌掺杂的 MCM-41 分子筛(Nb-MCM-41)。Nb-MCM-41 分子筛的酸性比 Al-MCM-41 分子筛的弱,但稳定性高,表面酸中心主要为 L 酸[31]。制备条件决定了 Ni-Si-O 孔材料的孔径大小和孔道结构[32~35]。

2 催化作用

2.1 铌化合物作为催化剂

铌酸和磷酸铌具有强酸性,在酸催化反应中显示出较高的活性,尤其是有水参与的反应,研究得较多[1,2]。纯粹的 Nb_2O_5 很难被还原[5],但在 Nb-Si-O 复合氧化物中,铌却体现出氧化-还原性[5],体现出催化氧化的活性。

2.1.1 水解反应

Hanaoka 等[36]在 1990 年发现铌酸可有效催化苯基环氧乙烷水解为苯基乙二醇,活性高于 $Al_2O_3-SiO_2$ 和 ZSM-5 等固体酸。戊二醛是重要的化工中间体和精细化工产品,文献[37]报道了铌酸催化二氢吡喃衍生物水解为戊二醛,在 363 K 常压下液相反应,戊二醛收率可达 94%。Sun 等[10]发现,在铌酸和磷酸铌上,甲缩醛可 100% 水解为甲醛和甲醇,没有二甲醚等副产物生成,铌酸和磷酸铌与 $CuZnO/Al_2O_3$ 组成的复合催化剂具有良好的甲缩醛重整制氢性能。Gallo 等[38]发现,经过铌交换,蒙脱土的酸性增强。在 333 K、铌交换后的蒙脱土上反应 30 min,环氧化油酸可完全醇解为 -羟基酯,比铌交换前的蒙脱土反应速率快 3 倍。铌酸可负载于钛硅分子筛上成为双功能催化剂,用于辛烯生成辛二醇的反应[39]。辛烯先在氧化中心上(钛氧物种)氧化为环氧辛烷,然后在酸中心(铌氧物种)上水解为辛二醇。与非负载的钛硅分子筛相比,负载了铌酸的钛硅分子筛的活性提高了 4 倍,诱导期由 24 h 缩短为 3 h[39]。

2.1.2 水合反应

Li 等[40]将负载的 Nb_2O_5 催化剂用于环氧乙烷(EO)水解制乙二醇(MEG)。用 $\alpha-Al_2O_3$ 负载的 Nb_2O_5 催化剂,在 423 K、15 MPa、H_2O 与 EO 的摩尔比为 22 的条件下,EO 转化率由无催化剂时的 34% 增至 99.8%,MEG 的选择性为 89%,催化剂寿命大于 1 000 h[41]。$Nb_2O_5/\alpha-Al_2O_3$ 催化剂用 Sn 和 $MgAl_2O_4$ 等修饰后,MEG 的选择性进一步增至 94%[42~44]。

2.1.3 脱水反应

以糠醛或羟甲基糠醛(HMF)为基础可合成塑料或燃料,所合成的塑料废弃后可完全降解,环境友好[45]。HMF 可由果糖等脱水生成。以磷酸铌为脱水催化剂,373 K 时,果糖转化率为 27%,HMF 选择性可达 100%,活性远高于磷酸锆和离子交换树脂等固体酸催化剂[46]。Dias 等[47]将 Nb-Si-O 孔材

料用于木糖液相脱水,在 433 K 下反应 6 h,木糖转化率为 90%,糠醛收率达 50%,催化剂不失活,活性高于 H – Y 分子筛。Brandao 等[48] 将微孔 Nb – Si – O 材料用于醇脱水反应时发现,升高反应温度,不仅有利于提高醇的转化率,还有利于醇发生分子内脱水生成烯烃。对于乙醇脱水反应,453 K 时,乙醇转化率为 18%,乙醚选择性为 45%,乙烯选择性为 55%;反应温度升至 573 K 时,乙醇转化率为 100%,乙烯选择性为 100%。

2.1.4　酯交换反应

β – 羰基酯是有机合成中的重要中间体。文献[49]报道,Nb_2O_5 可有效地催化 β – 羰基酯与醇进行酯交换反应,生成新的 β – 羰基酯。β – 羰基酯的转化率可达 65% ~100%,收率 50% ~80%,催化剂可重复使用。

2.1.5　烷基化反应

工业磷酸铌可用于催化苯、甲苯、对二甲苯等和苯甲醇的液相苄基化反应,410 K 时,苯甲醇可完全转化,反应产物主要为单烷基化物,副产物醚较少[50],活性高于 $Zr(SO_4)_2$ 和大孔树脂等固体酸催化剂。

2.1.6　裂化反应

Na – Y 分子筛经掺杂铌后,其异丙基苯催化裂化活性显著提高,673 K 时,异丙苯转化率由原来的 3% 提高到 91%[4]。在甲苯、乙苯和异丙苯的裂化反应中,W – Nb 混合氧化物的催化活性高于 WO_3/ZrO_2、丝光沸石和 $Al_2O_3 – SiO_2$。在 573 K 时,W – Nb – O 上甲苯的转化率为 14%,而在 WO_3/ZrO_2、丝光沸石和 $Al_2O_3 – SiO_2$ 上甲苯转化率分别只有 6%,7%,0%[51]。

2.1.7　其他酸催化反应

$NbCl_5$ 作为一种新型酸催化剂,可用于多种有机合成反应。如 β – 羰基酯的合成[52]、胺或硫醇与乙酸酐的乙酰化反应[53]、Knoevenagel 缩合制亲电烯烃[54] 和亚胺偶合生成邻二胺[55] 等。

2.1.8　氧化和环氧化反应

Nb – Si – O 材料中的铌具备一定的氧化 – 还原能力[5],在许多氧化反应中显示出催化活性。

Parvulescu 等[56] 发现,铌掺杂的 MCM – 41 分子筛可有效地催化 H_2O_2 氧化苯乙烯,343 K 时,苯乙烯的转化率为 87%,苯乙醛选择性为 99%。但在相同反应条件下,苯和甲苯在该催化剂上的转化率分别只有 1% 和 2%[56],远低于掺杂 V 和 Ti 的 MCM – 41 分子筛的转化率(分别为 78% 与 16%)[57]。Vetrivel 等[58] 发现,制备方法影响 Nb – Si – O 材料的氧化性能,在胺基甲苯的氧化反应中,浸渍法合成的 Nb/MCM – 4 材料的催化活性高于水热法合成的 Nb/MCM – 41 材料,523 K 时,在 Nb/MCM – 41 材料上胺基甲苯的转化率为 41%,胺基苯甲酸的选择性为 73%,胺基苯甲醛的选择性为 25%;而在 Nb – MCM – 41 材料上,相应的转化率和选择性分别为 32%,60%,33%。Mal 等[26] 用微孔磷酸铌催化氧化萘酚生成 1,4 – 萘醌时,萘酚的转化率为 9%,1,4 – 萘醌的选择性为 83%;而在苯酚氧化生成邻苯二酚的反应中,萘酚的转化率与 1,4 – 萘醌的选择性分别为 46%,95%[27]。

Nowak 等[34] 发现,中孔和大孔 Nb – Si – O 材料可有效催化 H_2O_2 氧化环己烯生成环氧己烷,如以 Nb – MCM – 41 为催化剂时,在 318 K 下反应 30 min,环己烯转化率可达 44%,环氧己烷的选择性可达 95%,孤立的铌物种被认为是活性中心[59]。Liu 等[60] 发现,六方孔结构的中孔 Nb – Si – O 材料对丙烯环氧化反应有较高的催化活性。Somma 等[61,62] 将大孔 Nb – Si – O 材料或含铌气溶胶用于烯烃环氧化反应时发现,催化活性稳定,环氧化产物的收率高,催化剂不流失,循环反应数次后催化活性基本不变。Bouh 等[63,64] 用 CH_3ReO_3/Nb_2O_5 催化不饱和脂肪酸的液相环氧化反应时发现,在 H_2O_2 为氧化剂、反应温度 297 ~323 K、反应时间 2 h 时,环氧化产物的收率为 80% ~100%。

2.2　含铌载体

Nb_2O_5 作载体时,与负载金属间存在强烈的相互作用(SMSI)[3~5,65],导致金属上的电子云密度增大,削弱了 H_2 在金属上的吸附,从而降低了对烃类加氢反应的催化活性,但增高了 CO 加氢生成烃类的催化活性[66]。与 SiO_2 和 Al_2O_3 等载体相比,Nb_2O_5 的氧化 – 还原性提高了其负载的金属氧化物催化剂的氧化能力[5]。

2.2.1　F – T 合成

在 F – T 合成反应中,Nb_2O_5 负载的贵金属比使用其他载体时显示出更高的活性。如 493 K 时,在 Ru/Nb_2O_5 催化剂上 CO 的转化率为 76%,而在 Ru/Al_2O_3 催化剂上 CO 的转化率只有 1.7%;Ru 在不同载体上的 CO 加氢活性高低顺序为:$Nb_2O_5 > ZrO_2 > Al_2O_3 > SiO_2 > MgO$[67]。Schmal 等[68] 比较了不同载体负载的 Co 催化剂在 F – T 合成中的产物分布,在 Co/Al_2O_3 催化剂上 CH_4 和 C_2^+ 的选择

性分别为 55% 和 37%，而在 Co/Nb_2O_5 催化剂上 CH_4 和 C_2^+ 的选择性分别为 14% 和 74%，说明以 Nb_2O_5 为载体时有利于链的增长反应。Mendes 等[69]用程序升温反应和原位漫反射紫外 - 可见光谱技术研究了 Co/Al_2O_3 和 $Co/Al_2O_3 - Nb_2O_5$ 催化剂催化 CO 加氢的反应性能，认为 $Co^{2+} - Co^0$ 物种催化甲烷化反应，而 $Co^0 - NbO_x$ 物种催化烃的链增长反应。

2.2.2 不饱和烃加氢

Jasik 等[70]比较了不同金属氧化物负载的 Ni 催化剂的苯加氢反应性能，实验结果表明，Ni/SiO_2 催化剂的活性最高，而 Ni/Nb_2O_5 催化剂则几乎没有活性。Jasik 等认为这是 Ni 与 Nb_2O_5 载体间的强相互作用所致。Ahn 等[71]研究了 Pd/SiO_2 催化剂上乙炔的加氢反应性能，实验结果表明，催化剂经 Nb_2O_5 改性后，乙炔的转化率和乙烯的选择性大幅度提高，且延长了催化剂的使用寿命。Ahn 等认为，Nb_2O_5 经 773 K H_2 还原后具有一定的加氢活性，提供了额外的乙炔加氢活性，且通过对聚合生成的油状副产物的加氢，减缓了催化剂的失活。

2.2.3 加氢脱硫与脱氯

加氢脱硫与脱氯反应在工业上很重要，加入 Nb_2O_5 往往能提高催化剂的活性。文献[72]报道，经 673 K 硫化，Mo/Nb_2O_5 催化剂上的异丙苯氢解活性为 Mo/Al_2O_3 催化剂的 60 倍，这是因为硫化后生成的 NbS_3 具有很高的催化活性。Damyanova 等[73,74]研究了加入 Nb_2O_5 对 Mo 在 SiO_2 上分散性的影响，实验结果表明，Nb_2O_5 与 SiO_2 之间有较强的相互作用，加入 Nb_2O_5 后，生成了新的酸中心，并促进了金属 Mo 的分散，当 Nb_2O_5 的质量分数为 5.4% 时，$Mo/Nb_2O_5 - SiO_2$ 催化剂的脱硫活性最高。Gaborit 等[75]发现，$Nb_xMo_{1-x}S_2/Al_2O_3$ 催化剂在 H_2S 分压达为 26.6 kPa 时，仍能保持稳定的加氢脱硫活性，而传统的 $MoNi/Al_2O_3$ 催化剂的加氢脱硫活性随 H_2S 分压的升高而迅速降低。Caero 等[76]考察了 Nb_2O_5 的加入方式对 TiO_2 负载的 Mo 催化剂的噻吩加氢脱硫性能的影响，实验结果表明，浸渍法制备的 $Mo/(Nb_2O_5/TiO_2)$ 催化剂的加氢脱硫活性远高于 Nb - Ti 混合氧化物负载的催化剂(Mo/Nb - Ti - O)。Caero 等认为，$Mo/(Nb_2O_5/TiO_2)$ 催化剂硫化后易在表面形成 MoS_2 阴离子活性中心，提高了脱硫活性。Chary 等[77,78]用氢吸附等技术研究了 Nb_2O_5 负载的 Ni 催化剂的性能，实验结果表明，Ni/Nb_2O_5 催化剂上存在氢溢流，负载量为 6% 的 Ni/Nb_2O_5 催化剂上氢溢流最显著，在三氯苯加氢脱氯反应中的活性也最高。

2.2.4 氧化与氨氧化

Marques 等[79]将 Nb_2O_5 和 Al_2O_3 负载的 Pt 和 Pt - Sn 催化剂用于 H_2 气氛中 CO 的优先氧化，433 K 时，CO 在 $Pt - Sn/Nb_2O_5$ 催化剂上的转化率为 100%，而在 $Pt - Sn/Al_2O_3$ 催化剂上的转化率仅为 7%；但在 $Pt - Sn/Nb_2O_5$ 催化剂上，CO 被氧化的同时大量 H_2 亦被氧化。

苄腈可作为合成树脂的前体或燃料添加剂。Chary 等研究了 Mo/Nb_2O_5 和 V_2O_5/Nb_2O_5 催化剂上甲苯氨氧化为苄腈的活性，673 K 时，负载量为 10% 的 Mo/Nb_2O_5 催化剂上甲苯转化率为 65%，苄腈选择性为 71%[80]；640 K 时，6% V_2O_5/Nb_2O_5 催化剂上甲苯转化率为 81%，苄腈选择性为 93%[81]；反应性能优于以往文献报道的其他催化体系。他们还将 Nb - Ti 混合氧化物负载的 V_2O_5 催化剂用于该反应，643 K 时，负载量为 5% 的 $V_2O_5/Nb_2O_5 - TiO_2$ 催化剂上甲苯转化率为 85%，苄腈选择性为 90%[82]。3 - 甲基吡啶经氨氧化可生成 3 - 腈基吡啶，后者可水解为烟酰胺，烟酰胺本身是一种药物，也可作为药物合成的中间体。Chary 等[83]发现，633 K 时，负载量为 6% 的 V_2O_5/Nb_2O_5 催化剂上甲基吡啶转化率可达 90%，腈基吡啶选择性为 98%。

2.3 铌的助剂作用

低碳烷烃经氧化脱氢可得更有价值的低碳烯烃，也可选择氧化或氨氧化为附加值更高的酸、酐和腈等产物，是近年来的研究热点。铌作为助剂加入到各种催化体系中，以提高烃的转化率和目标产物的选择性。

2.3.1 烷烃氧化脱氢

Union Carbide 公司[84]在 1981 年申请了 Mo - V - Nb 复合氧化物体系催化乙烷氧化脱氢生成乙烯的专利，在 $Mo_{16}V_4Nb_2$ 复合氧化物催化剂上(常压)，乙烷转化率为 10%，乙烯选择性为 100%，在 Mo - V 催化体系中加入铌可将反应温度由 813 K 降至 659 K，而乙烷转化率和乙烯选择性不降低；加压到 0.5 ~ 0.9 MPa 时，乙烷转化率增至 69% ~ 75%，而乙烯选择性降至 68% ~ 71%。Heracleous 等将经铌改性的 Ni/Al_2O_3 催化剂用于乙烷氧化脱氢，实验结果表明，加入铌能促进 Ni 的分散[85]，并促使 C — H 键活化，降低反应的活化能[86,87]，从而提高乙烷转化率；铌的加入还减少了与完全氧化相

关的表面亲电氧物种[86,87],因而提高了乙烯的选择性。Xie 等[88]用浆态法制备了 $MoV_{0.31}Te_{0.2}Nb_{0.1}$ 复合氧化物催化剂,并用于乙烷氧化脱氢,673 K 时,乙烷转化率为 90%,乙烯选择性为 87%,乙烯时空收率可达 176 g/(kg · h)。

Karamullaoglu 等[89]将 Cr – V – Nb 复合氧化物催化剂用于异丁烷氧化脱氢生成异丁烯,846 K 时,异丁烷的转化率为 45%,异丁烯的选择性为 90%。

丙烷的氧化脱氢比乙烷难,V – Nb – O 催化剂对丙烷氧化脱氢为丙烯具有较好的催化性能,在 773 ~ 823 K 时,丙烷转化率可达 20% ~ 40%,丙烯选择性为 30% ~ 50%[90~92]。

2.3.2　烃选择氧化与氨氧化

丙烯酸是重要的化工原料,全世界每年需求数百万吨,工业上一般通过丙烯氧化合成[3]。文献[93,94]报道了在丙烷选择氧化为丙烯酸和氨氧化为丙烯腈的催化反应中,铌对 Mo – V – Te 复合氧化物体系具有助催化效应,在 $Mo_1V_{0.3}Te_{0.23}Nb_{0.12}O_n$ 催化剂上,653 K 时,丙烷转化率达 84%,丙烯酸选择性为 63%;将该催化剂用于丙烷氨氧化反应,丙烷转化率可达 92 %,丙烯腈选择性为 64%。Lin 等[95]综述了丙烷氧化为丙烯酸的反应途径及相关催化剂的结构特征。一般认为,Mo – V 是主催化组分,铌的加入抑制了深度氧化的进行,提高了产物丙烯酸和丙烯腈的选择性[96~97];至于铌的助剂效应及其催化作用机理,文献主要从催化剂的结构[98,99]、酸碱性[100]、氧化 – 还原性[101]、组分间的协同效应[102~105]等方面考虑,但尚无统一的观点和看法。

Roussel 等[106,107]将 Mo – V – Nb – O 催化剂用于乙烷选择氧化为乙酸的反应,在 Mo – V – O 催化体系中加入铌,使乙烷转化率由 4% 提高到 15%,乙酸选择性由 73% 提高到 96%。

工业上采用钒磷氧(VPO)催化剂将丁烷选择氧化为马来酸酐。Pries 等[108,109]在 VPO 催化体系中加入磷酸铌,提高了催化剂的活性及选择性,马来酸酐的收率由 25% 增至 54%,同时反应诱导期大幅度缩短,催化剂的机械强度也得到了提高。

将吡啶交换的磷钼酸铌($NbPMo_{12}Pyr$)和磷钼钒酸铌($NbPMo_{11}VPyr$)用于烷烃选择氧化反应,实验结果表明,对于乙烷选择氧化为乙酸的反应,催化剂的活性高于 Mo – V – Nb – O 催化剂[110];对于丙烷选择氧化为丙烯酸的反应,催化剂的活性高于 Mo – V – Te – Nb – O 催化剂[111];而对于丁烷选择氧化为马来酸酐的反应,催化剂的活性高于 VPO 催化剂[111]。

2.4　光催化及其他催化反应

2.4.1　光催化制氢

层状结构的 Ni – $K_4Nb_6O_{17}$ 在紫外光照下可催化水分解生成 H_2 和 O_2[112,113]。Domen 等[113]推测其机理为:通过光照,在 $K_4Nb_6O_{17}$ 的层面上产生电子空穴对(e – h),电子与水在层面上反应生成 H_2,空穴与水在另一面反应生成 O_2,生成的 H_2 与 O_2 从层间通道逸出。由于催化剂预先经过处理(773 K 下 H_2 还原后再经 473 K 下 O_2 氧化),催化剂层外的 Ni 颗粒呈氧化态,而层间的 Ni 颗粒呈还原态。还原态的层间 Ni 增加了 $K_4Nb_6O_{17}$ 产生 e – h 的能力,而氧化态的层外 Ni 可避免生成的 H_2 与 O_2 复合为水,因此,Ni – $K_4Nb_6O_{17}$ 具有较高的光催化活性[113]。Abe 等[114]认为,有光催化活性的物质(如 La_3NbO_7 等)均具有八面体结构单元,这些单元通过共角形成网络结构,使电子和空穴的移动更加容易,因此,这类催化剂具有较高的光催化活性。铌酸盐负载的 Pt 和 Ni 等催化剂均显示了较高的光催化活性[115,116]。

2.4.2　其他催化反应

铌作为活性组分或助剂,还可应用于其他多种催化反应,如脱除 NO_x 反应[117,118]、水煤气变换反应[119]、甲烷重整反应[120]、光催化降解有机污染物[121,122]、手性催化反应[123]等。

3　结语

铌化合物可作为主催化组分、催化剂载体和助剂,应用于多种催化反应。铌酸和磷酸铌在酸催化反应中(尤其在有水分子参与的酸催化反应中)显示出很高的活性。在含铌负载的金属催化剂中,存在着金属 – 载体间强的相互作用,能调变金属催化剂的加氢性能。Nb^{5+} 具有一定的氧化 – 还原能力,特别是在 Nb – Si – O 复合氧化物催化剂的环氧化催化反应中,表现了优异的催化性能,而 Nb_2O_5 负载的金属氧化物催化剂的催化氧化活性也因此得到提高。在低碳烷烃氧化脱氢和选择氧化反应中,铌主要作为 V – Mo 催化剂的助剂,表现了良好的助催化性能,通过抑制深度氧化反应的进行,使目标产物烯烃、酸和腈等的收率大幅度提高,但铌助催化效应的作用机制仍不清楚。此外,近年来的研究表明,铌化合物还在光催化制氢、光催化降解有机物、脱除 NO_x 反应、手性催化等方面表现出了特殊的催化活性。国外对于铌的催化作用研究已进行了 25 年以上,国内对铌的催化作用的研究开

展得相对较晚,侧重于研究铌的酸催化性能,无论是深度、广度都与国外同行有一定的差距。深入、广泛地开展铌催化剂的研究,对于开发新的催化剂与催化反应或改进现有的催化过程都具有重要的意义。

参 考 文 献

1 Tanabe K. Application of Niobium Oxides as Catalysts. *Catal Today*, 1990, **8**(1):1~11

2 Tanabe K, Okazaki S. Various Reactions Catalyzed by Niobium Compounds and Materials. *Appl Catal, A*, 1995, **133**(2):191~218

3 Tanabe K. Catalytic Application of Niobium Compounds. *Catal Today*, 2003, **78**(1~4):65~77

4 Nowak I, Ziolek M. Niobium Compounds:Preparation, Characterization, and Application in Heterogeneous Catalysis. *Chem Rev*, 1999, **99**(12):3 603~3 624

5 Ziolek M. Niobium – Containing Catalysts——The State of the Art. *Catal Today*, 2003, **78**(1~4):47~64

6 李应成,岳斌,杨为民等. 铌酸/氧化铌在多相催化反应中的应用. 化学通报, 2005, **68**(3):172~178

7 Jehng J M, Wachs I E. Structural Chemistry and Raman – Spectra of Niobium Oxides. *Chem Mater*, 1991, **3**(1):100~107

8 Ushikubo Takashi, Koike Yasuo, Wada Keisuke, et al. Study of the Structure of Niobium Oxide by X – Ray Absorption Fine Structure and Surface Science Techniques. *Catal Today*, 1996, **28**(1~2):59~69

9 Tanabe K. Niobic Acid as an Unusual Acidic Solid Material. *Mater Chem Phys*, 1987, **17**(1~2):217~225

10 Sun Qing, Auroux A, Shen Jianyi. Surface Acidity of Niobium Phosphate and Steam Reforming of Dimethoxymethane over $CuZnO/Al_2O_3$ – NbP Complex Catalysts. *J Catal*, 2006, **244**(1):1~9

11 Maurer S M, Ko E I. Structural and Acidic Characterization of Niobia Aerogels. *J Catal*, 1992, **135**(1):125~134

12 Armaroli T, Busca G, Carlini C, et al. Acid Sites Characterization of Niobium Phosphate Catalysts and Their Activity in Fructose Dehydration to 5 – Hydroxymethyl – 2 – Furaldehyde. *J Mol Catal A:Chem*, 2000, **151**(1~2):233~243

13 Uekawa N, Kudo T, Mori F, et al. Low – Temperature Synthesis of Niobium Oxide Nanoparticles from Peroxo Niobic Acid Sol. *J Colloid Interf Sci*, 2003, **264**(2):378~384

14 Ristic M, Popovic S, Music S. Sol – Gel Synthesis and Characterization of Nb_2O_5 Powders. *Mater Lett*, 2004, **58**(21):2 658~2 663

15 Kresge C T, Leonowicz M E, Roth W J, et al. Ordered Mesoporous Molecular Sieves Synthesized by a Liquid – Crystal Template Mechanism. *Nature*, 1992, **359**(6 397):710~712

16 Beck J S, Vartuli J C, Roth W J, et al. A New Family of Mesoporous Molecular Sieves Prepared with Liquid Crystal Templates. *J Am Chem Soc*, 1992, **114**(27):10 834~10 843

17 Sayari A, Liu P. Non – Silica Periodic Mesostructured Materials: Recent Progress. *Microporous Mater*, 1997, **12**(4~6):149~177

18 Ciesla U, Schuth F. Ordered Mesoporous Materials. *Microporous Mesoporous Mater*, 1999, **27**(2~3):131~149

19 Schuth F. Non – Siliceous Mesostructured and Mesoporous Materials. *Chem Mater*, 2001, **13**(10):3 184~3 195

20 Antonelli D M, Nakahira A, Ying J Y. Ligand – Assisted Liquid Crystal Templating in Mesoporous Niobium Oxide Molecular Sieves. *Inorg Chem*, 1996, **35**(11):3 126~3 136

21 Antonelli D M, Ying J Y. Synthesis of a Stable Hexagonally Packed Mesoporous Niobium Oxide Molecular Sieve Through a Novel Ligand – Assisted Templating Mechanism. *Angew Chem, Int Edit*, 1996, **35**(4):426~430

22 Antonelli D M. Synthesis of Macro – Mesoporous Niobium Oxide Molecular Sieves by a Ligand – Assisted Vesicle Templating Strategy. *Microporous Mesoporousr Mater*, 1999, **33**(1~3):209~214

23 Hiyoshi Mayako, Lee Byongjin, Lu Daling, et al. Supermicroporous Niobium Oxide as an Acid Catalyst. *Catal Lett*, 2004, **98**(4):181~186

24 Lee Byongjin, Lu Daling, Kondo Junko N, et al. Three – Dimensionally Ordered Mesoporous Niobium oxide. *J Am Chem Soc*, 2002, **124**(38):11 256~11 257

25 Lee Byongjin, Lu Daling, Kondo Junko N, et al. Preparation of Ordered Supermicroporous Niobium Oxide. *Chem Lett*, 2002, (10):1 058~1 059

26 Mal Nawal Kishor, Fujiwara Masahiro. Synthesis of Hexagonal and Cubic Super – Microporous Niobium Phosphates with Anion Exchange Capacity and Catalytic Properties. *Chem Commun*, 2002, (22):2 702~2 703

27 Mal Nawal Kishor, Bhaumik Asim, Kumar Prashant, et al. Microporous Niobium Phosphates and Catalytic Properties Prepared by a Supramolecular Templating Mechanism. *Chem Commun*, 2003, (7):872~873

28 Mal Nawal Kishor, Bhaumik Asim, Fujiwara Masahiro, et al. Novel Organic – Inorganic Hybrid and Organic – Free Mesoporous Niobium Oxophosphate Synthesized in the Presence of an Anionic Surfactant. *Microporous Mesopoousr Mater*, 2006, **93**(1~3):40~45

29 National Institute of Advanced Industrial Science and Technology. Method for Producing Mesoporous Niobium Phosphate and Surfactant – Niobium Phosphate Composite. JP Pat Appl, JP 2003327420. 2003

30 Ziolek M, Nowak I. Synthesis and Characterization of Niobium – Containing MCM – 41. *Zeolites*, 1997, **18**(5~6):356~360

31 Ziolek M, Nowak I, Lavalley J C. Acidity Study of Nb – Containing MCM – 41 Mesoporous Materials. Comparison with that of Al – MCM – 41. *Catal Lett*, 1997, **45**(3~4):259~265

32 Nowak I. Textural and Structural Properties of Niobium – Containing Micro – , Meso – and Macroporous Molecular Sieves. *Colloid Surf,A*, 2004, **241**(1~3):103~111

33 Nowak I, Jaroniec M. Three – Dimensional Cubic Mesoporous

Molecular Sieves of FDU – 1 Containing Niobium: Dependence of Niobium Source on Structural Properties. *Langmuir*, 2005, **21**(2): 755 ~ 760

34 Nowak I, Kilos B, Ziolek M, et al. Epoxidation of Cyclohexene on Nb – Containing Meso – and Macroporous Materials. *Catal Today*, 2003, **78**(1 ~ 4): 487 ~ 498

35 Nowak I, Ziolek M, Jaroniec M. Synthesis and Characterization of Polymer – Templated Mesoporous Silicas Containing Niobium. *J Phys Chem B*, 2004, **108**(12): 3 722 ~ 3 727

36 Hanaoka Takaaki, Takeuchi Kazuhiko, Matsuzaki Takehiko, et al. Solvolysis and Isomerization of Phenyloxirane Catalyzed with Niobic Acid. *Catal Lett*, 1990, **5**(1): 13 ~ 16

37 **上海华谊丙烯酸有限公司. 一种二氢吡喃衍生物水解的铌催化剂及其应用. 中国,** CN 1586722. 2005

38 Gallo J M R, Teixeira S, Schuchardt U. Synthesis and Characterization of Niobium Modified Montmorillonite and Its Use in the Acid – Catalyzed Synthesis of β – Hydroxyethers. *Appl Catal, A*, 2006, 311: 199 ~ 203

39 Prasetyoko D, Ramli Z, Endud S, et al. Preparation and Characterization of Bifunctional Oxidative and Acidic Catalysts Nb_2O_5/TS – 1 for Synthesis of Diols. *Mater Chem Phys*, 2005, **93**(2 ~ 3): 443 ~ 449

40 Li Yingcheng, Yue Bin, Yan Shirun, et al. Preparation of Ethylene Glycol via Catalytic Hydration with Highly Efficient Supported Niobia Catalyst. *Catal Lett*, 2004, **95**(3 ~ 4): 163 ~ 166

41 Li Yingcheng, Yan Shirun, Yue Bin, et al. Selective Catalytic Hydration of Ethylene Oxide over Niobium Oxide Supported on α – Alumina. *Appl Catal, A*, 2004, **272**(1 ~ 2): 305 ~ 310

42 Li Yingcheng, Yan Shirun, Yang Weimin, et al. Effects of Support Modification on Nb_2O_5/α – Al2O3 Catalyst for Ethylene Oxide Hydration. *J Mol Catal A: Chem*, 2005, **226**(2): 285 ~ 290

43 Li Yingcheng, Yan Shirun, Qian Linping, et al. Effect of tin on Nb_2O_5/α – Al_2O_3 Catalyst for Ethylene Oxide Hydration. *J Catal*, 2006, **241**(1): 173 ~ 179

44 **中国石油化工股份有限公司上海石油化工研究院. 用于环氧乙烷水合制乙二醇催化剂的制备方法. 中国,**CN 1751793. 2006

45 Huber G W, Cheda J N, Barrett C J, et al. Production of Liquid Alkanes by Aqueous – Phase Processing of Biomass – Derived Carbohydrates. *Science*, 2005, **308**(5 727): 1 446 ~ 1 450

46 Carlini C, Giuttari M, Maria R G A, et al. Selective Saccharides Dehydration to 5 – Hydroxymethyl – 2 – Furaldehyde by Heterogeneous Niobium Catalysts. *Appl Catal, A*, 1999, **183**(2): 295 ~ 302

47 Dias A S, Lima S, Brandao P, et al. Liquid – Phase Dehydration of D – Xylose over Microporous and Mesoporous Niobium Silicates. *Catal Lett*, 2006, **108**(3 ~ 4): 179 ~ 186

48 Brandao P, Philippou A, Rocha J, et al. Dehydration of Alcohols by Microporous Niobium Silicate AM – 11. *Catal Lett*, 2002, **80**(3 ~ 4): 99 ~ 102

49 de Sairre M I, Bronze – Uhle E S, Donate P M. Niobium(Ⅴ) Oxide: A New and Efficient Catalyst for the Transesterification of β – Keto Esters. *Tetrahedron Lett*, 2005, **46**(15): 2 705 ~ 2 708

50 de la Cruz M H C, da Silva J F C, Lachter E R. Liquid Phase Benzylation of Aromatic Compounds with Benzyl Alcohol Catalyzed by Niobium Phosphate. *Appl Catal, A*, 2003, **245**(2): 377 ~ 382

51 Hino Makoto, Kurashige Mitsuhiko, Arata Kazushi. Synthesis of a Solid Acid of Tungsta – Niobia More Active than Aluminosilicates for Decompositions of Cumene, Ethylbenzene, and Toluene. *Catal Commun*, 2004, **5**(3): 107 ~ 109

52 Yadav J S, Reddy B V S, Eeshwaraiah B, et al. Niobium(Ⅴ) Chloride – Catalyzed C — H Insertion Reactions of α – Diazoesters: Synthesis of β – Keto Esters. *Tetrahedron*, 2005, **61**(4): 875 ~ 878

53 Yadav J S, Narsaiah A V, Basak A K, et al. Niobium Pentachloride: An Efficient Catalyst for the Selective Acetylation of Amines and Thiols Under Mild Conditions. *J Mol Catal A: Chem*, 2006, **255**(1 ~ 2): 78 ~ 80

54 Leelavathi P, Kumar S R. Niobium (Ⅴ) Chloride Catalyzed Knoevenagel Condensation: An Efficient Protocol for the Preparation of Electrophilic Alkenes. *J Mol Catal A: Chem*, 2005, **240**(1 ~ 2): 99 ~ 102

55 Arai Shigeru, Takita Satoshi, Nishida Atsushi. A Facile Synthesis of Vicinal Diamines Promoted by Low – Valent Niobium: Preparation of Chiral Octahydrobiisoquinolines and Their Application to Catalytic Asymmetric Synthesis. *Eur J Org Chem*, 2005, (24): 5 262 ~ 5 267

56 Parvulescu V, Constantin C, Su B L. Liquid Phase Oxidation of Aromatic Hydrocarbons Using Highly Ordered Nb and NbCo – MCM – 41 Nanoreactors. *J Mol Catal A: Chem*, 2003, **202**(1 ~ 2): 171 ~ 178

57 Parvulescu V, Anastasescu C, Constantin C, et al. Mono (V, Nb) or Bimetallic (V – Ti, Nb – Ti) Ions Modified MCM – 41 Catalysts: Synthesis, Characterization and Catalysis in Oxidation of Hydrocarbons (Aromatics and Alcohols). *Catal Today*, 2003, **78**(1 ~ 4): 477 ~ 485

58 Vetrivel S, Pandurangan A. Oxidative Property of Nb – Containing MCM – 41 Molecular Sieves for Vapor Phase Oxidation of *m* – Toluidine. *Catal Lett*, 2005, **99**(3 ~ 4): 141 ~ 150

59 Nowak I, Ziolek M. Effect of Texture and Structure on the Catalytic Activity of Mesoporous Niobosilicates for the Oxidation of Cyclohexene. *Microporous Mesoporous Mater*, 2005, **78**(2 ~ 3): 281 ~ 288

60 Liu Yanyong, Murata Kazuhisa, Inaba Megumu. Synthesis and Catalytic Activity of Niobium – Containing Hexagonal Mesoporous Silica. *Chem Lett*, 2003, **32**(11): 992 ~ 993

61 Somma F, Canton P, Strukul G. Effect of the Matrix in Niobium – Based Aerogel Catalysts for the Selective Oxidation of Olefins with Hydrogen Peroxide. *J Catal*, 2005, **229**(2): 490 ~ 498

62 Somma F, Puppinato A, Strukul G. Niobia – Silica Aerogel Mixed Oxide Catalysts: Effects of the Niobium Content, the Calcination Temperature and the Surface Hydrophilicity on the Epoxidation of Olefins with Hydrogen Peroxide. *Appl Catal, A*,

2006, **309**(1):115~121

63 Bouh A O, Espenson J H. Epoxidation Reactions with Urea – Hydrogen Peroxide Catalyzed by Methyltrioxorhenium (Ⅶ) on Niobia. *J Mol Catal A*:*Chem*, 2003, **200**(1~2):43~47

64 Li Ming, Espenson J H. Kinetic Study of Epoxidations by Urea – Hydrogen Peroxide Catalyzed by Methyltrioxorhenium (Ⅶ) on Niobia. *J Mol Catal A*:*Chem*, 2004, **208**(1~2):123~128

65 Decyk P. States of Transition Metal Ions in Modified Mesoporous MCM – 41 and in Microporous ZSM – 5 Studied by ESR Spectroscopy. *Catal Today*, 2006, **114**(2~3):142~153

66 Vannice M A. The Influence of MSI (Metal – Support Interactions) on Activity and Selectivity in the Hydrogenation of Aldehydes and Ketones. *Top Catal*, 1997, **4**(3~4):241~248

67 Iizuka Tokio, Tanaka Yukari, Tanabe Kozo. Hydrogenation of Carbon Monoxide and Carbon Dioxide over Supported Rhodium Catalysts. *J Mol Catal*, 1982, **17**(2~3):381~389

68 Schmal M, Aranda D A G, Soares R R, et al. A Study of the Promoting Effect of Noble Metal Addition on Niobia and Niobia Alumina Catalysts. *Catal Today*, 2000, **57**(3~4):169~176

69 Mendes F M T, Perez C A C, Noronha F B, et al. TPSR of CO Hydrogenation on $Co/Nb_2O_5/Al_2O_3$ Catalysts. *Catal Today*, 2005, **101**(1):45~50

70 Jasik A, Wojcieszak R, Monteverdi S, et al. Study of Nickel Catalysts Supported on Al_2O_3, SiO_2 or Nb_2O_5 Oxides. *J Mol Catal A*:*Chem*, 2005, **242**(1~2):81~90

71 Ahn In Young, Kim Woo Jae, Moon Sang Heup. Performance of La_2O_3 – or Nb_2O_5 – Added Pd/SiO_2 Catalysts in Acetylene Hydrogenation. *Appl Catal*, *A*, 2006, **308**:75~81

72 dos Santos A C B, Grange P, Faro Jr A C. Effect of Support Sulphidation on the Hydrocracking Activity of Niobia – Supported Nickel and Molybdenum Catalysts. *Appl Catal*, *A*, 1999, **178**(1):29~38

73 Damyanova S, Dimitrov L, Petrov L, et al. Effect of Niobium on the Surface Properties of Nb_2O_5 – SiO_2 – Supported Mo Catalysts. *Appl Surf Sci*, 2003, **214**(1~4):68~74

74 Damyanova S, Andonova S, Stereva I, et al. Molybdenum HDS Catalysts Supported on Niobia – Silica. *React Kinet Catal Lett*, 2003, **79**(1):35~42

75 Gaborit V, Allali N, Danot M, et al. Hydrotreating Properties of Mixed $Nb_xMo_{1-x}S_2$ Alumina Supported Catalysts. *Catal Today*, 2003, **78**(1~4):499~505

76 Caero L C, Romero A R, Ramirez J. Niobium Sulfide as a Dopant for Mo/TiO_2 Catalysts. *Catal Today*, 2003, **78**(1~4):513~518

77 Chary K V R, Lakshmi K S, Murthy M, et al. Hydrodechlorination of 1,2,4 – Trichlorobenzene over Niobia Supported Nickel Catalysts. *Catal Commun*, 2003, **4**(10):531~535

78 Chary K V R, Lakshmi K S, Rao P V R, et al. Characterization and Catalytic Properties of Niobia Supported Nickel Catalysts in the Hydrodechlorination of 1,2,4 – Trichlorobenzene. *J Mol Catal A*:*Chem*, 2004, **223**(1~2):353~361

79 Marques P, Ribeiro N F P, Schmal M, et al. Selective CO Oxidation in the Presence of H_2 over Pt and Pt – Sn Catalysts Supported on Niobia. *J Power Sources*, 2006, **158**(1):504~508

80 Chary K V R, Reddy K R, Bhaskar T, et al. Dispersion and Reactivity of Mo/Nb_2O_5 Catalysts in the Ammoxidation of Toluene to Benzonitrile. *Green Chem*, 2002, **4**(3):206~209

81 Chary K V R, Kumar C P, Murali A, et al. Studies on Catalytic Functionality of V_2O_5/Nb_2O_5 Catalysts. *J Mol Catal A*:*Chem*, 2004, **216**(1):139~146

82 Kumar C P, Reddy K R, Rao V V, et al. Vapour Phase Ammoxidation of Toluene over Vanadium Oxide Supported on Nb_2O_5 – TiO_2. *Green Chem*, 2002, **4**(5):513~516

83 Chary K V R, Kishan G, Kumar C P, et al. Characterization and Reactivity of Vanadium Oxide Catalysts Supported on Niobia. *Appl Catal*, *A*, 2003, **245**(2):303~316

84 Union Carbide Corp. Low Temperature Oxydehydrogenation of Ethane to Ethylene. US Pat Appl, US 4250346. 1980

85 Heracleous E, Lee A F, Wilson K, et al. Investigation of Ni – Based Alumina – Supported Catalysts for the Oxidative Dehydrogenation of Ethane to Ethylene:Structural Characterization and Reactivity Studies. *J Catal*, 2005, **231**(1):159~171

86 Heracleous E, Lemonidou A A. Ni – Nb – O Mixed Oxides as Highly Active and Selective Catalysts for Ethene Production via Ethane Oxidative Dehydrogenation. Part Ⅰ:Characterization and Catalytic Performance. *J Catal*, 2006, **237**(1):162~174

87 Heracleous E, Lemonidou A A. Ni – Nb – O Mixed Oxides as Highly Active and Selective Catalysts for Ethene Production via Ethane Oxidative Dehydrogenation. Part Ⅱ:Mechanistic Aspects and Kinetic Modeling. *J Catal*, 2006, **237**(1):175~189

88 Xie Qi, Chen Luqian, Weng Weizheng, et al. Preparation of MoVTe(Sb)Nb Mixed Oxide Catalysts Using a Slurry Method for Selective Oxidative Dehydrogenation of Ethane. *J Mol Catal A*:*Chem*, 2005, **240**(1~2):191~196

89 Karamullaoglu G, Onen S, Dogu T. Oxidative Dehydrogenation of Ethane and Isobutane with Chromium – Vanadium – Niobium Mixed Oxide Catalysts. *Chem Eng Process*, 2002, **41**(4):337~347

90 Ballarini N, Calestani G, Catani R, et al, The Synthesis, Characterization and Use of Metal Niobates as Catalysts for Propane Oxidehydrogenation. *Stud Surf Sci Catal*,2005, **155**:81~94

91 Moggi P, Devillers M, Ruiz P, et al. Oxidative Dehydrogenation of Propane on Pure and Silica – Dispersed Multimetallic Oxides Based on Vanadium and Niobium Prepared via Hydrolytic and Non – Hydrolytic Sol – Gel Methods. *Catal Today*, 2003, **81**(2):77~85

92 Sarzi – Amade M, Morselli S, Moggi P, et al. The Effect of Sol – Gel Promoters on the Characteristics of Mixed V – Nb Oxides and Their Catalytic Properties in Propane Oxidative Dehydrogenation. *Appl Catal*, *A*, 2005, **284**(1~2):11~20

93 Mitsubishi Chemical Corp. Production of Nitrile. JP Pat Appl, JP 5279313. 1993

94 Mitsubishi Chemical Corp. Preparation of Mixed Metal Oxide Catalysts and Preparation of Acrylic Acid from Propane by

Using the Catalysts. JP Pat Appl, JP 1057813. 1998

95 Lin M M. Selective Oxidation of Propane to Acrylic Acid with Molecular Oxygen. *Appl Catal*, *A*, 2001, **207**(1 ~ 2): 1 ~ 16

96 Botella P, Concepcion P, Lopez Nieto J M, et al. The Influence of Te – Precursor in Mo – V – Te – O and Mo – V – Te – Nb – O Catalysts on Their Catalytic Behavior in the Selective Propane Oxidation. *Catal Today*, 2005, **99**(1 ~ 2): 51 ~ 57

97 Gaffney A M, Chaturvedi S, Clark M B, et al. Characterization and Catalytic Studies of PVD Synthesized Mo/V/Nb/Te Oxide Catalysts. *J Catal*, 2005, **229**(1): 12 ~ 23

98 Holmberg J, Grasselli R K, Andersson A. Catalytic Behavior of M1, M2, and M1/M2 Physical Mixtures of the Mo – V – Nb – Te – Oxide System in Propane and Propene Ammoxidation. *Appl Catal*, *A*, 2004, **270**(1 ~ 2): 121 ~ 134

99 Ueda W, Vitry D, Katou T. Crystalline MoVO Based Complex Oxides as Selective Oxidation Catalysts of Propane. *Catal Today*, 2005, **99**(1 ~ 2): 43 ~ 49

100 Baca M, Pigamo A, Dubois J L, et al. Fourier Transform Infrared Spectroscopic Study of Surface Acidity by Pyridine Adsorption on the M1 Active Phase of the MoVTe(Sb)NbO Catalysts Used in Propane Oxidation. *Catal Commun*, 2005, **6**(3): 215 ~ 220

101 Guerrero – Perez M O, Al – Saeedi J N, Guliants V V, et al. Catalytic Properties of Mixed Mo – V – Sb – Nb – O Oxides Catalysts for the Ammoxidation of Propane to Acrylonitrile. *Appl Catal*, *A*, 2004, **260**(1): 93 ~ 99

102 Guliants V V, Bhandari R, Swaminathan B, et al. Roles of Surface Te, Nb, and Sb Oxides in Propane Oxidation to Acrylic Acid over Orthorhombic Mo – V – O Phase. *J Phys Chem B*, 2005, **109**(50): 24 046 ~ 24 055

103 Ballarini N, Cavani F, Cimini M, et al. Role of Nb in Rutile – Type Cr/V/Sb/Nb Mixed Oxides, Catalysts for Propane Ammoxidation to Acrylonitrile. *J Catal*, 2006, **241**(2): 255 ~ 267

104 Grasselli R K, Burrington J D, Buttrey D J, et al. Multifunctionality of Active Centers in (Amm) Oxidation Catalysts: From Bi – Mo – O_x to Mo – V – Nb – (Te, Sb) – O_x. *Top Catal*, 2003, **23**(1 ~ 4): 5 ~ 22

105 Grasselli R K, Buttrey D J, Burrington J D, et al. Active Centers, Catalytic Behavior, Symbiosis and Redox Properties of MoV(Nb, Ta)TeO Ammoxidation Catalysts. *Top Catal*, 2006, **38**(1 ~ 3): 7 ~ 16

106 Roussel M, Bouchard M, Bordes – Richard E, et al. Oxidation of Ethane to Ethylene and Acetic Acid by MoVNbO Catalysts. *Catal Today*, 2005, **99**(1 ~ 2): 77 ~ 87

107 Roussel M, Bouchard M, Karim K, et al. MoVO – Based Catalysts for the Oxidation of Ethane to Ethylene and Acetic Acid——Influence of Niobium and/or Palladium on Physicochemical and Catalytic Properties. *Appl Catal*, *A*, 2006, **308**: 62 ~ 74

108 Pries de Oliveira P G, Eon J G, Chavant M, et al. Modification of Vanadium Phosphorus Oxides Used for n – Butane Oxidation to Maleic Anhydride by Interaction with Niobium Phosphate. *Catal Today*, 2000, **57**(3 ~ 4): 177 ~ 186

109 de Farias A M D, Gonzalez W D, de Oliveira P G P, et al. Vanadium Phosphorus Oxide Catalyst Modified by Niobium Doping for Mild Oxidation of n – Butane to Maleic Anhydride. *J Catal*, 2002, **208**(1): 238 ~ 246

110 Galownia J M, Wight A P, Blanc A, et al. Partially Reduced Heteropolyanions for the Oxidative Dehydrogenation of Ethane to Ethylene and Acetic Acid at Atmospheric Pressure. *J Catal*, 2005, **236**(2): 356 ~ 365

111 Holles J H, Dillon C J, Labinger J A, et al. A Substrate – Versatile Catalyst for the Selective Oxidation of Light Alkanes Ⅰ. *Reactivity. J Catal*, 2003, **218**(1): 42 ~ 53

112 Domen Kazunari, Kudo Akihiko, Shinozaki A, et al. Photodecomposition of Water and Hydrogen Evolution from Aqueous Methanol Solution over Novel Niobate Photocatalysts. *J Chem Soc*, *Chem Commun*, 1986, (4): 356 ~ 357

113 Domen Kazunari, Kudo Akihiko, Tanaka Akira, et al. Overall Photodecomposition of Water on a Layered Niobiate Catalyst. *Catal Today*, 1990, **8**(1): 77 ~ 84

114 Abe Ryu, Higashi Masanobu, Sayama Kazuhiro, et al. Photocatalytic Activity of R_3MO_7 and $R_2Ti_2O_7$ (R = Y, Gd, La; M = Nb, Ta) for Water Splitting into H_2 and O_2. *J Phys Chem B*, 2006, **110**(5): 2 219 ~ 2 226

115 Tian Mengkui, Shangguan Wenfeng, Yuan Jian, et al. $K_4Ce_2M_{10}O_{30}$ (M = Ta, Nb) as Visible Light – Driven Photocatalysts for Hydrogen Evolution from Water Decomposition. *Appl Catal*, *A*, 2006, **309**(1): 76 ~ 84

116 Ikeda Shigeru, Fubuki Minori, Takahara Yoshiko K, et al. Photocatalytic Activity of Hydrothermally Synthesized Tantalate Pyrochlores for Overall Water Splitting. *Appl Catal*, *A*, 2006, **300**(2): 186 ~ 190

117 Wang Xueguang, Hou Wenhua, Wang Xiaoshu, et al. Preparation, Characterization and Activity of Novel Silica – Pillared Layered Titanoniobate Supported Copper Catalysts for the Direct Decomposition of NO. *Appl Catal*, *B*, 2002, **35**(3): 185 ~ 193

118 Mitadera Jun, Hinode Hirofumi. Catalytic Reduction of Nitric Monoxide by Ethene over Nb/TiO_2 in the Presence of Excess Oxygen. *Appl Catal*, *B*, 2002, **39**(3): 205 ~ 210

119 Zhang Fengli, Zheng Qi, Wei Kemei, et al. Improved Performance of Au/Fe_2O_3 Catalysts Promoted with ZrO_2 and Nb_2O_5 in the WGS Reaction Under Hydrogen – Rich Conditions. *Catal Lett*, 2006, 108(3 ~ 4): 131 ~ 136

120 Ramirez – Cabrera E, Laosiripojana N, Atkinson A, et al. Methane Conversion over Nb – DopZed Ceria. *Catal Today*, 2003, **78**(1 ~ 4): 433 ~ 438

121 Hur Su Gil, Kim Tae Woo, Hwang Seong Ju. Synthesis of New Visible Light Active Photocatalysts of $Ba(In_{1/3}Pb_{1/3}M'_{1/3})O_3$ (M′ = Nb, Ta): A Band Gap Engineering Strategy Based on Electronegativity of a Metal Component. *J Phys Chem B*, 2005, **109**(31): 15 001 ~ 15 007

122 Muktha B, Priya M H, Madras G, et al. Synthesis, Structure, and Photocatalysis in a New Structural Variant of the Aurivillius

Phase：$LiBi_4M_3O_{14}$（M = Nb，Ta）. *J Phys Chem B*，2005，**109**（23）：11 442～11 449

123 Kobayashi Shu，Arai Kenzo，Shimizu Haruka，et al. A Novel Dinuclear Chiral Niobium Complex for Lewis Acid Catalyzed Enantioselective Reactions：Design of a Tridentate Ligand and Elucidation of the Catalyst Structure. *Angew Chem*，*Int Edit*，2005，**44**（5）：761～764

（编辑 赵红雁）

Publication IV

Available online at www.sciencedirect.com
ScienceDirect
Applied Catalysis A: General xxx (2007) xxx–xxx
APPLIED CATALYSIS A: GENERAL
www.elsevier.com/locate/apcata

Structural, acidic and redox properties of V_2O_5/NbP catalysts

Qing Sun [a,b], Dongmei Fang [a], Suming Wang [a], Jianyi Shen [a,*], Aline Auroux [b,**]

[a] *Laboratory of Mesoscopic Chemistry, School of Chemistry and Chemical Engineering, Nanjing University, Nanjing 210093, China*
[b] *Institut de recherches sur la catalyse et l'environnement de Lyon, UMR 5256, CNRS–Université Lyon 1, 2 avenue Albert-Einstein, 69626 Villeurbanne cedex, France*

Received 21 March 2007; received in revised form 7 May 2007; accepted 8 May 2007

Abstract

V_2O_5 supported on niobium phosphate (NbP) with V_2O_5 loadings from 5 to 25 wt% were investigated by using different techniques. The structural properties were characterized by O_2 chemisorption, X-ray diffraction (XRD), Raman spectroscopy (LRS) and X-ray photoelectron spectroscopy (XPS). The surface acidity was determined by the techniques of microcalorimetry and infrared spectroscopy (FTIR) using NH_3 as a probe molecule. Isopropanol (IPA) and methanol probe reactions in the presence of O_2 were employed to provide the information about the surface acidity and redox property simultaneously. V_2O_5 is well dispersed on the surface of NbP according to the results from XRD and LRS with a V_2O_5 loading lower than 15 wt%. The vanadium and niobium elements in V_2O_5/NbP catalysts were present in the +5 oxidization state as observed from XPS. Chemical adsorption of O_2 showed that vanadia dispersed on NbP with about 60% dispersion. The results from NH_3 adsorption microcalorimetry suggested that the loaded V_2O_5 weakened the surface acidity of NbP while increased the proportion of weak acid sites. The results from IPA conversion reaction pointed out that IPA only converted to dehydration products (propylene (PPE) and diisopropyl ether (DIPE)) on NbP. The addition of V_2O_5 on NbP led to an oxidative product acetone (ACE), but not as much as on bulk V_2O_5. These results indicated that NbP possessed only surface acidity and weakened the redox property of supported V_2O_5. Accordingly, NbP produced only dimethyl ether (DME) from the dehydration of methanol owing to the lack of redox property, while the V_2O_5/NbP catalysts produced mainly dimethoxymethane (DMM) due to its acidic-redox bi-functional character. Specifically, methanol was first oxidized on the redox sites of V_2O_5/NbP to produce formaldehyde (FA) which was then condensed with additional methanol on the acidic sites of V_2O_5/NbP to form DMM.

Keywords: V_2O_5/NbP catalyst; Adsorption microcalorimetry; Acidic and redox properties; Isopropanol probe reaction; Methanol probe reaction

1. Introduction

Supported vanadia are extensively used as industrial catalysts for various processes such as selective oxidation of methanol to formaldehyde (FA) [1] and methyl formate (MF) [2], selective oxidation of o-xylene to phthalic anhydride [3,4], ammoxidation of alkyl aromatic hydrocarbons [5,6], removal of NO_x and SO_x [7], oxidation of SO_2 to SO_3 [8], selective catalytic reduction (SCR) of nitric oxides [9], etc.

Due to the restrictions of thermal stability, mechanical strength and surface area of bulk V_2O_5, it is generally not used directly as a catalyst in industry. It is usually supported on different carriers for different purposes. With a suitable support, its surface area, thermal stability and mechanical strength could be improved [10]. Studies indicated that the intensive interactions between a support and V_2O_5, and the dispersion and surface structures as well as the redox and acid-base properties of V_2O_5 would be modified by supports [11,12]. Hence, the supported V_2O_5 are sometimes used as model catalysts [13]. In fact, by employing different supports (such as SiO_2, Al_2O_3 and TiO_2) and loadings, the surface structure [14,15] and number of surface sites as well as the surface acid-base [16–18] and redox properties [19] can be intentionally monitored. The catalytic properties of the active vanadia phase can be greatly influenced by the nature of support and the dispersion of active components.

Nb_2O_5 is a solid acid that can be used as a support or a promoter in various catalysts [20]. The surface acidity could be enhanced by addition of P to form niobium phosphate (NbP) [21]. In recent years, the dispersion and structure of V_2O_5/Nb_2O_5 catalysts have been studied by using different spectroscopic techniques, such as X-ray diffraction (XRD), 51V NMR

* Corresponding author. Tel.: +86 25 83594305; fax: +86 25 83594305.
** Corresponding author.
E-mail address: jyshen@nju.edu.cn (J. Shen).

0926-860X/$ – see front matter © 2007 Elsevier B.V. All rights reserved.
doi:10.1016/j.apcata.2007.05.016

[22–24], X-ray photoelectron spectroscopy (XPS) [25], infrared spectroscopy (FTIR) [26], Raman spectroscopy (LRS) [26], EPR [27] and LEIS [28]. Their catalytic behavior in selective oxidation reactions was also studied [25–31]. In this work, we used niobium phosphate to support vanadia. The acidic and redox properties as well as the structure of the catalysts with different loadings were characterized. Specifically, the surface acidity was characterized by employing NH_3 adsorption microcalorimetry and infrared spectroscopy, while the surface acidic and redox properties were probed by the reactions of isopropanol conversion and methanol oxidation in the presence of O_2. The purpose of this work was to determine the relation between acidic-redox properties and dispersion of V_2O_5 on NbP.

2. Experimental

2.1. Catalyst preparation

The niobium phosphate supports were prepared as described in the literature [32]. Specifically, 2.73 g of $NbCl_5$ (Alfa Aesar, 99%) was partially hydrolyzed in 50 ml of H_2O, followed by the addition of 2.30 g of H_3PO_4 (Aldrich, 85% aqueous solution) to initiate a vigorous hydrolytic reaction. An additional 50 ml of H_2O was then added, and the reaction mixture was stirred for 30 min. The pH of the reaction mixture was adjusted to 2.60 with an ammonia solution. After stirring, the slurry was filtered and washed with deionized water to obtain a chlorine-free gel. The gel was mixed with 10 ml of H_2O and 1.45 g of hexadecylamine (Aldrich, 90%) and stirred for 30 min. Then 0.92 g H_3PO_4 (85%) was added, and the pH of the mixture was adjusted to 3.88. After mixing was complete, the slurry was heated in a Teflon-lined stainless steel autoclave at 338 K under autogenous pressure for two days. The final product was filtered, washed with deionized water, dried at 373 K overnight, and calcined at 723 K in air for 40 h.

The V_2O_5/NbP catalysts with various loadings (5–25 wt% of V_2O_5) were prepared by using the incipient wetness impregnation method. Specifically, for each preparation, a known amount of NbP was added into the aqueous solution containing the desired amount of vanadium oxalate and stirred. After being kept at room temperature overnight, it was dried at 383 K overnight and then calcined in air at 673 K for 5 h. A comparative sample of bulk V_2O_5 was obtained from the calcination of ammonium metavanadate in air at 673 K for 5 h.

2.2. Catalyst characterization

The X-ray diffraction measurements were carried out on a Bruker D5005 diffractometer scanning from 3° to 80° (2θ) at a rate of 0.02° s^{-1} using a Cu Kα radiation (λ = 0.15418 nm) source. The applied voltage and current were 50 kV and 35 mA, respectively. Elemental analysis was performed using the ICP atomic emission spectroscopy (Spectroflame-ICP D, Spectro). The surface areas were measured by nitrogen adsorption at 77 K after heat pretreatment under vacuum at 623 K for 4 h.

The X-ray photoelectron spectra were measured on a SSI 301 instrument equipped with a hemispherical electron analyzer and an Al anode (Al Kα = 1486.6 eV) powered at 100 W. The residual pressure in the spectrometer chamber was 5×10^{-8} Pa during data acquisition.

The skeletal FTIR spectra were recorded with a Bruker Vector 22 FTIR spectrophotometer (DTGS detector). The range, resolution and acquisition applied were 4000–400, 2 cm^{-1} and 100 scans, respectively. In each experiment, 2 mg of sample were mixed with 198 mg of KBr. A spectrum was recorded at room temperature.

Raman spectra were obtained using a Dilor XY spectrometer coupled to an Olympus BH-2 microscope. The excitation was provided by the 514.5 nm line of an Ar^+ ion laser (Spectra Physics) employing a laser power of 2.5 mW. The range and resolution applied were 100–1100 cm^{-1} and 0.5 cm^{-1}, respectively.

H_2-TPR measurements were carried out with a continuous mode using a U-type quartz microreactor (3.5 mm in diameter). A sample of about 50 mg was contacted with a H_2:N_2 mixture (5.13% volume of H_2 in N_2) at a total flow rate of 40 ml min^{-1}. The sample was heated at a rate of 10 K min^{-1} from room temperature to 1073 K. The hydrogen consumption was monitored using a thermal conductive detector (TCD). The reducing gas was first passed through the reference arm of the TCD before entering the reactor. The reactor exit was directed through a trap filled with $Mg(ClO_4)_2$ (to remove produced water) and then to the second arm of the TCD.

The dispersion of vanadium species was measured by using the high temperature oxygen chemisorption method (HTOC) [33]. A sample was reduced in flowing H_2 at 640 K for 2 h, and then oxygen uptake was measured at the same temperature.

The microcalorimetric studies of ammonia adsorption were performed at 423 K in a heat flow calorimeter (C80 from Setaram) linked to a conventional volumetric apparatus equipped with a Barocel capacitance manometer for pressure measurements. Ammonia used for measurements (purity > 99.9%) was purified by successive freeze–pump–thaw cycles. About 100 mg of sample was pretreated in a quartz cell under evacuation overnight at 623 K. The differential heats of adsorption were measured as a function of coverage by repeatedly introducing small doses of ammonia gas onto the catalyst until an equilibrium pressure of about 66 Pa was reached. The sample was then outgassed for 30 min at the same temperature and a second adsorption was performed at 423 K until an equilibrium pressure of about 27 Pa was attained in order to calculate the irreversibly chemisorbed amount of ammonia at this pressure.

The NH_3 adsorption infrared spectra were recorded with a Bruker Vector 22 FTIR spectrophotometer (DTGS detector). The range, resolution and acquisition applied were 4000–400, 2 cm^{-1} and 50 scans, respectively. The self-supporting wafer (10–30 mg, 18 mm diameter) was first activated in situ in the IR cell at 673 K in flowing O_2 for 12 h, evacuated at the same temperature for 2 h, and then exposed to NH_3 (purity > 99.9%) at room temperature for 5 min. The desorption was carried out by evacuation for 30 min each at room temperature, 323, 373, 473,

523, 573 and 673 K, respectively. A spectrum was recorded at room temperature after desorption at each temperature.

2.3. Catalytic reaction

Isopropanol conversion probe reaction was used to characterize the surface acidity. The probe reaction was carried out in a fixed-bed glass tube reactor. About 100 mg sample was loaded for each reaction. Isopropanol was introduced to the catalysts by bubbling air through a glass saturator filled with isopropanol maintained at 295 K. Isopropanol and reaction products were analyzed by an online gas chromatograph, using a PEG 20M packed column connected to a flame ionization detector (FID). Each catalyst was pretreated by heating in air at 673 K for 1 h and then cooled in the same flow to the reaction temperature. After that, the isopropanol was introduced to the catalyst. Then, the tail gas was analyzed after 0.5 h of isopropanol stream in isothermal reaction conditions. At each reaction temperature, four successive doses of tail gas were analyzed and the total reaction time was 1.5 h.

The oxidation of methanol was carried out in a fixed-bed microreactor made of glass with an inner diameter of 6 mm. The methanol was introduced to the reaction zone by bubbling O_2/N_2 (1/5) through a glass saturator filled with methanol (99.9%) maintained at 278 K. In each test, 0.2 g catalyst was loaded, and the gas hourly space velocity (GHSV) was 11400 ml g^{-1} h^{-1}. The feed composition was maintained as methanol:O_2:N_2 = 1:3:15 (v/v). The tail gas out of the reactor was analyzed by an on-line GC equipped with an FID detector and a TCD detector. The column used was PORAPAK N for the separation of methanol, DMM and other organic compounds. The gas lines were kept at 373 K to prevent condensation of the reactant and products. The reaction was carried out at atmospheric pressure. Each catalyst was pretreated by heating in air at 673 K for 1 h and then cooled in the same flow to the reaction temperature. At each reaction temperature, the reaction time was the same as that for isopropanol conversion reaction.

3. Results and discussion

3.1. Surface structures

The XRD patterns of NbP and V_2O_5/NbP samples are presented in Fig. 1. It can be seen from the figure that all the samples showed two broad peaks with 2θ located around 25 and 52° typical of amorphous NbP [34]. No other crystalline niobia phases were observed in this work. The absence of XRD peaks due to V_2O_5 for 5V/NbP and 15V/NbP samples indicates that vanadium oxide is present in a highly dispersed manner on the surface of NbP, while weak signs of V_2O_5 were observed for 25V/NbP sample, suggesting the appearance of crystalline V_2O_5 above this loading. Chary et al. observed the formation of β-$(Nb,V)_2O_5$ phase for V_2O_5/Nb_2O_5 samples with high V_2O_5 loading [25]. Wadsley and Andersson reported that in this β-phase vanadium replaces the niobium present in isolated tetrahedral sites at the junction of blocks of NbO_6 octahedra [35]. In this work, we did not observe any peak for this β-$(Nb,V)_2O_5$ phase. However, the presence of crystallites with size less than 4 nm cannot be excluded which is beyond the detection capacity of the powder XRD technique.

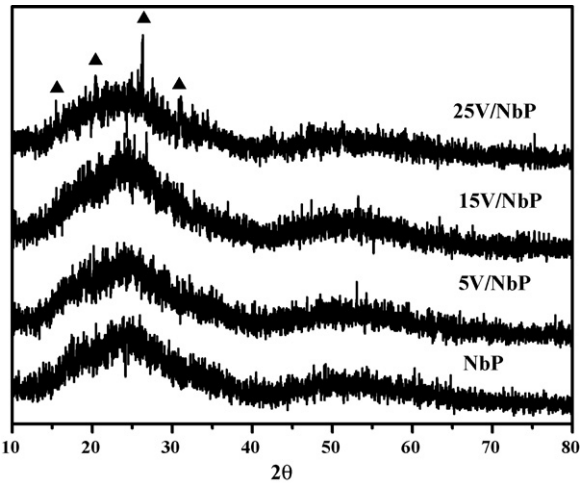

Fig. 1. X-ray diffraction (XRD) patterns of NbP and V_2O_5/NbP catalysts. (▲) Reflections due to crystalline V_2O_5.

The surface areas of the catalysts are given in Table 1. The support NbP, obtained by using a template had a BET surface area of 280 m^2 g^{-1}. The surface areas of supported V_2O_5 samples decreased with the increase of V_2O_5 loading. The decrease of surface area might primarily be due to some pore blocking of NbP by the vanadia species, since there is no new compound formed after calcination of the V_2O_5/NbP samples according to the XRD results. The bulk V_2O_5 sample prepared by decomposition of ammonium metavanadate had low surface area.

Table 1
Surface areas, O_2 uptakes, densities of adsorbed O, and calculated densities of V on the surface of NbP and V_2O_5/NbP catalysts

Catalyst	V_2O_5 loading on NbP (wt/wt%)	S_{BET} (m^2/g)	O_2 uptake (mmol/g)[a]	O density measured (O/nm^2)[b]	O density calculated (V/nm^2)[c]	V dispersion
NbP	0	280	0	–	–	–
5V/NbP	5	201	0.159	0.95	1.56	61%
15V/NbP	15	162	0.472	3.5	5.56	63%
25V/NbP	25	121	0.741	7.4	13.1	56%
V_2O_5	100	5	n.a.[d]	n.a.[d]	n.a.[d]	n.a.[d]

[a] Reduction of samples by H_2 and O_2 adsorption were both performed at 640 K.
[b] Supposing that each surface V adsorbs an oxygen atom.
[c] Supposing that all the vanadium atoms are located on the surface.
[d] Not available.

The monolayer dispersion capacity for V_2O_5 can be calculated [36]. In this work, we prepared the catalysts with different loadings (5–25%) in order to investigate the dispersion of V_2O_5 on NbP. The dispersion strongly depends on the preparation method and interactions between the support and supported species. V_2O_5 may not be dispersed monolayerly even if the loading is lower than the monolayer dispersion capacity.

Oxygen adsorption can be used to evaluate the dispersion of a metal oxide on the surface of a support. Parekh and Weller [37,38] proposed a low temperature oxygen adsorption method (LTOC) while Oyama et al. [33] suggested a high temperature oxygen adsorption method (HTOC). It was also suggested that the HTOC might propose less possibility for the bulk reduction and yield reasonably better values of dispersion [39], and therefore, we adopted this method for the measurements of vanadium dispersion in this work.

Table 1 gives the density of surface oxygen atom obtained in this way. NbP itself did not adsorb any O_2 after H_2 pretreatment at 640 K, indicating its nonredox property. Addition of V_2O_5 generated the O_2 uptake, which amount increased with increasing V_2O_5 loading and reached a maximum (0.741 mmol g^{-1}) at the loading of 25 wt%.

It was possible to estimate the surface V density (SVD) and V_2O_5 dispersion by supposing a 1/1 ratio for O/V. The SVD measured for 5V/NbP, 15V/Nb and 25V/NbP samples were 0.95, 3.5 and 7.4 V nm^{-2}, respectively. Dispersion is defined as the fraction of total oxygen atoms to total vanadium atoms in the sample. Thus, the corresponding V_2O_5 dispersions were 61, 63 and 56%, respectively, which indicated that vanadia was highly dispersed on the support even if it did not reach 100% at 5 wt% loading of V_2O_5. These results are in agreement with those from XRD. A similar high dispersion of vanadia was also observed on Nb_2O_5 [25] and TiO_2 [40]. Wadsley and Andersson [35] suggested vanadium replaced the niobium present in isolated tetrahedral sites at the junction of blocks of NbO_6 octahedra with formation of β-$(Nb,V)_2O_5$ phase. Therefore, the number of surface vanadium species titrated might decrease.

The skeletal IR spectra are reported in Fig. 2. A broad band around 1000 cm^{-1} was observed for all samples, which could be assigned to the O=P=O asymmetric stretching mode of phosphate or polyphosphate species [34]. In addition, all the samples exhibited a broad band around 626 cm^{-1}, probably due to the Nb–O–Nb stretching mode related to the slightly disordered octahedral NbO_6 [34]. There were three additional bands detected for 25V/NbP sample which were located at 1010, 838 and 480 cm^{-1}, respectively. The band at 1010 cm^{-1} could be assigned to $(V{=}O)^{3+}$ double bond stretching mode [41,42]. The bands at 838 and 480 cm^{-1} are due to the asymmetric stretching mode [43] and the rotation mode of V–O–V vibrations [44], respectively. The spectra due to V_2O_5 phase was observed only at 25 wt% V_2O_5 loading. These data suggested that V_2O_5 was highly dispersed on the surface of NbP at low V_2O_5 loading, in good agreement with those from XRD.

The Raman spectra of V_2O_5/NbP samples are presented in Fig. 3. For 5V/NbP and 15V/NbP samples, a strong broad vibration around 700 cm^{-1} might be due to the electronic defects corresponding to the presence of amorphous NbP [45].

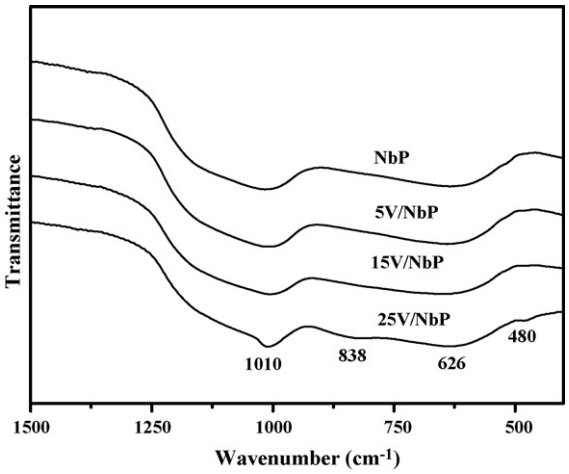

Fig. 2. FTIR skeletal spectra of NbP and V_2O_5/NbP catalysts. (2 mg sample in 198 mg KBr).

A weak Raman band was present around 1014 cm^{-1}, characteristic of the terminal V=O bond of the surface vanadium oxide species [46]. The intensity of this band increased with the V_2O_5 loading, which might suggest the higher population of V=O species with the increase of V_2O_5. The band of V=O stretching vibration shifted from 1014 to 1028 cm^{-1} with the V_2O_5 amount increasing from 5 to 15 wt%, which could be ascribed to distortions of the surface VO_x species with extent of polymerization as suggested by Zhao et al. [26]. In addition, it seemed that there was a very weak broad band centered around 933 cm^{-1} for 15V/NbP sample, which might arise from bridging V–O–V or V–O–Nb bond [26]. For the sample with 25 wt% V_2O_5 loading, the Raman features for crystalline V_2O_5 with bands around 994, 701, 526, 403, 302 and 284 cm^{-1} were presented. The absence of the bands due to V=O and V–O–V vibrations did not mean that only crystalline V_2O_5 existed for 25V/NbP sample since Raman response is much more sensitive for crystalline phase. The Raman spectra for V_2O_5/NbP samples demonstrated that at low V_2O_5 loading, V_2O_5 was highly dispersed on NbP. Crystalline V_2O_5 began to appear when V_2O_5 loading increased to 25 wt%, which is in agreement with the results of XRD and skeletal IR.

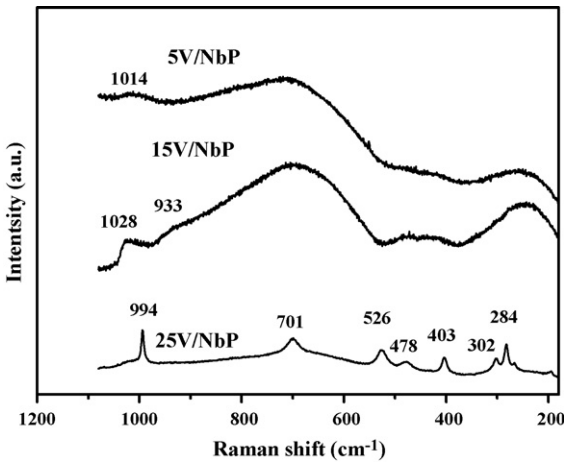

Fig. 3. Raman spectra of V_2O_5/NbP catalysts.

Table 2
Binding energies, V/Nb atomic ratios for surface and bulk composition of NbP and V_2O_5/NbP samples

Catalyst	Binding energy (eV)				V/Nb (surface atomic ratio)	V/Nb (bulk atomic ratio)
	O 1s	V $2p_{3/2}$	Nb $3d_{5/2}$	P 2p		
NbP	531.2	–	207.2	133.1	–	–
5V/NbP	531.2	517.2	207.1	133.1	0.11/1	0.10/1
15V/NbP	531.1	517.3	207.1	133.0	0.38/1	0.32/1
25V/NbP	530.7	517.3	207.1	133.0	0.81/1	0.64/1

Table 3
Number and strength of acid sites as determined by NH_3 adsorption at 423 K

Sample	V_{tot} (67 Pa) (μmol g^{-1})[a]	V_{tot} (27 Pa) (μmol g^{-1})[b]	V_{irr} (27 Pa) (μmol g^{-1})[c]	Q_{init} (kJ mol^{-1})[d]	Q_{int} (27 Pa) (J g^{-1})[e]
NbP	644	532	277	169	56.2
5V/NbP	641	510	233	168	51.3
15V/NbP	547	411	169	165	41.3
25V/NbP	426	332	128	151	31.8

[a] Total amount of NH_3 retained as determined at 67 Pa of equilibrium pressure.
[b] Total amount of NH_3 retained as determined at 27 Pa of equilibrium pressure.
[c] "Irreversible" amount of NH_3 retained as determined from the difference between the amounts adsorbed in the first and second adsorptions at 27 Pa, which represents the amount of strong sites.
[d] Heat evolved from the first NH_3 dose.
[e] Integral heat evolved at 27 Pa of NH_3 equilibrium pressure.

The results of binding energies (BE) as well as the surface and bulk V/Nb ratio from XPS and chemical analysis are shown in Table 2. The C 1s peak at 284.6 eV was used as an internal standard for correction of binding energies. The binding energies of V $2p_{3/2}$ for 5V/NbP, 15V/NbP and 25V/NbP samples are 517.2, 517.3 and 517.3 eV, respectively. Literature data show that the binding energy for V^{5+} in V_2O_5 is between 517.4 and 516.4 eV, while it is between 515.7 and 515.4 eV for V^{4+} in V_2O_4 [47]. Thus, the values indicated that the vanadia surface species were fully oxidized (oxidation state V^{5+}). The binding energy for O anions shifted negatively with the increasing of V_2O_5 loading which might be ascribed to the formation of V–O–Nb bond. NbP and V_2O_5/NbP catalysts showed similar Nb $3d_{5/2}$ and P 2p binding energy values around 207.1 and 131.1 eV suggesting the presence of one type of Nb cation and one type of P cation, which agree well with the results in the literature [25]. The bands for Nb and P were weakened with increasing V_2O_5 loading indicating an increasing coverage of NbP by V_2O_5 (figures are not given). In addition, XPS and chemical analysis results showed that surface vanadia might be enriched in comparison with the global vanadia amount of the samples (See Table 2).

3.2. Surface acidity

Ammonia adsorption microcalorimetry measurements were carried out to determine the number, strength and strength distribution of the surface acid sites of the catalysts [48]. The surface acidity in terms of number of acid sites and site strengths was titrated by adsorption microcalorimetry of ammonia and the results are presented in Fig. 4. The initial heat and saturation coverage for ammonia adsorption on NbP used in this work was found to be about 169 kJ mol^{-1} and 644 mol g^{-1}, which indicated that NbP was a fairly strong solid acid in agreement with those results from Hammett titration [49]. The acidic and adsorption properties of commercial Nb_2O_5 and NbP have been extensively studied by microcalorimetry adsorption of different probe molecules [50]. Addition of V_2O_5 decreased both the initial heat and the coverage for NH_3 adsorption. Specifically, the initial heats were 168, 165 and 151 kJ mol^{-1} and the saturation coverages for NH_3 adsorption were 641, 547 and 426 μmol g^{-1} for 5V/NbP, 15V/NbP and 25V/NbP, respectively, which suggested that the surface acidity decreased with the increase of V_2O_5 loading. In addition, both the number of the total population of acid sites ($V_{NH_3,\,tot}$) and that of strong sites ($V_{NH_3,\,irr}$) decreased (see Table 3). Surely, the weakness of surface acidity should be due to the decrease of the surface area. Moreover, the coverage by V_2O_5 gave rise to vanadium centers which are probably

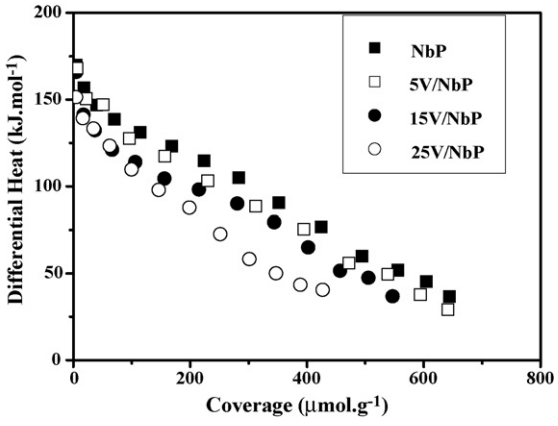

Fig. 4. Differential heat vs. coverage (in μmol per gram of catalyst) for NH_3 adsorption at 423 K over NbP and V_2O_5/NbP catalysts.

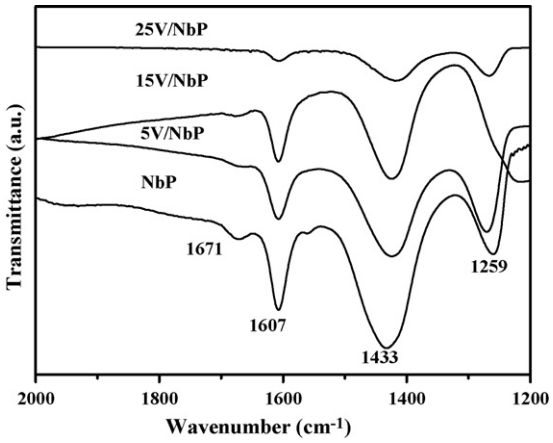

Fig. 5. FTIR spectra for NH_3 adsorption and desorption at 300 K on NbP and V_2O_5/NbP catalysts.

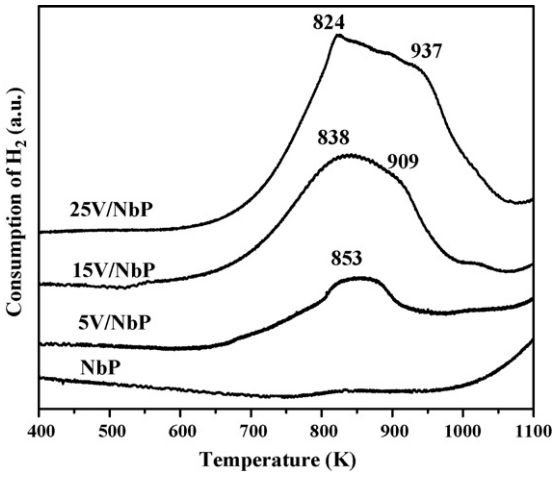

Fig. 6. TPR profiles of NbP and V_2O_5/NbP catalysts.

characterized by a lower acid strength than the acid centers of NbP [51]. Thus the proportion of strong acid sites decreased while that of weak acid sites increased. The heat of NH_3 adsorption gradually decreased with increasing NH_3 coverage revealing heterogeneous strength distributions of NbP and V_2O_5/NbP samples studied in this work. Similar results have been reported for V_2O_5/TiO_2 and V_2O_5/Al_2O_3 catalysts [51,52].

FTIR spectra for ammonia adsorption on NbP and V_2O_5/NbP samples desorbed at 300 K are shown in Fig. 5. It is generally believed that the IR peaks around 1433, and 1671 cm^{-1} are due to the deformation vibrations of NH_4^+ produced by NH_3 adsorption on Brønsted (B) acid sites, while the peaks around 1607 and 1259 cm^{-1} are due to coordinatively adsorbed NH_3 on Lewis (L) acid sites [53]. Literature data showed that both pure V_2O_5 [54] and pure NbP [34] displayed more Brønsted acidity than Lewis acidity. The addition of V_2O_5 on NbP decreased both the B and L acidity of NbP according to the relative intensities of the peaks around 1433 and 1607 cm^{-1}, which is in good agreement with the microcalorimetry results of NH_3 adsorption.

3.3. Redox properties

The TPR profiles for NbP and V_2O_5/NbP samples are shown in Fig. 6. NbP could not be reduced until 1000 K. Addition of 5% V_2O_5 into NbP brought a peak of H_2 consumption around 853 K. This peak was attributed to the reduction of surface monomeric or dimeric surface vanadia species which were well documented for supported vanadia samples [54,55]. It was found that the intensity of this peak increased while the corresponding T_{max} value of that decreased with the increasing V_2O_5 loading. It seems that there is a small shoulder around 909 and 937 K for 15V/NbP and 25V/NbP, respectively, which could be assigned to the existence of small amounts of crystalline V_2O_5 in the samples at high V_2O_5 loading [25]. It should be noted that V_2O_5/NbP displayed totally different redox properties from bulk V_2O_5 which possessed four peaks around 972, 1047, 1153 and 1218 K, respectively [54].

3.4. Isopropanol probe reaction

It is well known that IPA undergoes dehydration reactions to produce propylene (PPE) and diisopropyl ether (DIPE) on acid sites while it proceeds via a dehydrogenation reaction to acetone (ACE) on base sites in inert atmosphere [56]. In addition, IPA can also be oxidatively dehydrogenated to ACE in an oxidation atmosphere, which can be used to probe the surface redox properties [54,57–59]. Thus, the conversion of IPA and selectivities to PPE, DIPE and ACE in air can be used to probe the strength of surface acidic sites and redox properties.

Table 4 presents the results for the probe reaction of IPA on NbP, V_2O_5/NbP and V_2O_5 catalysts in air at 413 K. It can be seen that only PPE and DIPE were produced on NbP. Addition of V_2O_5 produced ACE, and the selectivity to ACE increased with the loading of V_2O_5. These results suggested that NbP displayed surface acidity only while the V_2O_5/NbP possessed both acidic and redox properties. In addition, the selectivity to propylene decreased with the loading of V_2O_5, while the selectivity to isopropyl ether increased. It is believed that the rate of PPE formation increases with the increase of surface acidity [60] while DIPE is usually produced on weak acid sites [56]. Thus, it seems that the addition of V_2O_5 weakened the surface acidity while enhancing the weak acidity of NbP. These results are in agreement with those from NH_3 adsorption microcalorimetry and FTIR. Furthermore, since the surface

Table 4
Catalytic activities of NbP, V_2O_5/NbP and V_2O_5 catalysts in isopropanol probe reaction at 413 K in air

Sample	Conversion of IPA (%)	Selectivity (%)		
		PPE	DIPE	ACE
NbP	4.1	82	18	0
5V/NbP	4.5	75	19	6
15V/NbP	5.0	60	21	19
25V/NbP	5.1	50	28	22
V_2O_5	3.4	30	53	17

Note: IPA, PPE, DIPE and ACE represent isopropanol, propylene, diisopropyl ether and acetone, respectively.

areas of V_2O_5/NbP are much higher than that of bulk V_2O_5 while the activities of V_2O_5/NbP for the IPA conversion are only slightly higher than that of bulk V_2O_5, it seems that NbP support decreased the activity of V_2O_5 for the conversion of IPA.

3.5. Methanol probe reaction

Methanol is one of the most important chemical intermediates used in industrial chemistry [61]. The catalytic oxidation of methanol is a convenient structure-sensitive reaction, widely used to characterize the oxide surfaces in terms of acidity-basicity and redox properties [61,62]. The products distribution from the oxidation of methanol at low conversions reflects the nature of the surface active sites since methanol is converted to formaldehyde and methyl formate (MF) on redox sites, to dimethyl ether (DME) on acidic sites and to dimethoxymethane (DMM) on acidic and redox bi-functional sites [62,63]. Therefore, we used the methanol probe reaction to characterize the surface acidic and redox properties of NbP, V_2O_5/NbP and V_2O_5 catalysts and the results are shown in Table 5. Although the conversion of methanol was low at 413 K on the catalysts, the conversion of methanol increased with V_2O_5 loading. Methanol converted to DME with 100% selectivity on NbP since it possesses acidic properties only. Addition of V_2O_5 on NbP mainly produced DMM due to their bi-functional character. Methanol was first oxidized on the redox sites to produce formaldehyde which was then condensed with additional methanol on the acidic sites to form DMM. The selectivity to DMM was high on all the catalysts at 413 K which indicated that the V_2O_5/NbP catalysts possessed suitable acidic and redox properties. However, it was also observed that with the increase of reaction temperature, the selectivity to DMM decreased rapidly while the amount of FA in the tail gas increased to be the predominant product. Such results revealed that at high temperature the acidities of V/NbP catalysts were still not strong enough to catalyze all the dehydration reaction between surface adsorbed formaldehyde species and additional molecular methanol. Thus, the adsorbed formaldehyde species desorbed as gas phase FA at high temperature. In addition, it seems that the NbP addition decreased the activity of pure V_2O_5 catalysts since V_2O_5/NbP was only slightly more active than V_2O_5 in methanol oxidation probe reaction although V_2O_5/NbP catalysts had much larger surface area than V_2O_5. The reason might be that some of vanadium ions replaced the niobium present in isolated tetrahedral sites at the junction of blocks of NbO_6 octahedra [35], which stabilized the valence state of V in V_2O_5/NbP, leading to the weakened redox properties of V_2O_5/NbP. Therefore, the catalyst exhibited relative low activity in the reaction of oxidation of methanol.

Table 5
Catalytic activities of NbP, V_2O_5/NbP and V_2O_5 catalysts in the methanol oxidation reaction

Sample	Temperature (K)	Conversion of methanol (%)	Selectivity (%)			
			DMM	FA	MF	DME
NbP	413	0.3	0	0	0	100
	433	0.9	0	0	0	100
	453	3.9	0	0	0	100
	473	6.1	0	0	0	100
5V/NbP	413	2.8	93	0	0	7
	433	4.8	86	3	0	12
	453	7.5	52	26	1	21
	473	12.9	14	51	3	32
15V/NbP	413	3.8	96	0	0	4
	433	6.3	88	6	0	6
	453	9.8	53	34	1	12
	473	16.2	14	65	3	18
25V/NbP	413	3.2	96	0	0	4
	433	5.7	89	5	0	6
	453	8.5	51	36	0	13
	473	15.5	12	67	3	18
V_2O_5	413	1.7	96	0	0	4

Note: DMM, FA, MF and DME represent dimethoxymethane, formaldehyde, methyl formate and dimethyl ether, respectively.

4. Conclusions

A series of V_2O_5/NbP catalysts with different V_2O_5 loading were synthesized by the wetness impregnation method. The results from XRD and LRS showed that V_2O_5 could be well dispersed on the surface of NbP. XPS showed that both vanadium and niobium were present in oxidized state of +5 in the samples. Adsorption of O_2 showed about 60% dispersion of V_2O_5 on NbP. The results of microcalorimetry and FTIR for NH_3 adsorption showed that the strength of surface acidity of NbP was decreased, while the proportion of the number of weak acid sites was increased upon the addition of V_2O_5 on NbP. The IPA probe reaction indicated that NbP exhibited acidity only. The addition of V_2O_5 produced acetone from IPA, but not as much as that on bulk V_2O_5. This indicates that the NbP support weakened the redox properties of V_2O_5. Accordingly, NbP produced only DME from the dehydration of methanol owing to its lack of redox property. In contrast, the V_2O_5/NbP catalysts produced mainly DMM due to its bifunctional character. Specifically, methanol was first oxidized on the redox sites of V_2O_5/NbP to produce formaldehyde which was then condensed with additional methanol on the acidic sites of V_2O_5/NbP to form DMM.

Acknowledgements

We acknowledge the financial supports from the French Ministry of Education, the CNRS–France, NSFC (20373023) and MSTC (2004DFB02900 and 2005CB221400).

References

[1] F. Roozeboom, P.D. Cordingley, P.J. Gellings, J. Catal. 68 (1981) 464.
[2] P. Forzatti, E. Tronconi, G. Busca, P. Tittarelli, Catal. Today 1 (1987) 209.
[3] M.S. Wainwright, N.R. Foster, Catal. Rev. Sci. Eng. 19 (1979) 211.
[4] V. Nikolov, D. Klissurski, A. Anastasov, Catal. Rev. Sci. Eng. 33 (1991) 319.
[5] P. Cavalli, F. Cavani, I. Manenti, F. Trifiro, Catal. Today 1 (1987) 245.
[6] M. Sanati, A. Andersson, J. Mol. Catal. 59 (1990) 233.

[7] J.N. Armor, Appl. Catal., B 1 (1992) 221.
[8] J.P. Dunn, P.R. Koppula, H.G. Stenger, I.E. Wachs, Appl. Catal., B 19 (1998) 103.
[9] H. Bosch, F. Janssen, F.M.G. Vandenkerkhof, J. Oldenziel, J.G. Vanommen, J.R.H. Ross, Appl. Catal. 25 (1986) 239.
[10] C.N. Satterfield, Heterogeneous Catalysis in Practice, McGraw-Hill, New York, 1980.
[11] G.C. Bond, S.F. Tahir, Appl. Catal. 71 (1991) 1.
[12] I.E. Wachs, Chem. Eng. Sci. 45 (1990) 2561.
[13] L.J. Burcham, I.E. Wachs, Catal. Today 49 (1999) 467.
[14] G.T. Went, S.T. Oyama, A.T. Bell, J. Phys. Chem. 94 (1990) 4240.
[15] A. Khodakov, B. Olthof, A.T. Bell, E. Iglesia, J. Catal. 181 (1999) 205.
[16] T. Kataoka, J.A. Dumesic, J. Catal. 112 (1988) 66.
[17] M. Li, J. Shen, J. Catal. 205 (2002) 248.
[18] H. Zou, M. Li, J. Shen, A. Auroux, J. Therm. Anal. Calorim. 72 (2003) 209.
[19] F. Arena, F. Frusteri, A. Parmaliana, Appl. Catal., A 176 (1999) 189.
[20] K. Tanabe, Catal. Today 78 (2003) 65.
[21] M. Ziolek, Catal. Today 78 (2003) 47.
[22] R.H.H. Smits, K. Seshan, J.R.H. Ross, A.P.M. Kentgens, J. Phys. Chem. 99 (1995) 9169.
[23] C. Martin, D. Klissurski, J. Rocha, V. Rives, Phys. Chem. Chem. Phys. 2 (2000) 1543.
[24] D.E. Keller, D.C. Koningsberger, B.M. Weckhuysen, J. Phys. Chem. B 110 (2006) 14313.
[25] K.V.R. Chary, G. Kishan, C.P. Kumar, G.V. Sagar, J.W. Niemantsverdriet, Appl. Catal., A 245 (2003) 303.
[26] C. Zhao, I.E. Wachs, Catal. Today 118 (2006) 332.
[27] K.V.R. Chary, C.P. Kumar, A. Murali, A. Tripathi, A. Clearfield, J. Mol. Catal. A: Chem. 216 (2004) 139.
[28] R.H.H. Smits, K. Seshan, J.R.H. Ross, L.C.A. Vandenoetelaar, J.H.J.M. Helwegen, M.R. Anantharaman, H.H. Brongersma, J. Catal. 157 (1995) 584.
[29] T.C. Watling, G. Deo, K. Seshan, I.E. Wachs, J.A. Lercher, Catal. Today 28 (1996) 139.
[30] C.P. Kumar, K.R. Reddy, V.V. Rao, K.V.R. Chary, Green Chem. 4 (2002) 513.
[31] K.V.R. Chary, C.P. Kumar, K.R. Reddy, T. Bhaskar, T. Rajiah, Catal. Commun. 3 (2002) 7.
[32] N.K. Mal, M. Fujiwara, Chem. Commun. (2002) 2702.
[33] S.T. Oyama, G.T. Went, K.B. Lewis, A.T. Bell, G.A. Somorjai, J. Phys. Chem. 93 (1989) 6786.
[34] Q. Sun, A. Auroux, J. Shen, J. Catal. 244 (2006) 1.
[35] A.D. Wadsley, S. Andersson, In: J.D., Dunitz, J.A., Ibers, (Eds.), Wiley, New York, 1970, p. 19.
[36] F. Roozeboom, M.C. Mittelmeijerhazeleger, J.A. Moulijn, J. Medema, V.H.J. Debeer, P.J. Gellings, J. Phys. Chem. 84 (1980) 2783.
[37] B.S. Parekh, S.W. Weller, J. Catal. 47 (1977) 100.
[38] S.W. Weller, Acc. Chem. Res. 16 (1983) 101.
[39] B.M. Reddy, B. Manohar, E.P. Reddy, Langmuir 9 (1993) 1781.
[40] K.V.R. Chary, G. Kishan, K. Lakshmi, K. Ramesh, Langmuir 16 (2000) 7192.
[41] L.D. Frederickson, D.M. Hausen, Anal. Chem. 35 (1963) 818.
[42] H.-L. Zhang, W. Zhong, X. Duan, X.-C. Fu, J. Catal. 129 (1991) 426.
[43] A. Andersson, J.-O. Bovin, P. Walter, J. Catal. 98 (1986) 204.
[44] K. Tarama, S. Youshida, S. Ishida, H. Kakioka, Bull. Chem. Soc. Jpn. 41 (1968) 2840.
[45] M. Cherian, M.S. Rao, G. Deo, Catal. Today 78 (2003) 397.
[46] G. Busca, J. Raman Spectrosc. 33 (2002) 348.
[47] V.I. Bukhtiyarov, Catal. Today 56 (2000) 403.
[48] A. Auroux, Top. Catal. 4 (1997) 71.
[49] K. Tanabe, Mater. Chem. Phys. 17 (1987) 217.
[50] P. Carniti, A. Gervasini, S. Biella, A. Auroux, Chem. Mat. 17 (2005) 6128.
[51] A. Gervasini, P. Carniti, J. Keranen, L. Niinisto, A. Auroux, Catal. Today 96 (2004) 187.
[52] J. Le Bars, J.C. Védrine, A. Auroux, S. Trautmann, M. Baerns, Appl. Catal., A 119 (1994) 341.
[53] J.Y. Shen, R.D. Cortright, Y. Chen, J.A. Dumesic, J. Phys. Chem. 98 (1994) 8067.
[54] X. Gu, J. Ge, H. Zhang, A. Auroux, J. Shen, Thermochim. Acta 451 (2006) 84.
[55] H. Eckert, I.E. Wachs, J. Phys. Chem. 93 (1989) 6796.
[56] A. Gervasini, J. Fenyvesi, A. Auroux, Catal. Lett. 43 (1997) 219.
[57] X.D. Gu, C. Hui, J.Y. Shen, Chin. J. Catal. 24 (2003) 885.
[58] D. Haffad, A. Chambellan, J.C. Lavalley, J. Mol. Catal. A: Chem. 168 (2001) 153.
[59] D. Kulkarni, I.E. Wachs, Appl. Catal., A 237 (2002) 121.
[60] N.S. Figoli, S.A. Hillar, J.M. Parera, J. Catal. 20 (1971) 230.
[61] J.M. Tatibouet, Appl. Catal., A 148 (1997) 213.
[62] M. Badlani, I.E. Wachs, Catal. Lett. 75 (2001) 137.
[63] J.-M. Tatibouet, H. Lauron-Pernot, J. Mol. Catal. A: Chem. 171 (2001) 205.

Publication V

Journal of Molecular Catalysis A: Chemical, 2007, in press

Dehydration of methanol to dimethyl ether over Nb_2O_5 and $NbOPO_4$ catalysts: Microcalorimetric and FT-IR studies

Qing Sun[a, b], Yuchuan Fu[a], Haixia Yang[a], Aline Auroux[b] and Jianyi Shen*[a]

[a]Lab of Mesoscopic Chemistry, School of Chemistry and Chemical Engineering, Nanjing University, Nanjing 210093, China

[b]Institut de Recherches sur la Catalyse et l'Environnement de Lyon, UMR 5256, CNRS-Université Lyon 1, 2 Avenue Albert Einstein, 69626 Villeurbanne Cedex, France

---

* Corresponding author E-mail: jyshen@nju.edu.cn

Phone: (+86)25-83594305 Fax: (+86)25-83594305

Abstract

The unique properties of Nb_2O_5 as a solid acid have led to catalytic applications in various reactions catalyzed by acids. The surface acidity and stability of Nb_2O_5 can be enhanced by the addition of phosphate ions. In this work, amorphous Nb_2O_5 and $NbOPO_4$ samples were synthesized. The interactions of ammonia, methanol, water and dimethyl ether with Nb_2O_5 and $NbOPO_4$ were investigated by means of adsorption microcalorimetry, adsorption infrared spectroscopy (FT-IR) and temperature-programmed desorption (TPD) techniques. The results of microcalorimetry and FT-IR for NH_3 adsorption have shown that $NbOPO_4$ is much more acidic than Nb_2O_5 due to its higher surface area, and that both Brønsted and Lewis acid sites are present on the surface of Nb_2O_5 and $NbOPO_4$. Water adsorption microcalorimetry results indicate that a small amount of water was strongly chemisorbed on Nb_2O_5 and $NbOPO_4$ while most of the adsorbed water corresponded to physical adsorption. The results of methanol adsorption microcalorimetry, methanol adsorption FT-IR and methanol TPD suggest that methanol is mainly strongly dissociatively adsorbed on Nb_2O_5 and $NbOPO_4$ to form methoxy species and DME could be produced from the dehydration of methoxy species. DME adsorption microcalorimetry and FT-IR showed that DME was mainly molecularly chemically adsorbed on Nb_2O_5 and $NbOPO_4$, while a small amount of DME was dissociatively adsorbed. The probe molecules (NH_3, methanol, H_2O and DME) used in this work were adsorbed more strongly on $NbOPO_4$ than on Nb_2O_5 because of the stronger acidity of $NbOPO_4$. In the reaction of methanol dehydration, although Nb_2O_5 and $NbOPO_4$ were not as active as a H-ZSM-5 zeolite, they exhibited 100% selectivity to the DME product and a good stability of the activity in the temperature range relevant to the reaction (453-573 K), without coke formation.

Key words: Nb_2O_5; Niobium phosphate; Methanol; DME; Adsorption microcalorimetry; Acidity

1. Introduction

Dimethyl ether (DME) has been widely used as an aerosol propellant to replace chlorofluoro carbons[1]. Additionally, it is an important chemical intermediate for producing many valuable chemicals such as lower olefins, methyl acetate, dimethyl sulfate …[2, 3]. In recent years, it has attracted global attention as a potential clean fuel substitute for LPG and diesel oil, due to its cleanness, non-toxicity and environmentally benign behaviour.[4, 5]

DME can be synthesized by dehydration of methanol over solid acidic catalysts.[6-9] It can also be synthesized directly from syngas via a so-called STD (syngas to DME) process by employing a hybrid catalyst comprising a methanol synthesis component and a solid acid[10, 11], which is more attractive in consideration of the equilibrium limitation. Typically, a $Cu/ZnO/Al_2O_3$ catalyst is used as the methanol synthesis component in the hybrid catalyst[11, 12], and the solid acids used for the dehydration of methanol are H-ZSM-5, H-Y zeolites, γ-Al_2O_3, modified γ-Al_2O_3, silica-alumina, etc.[8, 9, 11, 13, 14]

Among the solid acids used for methanol dehydration, H-ZSM-5 and γ-Al_2O_3 are the two catalysts that have been studied intensively both for academic and commercial purposes[6, 12, 15]. H-ZSM-5 has been reported to be an effective methanol dehydration catalyst, but on which hydrocarbon byproducts are generated, thus leading to a decrease of the activity[7, 11, 15]. This is due to the strong acidity of the H-ZSM-5, which catalyzes the conversion of methanol to hydrocarbons and even coke[11, 15]. Although the DME selectivity is high for methanol dehydration on γ-Al_2O_3[7, 15], it exhibits much lower activity than H-ZSM-5.[7, 11, 15]

Niobium pentoxide (Nb_2O_5) is a white solid, stable in air and insoluble in water. Hydrated niobium oxide ($Nb_2O_5 \cdot nH_2O$) exhibits strong acidity according to the Hammett titration ($H_0 \leq -5.6$). Its acid strength is equivalent to about 70% sulfuric acid.[16] It possesses both Lewis and Brønsted acid sites[17]. It usually exhibits high

activity for the acid catalyzed reactions in which water molecules participate[16, 18]. Niobium phosphate ($NbOPO_4$) has a similar structure to Nb_2O_5[19], but with a higher acid strength ($H_0 \leq -8.2$). Terminal P-OH and Nb-OH groups coexist at the surface of bulk and impregnated niobium phosphate catalysts[20]. On these materials, the P-OH groups are stronger Brønsted acids than Nb-OH[21]. The Lewis acid sites in niobium phosphate catalysts are the coordinatively unsaturated Nb^{5+} cations[21].

Okazaki et al. have reported that the activity of niobium oxide for the reaction of methanol dehydration to DME could be enhanced by the addition of H_3PO_4 on Nb_2O_5 [22].

In this work, amorphous Nb_2O_5 and $NbOPO_4$ samples were prepared. Adsorption microcalorimetry experiments using different gases (NH_3, methanol, water and DME) as probe molecules were carried out to determine the number and strength of the active sites on Nb_2O_5 and $NbOPO_4$, and adsorption FT-IR and TPD techniques were used to determine the nature of the adsorbed surface species. The catalytic activities of Nb_2O_5 and NbOPO4 were evaluated in the reaction of methanol dehydration to DME.

2. Experimental

2.1 Catalyst preparation

Nb_2O_5 was prepared by calcining commercial niobic acid ($Nb_2O_5 \cdot nH_2O$, CBMM, Brazil) at 623 K for 4 h in air flow. A porous niobium phosphate, denoted as $NbOPO_4$, was prepared by following a previously described procedure.[23] Specifically, 2.73 g of $NbCl_5$ (Alfa Aesar, 99%) was partially hydrolyzed in 50 ml H_2O, and 2.30 g H_3PO_4 (Aldrich, 85% aqueous solution) was added, upon which a vigorous hydrolytic reaction occurred. An additional 50 ml H_2O was then added and the reaction mixture was stirred for 30 min, after which an aqueous solution of ammonia (25%) was added to adjust the pH of the reaction mixture to 2.60. After stirring for a few minutes, the slurry was filtered and washed with deionized water to obtain a chloride-less gel. The gel was mixed with 10 ml H_2O and 1.45 g hexadecylamine (Aldrich, 90%) and stirred for 30 min. Then, 0.92 g H_3PO_4 (85%) was added and the pH of the mixture was adjusted to 3.9. After stirring for 30 min, the gel was heated in a Teflon lined stainless

steel autoclave at 338 K under autogenous pressure for 2 days. The final product was filtered, washed with deionized water, dried at 373 K overnight and calcined at 625 K in N_2 for 12 h, then in air up to 723 K for 40 h.

2.2 Catalyst characterization

The X-ray diffraction (XRD) measurements were carried out on a Bruker D5005 diffractometer scanning from 3^o to 80^o (2θ) at a rate of 0.02 degree/s using a Cu Kα radiation (λ = 0.15418 nm) source. The applied voltage and current were 50 kV and 35 mA, respectively. The surface area and pore size were measured by nitrogen adsorption at 77 K after heat pretreatment under vacuum at 673 K for 4 h. Elemental analysis was performed using ICP atomic emission spectroscopy (Spectroflame-ICP D, Spectro). The X-ray photoelectron spectra (XPS) were measured on a SSI 301 instrument equipped with a hemispherical electron analyzer and an Al anode (Al Kα =1486.6 eV) powered at 100 W. The residual pressure in the spectrometer chamber was 5×10^{-8} Pa during data acquisition.

The microcalorimetric studies of methanol, water and DME adsorption were performed at 303 K, while ammonia adsorption was performed at 423 K, in a heat flow calorimeter (C80 from Setaram) linked to a conventional volumetric apparatus equipped with a Barocel capacitance manometer for pressure measurements. All the gases used for measurements (purity > 99.9%) were purified by successive freeze–pump–thaw cycles. Before any adsorption, about 100 mg of sample was pretreated in a quartz calorimetric cell under evacuation overnight at 623 K. The differential heats of adsorption were measured as a function of coverage by repeatedly introducing small doses of gas or vapor onto the catalyst until an equilibrium pressure of about 66 Pa was reached.[24] The sample was then outgassed for 30 min at the same temperature and a second adsorption was performed at the same temperature until an equilibrium pressure of about 27 Pa was attained; this made it possible to calculate the irreversibly chemisorbed amount of probe molecule at this pressure.

Temperature-programmed desorption of water (or methanol) was performed on a Setaram TG-DSC 111 equipment coupled with a mass spectrometer (Thermostar from Pfeifer) as a detector. A capillary-coupling system was used. The TPD experiments

were carried out in a flow, with helium as the carrier gas (10 ml·min^{-1}). For each experiment, about 30 mg of a sample containing water (or methanol) absorbed in a previously performed microcalorimetric experiment was used. The sample was heated at 5 K·min^{-1} in helium up to 873 K. During this temperature increase, the gas phase composition was analyzed by mass spectrometry.

The gas adsorption FT-IR spectra were recorded with a Bruker Vector 22 FTIR spectrophotometer (DTGS detector) in the 4000–400 cm^{-1} range, with a resolution of 2 cm^{-1} and 50 acquisition scans. The self-supporting wafer (10–30 mg, 18mm diameter) was first activated in an in situ IR cell at 673 K in O_2 flow for 12 h, evacuated at the same temperature for 2 h, and then exposed to the different gases (NH_3, methanol and dimethyl ether) (purity>99.9%) at room temperature for 5 min. The desorption was carried out by evacuation for 30 min each at 300, 373, 473, 523, 573 and 673 K, respectively. A spectrum was recorded at room temperature after desorption at each temperature.

2.3 Catalytic reaction

The dehydration of methanol was carried out in a fixed micro-reactor made of stainless steel with an inner diameter of 6 mm. Methanol was introduced into the reaction zone by bubbling N_2 (99.999%) through a glass saturator filled with methanol (AR) maintained at 303 K. In each test, 0.2 g catalyst was loaded, and the gas hourly space velocity (GHSV) was 3400 ml·g^{-1}·h^{-1}. The feed composition was maintained at methanol:N_2 = 21:79. The tail gas out of the reactor was analyzed 30 minutes after reaching the reaction temperature by an on-line GC equipped with an FID detector. The column used was PEG 20M for the separation of methanol, DME and other organic compounds. The gas lines were kept at 383K to prevent condensation of the reactant and products. The reaction was carried out at atmospheric pressure.

3. Results and discussions

3.1 Structural characterizations

The XRD results shown in Fig. 1 indicate that the Nb_2O_5 and $NbOPO_4$ samples studied in this work were amorphous. They mainly exhibited two broad 2θ peaks

around 25 and 52°. The peaks were shifted to lower angles for $NbOPO_4$, implying some difference in bonding in $NbOPO_4$ compared to Nb_2O_5.

Results of bulk and surface elemental analysis, as well as the surface area and porosity data for the samples, are given in Table 1. $NbOPO_4$ presented a much higher surface area (511 $m^2 \cdot g^{-1}$) than Nb_2O_5 (110 $m^2 \cdot g^{-1}$), since $NbOPO_4$ was prepared by using a template. The pore diameter of $NbOPO_4$ (4.4 nm) was slightly smaller than that of Nb_2O_5 (6.0 nm), but the pore volume of $NbOPO_4$ (0.56 $ml \cdot g^{-1}$) was much larger than for Nb_2O_5 (0.16 $ml \cdot g^{-1}$). The chemical analysis showed a Nb/P atomic ratio of 1/1 in $NbOPO_4$. XPS results showed that P might be in slight excess on the surface (see Table 1).

Previous data had already shown the non-oxidative properties of Nb_2O_5 and $NbOPO_4$, evidenced by the absence of any hydrogen consumption peaks until 1100 K in temperature-programmed reduction experiments.[25]

3.2 Adsorption microcalorimetry

The surface acidity in terms of number of acid sites and site strengths was determined by ammonia adsorption microcalorimetry, and the results are presented in Fig. 2. Methanol, water and DME adsorption microcalorimetry measurements were carried out to determine the number, strength and strength distribution of the surface sites on Nb_2O_5 and $NbOPO_4$ and the results are shown in Figs. 3 to 6. Table 2 summarizes quantitative results for the initial heats of adsorption, irreversibly adsorbed volumes and total adsorbed volumes probed by different molecules (ammonia, methanol, water and DME) per m^2 of surface ($\mu mol \cdot m^{-2}$) and per gram of sample ($\mu mol \cdot g^{-1}$) under an equilibrium pressure of 27 Pa.

3.2.1 NH_3 adsorption microcalorimetry

Nb_2O_5 can be regarded as a strong acid according to Hammett titration.[16] It has been shown that its surface acidity can be enhanced and stabilized via addition of phosphate ions.[19] In this work, the initial heat and saturation coverage for ammonia adsorption on Nb_2O_5 were found to be about 165 $kJ \cdot mol^{-1}$ and 250 $\mu mol \cdot g^{-1}$, respectively (see Fig. 2). The initial heat did not vary with the addition of PO_4^{3-} into Nb_2O_5, However, the saturation coverage of NH_3 on $NbOPO_4$ was found to be about

850 μmol·g^{-1}, much higher than for Nb_2O_5, which is apparently due to the high surface area of $NbOPO_4$. In fact, when the surface coverage is expressed in terms of the amount of ammonia adsorbed on a unit surface area, the coverage on $NbOPO_4$ was lower than Nb_2O_5 (see Fig. 4 and Table 2).

3.2.2 H_2O adsorption microcalorimetry

Polar molecules with different gas phase affinities such as alcohol and water are usually used to measure the hydrophilic and hydrophobic properties of the surface of materials.[26-30] The differential heat and saturation coverage reflect the proton affinity and the strength of H-bonds or van der Waals forces on those samples.

The results of H_2O adsorption in terms of number and strength of adsorption sites on Nb_2O_5 and $NbOPO_4$ are shown in Fig. 3. The initial heats for H_2O adsorption on Nb_2O_5 and $NbOPO_4$ were very high, 179 and 189 kJ·mol^{-1}, respectively. With the increase of H_2O coverage, the differential heats first dropped sharply and then decreased gradually until the saturation coverage was reached at 67 Pa of equilibrium pressure (763 μmol·g^{-1} for Nb_2O_5 and 1800 μmol·g^{-1} for $NbOPO_4$). For example, on Nb_2O_5, the differential heat of H_2O adsorption first decreased dramatically to around 80 kJ·mol^{-1}, for a H_2O coverage of 1.5 μmol·m^{-2} (see Fig. 4), then it decreased slowly until it reached a value close to the latent heat of liquefaction of water (44 kJ·mol^{-1}). Bolis et al. have suggested that the high differential heat values (Q_{diff} >100 kJ·mol^{-1}) observed at low coverage are compatible with the energy of coordination of H_2O on Lewis acid sites, while adsorbed water on a Brønsted site acts as an H-bond acceptor of the Brønsted acidic proton with a differential heat of the order of 70 kJ·mol^{-1}. [31] Therefore, in this work, H_2O might be adsorbed first on the small amount of coordinatively unsaturated Nb^{5+} cations which act as Lewis acid sites, and then on Brønsted sites or on strongly polarized H_2O molecules already adsorbed on Lewis sites, as suggested in the literature[31].

The differential heats *vs.* coverage per m^2 for NH_3 adsorption and H_2O adsorption on Nb_2O_5 and $NbOPO_4$ are compared in Fig. 4. It can be seen that for both NH_3 and H_2O adsorption, the coverage per m^2 of surface was higher on Nb_2O_5 than on $NbOPO_4$. Moreover, the coverage for water adsorption was much higher than for

ammonia adsorption, which suggests a larger amount of physically adsorbed H_2O on Nb_2O_5 and $NbOPO_4$. It has been reported in the literature that the initial heats for water adsorption are 60 kJ·mol^{-1} on silica[27], 160 kJ·mol^{-1} on H-BEA zeolites[31] and 100 kJ·mol^{-1} on H-ZSM-5[32]. Thus, the Nb_2O_5 and $NbOPO_4$ samples studied in this work were quite hydrophilic and exhibited high strength of H-bonding, $NbOPO_4$ more so than Nb_2O_5.

3.2.3 Methanol adsorption microcalorimetry

Fig. 5 shows the results of methanol adsorption on Nb_2O_5 and $NbOPO_4$. The initial heats of adsorption and saturation coverage were found to be about 142 kJ·mol^{-1} and 533 μmol·g^{-1} on Nb_2O_5, respectively, while $NbOPO_4$ exhibited a slightly higher initial heat of 148 kJ·mol^{-1} and a much higher methanol coverage of 1563 μmol·g^{-1} due to its large surface area. However, the methanol coverage in terms of the amount per unit surface area on $NbOPO_4$ was lower than on Nb_2O_5, in agreement with what was observed for NH_3 adsorption (see Table 2). Both Nb_2O_5 and $NbOPO_4$ strongly interact with methanol as indicated by the differential heats, which are higher than those on silica (Q_{init} = 60 to 90 kJ·mol^{-1})[26, 28, 32-34] and H-ZSM-5 (Q_{init} = 115 kJ·mol^{-1})[32] but lower than on γ-Al_2O_3 (Q_{init} > 200 kJ·mol^{-1})[35].

It has been reported in the literature that there exist different methanol adsorption heat steps on silica[34] and on γ-Al_2O_3[35] at low and high coverage, indicating different methanol adsorption modes on them. Adsorption occurring at low coverage might be strong chemical adsorption, while adsorption at high coverage corresponds to physical adsorption in which hydrogen bonding plays an important role[35]. However, in the present work, the differential heats of methanol adsorption on Nb_2O_5 and $NbOPO_4$ decreased monotonically with increasing methanol coverage, and there was no apparent plateau observed in methanol adsorption heats. Note that outgassing at 673 K overnight (the pretreatment conditions used in this study) might remove more weak surface hydroxyl groups compared to the pretreatment conditions used in the literature (outgassing at 600 K for 2 hours)[34]. Therefore, only quite strong acid sites remained and methanol adsorbed strongly on them.

In addition, by comparing the total adsorbed methanol volume (V_{tot}) with the irreversibly adsorbed volume (V_{irr}) (see Table 2), it is clearly shown that most of adsorbed methanol was strongly chemisorbed on Nb_2O_5 and $NbOPO_4$. Moreover, both the total adsorbed methanol volume (V_{tot}) and the irreversibly adsorbed volume (V_{irr}) were much larger than those for NH_3 adsorption which titrates the surface acid sites. For example, on Nb_2O_5, the total adsorbed methanol volume (V_{tot}) and the irreversibly adsorbed volume (V_{irr}) were 483 and 341 $\mu mol \cdot g^{-1}$, respectively, while those for NH_3 adsorption were only 208 and 89 $\mu mol \cdot g^{-1}$. This might suggest that methanol was mainly dissociatively adsorbed on Nb_2O_5 and $NbOPO_4$, since the water formed by the dissociative adsorption of methanol might hydrate the surface of Nb_2O_5 and $NbOPO_4$, thereby generating new hydroxyl groups favoring further methanol adsorption.

3.2.4 DME adsorption microcalorimetry

DME was also used as a basic molecule to probe the surface acidity on the catalyst. The bridged oxygen in the DME molecule has unshared pairs of electrons and can act as electron donor.

Very few articles in the literature discuss DME adsorption microcalorimetry. It has been reported that DME is a better probe molecule than NH_3 in adsorption microcalorimetry for studying the acidity of sulfated metal oxides[36]. It is believed that the difference between NH_3 and DME adsorption is probably due to the different polarizabilities of these two probe molecules.[37] The basicity and polarizability of DME are more similar to those of light paraffins than to NH_3. So, DME could provide a more specific way to distinguish the interactions of solid acids with paraffins[37].

In this work, as depicted in Fig. 6, the initial heats for DME adsorption on Nb_2O_5 and $NbOPO_4$ were 130 and 133 $kJ \cdot mol^{-1}$, respectively. The corresponding saturation coverages for DME adsorption on Nb_2O_5 and NbOPO4 were 200 and 547 $\mu mol \cdot m^{-1}$ at an equilibrium pressure of 67 Pa, respectively. Measurements of the initial heats of DME adsorption on zirconium sulfate and iron sulfate have been reported in the literature, with values of 140 and 105 $kJ \cdot mol^{-1}$, respectively[36]. This suggests that the acidities of Nb_2O_5 and $NbOPO_4$ are stronger than that of iron sulfate but weaker than that of zirconium sulfate. It should be noted that the irreversible adsorption volumes

(see Table 2) for DME adsorption on Nb_2O_5 (117 μmol·g^{-1}) and $NbOPO_4$ (300 μmol·g^{-1}) were close to those for NH_3 adsorption (89 μmol·g^{-1} for Nb_2O_5 and 298 μmol·g^{-1} for $NbOPO_4$), which might suggest that one DME molecule is adsorbed on each acid site.

3.3 Temperature programmed desorption

3.3.1 Water TPD

Fig. 7 shows the H_2O-TPD results for the Nb_2O_5 and $NbOPO_4$ samples. Both of them exhibited a broad desorption peak which revealed the heterogeneous strength distribution of the adsorption sites on them, in agreement with the results of H_2O adsorption. It is usually not accurate to rank the sites strengths by simply comparing the desorption maxima because of complex diffusion effects, especially for porous materials. The temperatures of peak maxima were slightly higher for $NbOPO_4$ than for Nb_2O_5. In addition, the areas of the desorption peaks reflected the relative populations of adsorption sites, which clearly shows that $NbOPO_4$ possessed much more adsorption sites than Nb_2O_5, in good agreement with the microcalorimetric adsorption results.

3.3.2 Methanol TPD

The methanol-TPD results for Nb_2O_5 and $NbOPO_4$ are shown in Figs. 8 and 9, respectively. Both Nb_2O_5 and $NbOPO_4$ desorbed large amounts of water (*m/e* = 18) which might have been formed by methanol condensation on the surface of Nb_2O_5 and $NbOPO_4$. However, the possibility of the samples adsorbing some water in air during the transfer from one apparatus to the other could not be excluded. This suggested again the strong hydrophilic properties of Nb_2O_5 and $NbOPO_4$.

Fig. 8 shows that methanol (*m*/*e* = 31) adsorbed on Nb_2O_5 was released with a broad peak maximum around 470 K, followed by DME (*m*/*e* = 45), methane (*m*/*e* = 16, 15), and additional H_2O (*m*/*e* = 18) desorptions at 521 K, 672 K and 679 K, respectively. The weak peak appearing around 529 K for the *m*/*e* = 15 signal is due to the second fragmentation of DME in mass detection. From the relative intensities of the peaks, we might propose that a small amount of the adsorbed methanol is weakly bonded to Nb_2O_5, while most of the methanol interacts with Nb_2O_5 leading to the formation of methoxy groups (as seen by FT-IR). These surface methoxy groups

further formed DME with the increase of temperature, which is in good agreement with the results in the literature. It is interesting to observe that some methoxy species are very stable as they decompose to methane and H_2O at only 672 K. The desorption profile for $NbOPO_4$ displayed similar features, but the intensities of the peaks were much higher than for Nb_2O_5, as shown in Fig. 9. Additionally, the desorption peaks due to DME and methane both appeared at higher temperatures (532 and 680 K) than on Nb_2O_5, which suggests a better stability of methoxy species on $NbOPO_4$ than on Nb_2O_5. Note that we did not observe any signal due to CO (m/e = 28) and CO_2 (m/e = 44), suggesting the lack of oxidative properties of Nb_2O_5 and $NbOPO_4$.

3.4 Adsorption FT-IR

3.4.1 NH_3 adsorption FT-IR

Fig. 10 shows the FT-IR spectra of Nb_2O_5 and $NbOPO_4$ after NH_3 adsorption and desorption at 300 K. Both Brønsted and Lewis acid sites were present on the samples. The bands around 1671 and 1433 cm^{-1} are due to the deformation vibration of NH_4^+ formed by the interaction of NH_3 with Brønsted acid sites, while the bands at 1607 and 1259 cm^{-1} originate from the asymmetric and symmetric deformation vibrations, respectively, for NH_3 coordinated to Nb^{5+}. Apparently $NbOPO_4$ exhibited higher surface B and L acidities than Nb_2O_5, according to the relative intensities of the peaks around 1433 and 1607 cm^{-1}, respectively.

3.4.2 OH groups

The FT-IR spectra of the Nb_2O_5 and $NbOPO_4$ samples after outgassing from 300 K up to 773 K are reported in Figs. 11 and 12. In Fig. 12, the spectrum of Nb_2O_5 after outgassing at 300 K shows a sharp peak at 3706 cm^{-1} and a broad absorption band centered near 3400 cm^{-1}, which are assigned to the OH stretching mode of free Nb-OH groups and H-bonded hydroxyl groups[21]. The analysis of the lower frequency region showed a band present at 1612 cm^{-1}, due to the scissoring mode of adsorbed molecular water. Outgassing at 423 K caused a decrease of the broad absorption band around 3400 cm^{-1}, a notable reduction of the sharper component at 3706 cm^{-1} and a decrease of the intensity for the molecular adsorbed water. Upon evacuation at 573 K,

only small features could be observed on Nb_2O_5, suggesting that most of the surface hydroxyl species have been removed.

The spectrum of $NbOPO_4$ presents a strong sharp band at 3667 cm^{-1} (see Fig. 12) which could be assigned to the OH stretching mode of surface phosphate or pyrophosphate species as reported by Armaroli et al.[21]. This band is also accompanied by a broad band around 3300 cm^{-1} and a band due to scissoring mode of adsorbed molecular water at 1616 cm^{-1}. The bands on $NbOPO_4$ exhibited much higher intensity than those on Nb_2O_5 (see the comparison in Fig. 11, inset), suggesting the presence of much larger amounts of surface hydroxyl and adsorbed water on $NbOPO_4$ than on Nb_2O_5. Moreover, upon outgassing at increasing temperature, the surface hydroxyl groups and adsorbed water on $NbOPO_4$ were much more stable than those on Nb_2O_5.

3.4.3 Methanol adsorption FT-IR

The FT-IR spectra for methanol adsorbed on Nb_2O_5 and $NbOPO_4$ are shown in Figs. 13 and 14. On Nb_2O_5, which is shown in Fig. 13, a negative band appears at 3715 cm^{-1} due to the consumption of hydroxyl groups which were bonded with methanol, accompanied by a shoulder at 3400 cm^{-1} due to the hydrogen-bonded species. These features suggest the probable co-existence of molecularly adsorbed DME and CH_3O(a) (methoxy species) on the surface of Nb_2O_5. They are distinguishable by the characteristic symmetric ($\nu_s(CH_3)$) and antisymmetric ($\nu_{as}(CH_3)$) CH_3 stretching frequencies: 2829 and 2927 cm^{-1} for CH_3O(a), which are in good agreement with the results reported in the literature.[38, 39] The band observed at 2954 cm^{-1} could be assigned to the $\nu_{as}(CH_3)$ vibration mode of molecularly adsorbed DME species formed by methanol dehydration [40]. The band at 2884 cm^{-1} is due to the C-H vibration of $2\delta(CH_3)$ bending mode. In the region of low wave number, the $\delta(CH_3)$ bending vibrations led to bands at 1452 and 1439 cm^{-1} and the $\rho(CH_3)$ rocking mode is seen at 1154 cm^{-1}. In addition, a strong absorption band due to the C-O stretching mode of CH_3O(a) is visible at 1101 cm^{-1}, reflecting the presence of terminal methoxy adsorption species on the Nb_2O_5 surface. The band at 1616 cm^{-1} is due to the molecular adsorbed H_2O on Nb_2O_5, which might be produced via methanol

dehydration on the surface. Below the 1000 cm^{-1} region, the bands could not be observed due to the strong background of CaF_2 windows.

The features of these peaks indicate that most of the methanol is dissociatively adsorbed to form methoxy species most likely acting as on-top adsorbed species, and a small amount of methoxy species might dehydrate to DME adsorbed on the surface of Nb_2O_5. Upon evacuation at elevated temperature, the intensities of all these bands decrease, indicating the removal of the surface species. Upon desorbing at 673 K for 0.5 h, all the bands disappeared or became extremely weak.

Similar band features could be observed on $NbOPO_4$ (see Fig. 14), although the bands below 1300 cm^{-1} could not be observed due to the strong background of $NbOPO_4$. The bands in the C-H stretching region on $NbOPO_4$ shifted to higher wave numbers than for Nb_2O_5. This probably suggests that the methoxy species adsorb more strongly on P atoms than on Nb atoms, since P exhibits a higher electronegativity value (2.2) than Nb (1.6) and attracts electrons more strongly, which results in weaker O-C bonding and enhanced C-H bonding in methoxy species. This observation is in agreement with the results of methanol TPD.

3.4.4 DME adsorption FT-IR

The adsorption of DME on alumina[41], H-ZSM-5[42], ZrO_2[43] etc. has been studied by FT-IR. Chen et al. reported that DME was molecularly adsorbed on alumina surface at low temperature (150 K) while it formed surface methoxy species when heated to temperatures higher than 250 K[41]. Feng et al. suggested that the molecularly adsorbed DME was moderately dissociated on a dehydroxylated ZrO_2 surface, while it rapidly dissociated and no molecularly adsorbed DME could be observed on a fully hydroxylated ZrO_2 surface[43]. Fujino et al. suggested that DME molecules adsorbed on OH groups of H-ZSM-5 via hydrogen bonding irrespective of their acidity, and that the oxonium ions of DME were not produced on the studied surface[42].

The FT-IR results for DME adsorption on Nb_2O_5 and $NbOPO_4$ samples are shown in Figs. 15 and 16. In the case of $NbOPO_4$ (Fig. 16), the adsorption of DME caused an intense negative band at 3660 cm^{-1} which is surely due to the consumption of hydroxyl groups, suggesting DME adsorption on the hydroxyl groups of $NbOPO_4$.

On Nb_2O_5, this negative band feature was not apparent, perhaps because of the low density of OH groups on Nb_2O_5 (see Fig. 11) after pretreatment by outgassing at 673 K.

In the wave number region corresponding to C-H stretching, the bands at 2954 ($\nu_{as}(CH_3)$), 2880 ($2\delta(CH_3)$) and 2841 ($\nu_s(CH_3)$) cm^{-1} were observed on Nb_2O_5 (Fig. 15). The bands in the δ(C-H) region are also detectable at 1458 and 1471 cm^{-1} due to $\delta(CH_3)$ bending vibration mode. The bands observed at 1252 and 1151 cm^{-1} are due to the $\gamma(CH_3)$ vibration mode and $\rho(CH_3)$ rocking mode, respectively. The band observed at 1047 cm^{-1} is due to the ν_{as}(CO) stretching mode[44]. Since these bands appeared at different wave numbers compared to the methoxy species formed by methanol adsorption, these band features can therefore be assigned to the C-H stretching modes of DME molecularly coordinated to a Lewis acid site on the surface, which is in agreement with the observations on ZrO_2[40]. It is noted that there was also a weak band at 1616 cm^{-1} due to the scissoring vibration mode of molecular adsorbed water, which suggests that a small amount of DME was dissociatively adsorbed on the hydroxyl groups and thus formed H_2O. This might proceed by a mechanism in which DME molecules first react with an acidic proton to form a methanol molecule and a methyl group, and then the methanol thus formed can react with another Brønsted acid site to form H_2O(g) and a second methyl group[45]. However, the bands for methoxy species could not be observed, suggesting that the amount of dissociatively adsorbed DME is very small.

Similar bands were observed on $NbOPO_4$, indicating a similar adsorption situation. The bands for $NbOPO_4$ were shifted to higher wave numbers and exhibited higher intensities than on Nb_2O_5, implying the stronger interaction of adsorbed DME with $NbOPO_4$ than with Nb_2O_5.

Upon outgassing at 473 K, most of the bands disappeared on Nb_2O_5, while it seemed that some DME still remained on $NbOPO_4$, indicating again that DME is more strongly adsorbed on $NbOPO_4$ than on Nb_2O_5. A new band appearing at 1120 cm^{-1} upon outgassing at 473 K on Nb_2O_5 was not identified.

3.5 Reaction activity

The results for the dehydration of methanol to DME on Nb_2O_5 and $NbOPO_4$ catalysts are shown in Fig. 17. As a comparison, the results obtained on H-ZSM-5 and γ-Al_2O_3 catalysts in a previous work in our group are also given.[9] It can be seen that Nb_2O_5 and $NbOPO_4$ are much less active than H-ZSM-5, since the conversion of methanol on H-ZSM-5 reached the equilibrium at a temperature as low as 423 K,[9] while the conversions on Nb_2O_5 and $NbOPO_4$ were only 0.8% and 3.2%, respectively. Below 553 K, Nb_2O_5 and $NbOPO_4$ were much more active than γ-Al_2O_3, and among them $NbOPO_4$ was more active than Nb_2O_5. For example, at 513 K, the conversions of methanol on γ-Al_2O_3, Nb_2O_5 and $NbOPO_4$ were 3.0%, 12.8% and 28.5%, respectively. The activity of γ-Al_2O_3 increased quickly with increasing reaction temperature, while the activity of Nb_2O_5 and $NbOPO_4$ increased relatively slowly. The activity of $NbOPO_4$ reached a maximum at 593 K and then decreased with a further increase in temperature, which is due to the equilibrium limitation since the methanol dehydration reaction is exothermic. DME was the only organic product observed in the entire temperature range employed in this reaction, and no hydrocarbon by-products were detected on Nb_2O_5 and $NbOPO_4$. Moreover, no obvious deactivation of the Nb_2O_5 and $NbOPO_4$ catalysts could be observed during the time (12 h) over which the experiments were carried out. Moreover, very little coke was formed on Nb_2O_5 and $NbOPO_4$ after dehydration reaction. Comparatively, on H-ZSM-5, organic by-products were detected above 513 K, and the conversion of methanol decreased with the time on stream[9, 11].

The activity of a suitable dehydration catalyst should be sufficient but not too high in order to prevent the formation of hydrocarbon products, which causes coke deposition and deactivation of the catalysts. The results suggest that even though the activities of Nb_2O_5 and $NbOPO_4$ in the methanol dehydration reaction were lower than that of H-ZSM-5, they showed 100% selectivity to DME and good stability. Thus Nb_2O_5 and $NbOPO_4$ could be used as dehydration catalysts.

Note that the surface area of $NbOPO_4$ was much larger than that of Nb_2O_5, but the methanol dehydration activity of $NbOPO_4$ was only slightly higher than that of

Nb_2O_5 especially at high temperature. It has been reported that the strength of Lewis acid sites on γ-Al_2O_3 was decreased upon the adsorption of water[46], and the partial pressure of water had a strong negative effect on the activity of γ-Al_2O_3 for the dehydration of methanol to DME[7]. Thus, the observed behavior could be ascribed to the stronger adsorption of H_2O and DME as well as the higher stability of methoxy species on $NbOPO_4$ than Nb_2O_5, as identified by the results of adsorption microcalorimetry and adsorption FT-IR experiments. In the methanol dehydration reaction, water, DME and methanol might comparatively adsorb on the acid sites of Nb_2O_5 and $NbOPO_4$. Since water and DME are products of the methanol dehydration reaction, strongly adsorbed water and DME might occupy some active acid sites on $NbOPO_4$ and therefore decrease the methanol dehydration activity, which is in agreement with the results reported by Bandiera et al.[47].

4. Conclusions

Amorphous Nb_2O_5 and $NbOPO_4$ samples were synthesized. The results of microcalorimetry and FT-IR for NH_3 adsorption showed that $NbOPO_4$ is much more acidic than Nb_2O_5 due to its high surface area, and that both Brønsted and Lewis acid sites are present on the surface of Nb_2O_5 and $NbOPO_4$. Water adsorption microcalorimetry results indicated that a small amount of water was strongly adsorbed on the Lewis acid sites of Nb_2O_5 and $NbOPO_4$, while most of the water was adsorbed by physical adsorption. The results of methanol adsorption microcalorimetry and methanol adsorption FT-IR suggest that methanol was mainly strongly dissociatively adsorbed on the surface of Nb_2O_5 and $NbOPO_4$ to form methoxy species as well as small amounts of DME and water molecularly adsorbed on the surface as products of the dehydration of methoxy species, as confirmed by the methanol TPD results. DME adsorption microcalorimetry and adsorption DME FT-IR showed that DME was mainly molecularly chemisorbed on Nb_2O_5 and $NbOPO_4$, while a small amount of DME could also be dissociatively adsorbed. $NbOPO_4$ exhibited stronger interaction with the probe molecules (NH_3, methanol, H_2O and DME) than Nb_2O_5. In the reaction of methanol dehydration, although the activities of Nb_2O_5 and $NbOPO_4$ were lower

than that of H-ZSM-5, they exhibited 100% selectivity to the DME product and good stability of the activities, without coke formation.

Acknowledgements

We acknowledge the financial supports from the French Ministry of Education, the CNRS-France, NSFC (20373023) and MSTC (2004DFB02900 and 2005CB221400).

References

1 T. Shikada, K. Fujimoto, M. Miyauchi and H. Tominaga, *Appl. Catal.*, 1983, **7**, 361.
2 W. W. Kaeding and S. A. Butter, *J. Catal.*, 1980, **61**, 155.
3 G. Y. Cai, Z. M. Liu, R. M. Shi, C. Q. He, L. X. Yang, C. L. Sun and Y. J. Chang, *Appl. Catal. A*, 1995, **125**, 29.
4 T. H. Fleisch, A. Basu, M. J. Gradassi and J. G. Masin, in *Natural Gas Conversion Iv*, 1997, vol. 107, pp. 117.
5 J. Sehested, T. Mogelberg, T. J. Wallington, E. W. Kaiser and O. J. Nielsen, *J. Phys. Chem.*, 1996, **100**, 17218.
6 2 014 408, 1935.
7 M. T. Xu, J. H. Lunsford, D. W. Goodman and A. Bhattacharyya, *Appl. Catal. A*, 1997, **149**, 289.
8 J. H. Kim, M. J. Park, S. J. Kim, O. S. Joo and K. D. Jung, *Appl. Catal. A*, 2004, **264**, 37.
9 Y. C. Fu, T. Hong, J. P. Chen, A. Auroux and J. Y. Shen, *Thermochim. Acta*, 2005, **434**, 22.
10 *US Pat.,* 4 423 155, 1983.
11 T. Takeguchi, K. Yanagisawa, T. Inui and M. Inoue, *Appl. Catal. A*, 2000, **192**, 201.
12 *US Pat.,* 4 536 485, 1985.
13 *US Pat.,* 4 098 809, 1978.
14 *US Pat.,* 4 863 894, 1989.
15 V. Vishwanathan, K. W. Jun, J. W. Kim and H. S. Roh, *Appl. Catal. A*, 2004, **276**, 251.
16 K. Tanabe, *Mater. Chem. Phys.*, 1987, **17**, 217.
17 J.-M. Jehng and I. E. Wachs, *Catal. Today*, 1990, **8**, 37.
18 K. Tanabe, *Catal. Today*, 1990, **8**, 1.
19 I. Nowak and M. Ziolek, *Chem. Rev.*, 1999, **99**, 3603.
20 M. Ziolek, *Catal. Today*, 2003, **78**, 47.
21 T. Armaroli, G. Busca, C. Carlini, M. Giuttari, A. M. R. Galletti and G. Sbrana, *J. Mol. Catal. A*, 2000, **151**, 233.

22 S. Okazaki, M. Kurimata, T. Iizuka and K. Tanabe, *Bull. Chem. Soc. Jpn.*, 1987, **60**, 37.
23 N. K. Mal and M. Fujiwara, *Chem. Commun.*, 2002, 2702.
24 A. Auroux, *Top. Catal.*, 1997, **4**, 71.
25 Q. Sun, A. Auroux and J. Shen, *J. Catal.*, 2006, **244**, 1.
26 J. Cortes, M. Jensen and P. Araya, *J. Chem. Soc., Faraday Trans. I*, 1986, **82**, 1351.
27 Y. I. Tarasevich, V. E. Polyakov, A. A. Serdan and G. V. Lisichkin, *Colloid J.*, 2004, **66**, 592.
28 H. Thamm, *J. Chem. Soc., Faraday Trans. I*, 1989, **85**, 1.
29 B. Fubini, V. Bolis, A. Cavenago, E. Garrone and P. Ugliengo, *Langmuir*, 1993, **9**, 2712.
30 J. Janchen, J. van Wolput, W. J. M. Van Well and H. Stach, *Thermochim. Acta*, 2001, **379**, 213.
31 V. Bolis, C. Busco and P. Ugliengo, *J. Phys. Chem. B*, 2006, **110**, 14849.
32 C. C. Lee, R. J. Gorte and W. E. Farneth, *J. Phys. Chem. B*, 1997, **101**, 3811.
33 V. Bolis, A. Cavenago and B. Fubini, *Langmuir*, 1997, **13**, 895.
34 M. A. Natal-Santiago and J. A. Dumesic, *J. Catal.*, 1998, **175**, 252.
35 G. Busca, P. F. Rossi, V. Lorenzelli, M. Benaissa, J. Travert and J. C. Lavalley, *J. Phys. Chem.*, 1985, **89**, 5433.
36 Y. W. Han, H. Zou, J. Y. Shen, W. J. Ji and Y. Chen, *Chem. Lett.*, 1998, 1179.
37 J. C. Lavalley and J. Caillod, *J. Chim. Phys.*, 1980, **77**, 373.
38 W. C. Wu, C. C. Chuang and J. L. Lin, *J. Phys. Chem. B*, 2000, **104**, 8719.
39 V. Boiadjiev and W. T. Tysoe, *Chem. Mater.*, 1998, **10**, 334.
40 F. Ouyang and S. Yao, *J. Phys. Chem. B*, 2000, **104**, 11253.
41 J. G. Chen, P. Basu, T. H. Ballinger and J. T. Yates, *Langmuir*, 1989, **5**, 352.
42 T. Fujino, M. Kashitani, J. N. Kondo, K. Domen, C. Hirose, M. Ishida, F. Goto and F. Wakabayashi, *J. Phys. Chem.*, 1996, **100**, 11649.
43 Q. Y. Feng and S. L. Yao, *J. Phys. Chem. B*, 2000, **104**, 11253.
44 E. Finocchio, M. Daturi, C. Binet, J. C. Lavalley and G. Blanchard, *Catal. Today*, 1999, **52**, 53.
45 P. Cheung, A. Bhan, G. J. Sunley and E. Iglesia, *Angew. Chem. Int. Ed.*, 2006, **45**, 1617.
46 M. Li and J. Shen, *J. Catal.*, 2002, **205**, 248.
47 J. Bandiera and C. Naccache, *Appl. Catal.*, 1991, **69**, 139.

Figure Captions

Fig.1. XRD pattern of Nb_2O_5 and $NbOPO_4$ catalysts.

Fig. 2. Differential heat versus coverage (per gram of catalyst) for NH_3 adsorption at 423 K over Nb_2O_5 and $NbOPO_4$ catalysts.

Fig. 3. Differential heat versus coverage (per gram of catalyst) for H_2O adsorption at 303 K over Nb_2O_5 and $NbOPO_4$ catalysts.

Fig. 4. Differential heat versus coverage (per m^2 of catalyst) for NH_3 adsorption at 423 K and H_2O adsorption at 303 K over Nb_2O_5 and $NbOPO_4$ catalysts.

Fig. 5. Differential heat versus coverage (per gram of catalyst) for methanol adsorption at 303 K over Nb_2O_5 and $NbOPO_4$ catalysts.

Fig. 6. Differential heat versus coverage (per gram of catalyst) for DME adsorption at 303 K over Nb_2O_5 and $NbOPO_4$ catalysts.

Fig. 7. Temperature programmed desorption (TPD) profiles of adsorbed H_2O on Nb_2O_5 and $NbOPO_4$ catalysts as studied by TG-MS.

Fig. 8. Temperature programmed desorption (TPD) profiles of adsorbed methanol on Nb_2O_5.
(*m/e*: methanol 31, water 18, dimethyl ether 45, methane 15 and 16)

Fig. 9. Temperature programmed desorption (TPD) profiles of adsorbed methanol on $NbOPO_4$.
(*m/e*: methanol 31, water 18, dimethyl ether 45, methane 15 and 16)

Fig. 10. FT-IR spectra after NH_3 adsorption and desorption at 300 K on Nb_2O_5 and $NbOPO_4$ catalysts.

Fig. 11. FT-IR absorption bands of OH groups of the Nb_2O_5 desorbed at different temperatures. (a) 300 K, (b) 423 K,(c) 573 K. (Inset: FT-IR absorption bands of OH groups of the Nb_2O_5 and $NbOPO_4$ desorbed at 300 K)

Fig. 12. FT-IR absorption bands of OH groups of the $NbOPO_4$ desorbed at different temperatures. (a) 300 K, (b) 423 K,(c) 573 K, (d) 673 K, (e) 773 K.

Fig. 13. FT-IR spectra for methanol adsorption and desorption on Nb_2O_5 catalyst at different temperatures (a) 300 K, (b) 373 K, (c) 473 K, (d) 573 K, (e) 673 K.

Fig. 14. FT-IR spectra for methanol adsorption and desorption on $NbOPO_4$ catalyst at different temperatures (a) 300 K, (b) 373 K, (c) 473 K, (d) 573 K, (e) 673 K.

Fig. 15. FTIR spectra for dimethyl ether adsorption and desorption on Nb_2O_5 catalyst at different temperatures (a) 298 K, (b) 373 K, (c) 473 K, (d) 573 K, (e) 673 K.

Fig. 16. FTIR spectra for dimethyl ether adsorption and desorption on $NbOPO_4$ catalyst at different temperatures (a) 298 K, (b) 373 K, (c) 473 K, (d) 573 K, (e) 673 K.

Fig. 17. Conversion of methanol at different temperatures over Nb_2O_5, $NbOPO_4$, H-ZSM-5 and γ-Al_2O_3 catalysts. (The activities of H-ZSM-5 and γ-Al_2O_3 from the literature[9] are depicted as a comparison)

Table 1

Chemical analysis, X-ray photoelectronic spectroscopy analysis, BET surface area, microporous surface area, average pore radius, and pore volume of the samples

Sample	C.A. (wt%)		XPS (wt%)		BET ($m^2 \cdot g^{-1}$)	Average pore diameter (nm)	Pore volume ($ml \cdot g^{-1}$)
	Nb	P	Nb	P			
Nb_2O_5	---	---	---	---	110	6.0	0.16
$NbOPO_4$	42.6	12.4	12.1	12.7	511	4.4	0.56

Table 2

Number and strength of acid sites as determined by adsorption microcalorimetry under an equilibrium pressure of 27 Pa

Sample	Probe	V_{tot}[a] (27 Pa) ($\mu mol \cdot g^{-1}$)	V_{tot}[a] (27 Pa) ($\mu mol \cdot m^{-2}$)	V_{irr}[b] (27 Pa) ($\mu mol \cdot g^{-1}$)	V_{irr}[b] (27 Pa) ($\mu mol \cdot m^{-2}$)	Q_{init}[c] ($kJ \cdot mol^{-1}$)	Q_{int}[d] (27 Pa) ($J \cdot g^{-1}$)
Nb_2O_5	NH_3	208	1.9	89	0.8	165	22.4
$NbOPO_4$		716	1.4	298	0.6	165	76.5
Nb_2O_5	CH_3OH	483	4.4	341	3.1	142	44.0
$NbOPO_4$		1365	2.7	977	1.9	148	126.1
Nb_2O_5	DME	184	1.7	117	1.1	130	18.5
$NbOPO_4$		499	1.0	300	0.6	133	48.6
Nb_2O_5	H_2O	526	4.8	166	1.5	179	42.0
$NbOPO_4$		1260	2.5	411	0.8	189	101.2

Notes: [a] Total amount of NH_3, methanol, DME and water retained as determined at 27 Pa of equilibrium pressure.

[b] "Irreversible" amount of NH_3, methanol, DME and water retained as determined from the difference between the amounts adsorbed in the first and second adsorptions at 27 Pa, which represents the amount of strong sites.

[c] Heat evolved from the first NH_3, methanol, DME and water dose.

[d] Integral heat evolved at 27 Pa of NH_3, methanol, DME and water equilibrium pressure.

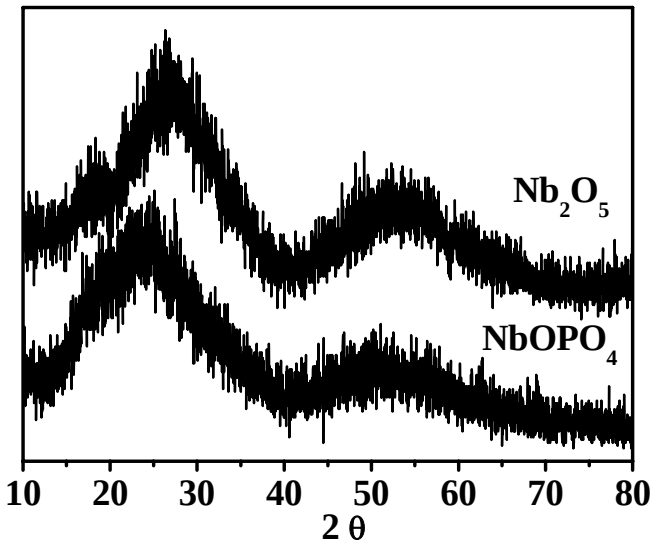

Fig.1. XRD pattern of Nb_2O_5 and $NbOPO_4$ catalysts.

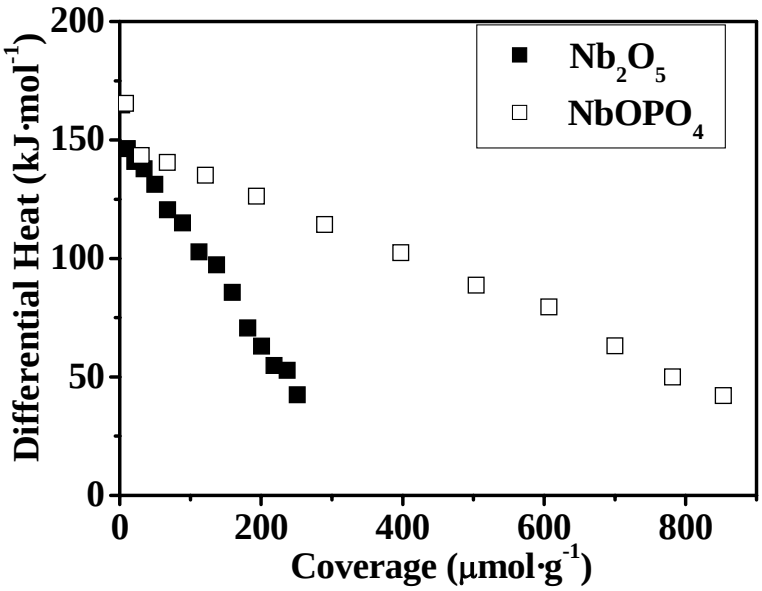

Fig. 2. Differential heat versus coverage (per gram of catalyst) for NH_3 adsorption at 423 K over Nb_2O_5 and $NbOPO_4$ catalysts.

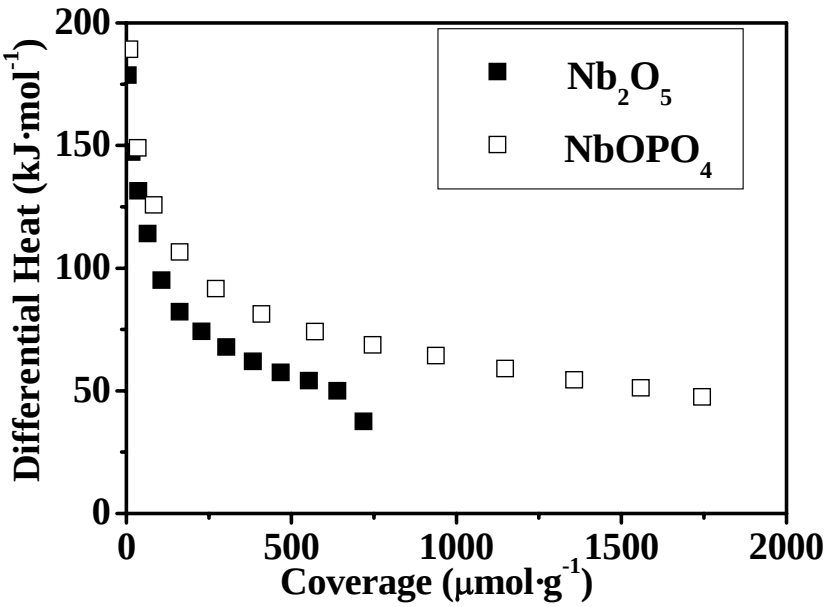

Fig. 3. Differential heat versus coverage (per gram of catalyst) for H_2O adsorption at 303 K over Nb_2O_5 and $NbOPO_4$ catalysts.

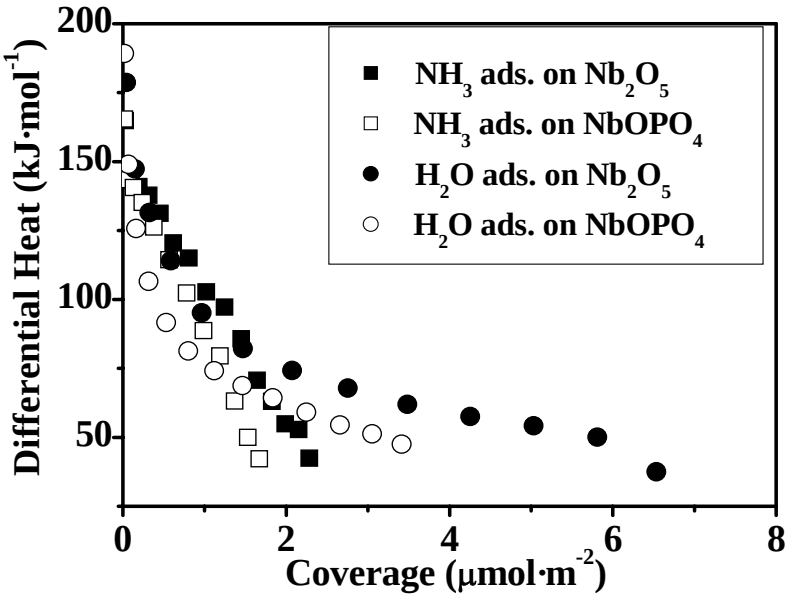

Fig. 4. Differential heat versus coverage (per m^2 of catalyst) for NH_3 adsorption at 423 K and H_2O adsorption at 303 K over Nb_2O_5 and $NbOPO_4$ catalysts.

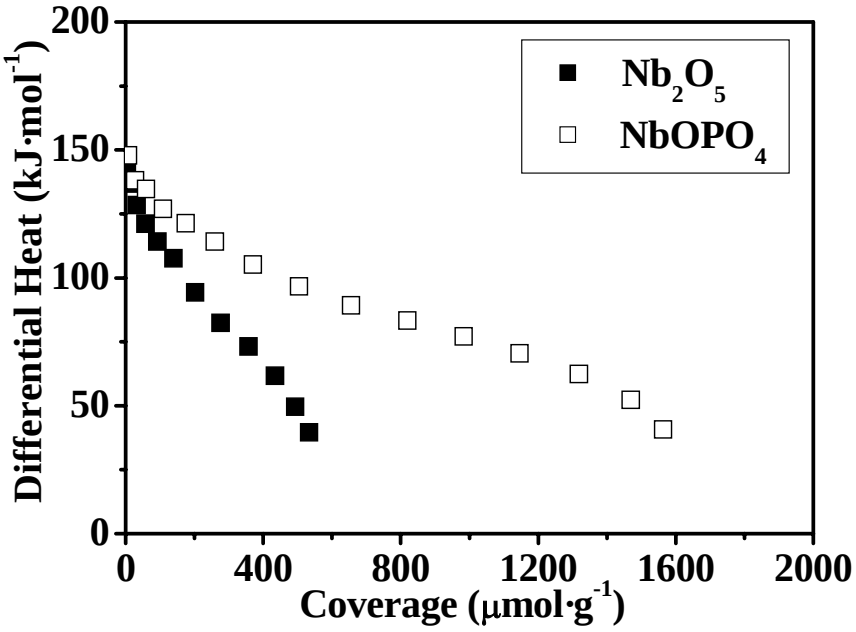

Fig. 5. Differential heat versus coverage (per gram of catalyst) for methanol adsorption at 303 K over Nb_2O_5 and $NbOPO_4$ catalysts.

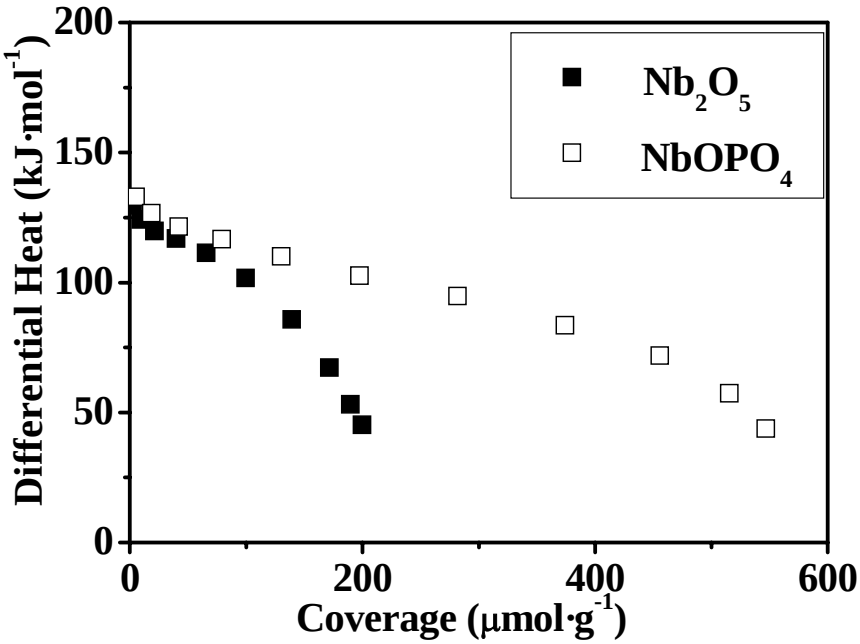

Fig. 6. Differential heat versus coverage (per gram of catalyst) for DME adsorption at 303 K over Nb_2O_5 and $NbOPO_4$ catalysts.

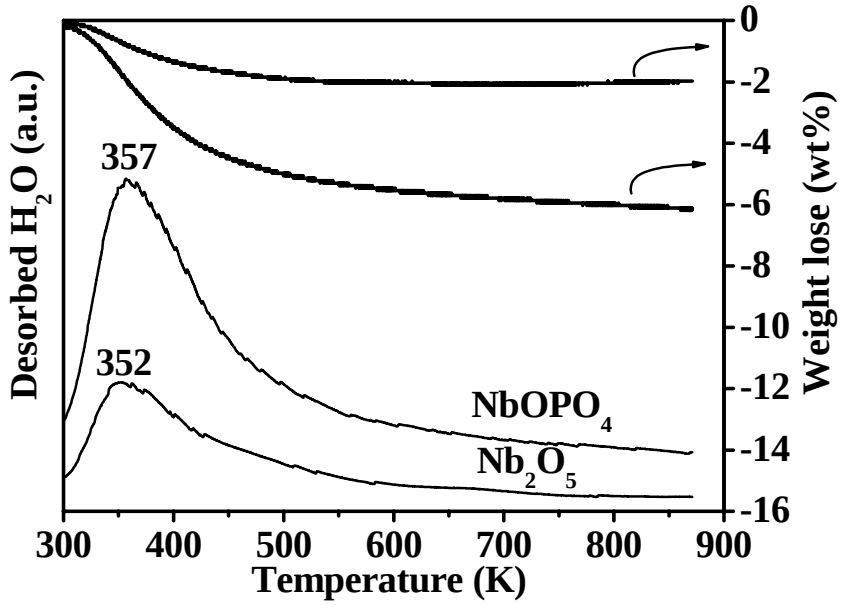

Fig. 7. Temperature programmed desorption (TPD) profiles of adsorbed H_2O on Nb_2O_5 and $NbOPO_4$ catalysts.

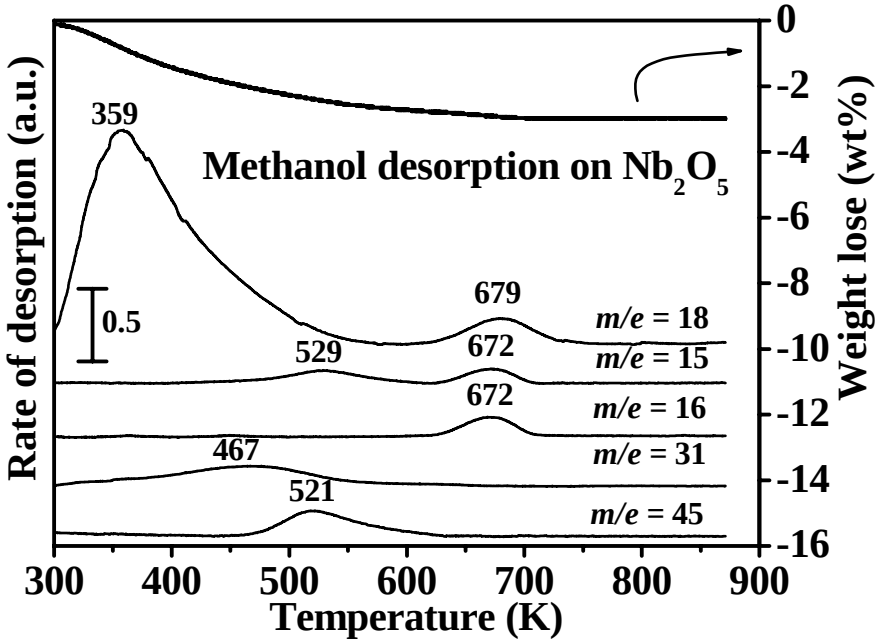

Fig. 8. Temperature programmed desorption (TPD) profiles of adsorbed methanol on Nb_2O_5. (*m/e*: methanol 31, water 18, dimethyl ether 45, methane 15 and 16)

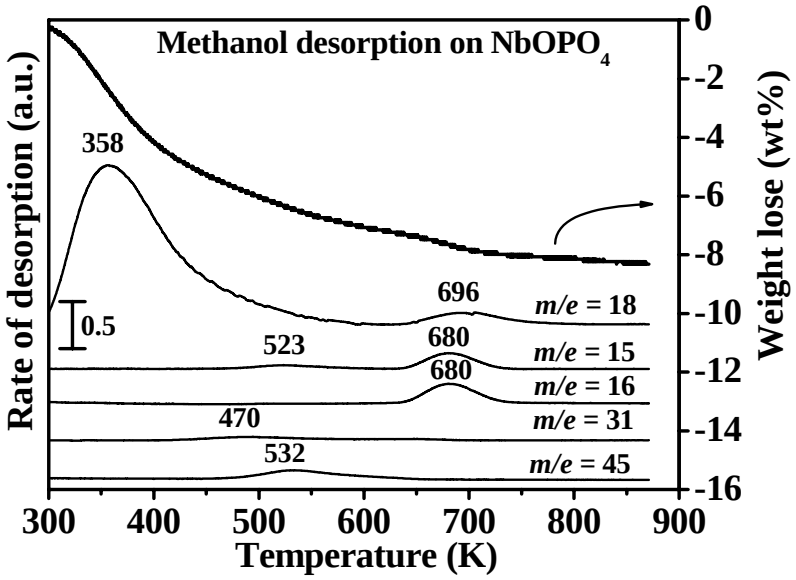

Fig. 9. Temperature programmed desorption (TPD) profiles of adsorbed methanol on $NbOPO_4$. (*m/e*: methanol 31, water 18, dimethyl ether 45, methane 15 and 16)

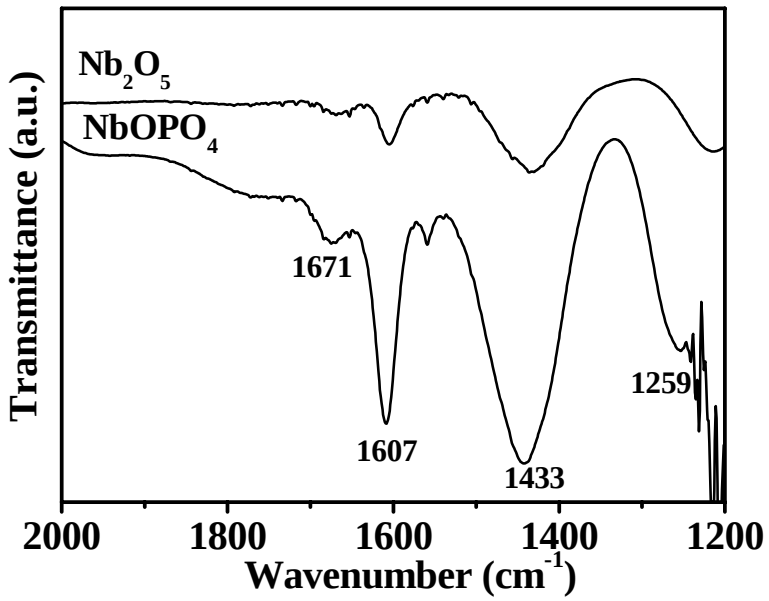

Fig. 10. FT-IR spectra after NH_3 adsorption and desorption at 300 K on Nb_2O_5 and $NbOPO_4$ catalysts.

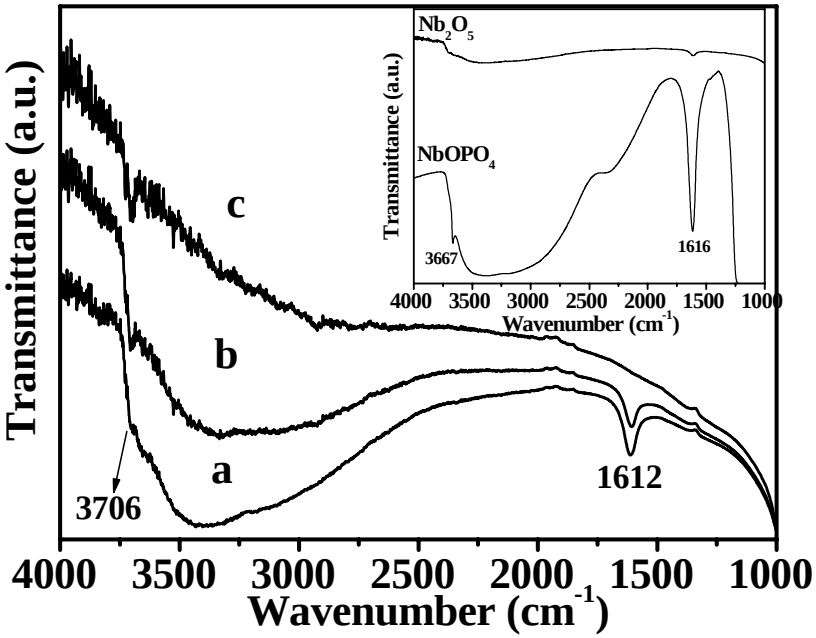

Fig. 11. FT-IR absorption bands of OH groups on Nb_2O_5 sample desorbed at different temperatures. (a) 300 K, (b) 423 K,(c) 573 K. (Inset: FT-IR absorption bands of OH groups of the Nb_2O_5 and $NbOPO_4$ samples desorbed at 300 K)

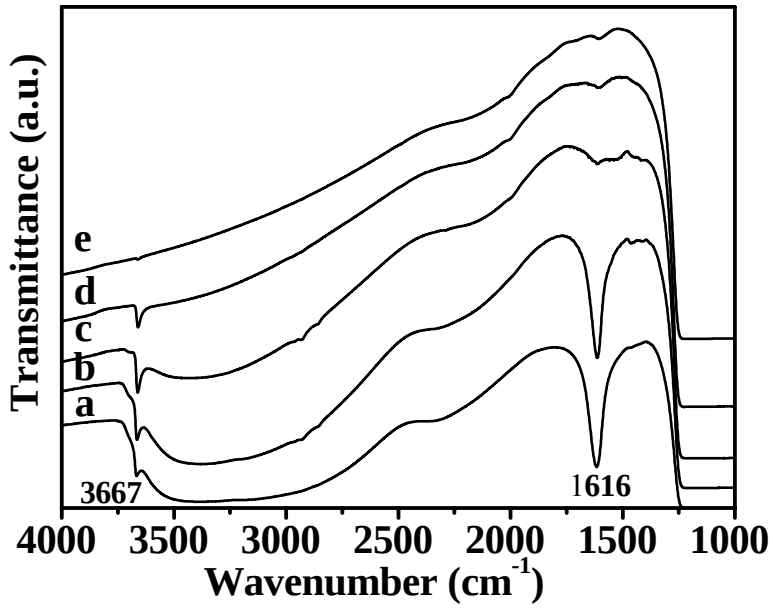

Fig. 12. FT-IR absorption bands of OH groups on $NbOPO_4$ sample desorbed at different temperatures. (a) 300 K, (b) 423 K,(c) 573 K, (d) 673 K, (e) 773 K.

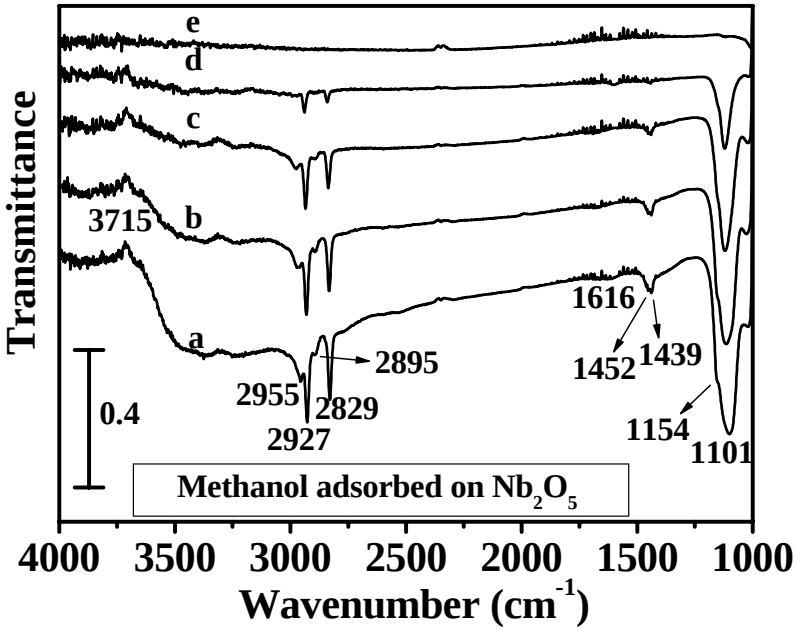

Fig. 13. FT-IR spectra for methanol adsorption and desorption on Nb_2O_5 catalyst at different temperatures (a) 300 K, (b) 373 K, (c) 473 K, (d) 573 K, (e) 673 K.

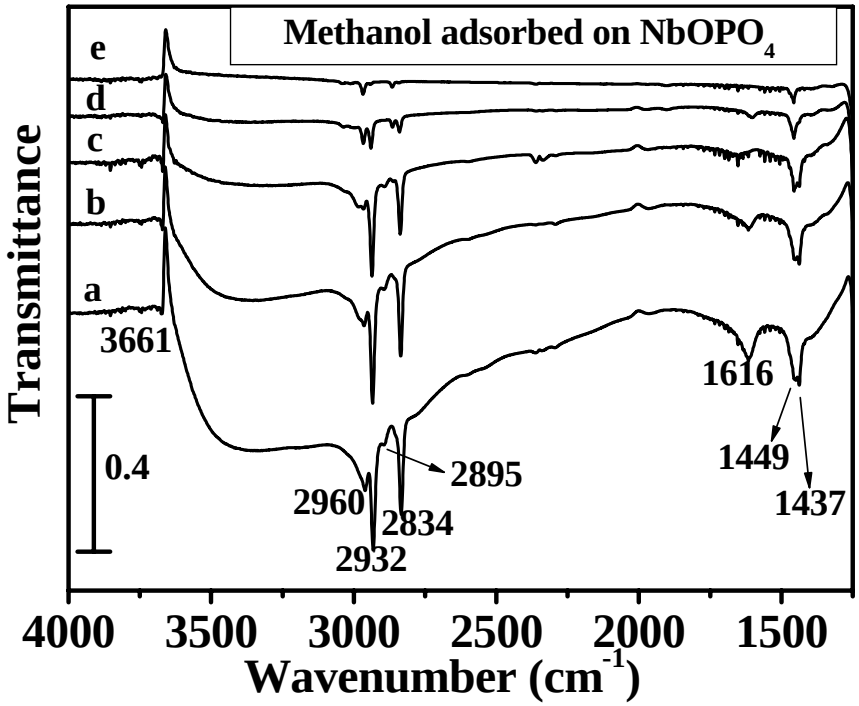

Fig. 14. FT-IR spectra for methanol adsorption and desorption on $NbOPO_4$ catalyst at different temperatures (a) 300 K, (b) 373 K, (c) 473 K, (d) 573 K, (e) 673 K.

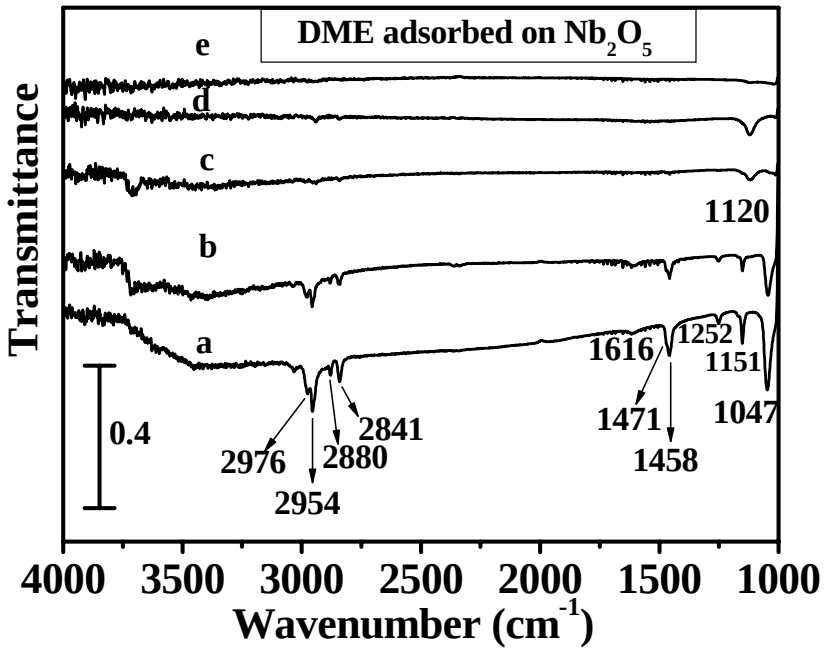

Fig. 15. FTIR spectra for dimethyl ether (DME) adsorption and desorption on Nb_2O_5 catalyst at different temperatures (a) 298 K, (b) 373 K, (c) 473 K, (d) 573 K, (e) 673 K.

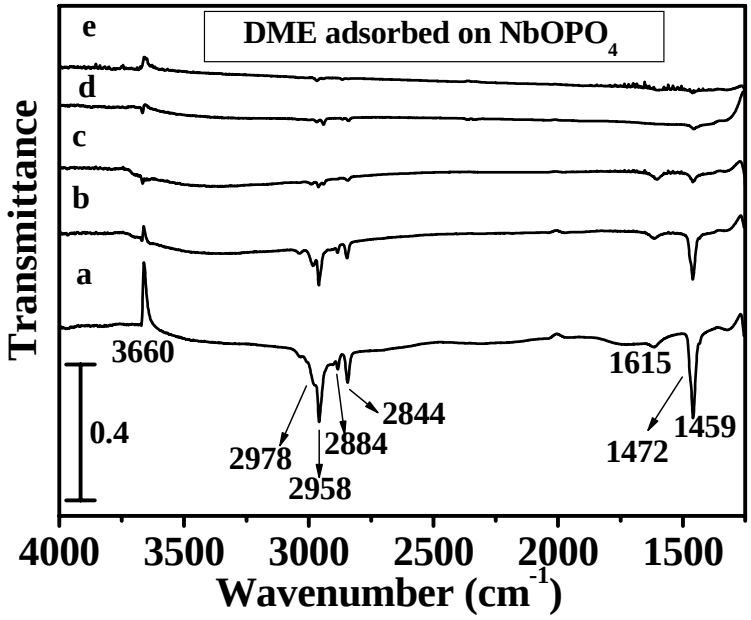

Fig. 16. FTIR spectra for dimethyl ether (DME) adsorption and desorption on $NbOPO_4$ catalyst at different temperatures (a) 298 K, (b) 373 K, (c) 473 K, (d) 573 K, (e) 673 K.

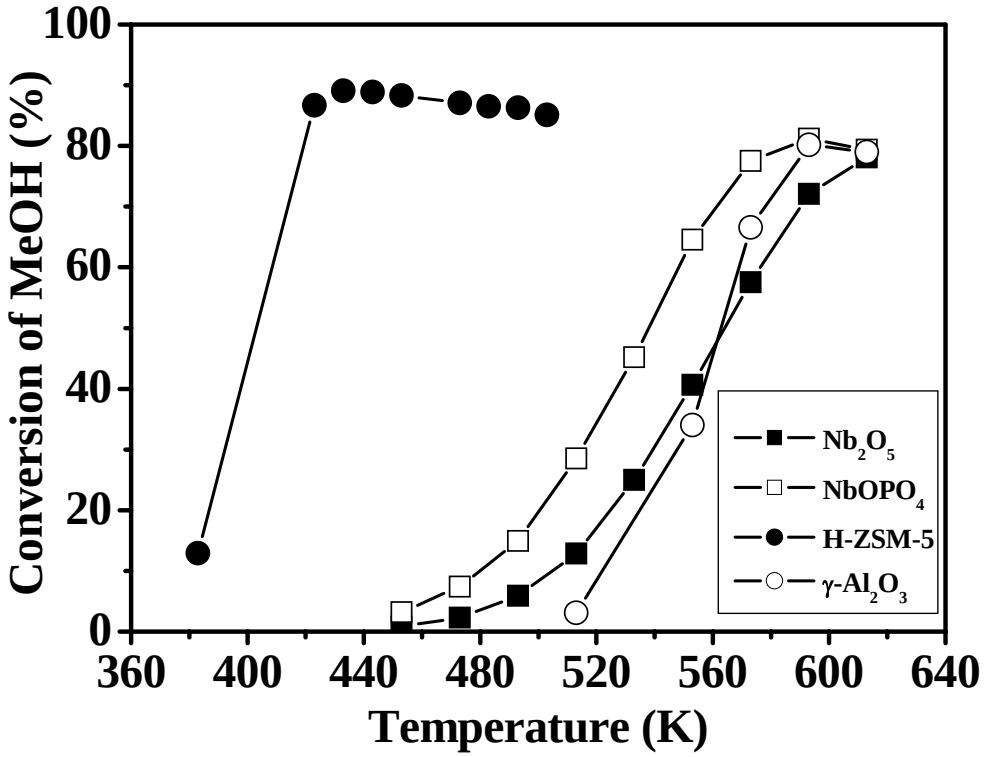

Fig. 17. Conversion of methanol at different temperatures over Nb_2O_5, $NbOPO_4$, H-ZSM-5 and γ-Al_2O_3 catalysts. (The activity of H-ZSM-5 and γ-Al_2O_3 from the literature[9] are depicted as a comparison)

Publication VI

Accepted in Applied Catalysis A: General

Structural, acidic and redox properties of V_2O_5-TiO_2-SO_4^{2-} catalysts

Qing Sun[1,2], Yuchuan Fu[1], Jingwei Liu[1], Aline Auroux[2], Jianyi Shen[1]*

[1]Laboratory of Mesoscopic Chemistry, School of Chemistry and Chemical Engineering, Nanjing University, Nanjing 210093, China

[2]Institut de Recherches sur la Catalyse et l'Environnement de Lyon, UMR 5256, CNRS-Université Lyon 1, 2 Avenue Albert Einstein, 69626 Villeurbanne Cedex, France

---

* Corresponding author E-mail: jyshen@nju.edu.cn

Phone: (+86)25-83594305 Fax: (+86)25-83594305

Abstract

A series of V_2O_5-TiO_2 (VT) catalysts with V_2O_5 contents from 15 to 75 wt% was prepared by the co-precipitation method, and the catalysts were doped with SO_4^{2-} ions. The structural properties were characterized by X-ray diffraction (XRD), Raman spectroscopy (LRS) and X-ray photoelectron spectroscopy (XPS). The surface acidity was determined by the techniques of NH_3 adsorption microcalorimetry and pyridine adsorption infrared spectroscopy (FT-IR). Isopropanol (IPA) and methanol probe reactions in the presence of O_2 were employed to provide information about the surface acidity and redox properties simultaneously. The results from XRD and LRS showed that V_2O_5 was well dispersed on the surface of TiO_2 when the vanadia content was below 25 wt%, with a surface V density of 11.5 $V{\cdot}nm^{-2}$. XPS showed that both vanadium and titanium were present in their fully oxidized states in all the samples. The SO_4^{2-} doped VT samples presented a sulfur oxidation state of +6. The results of NH_3 adsorption microcalorimetry and pyridine adsorption FT-IR indicate that the VT catalysts possess identical surface acid densities independently of the V_2O_5 content, and that both Brønsted and Lewis acid sites are present on their surface. The isopropanol probe reaction and methanol oxidation reaction results suggest that the surface acidity of VT catalysts was improved upon SO_4^{2-} doping, as evidenced by the simultaneous decrease in the amounts of oxidation products and increase in the amounts of dehydration products. A high selectivity of 90% to DMM was measured on the SO_4^{2-} modified 25%V_2O_5-75%TiO_2 catalyst, with 54% conversion of methanol at low temperature (413 K).

Key words: V_2O_5-TiO_2-SO_4^{2-}; Adsorption microcalorimetry; Acidic and redox properties; Isopropanol probe reaction; Methanol probe reaction

1. Introduction

V_2O_5/TiO_2 catalysts are widely used for many selective oxidation reactions. For example, they are used for ammoxidation of alkyl aromatics [1, 2], selective oxidation of methanol to formaldehyde [3] and methyl formate [4], selective oxidation of ethanol to acetaldehyde [5], selective oxidation of toluene to benzaldehyde and benzoic acid [6], selective oxidation of o-xylene to phthalic anhydride [7, 8], etc. Extensive studies have been devoted to such catalysts regarding the dispersion, surface structure, oxidation states and reducibility of the supported vanadia species under different conditions, and these properties have been correlated to the performance in selective oxidation reactions [9-12]. Excellent summaries about these studies can be found in references [13-15].

Methanol is one of the most important chemical intermediates used in industrial chemistry. The oxidation of methanol has been widely used as a probe reaction to characterize the activity of oxide catalysts [16, 17] and interpret it in terms of both structural and chemical (acidic and redox) properties, for example for molybdenum based systems supported on silica and vanadia on titanium oxide.

It appears from the literature that methanol can lead to different products by varying the nature of the catalyst and the reaction conditions. The main reaction product cited in the literature is formaldehyde (FA), because of its industrial interest. However, it is also reported that important amounts of dimethyl ether (DME), methyl formate (MF), dimethoxymethane (DMM) and carbon oxides can be formed by oxidation of methanol.

In the reaction of methanol oxidation, DMM has usually been regarded as a by-product and has never been studied intensively. DMM has an extremely low toxicity and can be used as an excellent solvent in pharmaceutical and perfume industries, as a reagent in organic synthesis [18], and as an intermediate for the production of concentrated formaldehyde [19]. We have also recently reported that DMM can be effectively steam reformed to produce H_2 for fuel cells [20]. Generally DMM is produced by condensation of formaldehyde with methanol over acidic catalysts [21]. It has been reported that DMM can also be synthesized by the direct oxidation of methanol on crystalline $SbRe_2O_6$ [22], $Re/\gamma\text{-}Fe_2O_3$ [23], heteropolyacids [24], or RuO_x/SiO_2 [25].

It has recently been reported that TiO_2-supported V_2O_5 catalysts modified by SO_4^{2-} ions possess a good activity in the selective catalytic reduction (SCR) of nitric oxides [26-29], suggesting that the surface acidity of the catalysts could be greatly enhanced by the addition of SO_4^{2-}.

In this work, high surface area V_2O_5-TiO_2 catalysts were prepared by a co-precipitation method and were doped with SO_4^{2-} ions. The structural properties and the acidic and redox properties of the catalysts have been characterized. The V_2O_5-TiO_2-SO_4^{2-} catalysts were tested in the methanol oxidation reaction and the results analyzed in relation with the addition of SO_4^{2-}.

2. Experimental

2.1. Catalyst preparation

High surface area vanadia-titania catalysts (denoted by VT) were prepared by a co-precipitation method. Specifically, stoichiometric $TiCl_4$ (99.9%) was dissolved in C_2H_5OH (1g $TiCl_4$ in 20 ml C_2H_5OH) in an ice bath, forming a titanium-containing solution (S1), while a vanadium-containing solution (S2) was obtained by dissolving $VOCl_3$ (99.9%, Aldrich) into H_2O (1g $VOCl_3$ in 20 ml H_2O). Then S1 was slowly dropped into S2 under continuous stirring to form a mixed solution (S3). An excess amount of diluted $NH_3.H_2O$ (4 wt % NH_3) was then dropped into S3 under vigorous stirring in an ice bath, and a brown precipitate formed immediately. This precipitate was first aged for 3 h at room temperature. It was then successively filtered, washed with deionized water until no chloride ions were detected, dried at 373 K overnight, and calcined at 673 K in air for 6 h. Pure TiO_2 and V_2O_5 were prepared by the same method.

The V_2O_5-TiO_2-SO_4^{2-} (VTS) samples were prepared by incipient wetness impregnation of 1 gram of above mentioned VT catalyst with an aqueous solution containing 50 mg $Ti(SO_4)_2$. After being kept at room temperature overnight, the resulting material was dried at 373 K overnight and then calcined in air at 673 K for 4 h.

2.2. Catalyst characterization

The X-ray diffraction (XRD) measurements were carried out on a Bruker D5005 diffractometer scanning from 3^o to 80^o (2θ) at a rate of 0.02 degree·s^{-1} using a Cu Kα

radiation (λ = 0.15418 nm) source. The applied voltage and current were 50 kV and 35 mA, respectively. Elemental analysis was performed using ICP atomic emission spectroscopy (Spectroflame-ICP D, Spectro). The surface areas were measured by nitrogen adsorption at 77 K after heat pretreatment under vacuum at 623 K for 4 h.

The X-ray photoelectron spectra (XPS) were measured on a SSI 301 instrument equipped with a hemispherical electron analyzer and an Al anode (Al Kα =1486.6 eV) powered at 100 W. The residual pressure in the spectrometer chamber was 5×10^{-8} Pa during data acquisition.

The skeletal FT-IR spectra were recorded with a Bruker Vector 22 FTIR spectrophotometer (DTGS detector) operating in the 4000–400 cm^{-1} range, with a resolution of 2 cm^{-1} and 100 acquisition scans. In each experiment, 2 mg of sample were mixed with 198 mg of KBr. A spectrum was recorded at room temperature.

Raman spectra were obtained using a Dilor XY spectrometer coupled to an Olympus BH-2 microscope. The excitation was provided by the 514.5 nm line of an Ar+ ion laser (Spectra Physics) employing a laser power of 2.5 mW. The range and resolution were 100-1100 cm^{-1} and 0.5 cm^{-1}, respectively.

H_2-TPR measurements were carried out in continuous mode using a U-type quartz microreactor (3.5 mm in diameter). A sample of about 50 mg was contacted with a H_2:N_2 mixture (5.13% volume of H_2 in N_2) at a total flow rate of 40 ml·min^{-1}. The sample was heated at a rate of 10 K·min^{-1} from room temperature to 1250 K. The hydrogen consumption was monitored using a thermal conductivity detector (TCD). The reducing gas was first passed through the reference arm of the TCD before entering the reactor. The flow out of the reactor was directed through a trap filled with $Mg(ClO_4)_2$ (to remove water from the product) and then to the second arm of the TCD.

The microcalorimetric studies of ammonia adsorption were performed at 423 K in a heat flow calorimeter (C80 from Setaram) linked to a conventional volumetric apparatus equipped with a Barocel capacitance manometer for pressure measurements. Ammonia used for the measurements (purity > 99.9%) was purified by successive freeze–pump–thaw cycles. About 100 mg of sample was pretreated in a quartz cell under evacuation overnight at 623 K. The differential heats of adsorption were measured as a

function of coverage by repeatedly introducing small doses of ammonia gas onto the catalyst until an equilibrium pressure of about 66 Pa was reached. The sample was then outgassed for 30 min at the same temperature, and a second adsorption was performed at 423 K until an equilibrium pressure of about 27 Pa was attained, in order to calculate the irreversibly chemisorbed amount of ammonia at this pressure.

The pyridine adsorption infrared spectra were recorded with a Bruker Vector 22 FTIR spectrophotometer (DTGS detector) in the 4000–400 cm^{-1} range, with a resolution of 2 cm^{-1} and 50 acquisition scans. The self-supporting wafer (10-30 mg, 18 mm diameter) was first activated in situ in the IR cell at 673 K in O_2 flow for 12 h, evacuated at the same temperature for 2 h, and then exposed to pyridine (purity > 99.9%) at room temperature for 5 minutes. The desorption was carried out by evacuation for 30 min each at room temperature, 323, 373, 473, 523 and 573 K successively. A spectrum was recorded at room temperature after desorption at each temperature.

2.3. Catalytic reaction

The reaction of isopropanol conversion was used to characterize the surface acidity. This probe reaction was carried out in a fixed-bed glass tube reactor. About 100 mg of sample was loaded for each reaction. Isopropanol was introduced onto the catalyst by bubbling air through a glass saturator filled with isopropanol maintained at 295 K. Isopropanol and reaction products were analyzed by an online gas chromatograph, using a PEG 20M packed column connected to a Flame Ionization Detector (FID). Each catalyst was pretreated by heating in air at 673 K for 1 h and then cooled in the same flow to the reaction temperature.

The oxidation of methanol was carried out in a fixed-bed micro-reactor made of glass with an inner diameter of 6 mm. The methanol was introduced into the reaction zone by bubbling O_2/N_2 (1/5) through a glass saturator filled with methanol (99.9%) maintained at 278 K. In each test, 0.2 g of catalyst was loaded, and the gas hourly space velocity (GHSV) was 11400 $ml.g^{-1}.h^{-1}$. The feed composition was maintained as methanol:O_2:N_2=1:3:15 (v/v). The tail gas out of the reactor was analyzed by an on-line GC equipped with an FID detector and a TCD detector. The column used was PORAPAK N for the separation of

methanol, DMM and other organic compounds. The gas lines were kept at 373 K to prevent condensation of the reactant and products. The reaction was carried out at atmospheric pressure.

3. Results and discussion

3.1. Surface structures

The XRD patterns of the VT samples are presented in Fig. 1. It can be seen from the figure that typical diffraction peaks characteristic of anatase TiO_2 are observed for all VT samples. The intensities of the peaks due to anatase TiO_2 decreased with increasing V_2O_5 content, as the concentration of TiO_2 decreased. For the VT samples with V_2O_5 contents lower than 25%, no crystalline vanadia phase was observed, indicating that vanadium oxide was present in a highly dispersed manner. The diffraction lines due to crystalline V_2O_5 began to appear when the V_2O_5 content increased to 50%, which suggests that agglomeration of V_2O_5 took place beyond this level of loading. Very similar XRD diffraction lines were observed for VT samples doped with SO_4^{2-}, indicating that the addition of SO_4^{2-} did not affect the dispersion of the VT samples. (Figure not shown)

The surface areas of the VT catalysts are shown in Table 1. TiO_2 possessed a surface area of 143 $m^2 \cdot g^{-1}$, which is higher than industrial TiO_2 such as DT 51 (100 m^2/g, Rhone Poulenc Ind.). It is usually reported in the literature that in V_2O_5/TiO_2 systems the surface area decreases with the V_2O_5 content. In this work, the VT sample containing 15 wt% V_2O_5, was found to display the largest surface area of 159 $m^2 \cdot g^{-1}$. This might be due to some conditions not controlled well during the catalysts preparation. Further increasing the vanadia content led to a monotonically linear decrease in the surface areas, down to the lowest value (21 m^2/g) for pure V_2O_5. Doping the VT catalysts with SO_4^{2-} decreased their surface area, which might be due to the collapse of some pores during the re-calcination of the VTS catalysts.

Table 1 also lists the binding energies (BE) as well as surface and bulk V/Ti ratios from XPS and chemical analysis. The C 1s peak at 284.6 eV was used as an internal standard for correction of binding energies. The binding energies of V $2p_{3/2}$ for the 15VT, 25VT, 50VT and V_2O_5 samples were 517.1, 517.1, 516.9 and 517.3 eV, respectively. It is

well known that the binding energy for V^{5+} in V_2O_5 is between 517.4 and 516.4 eV, while it is between 515.7 and 515.4 eV for V^{4+} in V_2O_4 [30]. Therefore, the observed values indicate that the vanadia surface species were fully oxidized (oxidation state V^{5+}). TiO_2, 15VT, 25VT and 50VT samples showed similar Ti $3d_{5/2}$ binding energy values around 458.5, 458.5, 458.3 and 458.3 eV, respectively. This suggests the presence of Ti^{4+}, which agrees well with the data reported in the literature [31, 32]. The bands for Ti were enhanced while those for V weakened with increasing V_2O_5 content, indicating a gradually increasing coverage of TiO_2 by V_2O_5 (Figures not shown). The XPS and chemical analysis results show that the surface vanadia content was higher than the overall vanadia amount in the 15VT and 25VT samples (See Table 2). For sample 50VT, the surface V/Ti atomic ratio was nearly the same as the bulk ratio, implying the accumulation of vanadia species.

For the 15VTS and 25VTS samples (15VT and 15VT doped with SO_4^{2-}, respectively), binding energies of 168.3 and 168.2 eV respectively were measured for the S 2p line. According to the literature data, these binding energy values are typical of sulfur in the S^{6+} oxidation state on the catalyst surface, as in Na_2SO_4 or $Fe_2(SO_4)_3$ [26, 33]. The peaks at 161-162.8 eV assigned to sulfide and at 164 eV to elemental sulfur were not observed. The S^{6+} species might be present in the form of bidentate sulfate on the surface of TiO_2, either chelating or bridging, as proposed in the literature [31, 34]. The results of chemical analysis (CA) for the S element (data not shown) showed that the S content in the VTS sample was very low (S < 0.3 wt%), beyond the detection capacity of CA, suggesting that most of the sulfate ions might have decomposed during the calcination of the VTS samples.

The skeletal IR spectra are reported in Fig. 2. No obvious bands could be observed for the TiO_2 sample. With the addition of V_2O_5, two thresholds around 1000 and 800 cm^{-1} appear for the VT samples, which could be assigned to the bands for monovanadate and polyvanadate species bonded to the surface of TiO_2 [35]. Increasing the V_2O_5 content to 50 wt% led to a sharp band at 1029 cm^{-1}, suggesting formation of crystalline V_2O_5 at this high V_2O_5 content. Four bands were detected for the V_2O_5 sample, located at 1022, 835, 627 and 480 cm^{-1}, respectively. The band at 1022 cm^{-1} could be assigned to the stretching mode of the $(V=O)^{3+}$ double bond [36, 37]. The bands at 835, 627 and 480 cm^{-1} are due to

the asymmetric stretching, symmetric stretching and rotation modes of V-O-V [38, 39], respectively. The features typical of crystalline V_2O_5 phase were observed when V_2O_5 content increased to 50%, in good agreement with the XRD results. It seems that adding SO_4^{2-} onto VT samples did not change the previously observed dispersion of V_2O_5, since the IR spectra of VTS samples are very similar to those of the corresponding VT samples.

The Raman spectra of the VT samples are presented in Fig. 3, from 1200 to 200 cm^{-1}, as a function of vanadia content. Strong Raman bands due to the covalent character of Ti-O bonds [40] appeared at 633, 514 and 403 cm^{-1} on all VT samples. For 15VT, a sharp band at 1028 cm^{-1} and a broad band at 925 cm^{-1} are assigned to terminal V=O and surface polymerized V-O-V species, respectively, in agreement with previous observations for supported vanadia catalysts [41]. When increasing V_2O_5 content from 15% to 25%, the intensities of both bands increased, suggesting that the populations of both isolated and polymerized surface vanadia species increased. In addition, the V=O stretching vibration band shifted from 1028 to 1034 cm^{-1}, which could be ascribed to distortions of the surface VOx species upon polymerization as suggested by Zhao et al [42]. The VT catalyst with high V_2O_5 content (50 wt%) exhibited typical Raman features of crystalline V_2O_5, showing bands around 994, 700, 525, 405, 301 and 282 cm^{-1}. Since the Raman response is very sensitive for crystalline phases, the absence of a crystalline V_2O_5 response for 25VT confirmed that the vanadia species were well dispersed below 25 wt% V_2O_5 loading, in good agreement with the results of XRD and skeletal IR. The literature on titania-supported vanadia samples usually reports maximum amounts of surface V atoms close to 7-8 $V{\cdot}nm^{-2}$, when reaching the monolayer dispersion [15, 41]. In this work, for the sample containing 25 wt% V_2O_5, the calculated surface vanadium amount is 11.5 $V{\cdot}nm^{-2}$, which suggests a higher vanadia loading could be achieved by using the co-precipitation method.

3.2. Surface acidity

Ammonia adsorption microcalorimetry measurements were carried out to determine the number, strength and strength distribution of the surface acid sites of the catalysts [43]. The surface acidity was thus determined in terms of number of acid sites and site strengths. The results are presented in Fig. 4.

The initial heat and saturation coverage for ammonia adsorption on TiO_2 were found to be about 187 $kJ \cdot mol^{-1}$ and 450 $\mu mol \cdot g^{-1}$, respectively, which indicated that the TiO_2 sample was quite acidic. The literature data concerning NH_3 adsorption microcalorimetry on TiO_2 indicates that different samples can have different acidic characters, from a low acidity [12] to a high acidity [44]. Thus, the surface acidity of TiO_2 might be different for different preparation methods. The addition of 15 wt% V_2O_5 into TiO_2 did not change much the initial heat and the saturation coverage, which became 193 $kJ \cdot mol^{-1}$ and 453 $\mu mol \cdot g^{-1}$, respectively. Further increasing the V_2O_5 content in VT catalysts led to a decrease of both the initial heat and the saturation coverage. For the 25VT and 50VT samples, the initial heats of adsorption were 181 and 179 $kJ \cdot mol^{-1}$ while the saturation coverages were 445 and 317 $\mu mol \cdot g^{-1}$, respectively. The decrease of the saturation coverage for VT catalysts was probably due to the decrease of the surface areas, since the surface coverages were the same when expressed per unit surface area (see Fig. 5, inset). Thus, the surface acid site density for TiO_2 and VT catalysts seemed to remain constant with different V_2O_5 contents. The pure V_2O_5 prepared in this work displayed a low initial heat (108 $kJ \cdot mol^{-1}$) and a low saturation coverage ($\mu mol \cdot g^{-1}$) indicating a much lower acidity than for VT samples. These results suggest that the acidity of V_2O_5 was greatly enhanced when supported on TiO_2. For all the catalysts studied in this work, the heat of NH_3 adsorption gradually decreased with NH_3 coverage, revealing the heterogeneous strength distribution of these catalysts. On V_2O_5/TiO_2 catalysts, similar results for NH_3 adsorption microcalorimetry have been reported in [44].

NH_3 adsorption microcalorimetry experiments were also performed on the VT samples doped with SO_4^{2-} in order to determine how the sulfate ions could influence the acidity of VT catalysts. However, during the experiments, endothermic peaks of differential heat were observed, which might due to an endothermic reaction occurring between the surface sulfate ions and adsorbed NH_3. This phenomenon has been already observed in the literature [45].

IR spectroscopy of pyridine adsorption on supported vanadium oxide surfaces has been examined widely in the literature [46-48], as it can be used to distinguish between the different types of surface acid sites in the catalysts.

Figs. 5 presents the IR spectra of pyridine adsorption on VT and VTS catalysts, after desorption at 300 K. The bands at 1608, 1574, 1488 and 1446 cm^{-1} have been assigned to the 8a, 8b, 19a and 19b vibrational modes of pyridine coordinated to Lewis acid sites (LAS) [46, 48]. Similarly, the bands at 1638 (ν8a), 1574 (ν8b), 1488 (ν19a) and 1536 cm^{-1} (ν19b), correspond to pyridinium ions bonded to Brønsted acid sites (BAS). The bands around 1488 (ν19a) and 1574 cm^{-1} (ν8b) are associated simultaneously to both Brønsted and Lewis acid sites.

Pure V_2O_5 presented low Brønsted and Lewis acidities, while TiO_2 exhibited strong Brønsted and Lewis acidities according to the relative intensities of the bands around 1536 and 1446 cm^{-1}. All the bands observed for the VT samples containing 15 wt% and 25 wt% V_2O_5 had intensities similar to those for TiO_2, indicating the similar acidities of these three samples, in good agreement with the results of NH_3 adsorption microcalorimetry. The 50VT sample seemed to have more LAS and fewer BAS since the intensity of the band at 1536 cm^{-1} remained constant while that at 1446 cm^{-1} decreased compared to 25VT. Upon addition of SO_4^{2-} on 25VT, the intensities of the bands decreased slightly compared to 25VT, probably due to the relative lower surface area of 25VTS than 25VT. The influence of SO_4^{2-} doping on the 25VT sample could not be observed from the results of pyridine adsorption IR. This could be due to the long pretreatment (activation in air flow at 673 K overnight and then evacuation at 673 K for 2 h) which could have removed all the surface bonded sulfate species.

3.3. Redox properties

TPR is frequently used to study the redox properties of metal oxide catalysts. The TPR profiles for the VT samples are shown in Fig. 6. Although a detailed description of these TPR profiles is difficult, some useful information can still be obtained by observing the systematic changes of these profiles.

For TiO_2, only a very weak H_2 consumption peak around 828 K was observed, which might be due to a slight reduction of the surface Ti species; this indicates the low reducibility of TiO_2. With addition of 15 wt% V_2O_5, the small peak observed for TiO_2 disappeared, probably suggesting the coverage of TiO_2 by vanadia species, while a new peak appeared around 750 K, ascribed to a reduction of the highly dispersed vanadia

species from V^{5+} to V^{3+} [49]. With the increase of V_2O_5 content, the intensity of this peak increased and the temperature of the maximum of the peak (Tmax) shifted to higher values, which might indicate that the surface vanadia species were present in increasing amounts and gradually changed to more polymeric vanadia species [49]. As the V_2O_5 content increased to 50 wt%, another peak appeared around 818 K, probably due to the reduction of highly polymeric vanadia or crystalline vanadia species. Upon further increasing the V_2O_5 content to 75 wt%, a reduction peak of crystalline V_2O_5 was clearly visible around 943 K, similar to that observed for bulk V_2O_5 [49].

The introduction of SO_4^{2-} had little effect. It seems that the addition of SO_4^{2-} might slightly inhibit the reduction of vanadia, since the reduction peak maxima slightly shifted to higher temperatures, possibly due to an increased proportion of polymeric vanadia species upon re-calcination.

3.4. Isopropanol probe reaction

It is well known that isopropanol (IPA) undergoes dehydration reactions to produce propylene (PPE) and diisopropyl ether (DIPE) on acid sites, while it undergoes a dehydrogenation reaction to acetone (ACE) on basic sites in inert atmosphere [50]. In addition, IPA can also be oxidatively dehydrogenated to ACE in an oxidative atmosphere, which can be used to probe the surface redox properties [51-54]. Thus, the conversion of IPA and selectivities to PPE, DIPE and ACE in air can be used to probe the strength of surface acidic sites and redox properties.

Table 2 presents the results for the probe reaction of IPA conversion on VT and VTS catalysts in air at 413 K. Pure TiO_2 presented a low IPA conversion. Addition of V_2O_5 greatly increased the catalytic activity. For example, the conversion of IPA on TiO_2 was only 6% while that on the 15VT sample was 11%. The activity of VT catalysts in the IPA conversion reaction reached a maximum value for a V_2O_5 content of 25 wt%, and then decreased with further increase of the V_2O_5 loading, probably due to the formation of crystalline vanadia. It can be seen from Table 2 that TiO_2 mainly produced the dehydration products (PPE and DIPE) with a total selectivity of 98%, suggesting the acidic character and lack of redox activity of TiO_2, in good agreement with the results from NH_3 adsorption microcalorimetry and TPR. Addition of 15 wt% V_2O_5 apparently created a

large amount of redox sites on the 15VT sample since the oxidative product ACE was produced with a high selectivity of 89%. Thus, the higher activity of VT catalysts in IPA conversion compared to TiO_2 was possibly due to the generation of redox sites upon the addition of V_2O_5. The selectivity to ACE reached the highest value on the 15VT catalyst and decreased with further increase of the V_2O_5 content. Pure V_2O_5 exhibited a very low activity for the IPA conversion. In addition, the dehydration products (PPE and DIPE) were obtained in larger quantities than the oxidation product (ACE), suggesting that, unlike the VT catalysts, V_2O_5 possessed more acidic sites than redox sites.

Doping with SO_4^{2-} seemed to decrease the activity of the VT samples for IPA conversion, which might be due to the decrease of the surface area. Moreover, some differences could be seen in the distribution of products. It appears that the dehydration products (PPE and DIPE) were formed in larger amounts, while there was less of the oxidation product ACE (see Table 2), although the difference was not large. Therefore, the surface acidic properties might be enhanced and the redox properties weakened upon the addition of SO_4^{2-} onto VT samples.

3.5. Methanol oxidation reaction

Methanol and its derivatives have been widely studied due to their industrial importance. Furthermore, the catalytic oxidation of methanol is a convenient structure-sensitive reaction, widely used to characterize oxide surfaces in terms of acid-base and redox properties [16, 17]. The distribution of products reflects the nature of the surface active sites: methanol is converted to formaldehyde (FA) and methyl formate (MF) on redox sites, to dimethyl ether (DME) on acidic sites, and to dimethoxymethane (DMM) on acidic and redox bi-functional sites [16, 17]. Therefore, we used the methanol oxidation reaction to characterize the surface acidic and redox properties of the VT and VTS catalysts. The results are shown in Table 3.

As shown in Table 3, V_2O_5 exhibited a high selectivity to DMM due to its acidic-redox bi-functional properties. However, it possessed a low activity for methanol conversion. Even at 433 K, the highest temperature employed in this work, the conversion of methanol was only 5% on V_2O_5. The VT catalysts presented much higher activities than V_2O_5. For

example, on 15VT, the conversion of methanol was 30% at 403 K, with selectivities to DMM, FA, MF and DME of 46%, 42%, 11% and 1%, respectively. Thus, activity was greatly enhanced on the VT catalysts. Moreover, the distribution of products on 15VT indicates that the surface acidity was not strong enough to effectively catalyze the reaction of FA condensation with methanol to produce DMM, leading to the production of large amounts of FA as well as its oxidation product MF. With an increase in temperature, the selectivity to DMM decreased while the selectivity to FA and MF increased, with a rapid increase in the total conversion of methanol. At 433 K, the conversion of methanol dramatically increased to 85%, and only oxidative products could be observed, with selectivities to FA, MF and COx of 8%, 75% and 17%, respectively. This suggests that VT catalysts mainly possess strong redox sites, whose activity was enhanced with the temperature increase, in good agreement with the results of IPA conversion. The methanol conversion and selectivities to the products were found to be very similar for the VT catalysts with different V_2O_5 contents from 15 to 50% (see Table 3), probably due to the high activity of all VT catalysts above 403 K.

Upon doping VT catalysts with SO_4^{2-}, the selectivity to DMM was greatly improved even at high conversions of methanol. On 25VTS, the highest yield to DMM was found at 413 K, a temperature at which the conversion of methanol was 54% and the selectivity to DMM was as high as 90%. The productions of FA and MF were greatly inhibited and no COx was detected. By contrast, the selectivities to DMM, FA and MF at the same temperature on the 25VT catalyst were 12%, 55% and 33% respectively, with a methanol conversion of 47%. The great improvement of the selectivity to DMM is apparently due to the enhancement of surface acidity with the addition of SO_4^{2-}. The improvement of surface acidity was also observed in the IPA conversion reaction. The improved acidity must be mainly due to some medium strength acid sites, since the selectivity to DME (usually created on strong acid sites) still remained at a very low level. A similar promoting effect of sulfate species has also been reported in the reaction of selective catalytic reduction of NO by NH_3 on a V_2O_5/TiO_2 system [28, 29]. Of all the catalysts studied in this work, the $25\%V_2O_5$-$75\%TiO_2$-SO_4^{2-} sample was found to be the most active one, probably due to the presence of the highest amount of vanadia surface species on its surface. Although the effect

of sulfate ions on acidity could not be observed from the results of pyridine adsorption IR, when considering the distribution of products in the methanol oxidation reaction it is clear that the surface acidity of the VT samples was greatly improved upon doping by SO_4^{2-}. This suggests that methanol oxidation is a good probe reaction for investigating the surface acidic and redox properties of catalysts.

4. Conclusions

V_2O_5-TiO_2 (VT) hybrid catalysts were prepared by a co-precipitation method and doped with SO_4^{2-} ions. The XRD, skeleton IR and Raman results suggest that vanadia species were well dispersed up to a vanadia loading of 25 wt%, corresponding to a high surface V density of 11.5 $V{\cdot}nm^{-2}$. The XPS results indicate that the V, Ti and S species present in the catalysts were all in fully oxidized states. The results of NH_3 adsorption microcalorimetry have shown that the surface acid site densities of VT catalysts remained constant with the increase of V_2O_5 content. Pyridine adsorption IR results indicated that both B and L acid sites were present on the surface of VT samples. However, pyridine adsorption IR did not reveal any obvious difference in the acidity upon SO_4^{2-} doping. The probe reactions of isopropanol conversion and methanol oxidation gave strong evidence that the surface acidity of the VT catalysts was greatly enhanced by SO_4^{2-} doping. Specifically, in the isopropanol conversion reaction, the yields of the dehydration products (propylene and diisopropyl ether) increased and those of the oxidative product (acetone) decreased simultaneously. In methanol oxidation, the oxidation products, formaldehyde and methyl formate, were greatly inhibited, while a large amount of DMM was produced by oxidation of methanol to formaldehyde and then formaldehyde condensation with two molecules of methanol. A high yield to DMM was observed on the SO_4^{2-}-doped 25%V_2O_5-75%TiO_2 catalyst at low temperature (413 K). The selectivity to DMM reached 90%, with 54% conversion of methanol.

Acknowledgments

We acknowledge the financial supports from the French Ministry of Education, the CNRS-France, NSFC (20373023) and MSTC (2004DFB02900 and 2005CB221400).

References

[1] P. Cavalli, F. Cavani, I. Manenti, F. Trifiro, Catal. Today 1 (1987) 245.
[2] M. Sanati, A. Andersson, J. Mol. Catal. 59 (1990) 233.
[3] F. Roozeboom, P.D. Cordingley, P.J. Gellings, J. Catal. 68 (1981) 464.
[4] P. Forzatti, E. Tronconi, G. Busca, P. Tittarelli, Catal. Today 1 (1987) 209.
[5] N.E. Quaranta, J. Soria, V.C. Corberan, J.L.G. Fierro, J. Catal. 171 (1997) 1.
[6] D.A. Bulushev, L. Kiwi-Minsker, V.I. Zaikovskii, A. Renken, J. Catal. 193 (2000) 145.
[7] M. Wainwright, N. Foster, Catal. Rev. Sci. Eng. 19 (1979) 211.
[8] V. Nikolov, D. Klissurski, A. Anastasov, Catal. Rev. Sci. Eng. 33 (1991) 319.
[9] G.C. Bond, K. Bruckman, Faraday Discuss. (1981) 235.
[10] G.C. Bond, S. Flamerz, Appl. Catal. 33 (1987) 219.
[11] G.C. Bond, J.C. Vedrine, Catal. Today 20 (1994) 1.
[12] M. Li, J. Shen, J. Catal. 205 (2002) 248.
[13] B. Grzybowska, Catal. Today 1 (1987) 341.
[14] G.C. Bond, S.F. Tahir, Appl. Catal. 71 (1991) 1.
[15] I.E. Wachs, B.M. Weckhuysen, Appl. Catal. A 157 (1997) 67.
[16] J.M. Tatibouet, Appl. Catal. A 148 (1997) 213.
[17] M. Badlani, I.E. Wachs, Catal. Lett. 75 (2001) 137.
[18] K. Fuji, S. Nakano, E. Fujita, Synthesis 4 (1975) 276.
[19] J. Masamoto, T. Iwaisako, M. Chohno, M. Kawamura, J. Ohtake, K. Matsuzaki, J. Appl. Polymer Sci. 50 (1993) 1299.
[20] Q. Sun, A. Auroux, J. Shen, J. Catal. 244 (2006) 1.
[21] S. Satoh, Y. Tanigawa, US Patent 6379507 (2002).
[22] Y.Z. Yuan, H.C. Liu, H. Imoto, T. Shido, Y. Iwasawa, J. Catal. 195 (2000) 51.
[23] Y.Z. Yuan, T. Shido, Y. Iwasawa, Chem. Comm. 15 (2000) 1421.
[24] H.C. Liu, N. Bayat, E. Iglesia, Angew. Chem. Int. Ed. 42 (2003) 5072.
[25] H.C. Liu, E. Iglesia, J. Phys. Chem. B 107 (2003) 10840.
[26] S.T. Choo, Y.G. Lee, I.-S. Nam, S.-W. Ham, J.-B. Lee, Appl. Catal. A 200 (2000) 177.
[27] S.M. Jung, P. Grange, Catal. Today 59 (2000) 305.
[28] S.M. Jung, P. Grange, Appl. Catal. B 36 (2002) 207.
[29] L. Baraket, A. Ghorbel, P. Grange, Appl. Catal. B 72 (2007) 37.
[30] V.I. Bukhtiyarov, Catal. Today 56 (2000) 403.
[31] J.P. Chen, R.T. Yang, J. Catal. 139 (1993) 277.
[32] J.P. Nogier, M. Delamar, Catal. Today 20 (1994) 109.
[33] M.H. Kim, I.-S. Nam, Y.G. Kim, J. Catal. 179 (1998) 350.
[34] D. Fraenkel, Ind. Eng. Chem. Res. 36 (1997) 52.
[35] G. Oliveri, G. Ramis, G. Busca, V.S. Escribano, J. Mater. Chem. 3 (1993) 1239.
[36] L.D. Frederickson, D.M. Hausen, Anal. Chem. 35 (1963) 818.
[37] H. Zhang, W. Zhong, X. Duan, X. Fu, J. Catal. 129 (1991) 426.
[38] A. Andersson, J.-O. Bovin, P. Walter, J. Catal. 98 (1986) 204.
[39] K. Tarama, S. Youshida, S. Ishida, H. Kakioka, Bull. Chem. Soc. Jpn. 41 (1968) 2840.

[40] I.E. Wachs, Catal. Today 27 (1996) 437.
[41] B.M. Weckhuysen, D.E. Keller, Catal. Today 78 (2003) 25.
[42] C. Zhao, I.E. Wachs, Catal. Today 118 (2006) 332.
[43] A. Auroux, Top. Catal. 4 (1997) 71.
[44] X.J. Liu, X.D. Gu, J.Y. Shen, Chin. J. Catal. 24 (2003) 674.
[45] F. Belkhadem, J.M. Clacens, A. Bengueddach, F. Figueras, Appl. Catal. A 298 (2006) 188.
[46] F. Hatayama, T. Ohno, T. Maruoka, T. Ono, H. Miyata, J. Chem. Soc.-Faraday Trans. 87 (1991) 2629.
[47] T. Blasco, A. Galli, J.M. Lopez Nieto, F. Trifiro, J. Catal. 169 (1997) 203.
[48] J. Keranen, A. Auroux, S. Ek, L. Niinisto, Appl. Catal. A 228 (2002) 213.
[49] S. Besselmann, C. Freitag, O. Hinrichsen, M. Muhler, Phys. Chem. Chem. Phys. 3 (2001) 4633.
[50] A.L. Petre, A. Auroux, A. Gervasini, M. Caldararu, N.I. Ionescu, J. Therm. Anal. 64 (2001) 253.
[51] X.D. Gu, H. Chen, J.Y. Shen, Chin. J. Catal. 24 (2003) 885.
[52] X. Gu, J. Ge, H. Zhang, A. Auroux, J. Shen, Thermochim. Acta 451 (2006) 84.
[53] D. Haffad, A. Chambellan, J.C. Lavalley, J. Mol. Catal. A 168 (2001) 153.
[54] A.P. Kulkarni, D.S. Muggli, Appl. Catal. A 302 (2006) 274.

Figure Captions

Fig. 1. X-ray diffraction (XRD) patterns of VT catalysts.

Fig. 2. FT-IR skeletal spectra of VT and VTS catalysts. (2 mg sample in 198mg KBr)

Fig. 3. Raman spectra of VT catalysts.

Fig. 4. Differential heat versus coverage (in μmol per gram of catalyst) for NH_3 adsorption at 423 K over VT catalysts.

Fig. 5. FT-IR spectra for pyridine adsorption and desorption at 300 K on VT and VTS catalysts.

Fig. 6. TPR profiles of VT and VTS catalysts.

Table 1

Binding energies, V/Ti atomic ratios for surface and bulk composition of VT and VTS catalysts

Catalyst	V_2O_5 loading in catalyst (wt/wt%)	S_{BET} (m^2/g)	Binding energy (eV)				V/Ti (surface atomic ratio)	V/Ti (bulk atomic ratio)
			O 1s	V $2p_{3/2}$	Ti $2p_{3/2}$	S 2p		
TiO_2	0	141	529.9	----	458.5	----	----	----
15VT	15	159	529.8	517.1	458.5	----	0.23	0.16
25VT	25	143	529.6	517.1	458.3	----	0.35	0.27
50VT	50	99	529.6	516.9	458.3	----	0.71	0.74
75VT	75	55	na[a]	na[a]	na[a]	----	na[a]	na[a]
15VTS	15	119	529.9	517.1	458.3	168.3	0.22	0.15
25VTS	25	99	530.0	517.0	458.5	168.2	0.33	0.26
50VTS	50	59	na[a]	na[a]	na[a]	na[a]	na[a]	na[a]
V_2O_5	100	21	530.2	517.3	----	----	----	----

[a] Not available

Table 2

Catalytic activities of VT and VTS catalysts in the isopropanol probe reaction at 393 K in air

Sample	Con. of IPA (%)	Selectivity (%)		
		PPE	ACE	DIPE
TiO_2	6	28	2	70
15VT	11	5	89	7
25VT	19	9	77	14
50VT	12	9	56	36
75VT	10	12	32	56
15VTS	6	8	83	9
25VTS	7	12	73	15
50VTS	5	16	53	31
V_2O_5	0.8	23	34	43

IPA = isopropanol, PPE = propylene, DIPE = diisopropyl ether, ACE = acetone

Table 3

Catalytic activities of the VT and VTS catalysts in the methanol oxidation reaction

Sample	Temp. (K)	Con. of methanol (%)	Selectivity (%)				
			DMM	FA	MF	DME	COx
15VT	403	30	46	42	11	1	0
	413	43	11	58	30	1	0
	423	78	1	22	71	1	5
	433	85	0	8	74	1	17
25VT	403	34	47	39	14	0	0
	413	47	12	55	33	1	0
	423	82	0	15	79	1	5
	433	91	0	6	69	1	23
50VT	403	32	47	40	12	1	0
	413	43	16	58	26	1	0
	423	75	1	27	67	1	5
	433	90	0	8	73	1	18
15VTS	403	16	98	0	2	0	0
	413	26	96	0	4	0	0
	423	38	88	3	9	0	0
	433	60	71	16	12	1	0
25VTS	403	34	95	0	5	0	0
	413	54	90	3	7	0	0
	423	69	56	21	23	1	0
	433	90	7	13	78	1	2
50VTS	403	10	92	8	0	0	0
	413	15	75	21	4	0	0
	423	21	44	47	9	1	0
	433	29	19	60	19	1	0
V_2O_5	403	1	97	0	0	3	0
	413	1.7	98	0	0	2	0
	423	3	96	0	0	4	0
	433	5	95	0	0	5	0

DMM = dimethoxymethane, FA = formaldehyde, MF = methyl formate,

DME = dimethyl ether, COx = CO_2 (or CO).

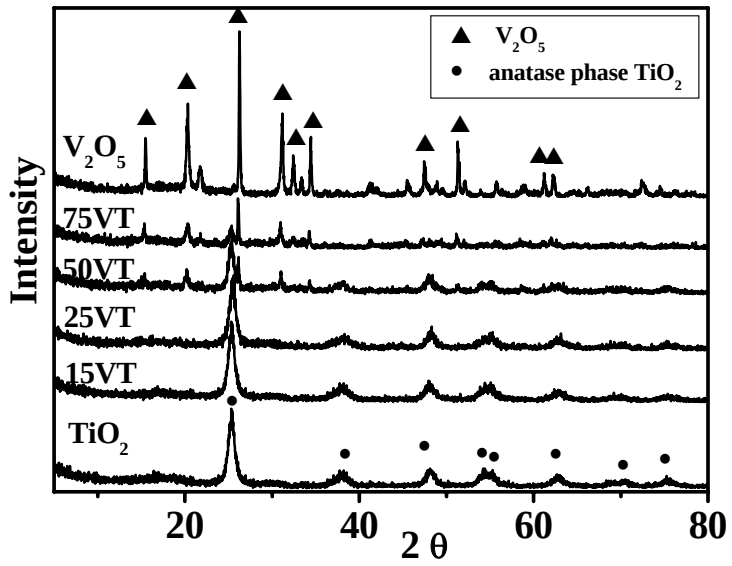

Fig.1. X-ray diffraction (XRD) patterns of VT catalysts.

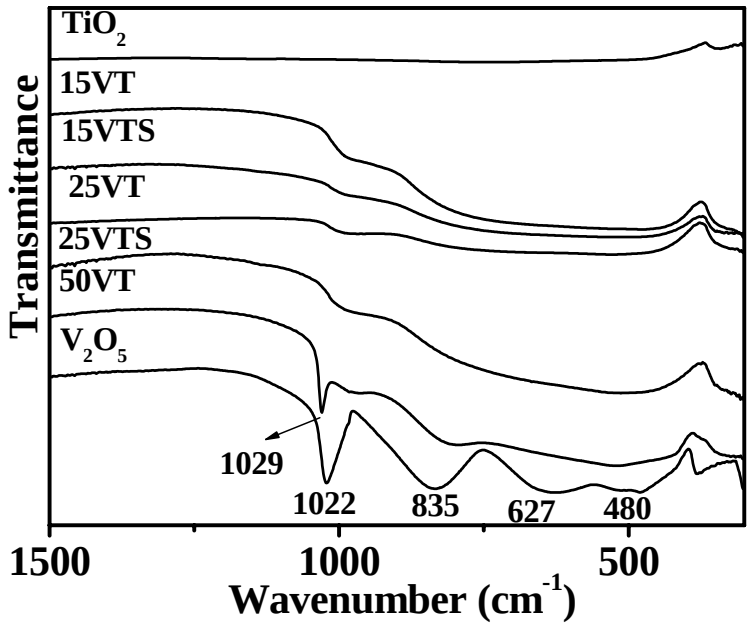

Fig. 2. FT-IR skeletal spectra of VT and VTS catalysts. (2 mg sample in 198mg KBr)

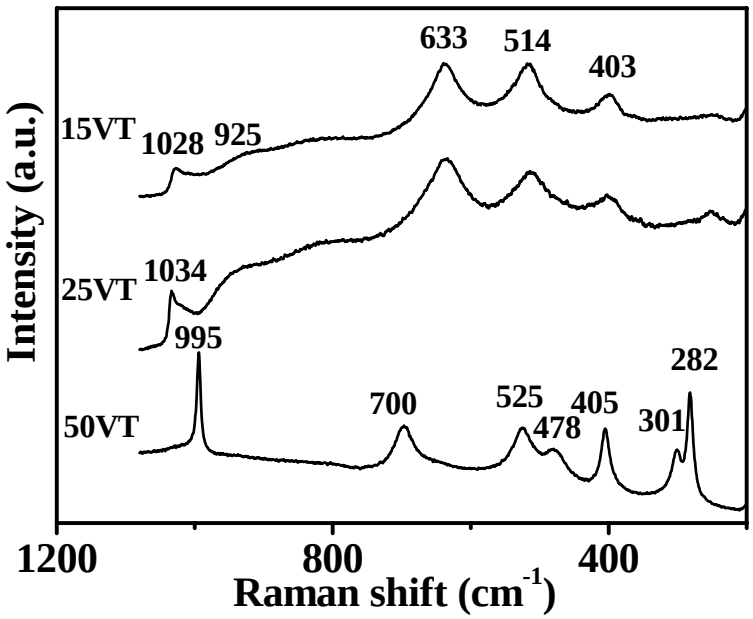

Fig. 3. Raman spectra of VT catalysts.

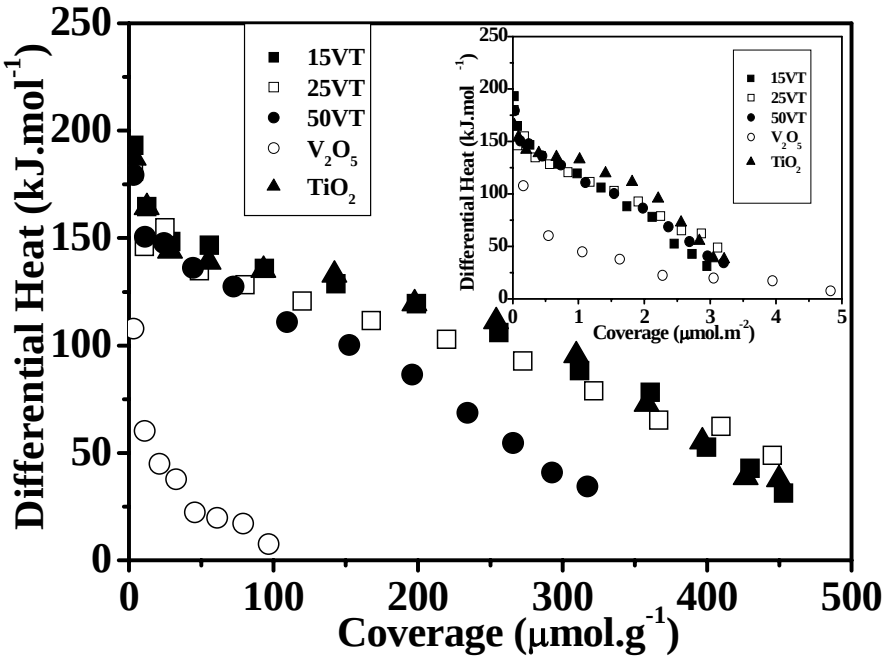

Fig. 4. Differential heat versus coverage in μmol per gram of catalyst and in μmol per m^2 of catalyst (inset) for NH_3 adsorption at 423 K over VT catalysts.

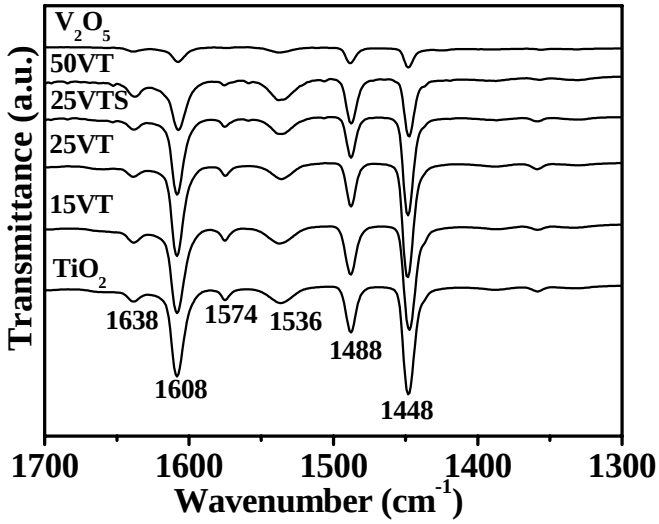

Fig. 5. FT-IR spectra for pyridine adsorption and desorption at 300 K on VT and VTS catalysts.

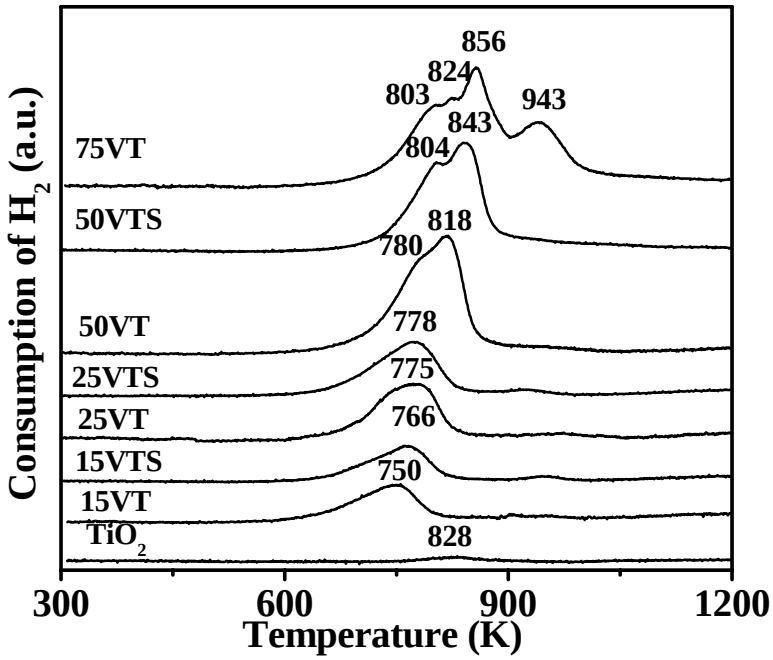

Fig. 6. TPR profiles of VT and VTS catalysts.

Publication VII

Submitted to Catalysis Communications

High surface area carbons as acidic components with Cu-ZnO/Al_2O_3 for the reforming of dimethoxymethane

Hao Shen[a], Yuchuan Fu[a], Qing Sun[a,b], Songlin Zuo[a], Aline Auroux[b] and Jianyi Shen[a,*]
Lab of Mesoscopic Chemistry, School of Chemistry and Chemical Engineering, Nanjing University, Nanjing 210093, China [a]
Institut de Recherches sur la Catalyse et l'Environnement de Lyon, UMR 5256, CNRS-Université Lyon 1, 2 Avenue Albert Einstein, 69626 Villeurbanne Cedex, France [b]

* Corresponding author E-mail: jyshen@nju.edu.cn
Phone and Fax: (+86) 25-83594305

Abstract:

Acidic carbon nano-fibers (H-CNF) has been known to be active for the hydrolysis of dimethoxymethane (DMM) to produce methanol and formaldehyde which were then steam reformed to produce H_2. In this work, high surface area H-CNF (H-HSCNF) was prepared via the activation of CNF by KOH and then by HNO_3, which had the surface area of 410 m^2/g and was highly active for the hydrolysis of DMM. Activation of phenolic resin (PR) with KOH and then HNO_3 produced acidic carbon with surface area as high as 1120 m^2/g (H-HSPRC), which was extremely active for the hydrolysis of DMM. The complex catalysts combining Cu-ZnO/γ-Al_2O_3 and H-HSPRC exhibited excellent performance for the reforming of DMM to produce H_2. The rate of H_2 production could be as high as 7400 ml $g_{cat}^{-1}h^{-1}$ from the reforming of DMM over the Cu-ZnO/γ-Al_2O_3-10%H-HSPRC, which was about 1.5 times higher than that from the reforming of methanol over the Cu-ZnO/γ-Al_2O_3.

Keywords: Acidic carbon nano-fibers; Acidic phenolic resin carbon; Surface acidity; Hydrolysis of DMM; Reforming of DMM; H_2 production;

1. Introduction

Fuel cell system has the advantages of cleanness and compactness with high energy density. Such system is promising for household and portable applications [1-3]. H_2 is the main fuel for such applications and can be produced through the reforming of hydrocarbons and oxygenated organic compounds [4-6]. The reforming of methanol received much attention. The disadvantage of using methanol as a fuel is that it is highly toxic. Since dimethoxymethane (DMM) is an environmentally benign chemical, the reforming of DMM to produce H2 has been reported recently [8, 9].

The reforming of DMM is generally composed of the following steps:

$$CH_3OCH_2OCH_3 + H_2O \rightarrow 2\ CH_3OH + CH_2O \quad (1)$$

$$CH_3OH + H_2O \rightarrow 3\ H_2 + CO_2 \quad (2)$$

$$CH_2O + H_2O \rightarrow 2\ H_2 + CO_2 \quad (3)$$

The overall reaction can be expressed as

$$CH_3OCH_2OCH_3 + 4H_2O \rightarrow 8\ H_2 + 3\ CO_2 \quad (4)$$

The catalysts for the reforming of DMM need an acidic component for the hydrolysis of DMM and the Cu-ZnO/γ-Al_2O_3 (CuZnAl) for the reforming of methanol and formaldehyde [8, 9].

The acidic carbon nano-fibers (H-CNF) with the surface area of 160 m^2/g was found to be active for the hydrolysis of DMM [9]. The complex catalyst Cu-ZnO/γ-Al_2O_3-40%H-CNF exhibited effective performance for the reforming of DMM. The rate of H_2 production reached 5200 ml $g_{cat}^{-1}h^{-1}$ from the reforming of DMM over the Cu-ZnO/γ-Al_2O_3-40%H-CNF, which was as high as that from the reforming of methanol over the Cu-ZnO/γ-Al_2O_3 [9].

Theoretically, the rate of H_2 production from the reforming of DMM might be higher than that from the reforming of methanol if the hydrolysis of DMM is fast enough since the step (3) was fast [9]. The aim of this work was to prepare acidic carbons with higher surface areas as the acidic components with Cu-ZnO/γ-Al_2O_3 for the reforming of DMM.

2. Experimental

2.1 Catalyst preparation

The complex catalysts for the reforming of DMM were mixed with the CuZnAl and an acidic component. CuZnAl used in this study was a commercial catalyst (CF105, a product of the Research Institute of Nanjing Chemical Industry Group, China) with a molar ratio of 63% Cu, 21% Zn, and 16% Al [9]. The CNF was prepared by the decomposition of propylene on an unsupported Cu-Ni (4:6 by weight) catalyst following the procedure described by Shen et al. [20]. The CNF was further activated by KOH [12-18]. Specifically, the CNF was mixed with KOH at the ratio of 1:6 (g/g) and heated in N_2 at 1073 K for 1 h [12]. A phonoic resin (PR) was also used as a precursor. The ratio of KOH to PR was 4:1 (g/g) and the mixture was heated in N_2 at 1073 K for 1 h [17]. After the activation with KOH, the resulted materials were washed thoroughly with deionized water to obtain the carbons with high surface areas (HSCNF and HSPRC). Such carbons were further treated in 63% nitric acid. Specifically, 30 ml concentrated nitric acid was added for one gram of each carbon sample and the mixture was refluxed for 30 min. Afterwards, the carbon samples were washed thoroughly and dried at 393 K for 12 h. The samples were termed as H-HSCNF and H-HSPRC, respectively.

2.2 Catalyst characterization

The surface areas of the catalysts were determined by N_2 adsorption at 77.3 K employing the BET method. The X-ray photoelectron spectra (XPS) were measured on an SSI 301 instrument equipped with a hemispherical electron analyzer and an Al anode (Al$K\alpha$ = 1486.6 eV) powered at 100 W. The residual pressure in the spectrometer chamber during data acquisition was 5×10^{-8} Pa. Microcalorimetric measurements of ammonia adsorption were performed to determine the surface acidity of the samples at 423 K. A C-80 calorimeter (Setaram, France) was connected to a volumetric system equipped with a Baratron capacitance manometer (USA) for the pressure measurement and gas handling [9]. The morphology of the different

samples has been examined using SEM and the images were obtained from a Jeol 55 CF (CMEABG Lyon).

2.3 Catalytic reaction

The hydrolysis and reforming of DMM were performed in a glass fixed-bed micro-reactor [9]. The DMM and H_2O were introduced to the reaction zone by bubbling N_2 (99,999%) through a glass saturator filled with DMM (Aldrich, 99%) maintained at 273 K and a glass saturator filled with H_2O maintained at 333 K. The feed composition was maintained at N_2:H_2O:DMM = 24:5:1 (v/v). The catalysts were usually pre-reduced at 533 K for 3 h in 12% H_2/N_2 with the flow rate of 50 ml min^{-1}. The tail gas out of the reactor was analyzed by FID and TCD detectors. The FID was connected to a Porapak N column for the separation of methanol, DMM and other organic compounds, while the TCD was connected to a TDX-01 column for the analysis of methane, CO_x and N_2. The amount of H_2 produced was usually calculated according to the conversion of DMM and the composition of other products and was checked using another gas chromatograph with a TDX-01 column [9].

3. Results and discussion

3.1. Characterization of catalysts

Table 1 presents the surface areas and compositions of the samples. The activation of CNF by KOH increased the surface area from 78 to 1100 m^2/g. The activation of phenolic resin by KOH led to a carbon with surface area of 2440 m^2/g. Upon the treatment by concentrated HNO_3, the surface areas of the samples were significantly decreased to 410 m^2/g for the H-HSCNF and 1120 m^2/g for the H-HSPRC. Treatment with nitric acid introduced functional groups on the carbon surface. In fact, XPS results revealed the significantly increased oxygen content for the carbon materials upon the treatment with HNO_3.

Fig. 1 shows the SEM images of CNF, H-HSCNF, HSPRC and H-HSPRC. It is seen that the treatments with KOH and then nitric acid did not seem to change the morphology of the CNF. Previous study showed that the CNF was mainly in the graphite

state even after the treatment with nitric acid [9]. In contrast, the SEM images in Fig. 1 showed that the HSPRC obtained from the activation of phenolic resin by KOH was in the glassy state and was not affected by the treatment with nitric acid. In addition, the HSPRC and H-HSPRC were highly porous with pores in the micrometer sizes. Apparently, the pores with the average size of 2.56 nm as determined by the N_2 desorption could not be seen by SEM, and they must be dispersed in the skeleton of the HSPRC. The thickness of the carbon skeleton among the large pores in micrometers seemed less than 50 μm, as can be seen in Fig. 1 d. Such bimodal distribution of pores facilitate the diffusion of the reactants and products. In fact, calculations using Knusen diffusion equation indicated that the diffusion of DMM was fast enough in the pores with the average size of 2.56 nm at 513 K with the space velocity of 3.2×10^4 ml g_{cat}^{-1} h^{-1}, as long as the particle size of the H-HSPRC was smaller than 100 μm.

The results of microcalorimetric adsorption of ammonia on the carbon materials are presented in Fig. 2. The H-HSCNF had higher surface area than H-CNF and therefore it had significantly more surface acidic sites than H-CNF. The initial heats for the CNF series samples were around 100 kJ/mol. Reductions were carried out at 533 K in 12% H_2/N_2 for 3 h, a condition used for the reduction of CuZnAl. The reduced H-HSCNF still possessed substantial surface acidity with 220 μmol/g acidic sites. Fig. 2 b showed that the HSPRC was non-acidic since the heat of adsorption of NH_3 measured for it was lower than 40 kJ/mol. The treatment with nitric acid greatly increased the initial heat (140 kJ/mol) and coverage (1300 μmol/g) for the adsorption of NH_3, indicating the greatly increased surface acidic sites. The reduction at 533 K in 12% H_2/N_2 did not influence the surface acidity of the H-HSPRC. It should be noted that the H-HSCNF and H-HSPRC exhibited different initial heats for the adsorption of ammonia. Such difference might reflect the different functional groups grown on the different carbon surfaces upon the treatment with HNO_3.

3.2. Hydrolysis of DMM

Fig. 3 shows the results of hydrolysis of DMM versus reaction time at 533 K. It is seen that the H-HSPRC was more active than H-HSCNF. In addition, the activity of H-HSPRC was stable while that of H-HSCNF decreased with time until 250 min. Thus, all the reaction data for the hydrolysis and reforming of DMM were collected after the reactions were stabilized.

Fig. 4 shows the effects of temperature and space velocity on the hydrolysis of DMM over the H-CNF, H-HSCNF and H-HSPRC. High space velocity (4.5×10^5 ml $gcat^{-1}$ h^{-1}) was used for the hydrolysis of DMM at different temperatures. The conversion of DMM increased with the reaction temperature and reached 21%, 74% and 99% at 533 K for the H-CNF, H-HSCNF and H-HSPRC, respectively. Higher space velocities were used at 513 K for the hydrolysis of DMM over the acidic carbons. The conversion of DMM decreased with the space velocity, but the conversion of DMM remained high (82%) over the H-HSPRC even at the very high space velocity of 1.35×10^6 ml $gcat^{-1}$ h^{-1}. The products of hydrolysis of DMM were mainly methanol and formaldehyde with less than 0.2% of DME.

3.3 Reforming of DMM

Table 2 presents the results for the reforming of DMM over the CuZnAl-H-CNF, CuZnAl-H-HSCNF and CuZnAl-H-HSPRC with 20% acidic component in the complex catalysts. The H-CNF did not seem to be active enough for the hydrolysis of DMM and thus the conversion of DMM over the complex catalyst CuZnAl-H-CNF was low. The produced methanol and formaldehyde could be reformed into H_2 and CO_2 and the selectivity to H_2 was high. The H-HSCNF was much more active than H-CNF and more DMM could be hydrolyzed over the H-HSCNF. However, the conversion of DMM was still lower than 90% at the temperatures used, indicating that H-HSCNF was not active enough either for the hydrolysis of DMM. Temperature seemed to affect the reforming of methanol on the CuZnAl component significantly. At the temperatures lower than 493 K, the selectivity to H_2 was lower than 89% while it was higher than 97% at the temperatures higher than 513 K. The H-HSPRC seemed

active enough for the hydrolysis of DMM at the high space velocity. In fact, the conversion of DMM was nearly 100% with high H_2 selectivity (>97%) on the CuZnAl-20%H-HSPRC at the temperatures higher than 513 K.

Less amount of H-HSPRC might be also possible for the complete hydrolysis of DMM. Table 3 gives the results about the effect of content of H-HSPRC in the complex catalysts on the reforming of DMM at the different space velocities. The data in Table 3 showed that the complex catalyst containing 5% H-HSPRC was not active enough for the hydrolysis of DMM. On the other hand, the complex catalyst containing 10% H-HSPRC seemed more appropriate since the conversion of DMM was higher than 96% for all the space velocities used. In particular, the conversion of DMM and selectivity to H_2 reached 96% and 93%, respectively, for the reforming of DMM over the CuZnAl-10%H-HSPRC at 513 K with the space velocity of GHSV=3.2×10^4 ml g_{cat}^{-1} h^{-1}, corresponding to the rate of H2 production of about 7400 ml g_{cat}^{-1} h^{-1}, which was about 1.5 times higher than that (5230 ml g_{cat}^{-1} h^{-1}) from the reforming of methanol over the Cu-ZnO/γ-Al_2O_3 [9].

4. Conclusion

In this work, we demonstrated that highly acidic carbon materials could be obtained via the activation of carbon nano-fibers (CNF) and phenolic resin with KOH followed by the treatment with concentrated HNO_3. Such acidic carbons were found to be highly active for the hydrolysis of dimethoxymethane (DMM) and thus could be used with Cu-ZnO/γ-Al_2O_3 for the reforming of DMM to produce H_2. Specifically, the activation of phenolic resin (PR) with KOH and then HNO_3 produced acidic carbon with surface area as high as 1120 m^2/g (H-HSPRC). The complex catalyst Cu-ZnO/γ-Al_2O_3-10%H-HSPRC exhibited excellent performance for the reforming of DMM to produce H_2. The rate of H_2 production over the catalyst at 513 K could be as high as 7400 ml $g_{cat}^{-1}h^{-1}$, which was about 1.5 times higher than that from the reforming of methanol over the Cu-ZnO/γ-Al_2O_3.

Acknowledgement

This work was supported by the Ministry of Science and Technology of China (2004DFB02900 and 2005CB221403), the National Science Foundation of China (20373023) and the High Tech. Program of Jiangsu Province of China (BG2006031).

References:

[1] P.G. Gray, M.I. Petch, Platinum Metals Rev. 44 (2000) 108.
[2] S. Golunski, Platinum Metals Rev. 42 (1998) 2.
[3] N. Edwards, S.R. Ellis, J.C. Frost, S.E. Golunski, A.N.J. van Keulen, N.G. Lindewald, J.G. Reinkingh, J. Power Sources 71 (1998) 123.
[4] A. Qi, S. Wang, G. Fu, C. Ni, D. Wu, Appl. Catal. A 281 (2005) 233.
[5] R.D. Cortright, R.R. Davda, J.A. Dumesic, Nature 418 (2002) 964.
[6] J.C. Amphlett, R.F. Mann, B.A. Peppley, P.R. Roberge, A. Rodrigues, J.P. Salvador, J.Power Sources 71 (1998) 179.
[7] Lambiotte & Cie, online publications (http://www.lambiotte.com/methylal.html).
[8] Q. Sun, A. Auroux, J. Shen, J. Catal. 244 (2006) 1.
[9] Y.C. Fu, Studies of Some Catalytic Reactions for the Synthesis and Conversion of Methanol-derived Chemicals, Ph. D. thesis, Nanjing University, 2005.
[10] J.-P. Shen, C. Song, Catal. Today 77 (2002) 89.
[11] B.A. Peppley, J.C. Amphlett, L.M. Kearns, R.F. Mann, Appl. Catal. A 179 (1999) 31.
[12] S.H. Yoon, S. Lim, Y. Song, Y. Ota, W.M. Qiao, A. Tanaka, I. Mochida, Carbon 42 (2004) 1723.
[13] H. Marsh, D. C. Crawford, T. M. O'Grady, A, Wennerberg, Carbon, 20 (1982) 419.
[14] A. N. Wennerberg, T. M. O'Grady, US Patent 4082694 (1978).
[15] N. M. Rodriguez, J. Mat. Res. 8 (1993) 3233.
[16] A. Ahmadpour, D.D. Do, Carbon 34 (1996) 471.
[17] H.S. Teng, S.C. Wang, Carbon 38 (2000) 817.
[18] M.J. Illan-Gomez, C.S.M. de Lecea, A. Linares-Solano, L.R. Radovic, Energy Fuels 12 (1998) 1256.
[19] S. Biniak, G. Szymanski, J. Siedlewski, A. Swiatkowski, Carbon 35 (1997) 1799.
[20] J. Shen, Q. Sun, H. Zhang, CN Patent 1562468 (2006).
[21] T. Otowa, Y. Nojima, T. Miyazaki, Carbon 35 (1997) 1315.

Figure Captions

Fig. 1 SEM images of (a) CNF, (b) H-HSCNF, (c) HSPRC and (d) H-HSPRC.

Fig. 2 Differential heat versus coverage for NH_3 adsorption at 423 K over (a) H-CNF and H-HSCNF, and (b) SPRC and H-HSPRC. The samples were either reduced at 533 K in 12% H_2/N_2 for 3 h or out gased at 523 K for 1 h before the measurements.

Fig. 3 Conversion of DMM versus time on stream over the H-HSPRC and H-HSCNF for the hydrolysis of DMM at 533 K with GHSV=4.5×10^5 ml g^{-1} h^{-1}.

Fig. 4 Effects of temperature (a) and space velocity (b) on the hydrolysis of DMM over the H-CNF, H-HSCNF and H-HSPRC. Reaction conditions: N_2/H_2O/DMM (v/v) = 24/5/1, T = 513 K (for different velocities) and GHSV = 4.5×10^5 ml $gcat^{-1}$ h^{-1} (for different temperatures).

Table 1
Surface area and composition of the carbon materials used in this study.

Sample	BET area (m^2/g)	Pore size (nm)	Surface composition from XPS		
			O	N	C
CNF	78	-	3.45	0.00	96.55
H-CNF	50	-	12.55	1.74	85.70
HSCNF	1100	-	3.76	0.27	95.97
H-HSCNF	410	3.5	11.99	0.69	87.32
HSPRC	2440	-	13.15	1.05	85.80
H-HSPRC	1120	2.6	18.18	1.02	80.80

Table 2

Reforming of DMM over the complex catalysts [a]

Catalyst [b]	Temp. (K)	DMM Conv. (%)	H_2 Sel. (%)	Sel. to carbonaceous products (%)				
				CO	CO_2	CH_3OH	DME	CH_4
CuZnAl-	473	11	97	n.d.	97	2	1	n.d.[c]
H-CNF	493	14	97	n.d.	97	1	2	n.d.
	513	26	97	n.d.	97	1	2	0
	533	36	96	n.d.	97	1	3	0.1
CuZnAl-	473	52	64	n.d.	68	32	0.1	n.d.
H-HSCNF	493	67	89	n.d.	90	10	0.1	n.d.
	513	80	98	n.d.	98	2	0.1	n.d.
	533	90	100	1	99	0.3	0.2	0
CuZnAl-	473	99	54	n.d.	60	41	0	n.d.
H-HSPRC	493	100	74	n.d.	77	23	0	n.d.
	513	100	97	n.d.	97	3	0	n.d.
	533	100	100	2	97	0.2	0	n.d.

[a] Conditions for DMM reforming: $N_2/H_2O/DMM=24/5/1$ (v/v) and GHSV=2.1×10^4 ml $g_{cat}^{-1}h^{-1}$.
[b] The content of H-CNF, H-HSCNF and H-HSPRC in the complex catalysts was 20%.
[c] n.d. denotes “not detectable”.

Table 3

Effect of content of H-HSPRC in the complex catalysts for the reforming of DMM at 513 K.

Catalyst	GHSV (ml $g_{cat}^{-1}h^{-1}$)	DMM Conv. (%)	Rate of H_2 production (ml $g_{cat}^{-1}h^{-1}$)	Selectivity (%)				
				H_2	CO	CO_2	CH_3OH	DME
CuZnAl-5% H-HSPRC	2.1×10^4	84	4636	99	0.9	98	1	0.2
	2.6×10^4	81	5494	98	0.6	98	2	0.2
	3.2×10^4	73	5770	96	0.3	96	3	0.2
CuZnAl-10% H-HSPRC	2.1×10^4	99	5475	99	0.8	98	1	0
	2.6×10^4	98	6497	96	0.6	96	4	0
	3.2×10^4	97	7412	93	0.3	93	6	0
CuZnAl-20% H-HSPRC	2.1×10^4	100	5421	97	n.d.	97	0	0

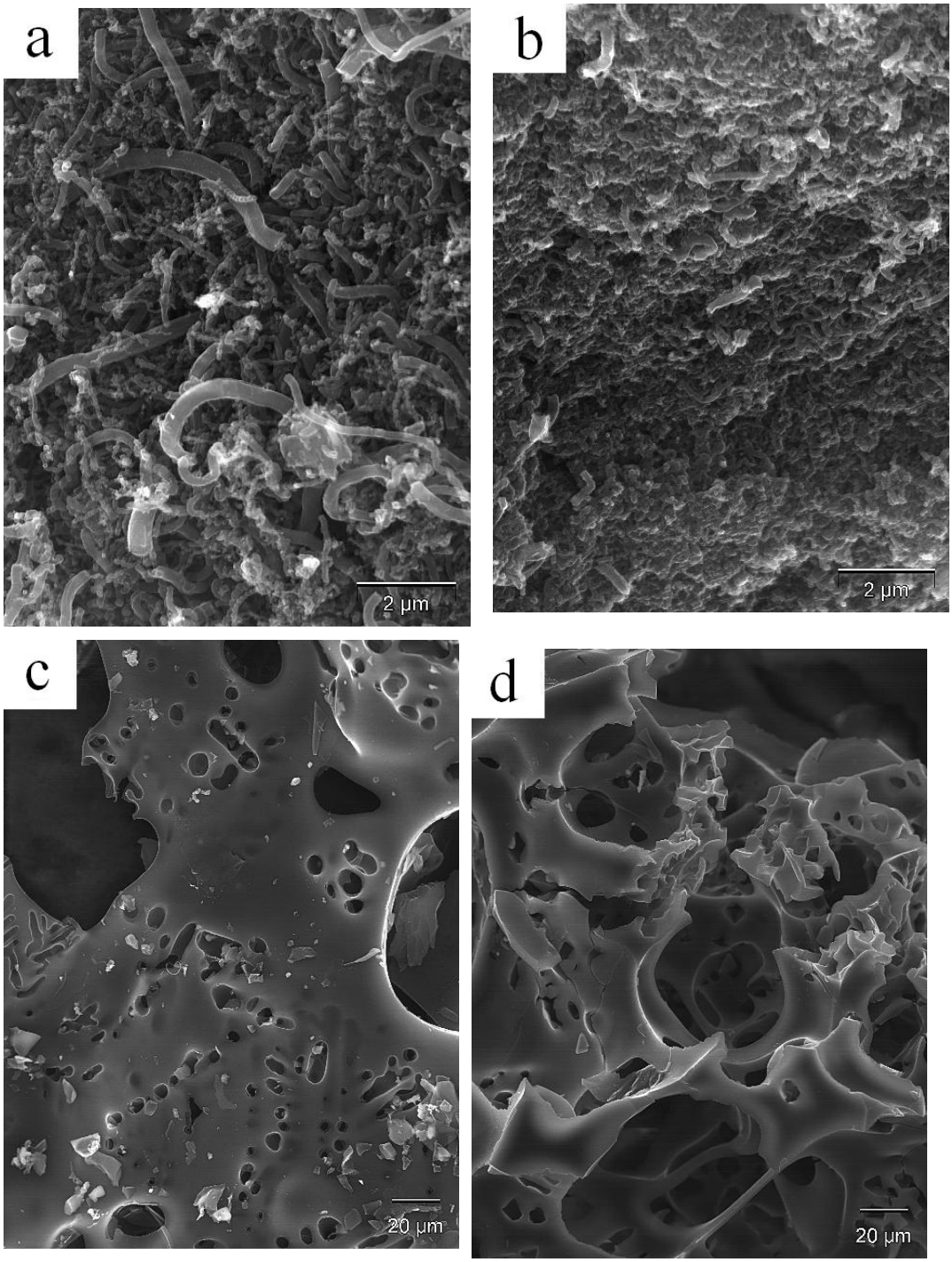

Fig. 1 SEM images of (a) CNF, (b) H-HSCNF, (c) HSPRC and (d) H-HSPRC.

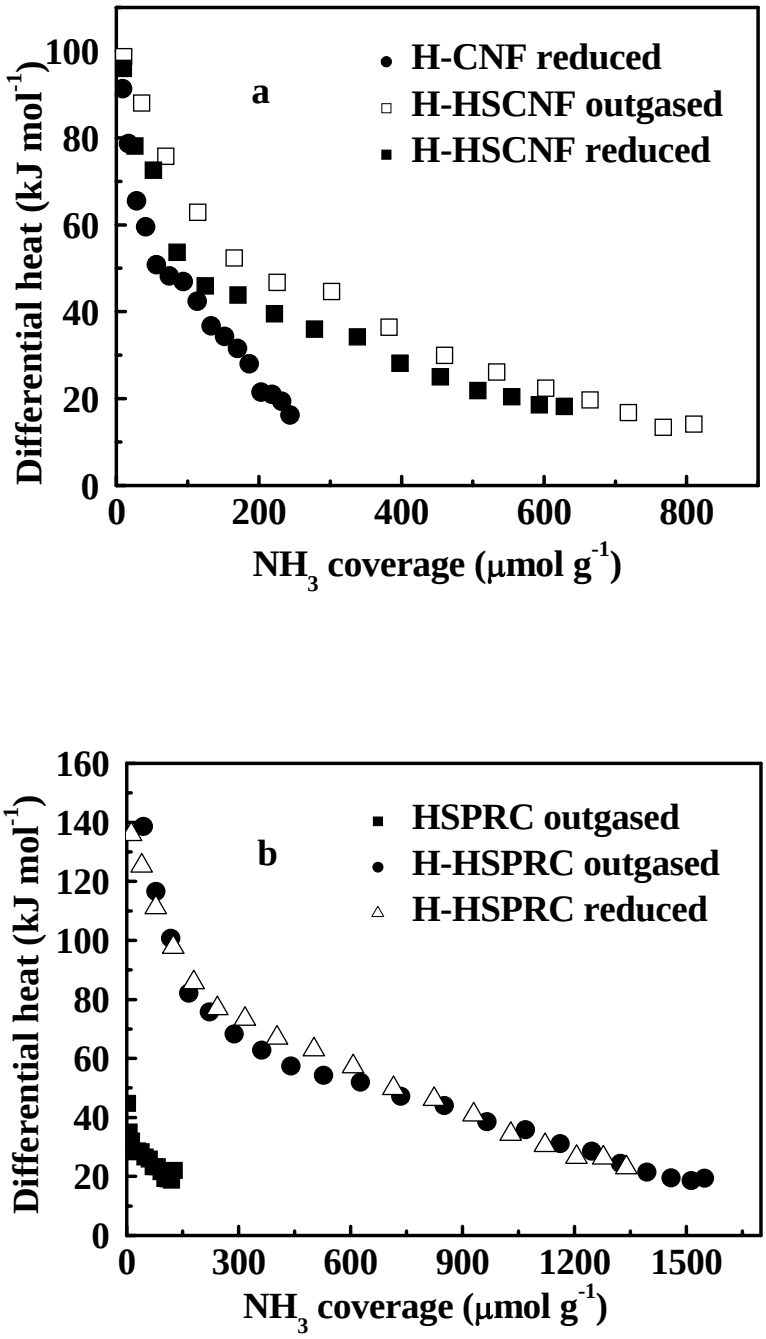

Fig. 2 Differential heat versus coverage for NH_3 adsorption at 423 K over (a) H-CNF and H-HSCNF, and (b) SPRC and H-HSPRC. The samples were either reduced at 533 K in 12% H_2/N_2 for 3 h or out gased at 523 K for 1 h before the measurements.

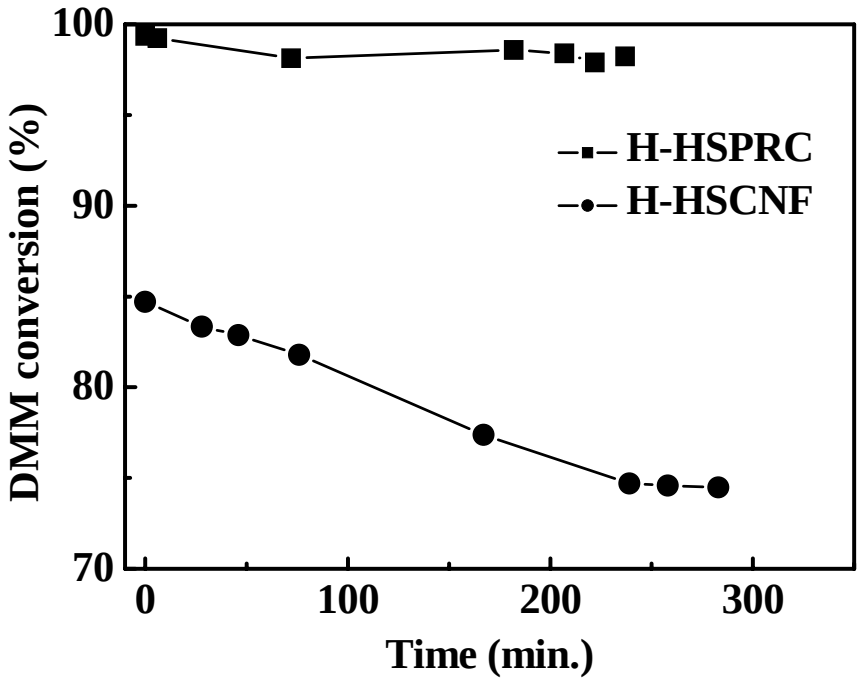

Fig. 3 Conversion of DMM versus time on stream over the H-HSPRC and H-HSCNF for the hydrolysis of DMM at 533 K with GHSV=4.5×10^5 ml g^{-1} h^{-1}.

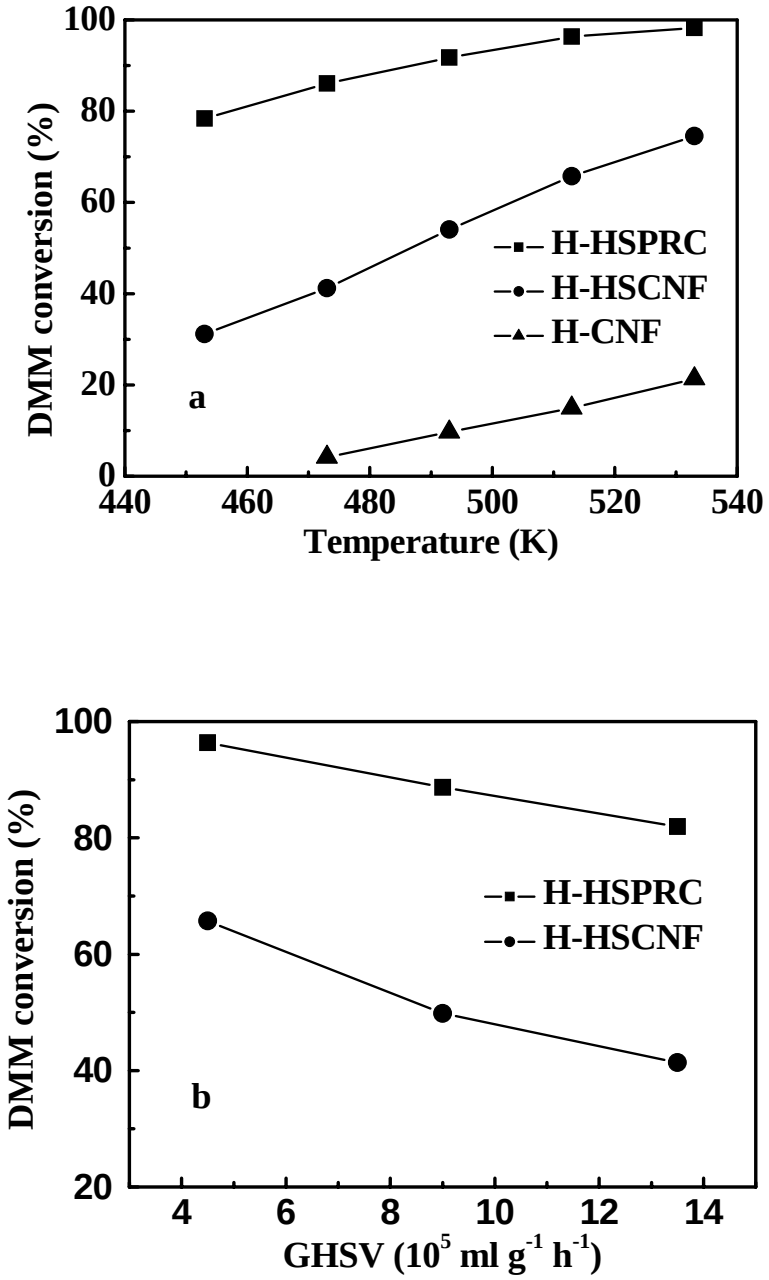

Fig. 4 Effects of temperature (a) and space velocity (b) on the hydrolysis of DMM over the H-CNF, H-HSCNF and H-HSPRC. Reaction conditions: N_2/H_2O/DMM (v/v) = 24/5/1, T = 513 K (for different velocities) and GHSV = 4.5×10^5 ml $gcat^{-1}$ h^{-1} (for different temperatures).

5. Summary of Results and Discussions

The main results of this work are summarized below.

(1) Steam reforming of DMM to produce H_2:

Dimethoxymethane (DMM) has very low toxicity and high hydrogen content, which may be suitable as a H_2 storage material for small H_2 sources instead of toxic methanol. H_2 could be produced via reforming of DMM. The reforming of DMM consists of the hydrolysis of DMM to methanol and formaldehyde, which are further reformed into H_2 and CO_2. In this work, we indicate that it is possible to directly reform DMM to produce H_2 if a proper acidic component is used with the traditional $CuZnO/Al_2O_3$ catalyst. A new complex catalyst combined with NbP and $Cu\text{-}ZnO/Al_2O_3$ was developed to produce H_2 from steam reforming of DMM.

Nb_2O_5 and NbP samples were prepared with different methods to be used as the solid acid component in the steam reforming of DMM reaction. The porous NbP obtained by using hexadecylamine as a template exhibited the highest surface area. Both Nb_2O_5 and NbP samples studied in this work possessed similar amorphous structure. The NbP samples were found to be more acidic than Nb_2O_5, especially the one with high surface area. Both Brønsted and Lewis acid sites were present on the surface of Nb_2O_5 and NbP, but more Brønsted sites were evidenced on niobium phosphates than on Nb_2O_5. The high surface area niobium phosphate exhibited great amount of surface acid sites (> 750 $\mu mol \cdot g^{-1}$) and was most active in catalyzing the reaction of isopropanol dehydration. Both Nb_2O_5 and NbP were active for the hydrolysis of DMM. The results of methanol reforming indicated that the addition of Nb_2O_5 or NbP into $CuZnO/Al_2O_3$ catalysts does not affect the conversion of methanol compared to $CuZnO/Al_2O_3$ alone and no DME or any other organic compounds were formed. Thus, Nb_2O_5 and NbP seemed suitable as hydrolysis components for the reforming of DMM. By combining Nb_2O_5 or NbP with an industrial $CuZnO/Al_2O_3$, the complex catalysts were effective for the reforming of DMM to produce H_2 above 493 K. DMM could be completely reformed into COx and H_2 over the complex catalysts at 493 K.

(2) Selective oxidation of methanol to DMM:

DMM is usually produced via a condensation of formaldehyde with methanol over acid catalysts. The direct synthesis of DMM would be more efficient if the process is industrialized. The selective oxidation of methanol to DMM may involve two steps: (1) oxidation of methanol to formaldehyde on redox sites and (2) condensation of formaldehyde produced with additional methanol to DMM on acidic sites. Thus, bi-functional catalysts with both redox and acidic characters are required for the reaction.

Two catalysts series of V_2O_5/NbP and V_2O_5-TiO_2-SO_4^{2-} respectively were prepared. The acidic and redox properties were studied by different techniques and correlated with the activities in the reaction of oxidation of methanol to DMM.

Specifically, a series of V_2O_5/NbP catalysts with different V_2O_5 loadings were synthesized by the wetness impregnation method. The results from XRD and LRS showed that V_2O_5 could be well dispersed on the surface of NbP. XPS showed that both vanadium and niobium were present in the oxidized state of +5 in the samples. Adsorption of O_2 showed about 60% dispersion of V_2O_5 on NbP. The results of microcalorimetry and FT-IR for NH_3 adsorption showed that the strength of surface acidity of NbP was decreased while the proportion of the number of weak acid sites was increased upon the addition of V_2O_5 on NbP. The IPA probe reaction indicated that NbP exhibited acidity only. The addition of V_2O_5 produced acetone from IPA, but not as much as that on bulk V_2O_5 (the activity being expressed in per m^2). This indicates that the NbP support weakened the redox properties of V_2O_5. Accordingly, NbP produced only DME from the dehydration of methanol owing to its lack of redox property. In contrast, the V_2O_5/NbP catalysts produced mainly DMM due to its bi-functional character. Specifically, methanol was first oxidized on the redox sites of V_2O_5/NbP to produce formaldehyde which was then condensed with additional methanol on the acidic sites of V_2O_5/NbP to form DMM.

V_2O_5-TiO_2 (VT) hybrid catalysts were prepared by a co-precipitation method and doped with SO_4^{2-}. XRD, skeleton IR and Raman results suggested that vanadia

high V surface density of 11.5 V/nm^2. XPS results indicated that V, Ti and S species in the catalysts were all existing in full oxidized state. The results of NH_3 adsorption microcalorimetry showed that the surface acid densities of VT catalysts remained constant with increasing V_2O_5 content. Pyridine adsorption IR indicated that both B and L acid sites were present on the surface of VT samples. Although from pyridine adsorption IR, no obvious difference was observed for an acidity enhancement upon SO_4^{2-} doping, the probe reactions of isopropanol conversion and methanol oxidation strongly suggested that the surface acidity of VT catalysts was greatly improved with SO_4^{2-} doping. Specifically, in isopropanol conversion reaction, the dehydration products, propylene and diisopropyl ether, increased and the oxidative product, acetone, decreased simultaneously. In methanol oxidation reaction, the oxidative products formaldehyde and methyl formate were greatly inhibited while a large amount of DMM was produced, which formed first by oxidation of methanol to formaldehyde and then formaldehyde condensation with two molecular methanol. A high yield of DMM was found on SO_4^{2-} doped 25%V_2O_5-75%TiO_2 catalyst at low temperature (413 K). The selectivity to DMM reached 90% with 54% conversion of methanol.

(3) Dehydration of methanol to produce DME:

Dimethyl ether (DME) has been widely used as an aerosol propellant to replace chlorofluoro carbons. Furthermore, it is an important chemical intermediate for producing many valuable chemicals such as lower olefins, methyl acetate, dimethyl sulfate, etc. In recent years, it has attracted global attention as a potential clean fuel substitute for LPG and diesel oil for its cleanness, non-toxic and environmentally benign behaviour. DME is generally synthesized by dehydration of methanol over solid acidic catalysts. It can also be synthesized directly from syngas via a so-called STD (syngas to DME) process by employing a hybrid catalyst comprising a methanol synthesis component and a solid acid, which is more attractive in consideration of the equilibrium limitation.

5. Summary of Results and Discussions

Nb_2O_5 and NbP samples were synthesized and used to adsorb NH_3, methanol, water and dimethyl ether, which were investigated by means of adsorption microcalorimetry, adsorption infrared spectroscopy (FT-IR) and temperature-programmed desorption (TPD) techniques. The results of microcalorimetry and FT-IR for NH_3 adsorption have shown that NbP is much more acidic than Nb_2O_5 due to its higher surface area, and that both Brønsted and Lewis acid sites are present on the surface of Nb_2O_5 and NbP. Water adsorption microcalorimetry results indicate that a small amount of water was strongly chemisorbed on Nb_2O_5 and NbP while most of the adsorbed water corresponded to physical adsorption. The results of methanol adsorption microcalorimetry, methanol adsorption FT-IR and methanol TPD suggest that methanol is mainly strongly dissociatively adsorbed on Nb_2O_5 and NbP to form methoxy species and DME could be produced from the dehydration of methoxy species. DME adsorption microcalorimetry and FT-IR showed that DME was mainly molecularly chemically adsorbed on Nb_2O_5 and NbP, while a small amount of DME was dissociatively adsorbed. The probe molecules (NH_3, methanol, H_2O and DME) used in this work were adsorbed more strongly on NbP than on Nb_2O_5 because of the stronger acidity of NbP. In the reaction of methanol dehydration, although Nb_2O_5 and NbP were not as active as a H-ZSM-5 zeolite, they exhibited 100% selectivity to the DME product and a good stability of the activity in the temperature range relevant to the reaction (453-573 K), without coke formation.

6. Conclusions

The work is related to the subject “Clean Energy”. The application of fuel cells based on hydrogen energy for electric power generation has immense potential since they offer efficiency and environmental and operational benefits better than those obtained from conventional technologies such like internal combustion engines. As a foundation of fuel cells based on hydrogen energy, the large-scale production of hydrogen in industry is available which can be realized by hydrocarbon reforming or coal gasification combined with water gas shift reaction. What is much more costly is the process of storage and transportation of hydrogen. One of the key techniques to solve this problem is the development of mobile hydrogen sources for fuel cells.

DMM (dimethoxymethane) is a hydrogen containing fuel which has the advantages of high content of hydrogen, nontoxicicity and to be environmentally benign and easy for storage and transportation at ambient conditions (a liquid). Therefore, it can be used as a preferring material for mobile H_2 storage and transportation.

DMM is industrially produced via the condensation of methanol and formaldehyde. In this work, we also studied a new process of selective oxidation of methanol to produce DMM on a redox-acidic bi-functional catalyst on which methanol was first oxidized on the redox sites to produce formaldehyde and formaldehyde then condensed with additional methanol on the acidic sites to form DMM. The redox-acidic bi-functional catalysts of V_2O_5/NbP and V_2O_5-TiO_2-SO_4^{2-} were prepared, characterized and evaluated in the reaction of selective oxidation of methanol to DMM.

In this work, we demonstrated the possibility of a new way to produce H_2 through the steam reforming of DMM. The steam reforming of DMM consists of the hydrolysis of DMM to methanol and formaldehyde, which are further reformed into H_2 and CO_2. Therefore, a complex bi-functional catalyst composed of a solid acid for the hydrolysis of DMM and a copper component for the reforming of methanol and formaldehyde are considered to be used for the steam reforming of DMM. The solid

acid Nb_2O_5 and NbP were prepared and used as acid components combined with $CuZnO/Al_2O_3$ catalyst for the steam reforming of DMM to produce H_2.

In addition, the adsorption properties and catalytic performance of solid acids Nb_2O_5 and NbP in the reaction of methanol dehydration to DME (dimethyl ether) were also studied.

The following is the summary of the general conclusions.

(1) Selective oxidation of methanol to DMM:

In V_2O_5/NbP catalysts, V_2O_5 can be well dispersed on the surface of NbP with a dispersion of 60% as indicated by the results from XRD, LRS and O_2 adsorption. Both vanadium and niobium were present in the oxidized state of +5. The addition of V_2O_5 on NbP resulted in a decrease of surface acidity and an increase of proportion of the number of weak acid sites to strong sites, suggested by the results of microcalorimetry and FT-IR for NH_3 adsorption. Both IPA probe reaction and methanol oxidation reaction indicated that NbP exhibited acidity only, while the addition of V_2O_5 on NbP generated redox sites to form redox-acidic bi-functional catalysts. However, it seemed that is the redox properties of V_2O_5 were weakened by the NbP support, since V_2O_5/NbP catalysts were not as active as bulk V_2O_5 in the reactions of isopropanol conversion and methanol oxidation.

High surface area V_2O_5-TiO_2 (VT) hybrid catalysts were obtained by a co-precipitation method and modified by doping with SO_4^{2-} ions doping. The XRD, skeleton IR and Raman results suggest that vanadia species are well dispersed with a high surface V density of 11.5 $V{\cdot}nm^{-2}$, which is higher than on supported vanadia catalysts (maximum 8 $V{\cdot}nm^{-2}$). The XPS results indicate that the V, Ti and S species present in the catalysts are all in fully oxidized states. The surface acid sites densities of VT catalysts remained constant with increasing V_2O_5 content as suggested by the results of NH_3 adsorption microcalorimetry. Both the reactions of isopropanol conversion and methanol oxidation gave strong evidence that the surface acidity of the VT catalysts was greatly enhanced by SO_4^{2-} doping. In the isopropanol conversion

reaction, the yields of the dehydration products (propylene and diisopropyl ether) increased and those of the oxidative product (acetone) decreased simultaneously. Similar catalytic performance was found in the reaction of methanol oxidation on VT catalyst doped with SO_4^{2-} ions. Specifically, the oxidation products, formaldehyde and methyl formate, were greatly inhibited, while a large amount of DMM was produced by oxidation of methanol to formaldehyde and then formaldehyde condensation with two molecules of methanol. The SO_4^{2-} doped 25%V_2O_5-75%TiO_2 catalyst exhibited a high yield of DMM (DMM selectivity: 90%, methanol conversion: 54%) at low temperature (413 K). These results showed that DMM can be effectively synthesized via selective oxidation of methanol on redox-acidic bi-functional VT-SO_4^{2-} catalysts.

(2) Steam reforming of DMM to produce H_2:

The Nb_2O_5 and NbP samples studied in this work exhibited amorphous structure. Both Nb_2O_5 and NbP exhibited strong acidity in which NbP was more acidic than Nb_2O_5 due to the larger surface area according to the results of NH_3 adsorption microcalorimetry. The results from NH_3 adsorption FT-IR suggested that both Brønsted and Lewis acid sites were present on the surface of Nb_2O_5 and NbP. In the reaction of hydrolysis of DMM, both Nb_2O_5 and NbP were tested to be active and no DME by-product was produced. In addition, the acid component (Nb_2O_5 or NbP) did not affect the methanol steam reforming effect on CuZnO/Al_2O_3 when combined together. These results suggested that Nb_2O_5 and NbP are suitable acids components for DMM hydrolysis reaction. Therefore, a complex catalyst combining Nb_2O_5 or NbP with an industrial CuZnO/Al_2O_3 was further tested to be effective for the reforming of DMM to produce H_2. It was found that DMM can be completely reformed into COx and H_2 over the complex catalysts at 493 K. Thus, DMM can be effectively reformed to produce H_2 on a complex catalyst composed of a solid acid (Nb_2O_5 or NbP) and a CuZnO/Al_2O_3 catalyst.

(3) Dehydration of methanol to produce DME:

Strong solid acids Nb_2O_5 and NbP samples were characterized and tested in the reaction of methanol dehydration. The results from water adsorption microcalorimetry indicated that most of the water was physically adsorbed while a small amount of water was strongly chemically adsorbed on the Lewis acid sites of Nb_2O_5 and NbP. The results from methanol adsorption microcalorimetry and methanol adsorption FT-IR suggested that methanol was mainly dissociatively adsorbed on Nb_2O_5 and NbP to form methoxy species, which further dehydrated to molecularly adsorbed DME and water, as confirmed by the results of methanol TPD. DME was mainly molecularly chemisorbed on Nb_2O_5 and NbP, while a small amount of DME could also be dissociatively adsorbed as seen from the results of DME adsorption microcalorimetry and FT-IR. NbP exhibited stronger interaction with the probe molecules (NH_3, methanol, H_2O and DME) than Nb_2O_5 due to its stronger surface acidity. In the reaction of methanol dehydration, although the catalytic activities of Nb_2O_5 and NbP were not as high as that of H-ZSM-5, they exhibited 100% selectivity to the DME product and good stability of the activities without coke formation. Thus, Nb_2O_5 and NbP could be used as a solid acid in the methanol dehydration reaction or as an acid component in the STD (syngas to DME) process.

Abbreviations

DMM Dimethoxymethane

DME Dimethyl ether

MF Methyl formate

FA Formaldehyde

IPA Isopropanol

NbP Niobium phosphate

XRD X-ray diffraction

BET Brunauer, Emmett, Teller

LRS Raman spectroscopy

XPS X-ray photoelectron spectroscopy

CA Chemical Analysis

FTIR Fourier Transformed Infrared spectroscopy

UV-vis spectroscopy Ultra violet-visible spectroscopy

TEM Transmission electron microscopy

TPD Temperature-programmed desorption

TPR Temperature-programmed reduction

Abstract (Chinese, English, French)

题目

甲缩醛和二甲醚的合成及重整制氢

摘要

本工作与“清洁能源”主题相关。甲缩醛（DMM）具有高含氢量、无毒等优点，适宜用作氢燃料电池汽车的储氢燃料。本工作发现DMM可以在固体酸（如氧化铌或磷酸铌）和$CuZnO/Al_2O_3$组成的复合催化剂上100％转化重整制氢。本工作还研究了磷酸铌担载的五氧化二钒催化剂以及硫酸根改性的钒钛催化剂体系在甲醇选择氧化制备DMM反应中的性能。此外，还对氧化铌和磷酸铌催化剂在甲醇脱水反应中的反应活性和吸附性能进行了研究。

关键词

甲缩醛重整，甲醇氧化，甲醇脱水，制氢，酸碱性和氧化-还原性，吸附量热

TITLE

Reforming and synthesis of dimethoxymethane and dimethyl ether for H_2 production

---

ABSTRACT

This work is related to the subject "Clean Energy". Dimethoxymethane (DMM) is a suitable H_2 storage material for mobile application due to its high H_2 content and non-toxicity. It was found that DMM can be 100% reformed to produce H_2 on a complex catalyst composed of an acid component such as Nb_2O_5 or niobium phosphate (NbP) combined with $CuZnO/Al_2O_3$ catalyst. Moreover, V_2O_5/NbP and V_2O_5-TiO_2-SO_4^{2-} catalysts were prepared and evaluated in the reaction of selective oxidation of methanol to DMM. The surface acidic and redox properties of V_2O_5-TiO_2-SO_4^{2-}were correlated to the reactive performance of the catalysts. The adsorption properties of Nb_2O_5 and NbP used in methanol dehydration reaction were also studied.

KEY WORDS

Reforming of dimethoxymethane, Oxidation of methanol, Dehydration of methanol, Production of H_2, Acidic and redox properties, Adsorption microcalorimetry

---

Abstract (Chinese, English, French)

TITRE

Reformage et synthèse des diméthoxyméthane et diméthyléther pour la production d’ hydrogène

---

RESUME

Ce travail est lié au sujet "Energies Propres". Le diméthoxyméthane (DMM) a un fort potentiel de stockage d’hydrogène comme source pour des applications mobiles du fait de son contenu élevé en hydrogène et de sa non toxicité. Il a été montré que le DMM peut être reformé à 100% pour produire de l’hydrogène sur un catalyseur complexe formé d’un solide acide tel que Nb_2O_5 ou du phosphate de niobium (NbP) associé à un catalyseur de type $CuZnO/Al_2O_3$. D’autre part, des catalyseurs V_2O_5/NbP et $V_2O_5/TiO_2–SO_4^{2-}$ ont été préparés et évalués dans la réaction d’oxydation sélective du méthanol en DMM. Les propriétés acides et redox de surface de ces catalyseurs ont été corrélées à leur performance catalytique. Les propriétés d’adsorption de Nb_2O_5 et NbP, testés en réaction de déshydratation du méthanol, ont été aussi évaluées.

DISCIPLINE

Chimie, Catalyse

MOTS-CLES

Reformage du diméthoxyméthane, Oxydation du méthanol, Déshydratation du méthanol, Production d’hydrogène, Propriétés acides et redox, Microcalorimétrie d’adsorption

---

INTITULE ET ADRESSE DU LABORATOIRE

Institut de Recherches sur la Catalyse et l'Environnement de Lyon,
UMR 5256 CNRS/Université Lyon 1,
2 avenue Albert Einstein, 69626 VILLEURBANNE Cedex, FRANCE